1-1-2012

Reliability model for ductile hybrid frp rebar using randomly dispersed chopped fibers

Bashar Ramzi Behnam
Wayne State University,

RELIABILITY MODEL FOR DUCTILE HYBRID FRP REBAR USING RANDOMLY DISPERSED CHOPPED FIBERS

by

BASHAR RAMZI BEHNAM

DISSERTATION

Submitted to the Graduate School

of Wayne State University,

Detroit, Michigan

in partial fulfillment of the requirements

for the degree of

DOCTOR OF PHILOSOPHY

2012

MAJOR: CIVIL ENGINEERING

Approved by:

_____
Advisor Date

_____

_____

_____

_____

DEDICATION

To My Mom
To the memory of my father

ACKNOWLEDGMENTS

I would like show my appreciation and gratitude to my advisor Dr. Christopher D. Eamon, Professor of Civil Engineering Department for his invaluable guidance and advice throughout the time of conducting this work. I sincerely thank him for the comments and academic materials provided which paved the way for advancement in this work.

I also would like to thank the committee members Dr Mumtaz Usmen, Dr Hwai-Chung Wu, and Dr Wen Li for their suggestions, comments, and encouragements.

Without those people, this work wouldn’t have been accomplished.

TABLE OF CONTENTS

LIST OF FIGURES

LIST OF TABLES

Chapter One

Introduction

In 2002, the U.S. Federal Highway Administration (FHWA) released a comprehensive study on the direct costs associated with metallic corrosion in almost every U.S. industry sector: infrastructure, transportation, production and manufacturing, government, and utilities (Figure 1-1) (Brongers, Koch, Thompson, Payer, and Virmani, 2002). Despite the fact that corrosion management has improved over the past several decades, the total annual direct cost of corrosion in the U.S. was estimated to be around $276 billion—approximately 3.1% of the nation's Gross Domestic Product (GDP). To reduce this cost, there is a need to encourage, support, and implement optimal corrosion control practices *or* find and use alternatives, non-corrosive materials.

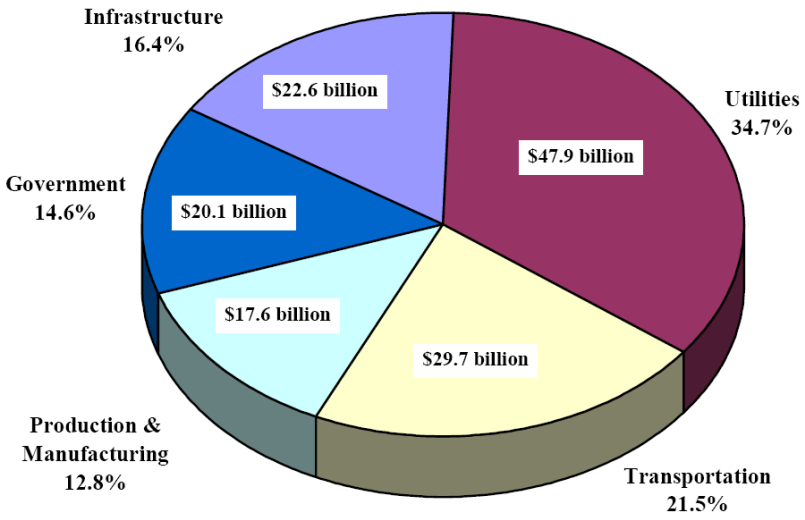

Figure (1-1): Direct costs associated with metallic corrosion in U.S. industries.

In the FHWA study, infrastructure was divided into the following sectors: highway bridges, gas and liquid transmission pipelines, waterways and ports, hazardous materials storage, airports, and railroads. The annual direct cost in infrastructure was estimated to be $22.6 billion (Figure 1-2).

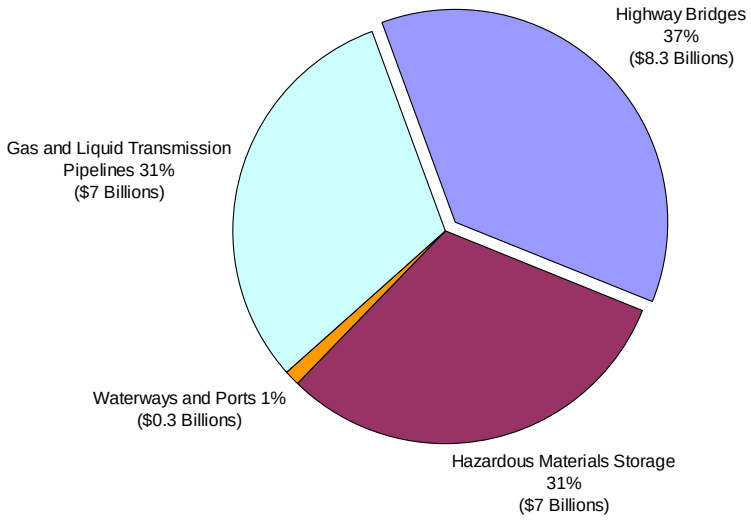

Figure (1-2): Cost of infrastructure corrosion.

1-1 Highway Bridges

According to FHWA (Brongers, Koch, Thompson, Payer, and Virmani, 2002), there are approximately 583,000 bridges in the U.S. Of this total, 200,000 are constructed of steel, 235,000 are conventional reinforced concrete, 108,000 are constructed using prestressed concrete, and the balance is made with other construction materials. Because of corroded steel and steel reinforcement, approximately 15% of these bridges are structurally deficient. Annual direct cost estimates total $8.3 billion, including $3.8 billion to replace deficient bridges over the next 10 years, $2 billion for maintenance and capital costs for concrete bridge decks and $2 billion for their concrete substructures, and $0.5 billion for maintenance painting of steel bridges. Indirect costs to the user, such as

traffic delays and lost productivity, were estimated to be as high as 10 times that of direct corrosion costs.

According to Brongers, Koch, Thompson, Payer, and Virmani (2002) “the dollar impact of corrosion on reinforced-concrete, prestressed concrete, and steel bridges is considerable, but the indirect costs, those incurred by users, increase expenses tenfold. For example, a traffic tie-up or detour caused by a bridge failure or its rehabilitation and maintenance can result in wear and tear on automobiles, increased gasoline use, delays in product transport, missed appointments, and other inconveniences that result in lost dollars. Increasing use of corrosion-resistant alloys, improved coatings, and durable concretes will further reduce the large direct and indirect expenses associated with bridge corrosion.”

1.2 Coating for Structural Steel Reinforcing Steel Rebars

Coatings are sometimes used on steel reinforcing bars to provide protection from corrosion. Currently, there are two common types of coating used:

1- Epoxy coating: This is a process of painting the reinforcing bar surface with a layer of epoxy. Although this is the most common way to protect steel from corrosion, the epoxy-coated rebar is subjected to several problems, which are:

- Pits or discontinuities in the epoxy film can lead to immediate corrosion at the uncoated site,
- The coating lacks abrasion resistance, and thus is easily damaged in transport to the job site and installation,
- Concrete vibrators (which are supposed to be covered with rubber) can damage the coating by vibrating a sharp piece of aggregate against the bar. (Ask Dr. Kalv, 2011).

2- Hot-dip galvanized bars: Hot dip galvanizing is the process of coating iron, steel, or aluminum with a thin zinc layer, by passing the metal through a molten bath of

zinc at a temperature of around 860 °F (460 °C). When exposed to the atmosphere, the pure zinc (Zn) reacts with oxygen (O_2) to form zinc oxide (ZnO), which further reacts with carbon dioxide (CO2) to form zinc carbonate ($ZnCO_3$), (Hot-dip galvanizing, 2011). However, this coating may cause embrittlement. There are three basic embrittlement[1] mechanisms (Lesay and Mraz, 2009):

- liquid metal embrittlement: liquid metal influences the plasticity of steels. The ductility decreases with increasing Zn content. The change of plasticity is associated with fracture.
- hydrogen embrittlement: this embrittlement is due to cracks induced by hydrogen. This is well know as "hydrogen induced cracking"
- strain ageing embrittlement: A loss in ductility accompanied by an increase in hardness and strength that occurs when low-carbon steel is aged following plastic deformation.

One solution to overcome the "painting" protection problems of structural steel is to use different materials. Fiber reinforced polymer (FRP) composite bars have been developed for this purpose. However, the two major problems with using FRP rebars are high costs and lack of ductility.

1-3 Fiber Reinforced Polymer FRP

Fiber Reinforced Polymers (FRPs) has been used in various civil engineering applications to retrofit and strengthen structural members such as columns in compression and beams in moment, and shear. FRP rebars have been recognized by many standards, such as ACI-440 (Guide for the Design and Construction of Structural Concrete Reinforced with FRP, 2006), AASHTO (AASHTO LRFD Bridge Design Guide Specifications for GFRP-Reinforced Concrete Bridge Decks and Traffic Railings, 2009), and PCI (PCI Bridge Design Manual, 2011) as reinforcement in reinforced concrete

[1] Embrittlement is a loss of ductility of a material, making it brittle.

structures. Because of the linear elastic properties and high strength of FRP materials, the design of structural beams is often based on an over-reinforced section with a great reduction factor (ϕ). This reduction factor is to account for lack of ductility of the FRP rebar. For example, according to ACI-318 for an under-reinforced beam section with steel reinforcement, ϕ is equal to 0.9, while ϕ is equal to 0.55 for an under-reinforced beam section using FRP reinforcement, according to ACI-440.

1-4 Advantages of Using FRP Reinforcement

The following are some advantages of current FRP reinforcement in concrete structures (Somboonsong, 1997).

1- Corrosion resistant: since FRP is a nonmetallic material, it doesn't corrode when it comes in contact with water and air or salt water and most soil conditions. Therefore, durability problems associated with steel reinforcement do not exist. Consequently, the life cycle of the composites is potentially longer with lower maintenance costs.
2- High strength: the tensile strength of some FRP composites is greater than steel when the load applied in the direction of loading. For example, the tensile strength of S-glass fibers is 4300 MPa (625 ksi) whereas the ultimate tensile strength of steel grade 60 is 650 MPa (95 ksi).
3- High specific Modulus: which is defined as the modulus of elasticity of the unidirectional fibers divided by the density of the material. For example; specific modulus of carbon fiber is between 15.7 to 85.6 whereas the specific modulus of steel is 3.9.
4- Lightweight: FRP composites are very light in general and this will reduce the cost of shipping and handling significantly. Moreover, the installation time may be reduced and the total weight of the structure will be less. FRP weighs three to six times less than steel.

5- Non-conductive and electromagnetic permeability: FRP composites are nonconductive and have electromagnetic transparency (permeable) which makes them suitable for structural applications involving *Magnetic Resonance Imaging* (MRI) medical equipment and when radar transparency is needed for military installations where conventional steel cannot be used.
6- Tailor-ability: FRP materials are more versatile than steel because the properties of FRP can be tailored to meet specific functional requirements.

1-5 Disadvantages of Using FRP Reinforcement

The following are some disadvantages of current FRP reinforcement in concrete structures (Somboonsong, 1997).

1- FRP materials are more expensive than steel. For example, High Modulus-Carbon fiber is 120 times more expensive that steel for the same volume.
2- Lack of consideration of the uncertainties associated with FRP bar resistance: since FRP composites are relatively new, few reliability analyses have been conducted on this material.
3- Lack of ductility: one of the biggest problems associated with use of FRP in civil engineering applications is ductility. However, hybrid bars can overcome brittle failure.
4- Small modulus of elasticity: Glass fiber reinforced polymer (GFRP) and aramid fiber reinforced polymer (AFRP) composites have small elastic moduli which may affect serviceability of the structure, particularly deflection. However, carbon fiber reinforced polymer (CFRP) has an elastic modulus close to that of steel and higher.
5- Lack of standards: although FRP composites have been recognized by ACI, AASHTO, PCI and other agencies, still there are no uniform manufacturing standards. For example, different manufacturers provide different FRP composite mechanical properties under the same designated name.

6- Lack of long term performance data: the performance of FRP composites are still under research regarding fatigue, creep, creep rupture, relaxation, thermal expansion, moisture, chemical deteriorations, and other environment effects.
7- Lower temperature of combustion: it has been concluded that both strength and stiffness of the FRP composite decrease when temperatures rise. At high temperatures, the resin becomes flammable. Fire resistant resins are currently under research.
8- Anisotropy of material properties: the mechanical properties are different in different directions, resulting in more complex analysis and design.

1-6 Objectives and Scope

The two primary objectives of this study are to:

1- develop the concept for a new Hybrid Ductile Fiber Reinforced Polymer rebar (H-D-FRP rebar) that could potentially replace conventional steel reinforcement in reinforced concrete structures. The bar uses randomly dispersed chopped fibers to lower the manufacturing cost, and multiple materials to provide ductility, addressing the two major shortcomings of current FRP bar construction. Existing analytical approaches are appropriately modified to model the H-D-FRP bar behavior.

2- address H-D-FRP rebar resistance uncertainties. A probabilistic model of bar resistance is developed, and uncertainty in bar resistance is quantified. A reliability analysis is conducted on the developed bars, and required material resistance factors are determined to insure that the developed bars meet current target reliability levels.

These two issues will be directly integrated in this research in that a reliability-based design optimization procedure will be developed and conducted to minimize bar

costs while accounting for uncertainties is bar performance by imposing probabilistic safety limits in the optimization procedure.

These two issues will be directly integrated in this research in that a reliability-based design optimization procedure is developed and implemented to minimize bar costs while accounting for uncertainties is bar performance by imposing probabilistic safety limits in the optimization procedure. Two schemes have been proposed in this research using randomly dispersed chopped fibers to develop a new Hybrid Ductile Fiber Reinforced Polymer rebar (H-D-FRP rebar) approach. Different types of fibers will be proposed to build these two H-D-FRP rebars: E-glass, Aramid (Kevlar-49), carbon with a small modulus of elasticity (SM-Carbon), and carbon with medium/intermediate modulus of elasticity (IM-Carbon) fibers. A small volume fraction of steel (20%) will be used in one of the schemes to add stiffness and ductility. The rebars are optimized to determine volume fractions of each fiber type. The optimization process is conducted for two civil engineering applications, with bars placed in reinforced concrete sections of bridge decks and building beams/girders. Ductility, moment capacity, and other important constraints are imposed. Many factors associated with chopped fibers are considered in designing the rebars such as chopped fiber length, orientation of these fibers, and their curvatures.

Due to the uncertainties in the mechanical properties of the materials and dimensions of cross sections used in developing these two schemes, a probabilistic model of bar resistance is constructed to properly propagate these uncertainties in a reliability analysis. The reliability analysis will be used to insure that the new schemes developed meet currently accepted target reliability levels associated with reinforced concrete beam design.

Chapter Two

Literature Review

2-1 FRP Rebar

One of the earliest attempts to use light engineering materials to control stress-strain behavior was done by Bunsell and Harris (1974). They used two types of fibers, carbon and glass, in a resin to construct their hybrid material. Bader and Manders (1981) used hybrid composites fabricated from glass and carbon fibers in an epoxy matrix. They found that failure strain in the carbon phase increased as the relative volume fraction of the carbon fiber was decreased and more finely dispersed. Multiple phase modes were observed when both constituents, carbon and glass were fibers, mixed together, and no catastrophic failure occurred until a considerable number of ligament fractures had accumulated. Tamuzs and Tepfers (1995) studied the ductility behavior of composite FRP rebars with necessary elongation and stress hardening. They used braided aramid fiber strands around a core of foam plastic, thin glass or carbon fibers. Somboonsong (1997), based his ductile hybrid FRP rebar model on core yarns, which are responsible for giving high stiffness, covered by a braided yarn structure which is responsible for giving ductility. Based on three different combinations of sleeve and core yarns, it was shown that twisting the core yarns did not significantly improve the composite initial yield strain. Furthermore, it reduced the composite initial modulus significantly. He also found that twist, crimp, and braiding angle on sleeve yarns had effects on composite initial modulus and the ratio of ultimate strain to yield strain. The new ductile hybrid FRP rebar improved bonding with concrete though ribs in the braiding. Belarabi, Chandrashekhar, and Watkins (1999) achieved ductility of hybrid FRP rebars by selecting fibers that would fail at different stains causing gradual failure. They tested two types of hybrid FRP rebars as reinforcement embedded in concrete beams. In the Three-

Fiber Hybrid rebar, Epoxy 9500 was used as resin and Mitsubishi K137HG, Mitsubishi K13710, and Zoltek Panex-33 used as fibers. In the Two-Fiber Hybrid rebar, they used Shell Epoxy 9500 as resin, and Mitsubishi K137HG, and Zoltek Panex-33 as fibers. In both cases, Zoltek fibers were used in the core, while Mitsubishi fibers were used around the core at an angle 20 degrees. The hybrid rebars used in the research by Saikia, Thomas, Ramaswamy, and Rao (2005) consisted of glass fiber reinforced polymer (GFRP) strands, helically wound on a steel rod, with epoxy binder material. They observed that failure of the hybrid rebar reinforced concrete beams was primarily due to delamination at the level of reinforcement, leading to anchorage failure resulting in loss of bond between rebar and concrete.

Terry (2006) came up with new model. It is a core-shell configuration with carbon fibers and Kevlar in the outer shell respectively and glass and steel fibers in the core. He used Epoxy as resin. About half of the reinforcement was steel fiber. The ductility indexes computed on the energy considerations of the FRP-reinforced beams were found to be very similar to those of companion steel-reinforced beams. Wu (2006) came up with a brilliant method for design reinforced concrete flexural members by using non ductile FRP bars in tension face and ductile steel mechanism in the compression face. Won, Park, and Jang (2007) found that their FRP bar showed elastic behavior up to the point of early fracture with very irregular behavior thereafter. Fibers in the sleeve were broken in very irregular lengths, while the fibers in the core were broken in a regular pattern. The new developed hybrid FRP bar by Cui, Cheung, Noruziaan, Lee, and Tao (2008) possess characteristics of alkaline resistance, good ductility, and increased modulus of elasticity with slightly higher cost than glass composite reinforcement bars. The core consists of steel and glass fiber while the shell consists of Twaron and carbon fibers. In the work by Wu (2008), a new structural scheme of providing ductility to RC members through compressive yielding (CY) instead of tensile yielding has been developed. The ductility demand of the compression yielding zone has been developed with a perforated block. The main reinforcement was FRP. In the study by Cui and Tao (2009), a new hybrid composite rebar has been developed. Both unidirectional tensile and corrosion resistance tests were performed. Accelerated alkali exposure tests with different durations were conducted. The tests have shown promising

potential for application in reinforced concrete structures. Zhou, Wu, and Leung (2009) investigated the ductility behavior of compression yielding of FRP reinforced beams numerically to illustrate the effects of key variables on the ductility performance. Wierschem and Andrawes (2010) used NiTi (nickel titanium) in their FRP rebar beside plastic fibers to add damping capability to reinforced concrete structures.

2-2 Reliability Analysis

Ang and Cornell (1974) introduced calculation of reliability index (β) with the First Order Second Moment (FOSM) method, and illustrated how it could be calculated instead of failure probability directly, to save significant computational effort by avoiding simulation. This calculation gave exact answers (in terms of failure probability) only for problems linear in standard normal space, however. Additionally, the approach suffered from the 'invariance problem', whereby different formulations of the same problem that were equivalent mathematically would result in different beta values. The invariance problem was corrected by Hasofer-Lind when the most probable point MPP was introduced. In their work, Hasofer and Lind (1974) developed the well-known "Hasofer-Lind (H-L) Method" to calculate the safety index (β), applicable for random variables which are statistically independent and normally distributed. This method is also known as the Advanced First Order Second Moment Method (AFOSM), and solved the invariance problem associated with the FOSM method. They presented two coordinate systems: the original coordinate system and the transformed or reduced coordinate system. The first system is in basic variable space while and second system is in standard normal space. Now, (β) can be calculated as the shortest distance from the origin of the axes in the second coordinate system to the limit state surface. The point on the limit state surface from which beta is calculated is called the "design point", checking point", or "most probable point of failure (MPP)". The MPP represents the peak of the joint probability density function (PDF) of the limit state function (g) that intersects the failure boundary g=0. This point is found by iteration. The Rackwitz-Fiessler (1974; 1878) procedure is a beta-based method that expands the Hasofer-Lind approach to account for

non-normal random variables (RVs) by transforming them to 'equivalent normal' RVs at the MPP. This method, referred to as the First Order Reliability Method (FORM) is based on equating the cumulative distribution function (CDF) and the PDF of the actual random variables and the equivalent normal random variables at the MPP. The important parameters are the mean and standard deviation. This method is easy to implement but becomes inaccurate if the actual non-normal distribution gets highly skewed. Fiessler, Neumann, and Rackwitz (1979), based their work on expanding the limit state surface g(x) = 0 into a second order Taylor series about the checking point P^* (x^*) shown in equation (2-1).

$$g(x) = g(x^*) + \frac{1}{1!}\sum_{i=1}^{n} \left.\frac{\partial g(x)}{\partial x_i}\right|_{x^*} \left(x_i - x_i^*\right) + \frac{1}{2!}\left[\sum_{i=1}^{n} \left.\frac{\partial^2 g(x)}{\partial x_i^2}\right|_{x^*} \left(x_i - x_i^*\right)^2 + 2\sum_{i=1}^{n-1}\sum_{j=i+1}^{n} \left.\frac{\partial^2 g(x)}{\partial x_i \partial x_j}\right|_{x^*} \left(x_i - x_i^*\right)\left(x_i - x_i^*\right)\right] = 0 \qquad \text{.....(2-1)}$$

and letting the original coordinate system (X) be rotated into a new system (Y) with the same origin such that the point P^* is on the Y_n-axis and has coordinates (0, 0, …., β) as shown in Figure (2-1).

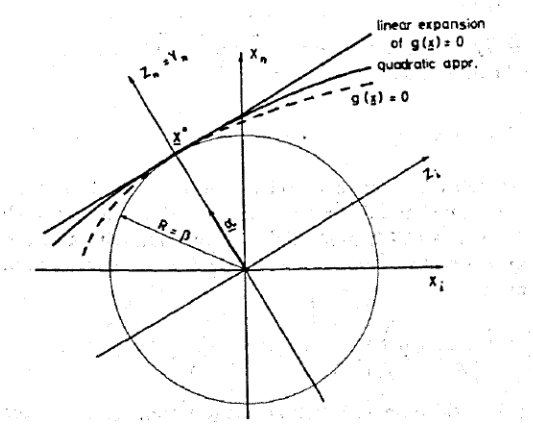

Figure (2-1): Derivation of rotational quadratic forms.

and by using some results of the statistical theory of quadratic forms in normal variants, the failure probability estimate can be obtained by use of the Chi-square distribution. In

their work, Chin and Lind (1983) proposed an extension of the Rackwitz-Fiessler (R-F) algorithm using a three-parameter approximation. The approximation is made such that the values of the cumulative distribution function F(x), the probability density function *f*(x), and its derivative *f'*(x) are identical at the approximation point x*. In addition to using the mean and standard deviation, a new constant α was introduced. For some cases, the proposed algorithm is more efficient than the R-F algorithm in the sense that it is fast, gives smaller errors, and does not require double precision computation.

Ayyub and Haldar (1984) based their work on FORM to calculate reliability index or safety index (β) with a modification to reduce the iteration numbers by introducing (β*) which is an initial value for the index which can be calculated by dividing the mean of the limit state function by its standard deviation. Taking this index as 3 often gives a good starting point for many realistic problems. Breitung (1984) used the theory of asymptotic approximation to present a simple closed-form solution for the probability computation with a second order approximation (quadratic) by using a Taylor series expansion. He also ignored the mixed terms and their derivatives in the Taylor series approximation which is also called a parabolic approximation. The new formula of probability of failure was given in terms of the distance of the limit surface (β) from the origin and the curvatures (κ) of the surface at the minimal distance points. This method is accurate when β is large. Harbitz (1986) developed an adaptive sampling method for failure calculations to improve both Monte Carlo and acceptance sampling techniques. The method is in terms of cumulative Chi-squared distribution $\Gamma_k(\beta^2)$. Three assumptions must be fulfilled: the limit state function defining the combination of the basic variables for which failure will occur is known, basic variables are independent and normally distributed, and the reliability index, β, is known. The main idea is to restrict the sampling domain in the basic variable space to the tail part of the joint distribution of the basic variables. A remarkable increase in efficiency is obtained compared to simple Monte-Carlo technique. he sampling reduction is proportional to 1 divided by the probability content outside the β-sphere ($1-\Gamma_k(\beta^2)$). Der Kiureghian, Lin, and Hwang (1987) considered second-order approximations in a rotated standard space Y' in which the y_n' axis coincides with design point as shown in figure (2-2). The limit state surface

has been approximated by two semi-parabolas (paraboloid). The approximating semi-parabola is defined by fitting to a set of discrete points selected on the limit-state surface at prescribed distances. This procedure helps to avoid the computation of the second-order derivative matrix which can be prohibitively costly when the dimension of the matrix is large. The advantages of this method are that is is simpler and needs less computation than the regular SORM. It is insensitive to noise in the limit state surface, approximately accounts for higher-order effects, and facilitates the use of an existing formula for the probability content of semi-parabola sets.

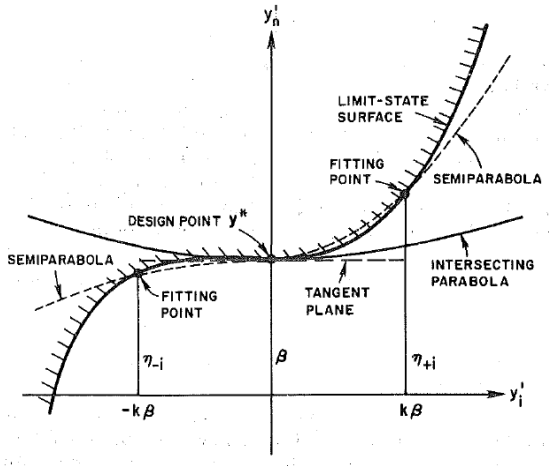

Figure (2-2): Fitting of semiparabola in rotated standard space.

Hohenbichier, Gollwitzer, Kruse, and Rackwitz (1987), applied the theory of first and second order reliability methods to a complex system (more than one failure surface). They improved results by using the concept of asymptotic analysis. Their computations reduced the system to a problem of non-linear multi-constraint optimization and simple algebraic manipulations instead of solving multi-normal integrals. Their work was also based on probabilistic rules of unions and intersections. The goal was to search for an optimal approximation point β on the boundary of the failure domain.

In the importance sampling method, the region of importance is usually not known in advance. The efficiency of the simulation can be improved if it can be estimated. Karamchandani, Bjerager, and Cornell (1989) proposed a multimodal sampling method based on the idea that as one samples, the knowledge of the failure

domain increases. If one keeps modifying the importance sampling density to reflect this increasing state of knowledge, one can develop a good sampling density and estimate the failure probability efficiently. In this paper by Karamchandani (1990), the failure-path approach was used with a multistate model. The multistate model consisted of a linear relationship between load and deformation. For tension brace members, a elastoplastic relationship was assumed, and for compression brace members, a three-stage model was assumed (an initial elastic state, back-slope negative stiffness state, and final zero stiffness state). For non-brace elements, a two stage model for tension and compression was assumed. FORM was used in computing the probability of occurrence of the union of the individual sequence events.

Ayyub and Chia (1992) suggested a simulation-based structural reliability method which is a generalization of the conditional expectation method (CE). In this method, Generalized Conditional Expectation (GCE), the conditional expectation has been generalized by allowing the number of control variables to be larger than one. GCE is used together with a variance reduction technique (VRT). This method was determined to be highly efficient, and converged to the correct probability of failure in a relatively small number of simulation cycles. However, the level of computational difficulty increased.

Bucher and Bourgund (1992) developed a response surface (RS) with a simple second degree polynomial with or without mix terms. The mean and standard deviation values were used to calculate the coefficients of the polynomial and the center point in each step was calculated using linear interpolation. Wu (1992) proposed an efficient, adaptive importance sampling (AIS) method for structural system reliability analysis. The features of the proposed AIS are: The initial sampling domain is the failure side of the system limit state surface constructed from approximate, parabolic surfaces; the sampling domain is varied incrementally by changing the curvatures of the parabolic surfaces at the most probable point of failure;, and the final sampling domain contains the system failure domain. The adaptive limit state surface provides high flexibility to develop a minimal sampling domain that contains, but is very close to, the system failure domain.

Engelund and Rackwitz (1993), reviewed 4 different methods of importance sampling and a set of evaluation criteria for comparison of these methods was chosen. These methods are; Direct, Static or Nonadaptive methods, Updating methods, Adaptive

schemes, and Spherical schemes. It is not possible to identify one of the methods as being the best under all circumstances. The three major criteria that control which importance sampling method is the best are: accuracy and efficiency, sensitivity to number of random variables, sensitivity to multiple important regions, and noisy limit state functions.

Saliby (1997) discussed an interesting issue which is the similarities between Descriptive Sampling (DS), which is based on a fully deterministic selection of the input sample values, and Latin Hypercube Sampling (LHS), which is a variance reduction technique in which the selection of sample values is highly controlled. He found that DS represents an improvement over LHS, being more efficient both in statistical terms and computing terms. The goal of Au and Beck's (2001) work was to compute small failure probabilities in reliability analysis of an engineering system. Markov chain Monte-Carlo simulation technique based on the Metropolis algorithm is presented for estimating conditional probabilities which cannot be estimated efficiently by standard Monte Carlo procedure. Atadero, Lee, and Karbhari (2004) used reliability analysis on three-layered carbon FRP strengthened bridge decks. Based on real data tests and using the Chi-square test, statistical distributions were assigned for strength, modulus, and thickness of the layers of the CFRP. Mote-Carlo simulation with 50,000 cycles was used to model the moment capacity of the section. Finally, the reliability index was calculated for two cases based on load and resistance as normally and log-normally distributed variables.

Gomes and Awruch (2004) carried out a comparison using RS and an Artificial Neural Network (ANN) with FORM, Direct Monte Carlo Simulation, and Adaptive Importance Sampling techniques. Au, Ching, and Beck (2007), presented the reliability analysis using three variants of Subset Simulation. The idea behind Subset Simulation is that a small failure probability can be expressed as a product of large conditional failure probabilities for some intermediate failure events. In this research by Eamon and Charumas (2011), an alternate approach to estimate reliability was presented for cases when other classical reliability method fail or when dealing with limited computational resources. Here, the limit state functions were simplified to two random variable problems. The procedure is a combination of estimating the PDF or CDF of a portion of the limit state and conditional expectation.

Despite the large body of work in reliability analysis and composite bar design, to date, uncertainties in bar resistance parameters have not been quantitatively considered, nor has a reliability model of this relatively new technology been conducted, even though the significance of load, resistance, and modeling uncertainties in engineering design is well recognized. In the last few decades, a large body of work has been conducted to quantify uncertainties and their effects on structural safety in a variety of other materials such as steel, concrete, and timber (Galambos and Ravindra, 1978; Ellingwood et al., 1980; Melchers 1999; Nowak and Szerszen, 2003). An example of the result of this effort is the development of the Load and Resistance Factor Design code format for civil engineering structures, which relies upon probabilistic calibration to obtain structural designs with consistent reliability levels (AASHTO 2010, ACI 2008; AISC 2005; NDS 2005; ASCE 2010). Recognition of the importance of reliability analysis has lead to the development of new fields of study as well, such as reliability-based design optimization (RBDO) (Lee and Kwak, 1995; Choi, Park, and Youn, 2001; Yang and Gu, 2004; Kharmanda, Olhoff, and El-Hami, 2004; Zou and Mahadevan, 2006; Agarwal, Mozumder, Renaud, and Watson, 2007).

2-3 Randomly Dispersed Chopped Fibers

The first notable and distinguished work to study the effect fiber orientation on elasticity and strength was made by Cox (1952). Theoretical expressions for strength and elasticity were derived for cases where there are short fibers aligned in the direction of loading and when there are fibers randomly oriented. An explanation to Cox's original work in an organized and simplified way with some figures was done by Pan (1993) since the presentation of Cox's work was difficult to understand. The goal of his work was to derive theoretically the optimum short fiber volume fraction and matrix in composite materials. His experimental work has been considered by some researchers to be a reliable source of data to validate their new proposed theoretical work. Manera (1977) conducted experimental work of randomly oriented short glass fiber composites.

He also suggested approximate equations for elastic properties for this type of composites.

Sun and Weng (1977) proposed a new method to calculate the effect of fiber length on elastic modulus of randomly-oriented chopped fiber composites based on a composite-cylinder model. The result was compared with existing experimental data and other existing models. The new method was found to give close results to experiment ones. Rosenthal, (1992) proposed a fiber orientation model to decouple fiber length effects from fiber orientation effects in reinforced composites. He used the modified rule-of-mixture and its factors as a base to compare the results with his experiment. Thomason, Vlug, Schipper, and Kirkor (1996) presented the effect of randomly oriented chopped fibers on strength and strain at failure. They compared the theoretical expression with experimental results. Based on this comparison, they came up with a single number for fiber orientation factor for ultimate strength of composites to be used in a strength modified rule-of-mixtures[1].

In their work, Fu and Lauke (1997) proposed a new equation to calculate the elastic modulus of randomly dispersed chopped fiber reinforced polymers based on a laminate analogy approach. They compared their theoretical results to the modified rule-of mixtures[2] and experimental data. The new method was found to be satisfactory and agree with existing experimental work. The comparison of their theoretical results gave slightly better results than the modified rule-of mixtures. Fu, Hu, And Yue (1999) presented a new method using the laminate analogy approach to predict the flexural modulus of randomly oriented shot fibers. They used different probability density functions to model fiber length and fiber orientation distributions. The theoretical result was compared with some existing experimental data and very good agreement was achieved, especially when fiber length was greater than 3mm and fiber content less than 40%.

Andersons, Sparnins and Joffe (2006) used the modified rule-of-mixtures to compare the results of modulus of elasticity and strength with experimental data. Flax fiber mats were used as reinforcement for polymer composites. Very good agreement of

[1] In their work, the called it the modified Kelly-Tyson prediction.
[2] In their original work, they called it the paper-physics approach.

strength and stiffness between theoretical and experimental results was found. In order to complete this section, Bert and Kline (1985), Chin, Lee, and Liu (1988) and Kortschot, and Jayaraman (1996) proposed equations to predict the physical properties of composite materials with randomly dispersed chopped fibers, but presented no experimental work for comparison.

2-4 Curved Fibers

In spite of the importance of fibers' curvature on the behavior of FRP composites and especially on the modulus of elasticity, only a few studies have been done so far in this field. Bažant (1968) theoretically studied the effect of curvature of continuous fibers for different curvature shapes. He came up with a set of five different equations; each one represents a specific case. Tarnopol'skil, Portnov, and Zhigum (1967) and Markov and Nikolaev (1971) compared theoretical results with their experimental data, and found excellent agreement. It should be noted that they used the same equation for composite modulus. Nosarev (1967) proposed a new method to calculate the effect of curvature of glass fibers on modulus of elasticity and Poisson's ratio of composite materials and compared the theoretical results with his experimental data. it was found that his new method was quite accurate.

2-5 Optimization

Karush (1939) and Kuhn and Tucker (1951) independently derived a new method for solving constrained optimization problems using nonlinear programming. This method is an extension of the Lagrangian method with inequality constrains. Many conditions should be satisfied before this method could be used. The conditions are known as the KKT (Karush-Kanh-Tucker) conditions. In order to use this method, two more requirements should be satisfied. For maximization problems, the objective

function should be concave and for minimization problem, the objective function should be convex, and for both cases, the design space should be a convex set.

Cheney and Goldstein (1959) and Kelly (1960) presented a new method or algorithm for solving convex programming problems with nearly linear objective and constraint functions. This method is known as the *cutting plane method* (CP) or *sequential linear programming* (SLP). A first-order Taylor series expansion about the current design vector can be used to generate a linear programming LP problem from the original nonlinear objective and constraint functions. The negative consequences of using the simplex method in solving this type of problem are: The method is instable[1], and if the algorithm is terminated before the optimal solution is obtained, no feasible solution is known and the computational effort is wasted.

Rosen, (1960, 1961) presented an approach in the method of feasible directions known as *Rosen's Gradient Projection Method* in solving nonlinear programming with linear or nonlinear constrains. This method is based on normalizing the search directions and uses the projection of the negative of the objective function gradient onto the current active constrains for minimization and positive of the objective function gradient for maximization. The advantages of this method are: it is easy to implement using computers since it deals with matrices, and it doesn't need to deal with linear optimization sets. The disadvantage of this method is that it is effective only when constraints are linear.

Zoutendijk (1960) presented his method of optimization using nonlinear programming with feasible directions. The idea behind his method is to start with an initial feasible point and move in the direction that maximizes or minimizes the objective function according to a feasible direction and suitable step length. Disadvantages of this method are that it deals with many variables, and it is computationally lengthy since it implies the need for solving linear programming sets. Wilson (1963) proposed the first sequential quadratic programming method (SQP) for the solution of constrained nonlinear optimization problems. SQP is one of the most popular methods for optimization. This method relies on the Newton method to solve a set of nonlinear equations, and applies the KKT conditions to the Lagrangian of the constrained

[1] The solution may be located at vertices very far from each other.

optimization problem to improve the quadratic approximation of Hessian matrix (Rao, 2009). A disadvantage of SQP is that it is difficult to implement so that the exact second derivatives (Hessian Matrix) can be used efficiently and reliably. When second derivatives are used, the quadratic programming sub-problem can be nonconvex.

Box (1965) presented a new method to solve constrained nonlinear optimization problems. This method is known as the “Complex Method” which is an extension of the simplex method for solving unconstrained optimization problems. This method is easy to perform and can be implemented by computers since it doesn’t require first or second derivatives of the objective function or the constraints. On the other hand, it has its own disadvantages which are: the method becomes inefficient rapidly as the number of design variables increases; it cannot be used to solve problems having equality constraints; if the feasible region is nonconcave, there is no guarantee that the centroid of all feasible points is also feasible; and the method needs an initial point vector X_i that is feasible.

In his work, Box (1966) made a comparison among eight unconstrained optimization methods applied to test problems. These methods are Rosenbrock, Davies-Swann-Campey, simplex, Powell-Fletcher-Davidon (Powell& Fletcher), Powell sum of squares, and Barnes. Davidon’s method was the most consistently successful. He also used a transformation technique to transform independent variables in the constraints which are functions of variables x_i such that all constraints are satisfied automatically. The advantage of the transformation is that it is easier to deal with an unconstrained optimization problem. The disadvantage of transformation is that the constraints have to be simple functions, as it may not possible to find transformation for certain constraints.

Many researchers have tried to improve the original SQP by Wilson. Two of them are Han (1977) and Powell (1978) who introduced two crucial improvements to this method. The first was the use of a QP sub-problem defined in terms of a positive-definite Quasi-Newton approximation. The second improvement was the use of a line search merit function, which is a scalar-valued function whose value provides a measure of quality of a given point as an estimate of a solution of the constrained problem, to obtain a sequence of improving the estimate of the solution.

Gabriele and Ragsdell (1977) presented one of the most powerful minimization methods in optimization known as the *Generalized Reduced Gradient* Method (GRG) for

solving constrained nonlinear convex set of problems which converts all inequality constrains to equalities using slack variables. The idea behind this method is the elimination of variables using the equality constraints. This method relies on the Steepest Descent Method which was first made by Cauchy (1847). In this method (GRG), a search direction is established tangent to the constraint lines in the direction reducing the objective function. As the search deviates from the equality constraint curves, repeated corrections are made to maintain feasibility. The advantages of the GRG may be summarized in two points: it is a very fast method that converges quickly, and it can be easily implemented in matrix form on a computer. On the other hand, the drawbacks of this method are it depends on the initial starting points, and it uses first derivatives in the solution.

Karmarkar (1984) invented a dramatic and powerful new algorithm for solving huge linear programming problems with an approach very different from the simplex method. This method is known as the *Interior-Point Algorithm*. The idea of this method begins with an initial solution that lies in the interior of the feasible region, then moves in the direction that improves the objective function value at the fastest rate. The projected gradient of the objective function onto the feasible region defines this movement. The third and last step in this method is to transform the feasible region to place the current trail solution near its center. Karmarkar used a sophisticated centering scheme in his work.

Chen, Kang, and Lee (2004) used the generalized reduced gradient (GRG) algorithm with 3 different searching methods to come up with an efficient method. These methods are the Conjugate gradient method, modified Cauchy's searching method, and the Broyden, Fletcher, Goldford, and Shanno (BFGS) method. A four-criterion comparison was performed that involved the effectiveness, efficiency, space occupation and solution precision by testing 25 testing problems. There was no single method that managed to converge in all the testing problems. The complexity of the QP sub-problem has been a major impediment to the formulation of the Hessian matrix in the SQL method. Gill, Murray, and Saunders (2005) have overcome this problem by eschewing second derivatives and by solving convex QP sub-problems defined with a positive semi-definite Quasi-Newton approximation Hessian. They apply an SQL method to a sequence

of regularized problems with penalty in which this amount is increased geometrically and will be terminated when a solution is found or the penalty reaches a pre-assigned upper limit.

Chapter Three

Theories and Justifications of Fiber Reinforced Polymer

Hybrid-Ductile Fiber Reinforced Polymer (H-D-FRP) rebars are made up of 2 or more types of different fibers plus resin. Fibers could be continuous or chopped. Continuous and chopped fibers have their own advantages and disadvantages. The main concern in this work is small or chopped fibers. In this chapter, however, we will discuss these two types of fibers, with focus on chopped fibers.

3-1 Constituent of Fiber Composites

In general, FRP composites in structural engineering consist of two major components, fibers as reinforcement and a matrix as a material to be reinforced.

3-1.1 Fibers

- **Glass Fiber**

  This type of fiber is a common material in structural engineering applications due to low cost, high strength, and high temperature resistance. The four common types of glass fibers are: Electric glass (E-Glass), high stiffness and strength glass (S-glass), chemical glass (C-glass), and Alkali resistance glass (A-glass). The diameter of an individual glass fiber or filament ranges between 3-24 μm. Glass fibers are sensitive to moisture in the presence of salt and elevated alkalinity.

- **Aramid Fibers**

Kevlar-49 and Twaron are the most common types of aramid fiber used today because of their high modulus of elasticity. They are the lightest of the high-performance fibers, having a density of 1.4 g/cm^3 (0.051 lb/in^3). Aramid fibers have a relatively high price, and high moisture absorption. On the other hand, they have high longitudinal tensile strength and modulus of elasticity.

- **Carbon Fibers**

Carbon fibers, in general, have stiffness (modulus of elasticity) close to that of steel, are very durable, and perform very well in hot and moist environments. The major obstacle of using carbon fibers is the high price. Carbon fibers have diameter between 5-10 μm.

Figure (3-1) shows a typical stress-strain curve for different fiber types and structural steel for reinforcement, while Table (3-1) shows some engineering and mechanical properties of different types of fibers.

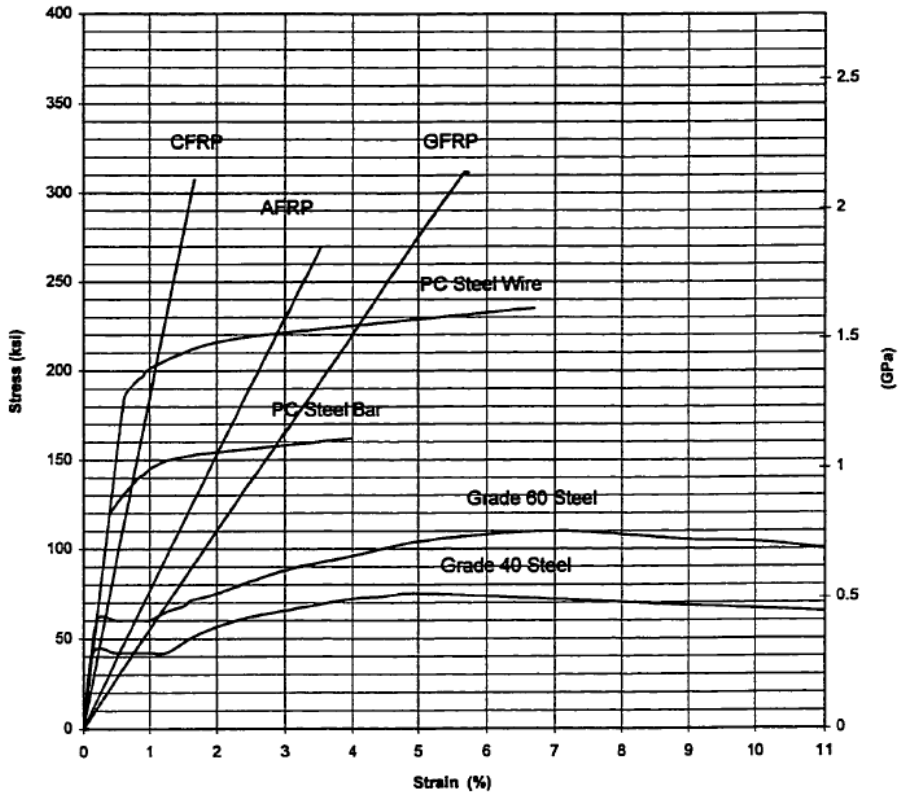

Figure (3-1): Stress-strain curves for different types of fibers and steel.

Table (3-1): Values and ranges of the engineering and mechanical properties of some common fibers.

		Glass		Aramid		Carbon		
		E-Glass	**S-Glass**	**Kevlar-29**	**Kevlar-49**	**Carbon HM**	**Carbon IM**	**Carbon SM**
Strength	**(MPa)**	3400	4445	2800-3600	2900-3600	2700	2910	3530
Young's Modulus	**(GPa)**	73-81.4	87-89	69-83	125	758-903-	380-647	230
Density	**gr/cm^3**	2.56-2.62	2.5-2.54	1.44	1.44	1.76-2.13	1.76-2	1.76
Ultimate Strain	**%**	4.4-4.88	4.9-5.7	3.6-4.4	2.2-2. 8	0.27-0.3	0.4-0.5	1.4-1.5

3-1.2 Matrices

The most common matrix materials for composites are polymeric. The reasons behind using polymeric materials are:

1- The stiffness, strength and other mechanical properties are low compared with metals and ceramics. So considerable benefit can be gained by reinforcing polymers and the reinforcement doesn't have to have exceptional properties.

2- The processing of polymer matrix composites doesn't involve high temperature and high pressure; consequently, problems associated with degradation of reinforcement during manufacture are less significant.

The two types of polymer matrices are *thermosets* and *thermoplastics*. Polyester resins and epoxy resins are examples of the first type. Polypropylene resin is an example of the second type. Table (3-2) shows some typical mechanical properties of some matrix materials (Mathews and Rawlings, 1999)

Table (3-2): Typical mechanical properties of Epoxy, Polyester, and Polypropylene resins.

	Epoxy	Polyester	Polypropylene
Density (Mg/m^3)	1.1-1.4	1.1-1.5	0.9
Young's Modulus (GPa)	2.1-6.0	1.3-4.5	1.9-1.4
Tensile Strength (MPa)	35-90	45-85	25-38
Fracture Toughness K_{IC} (MPa$\sqrt{m}$)	0.6-1.0	0.5	-

3-2 Continuous Fibers Composites

This kind of composite is well-established and not the main concern of this study. However, important general rules of behavior will be summarized.

3-2.1 Rule of Mixtures

In order to relate the longitudinal unidirectional composite stiffness and stiffness of the matrix and fibers, and stress in the composite to stresses in the matrix and fibers, a relationship based on linear elastic behavior has been derived using basic engineering mechanics and material properties.

3-2.1.1 Stiffness Rule of Mixtures

Tensile composite stiffness modulus[1] can be calculated according to the following equation

$$E_c = E_m v_m + \sum_i E_{fi} v_{fi} \qquad \text{.....(3-1)}$$

where

E_c : tensile stiffness modulus of the composite,
E_m : matrix/resin stiffness modulus,
v_m :volume fraction of the matrix/resin,
E_{fi} : fiber tensile stiffness modulus of type i,
v_{fi} : volume fraction of fiber type i.

[1] In this work, stiffness modulus, Young's modulus, and modulus of elasticity have been used interchangeably.

3-2.1.2 Strength Rule of Mixtures

The corresponding tensile stress in the composite, σ_c will be

$$\sigma_c = \left(E_m v_m + \sum_i E_{fi} v_{fi} \right) \varepsilon_c \qquad \text{.....(3-2a)}$$

where:

ε_c : composite strain,

If there is steel in the composite then, after reaching the yield stress σ_y, the above equation, with volume fraction of steel v_{steel}, will be:

$$\sigma_c = \left(E_m v_m + \sum_j E_{ji} v_{ji} \right) \varepsilon_c + \sigma_y v_{steel} \qquad \text{.....(3-2b)}$$

3-2.2 Work Justification 1

Experimental results of continuous Hybrid-Ductile FRP (D-H-FRP) rebars have shown good agreement with the results from the rule of mixtures. There are three major works that deal with H-D-FRP rebars. Belarbi, Chandrashekhara, and Watkins, (1999) used a rebar that consists of three different types of carbon fibers (Mitsubishi HG, Mitusbishi, and Zoltek), each having different failure stress and strain, as well as different stiffness modului. The experimental and theoretical results are shown in Figure (3-2).

Somboonsong (1999) used a rebar made of 2 layers; one layer is Carbon (Amoco T or P series) and the other one is Kevlar-49. Figure (3-3) shows experimental and theoretical results based on this work. Terry (2006) used three different types of fibers and steel grade 60 in his work. He used E-glass fibers, Twaron Kevlar fibers, and Zoltek carbon fibers. The result is shown in Figure (3-4). According to his comments, the difference between the theoretical and experimental results is due to shock wave propagation from broken fibers impacting other fibers (premature failure of fibers).

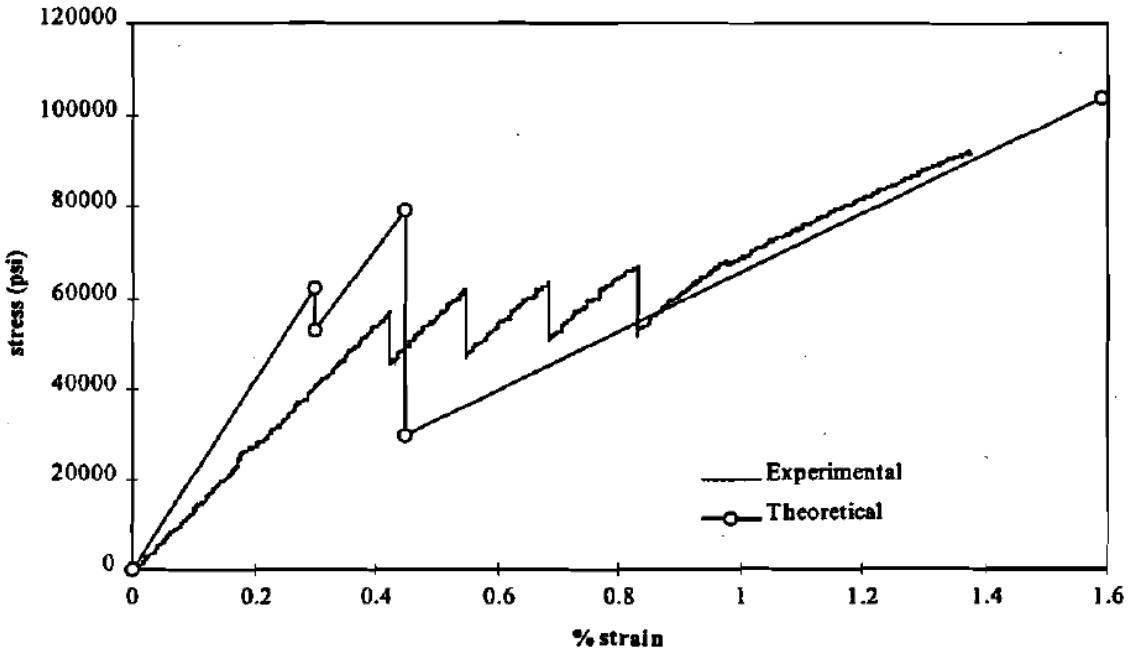

Figure (3-2): Experimental and theoretical results of stress-strain curves by Belarbi, et al., (1999).

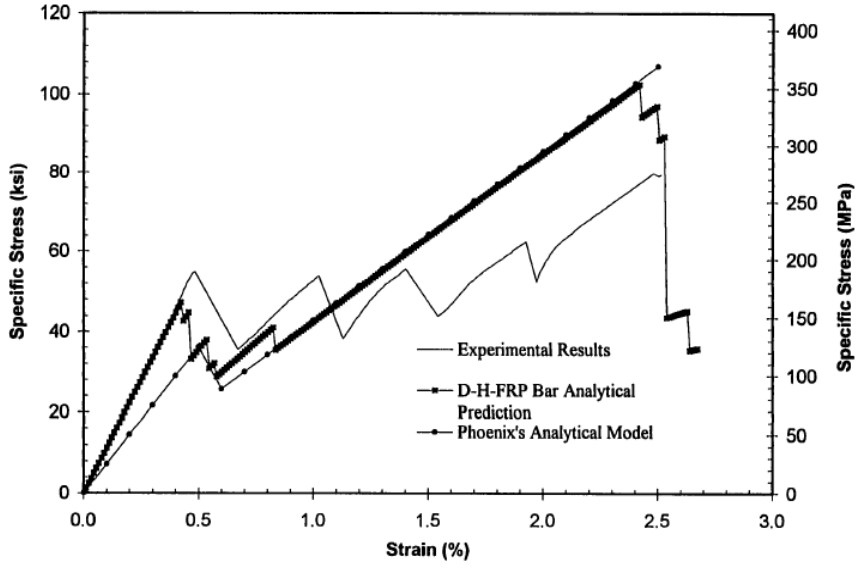

Figure (3-3): Experimental and theoretical results of stress-strain curves by Somboonsong (1999).

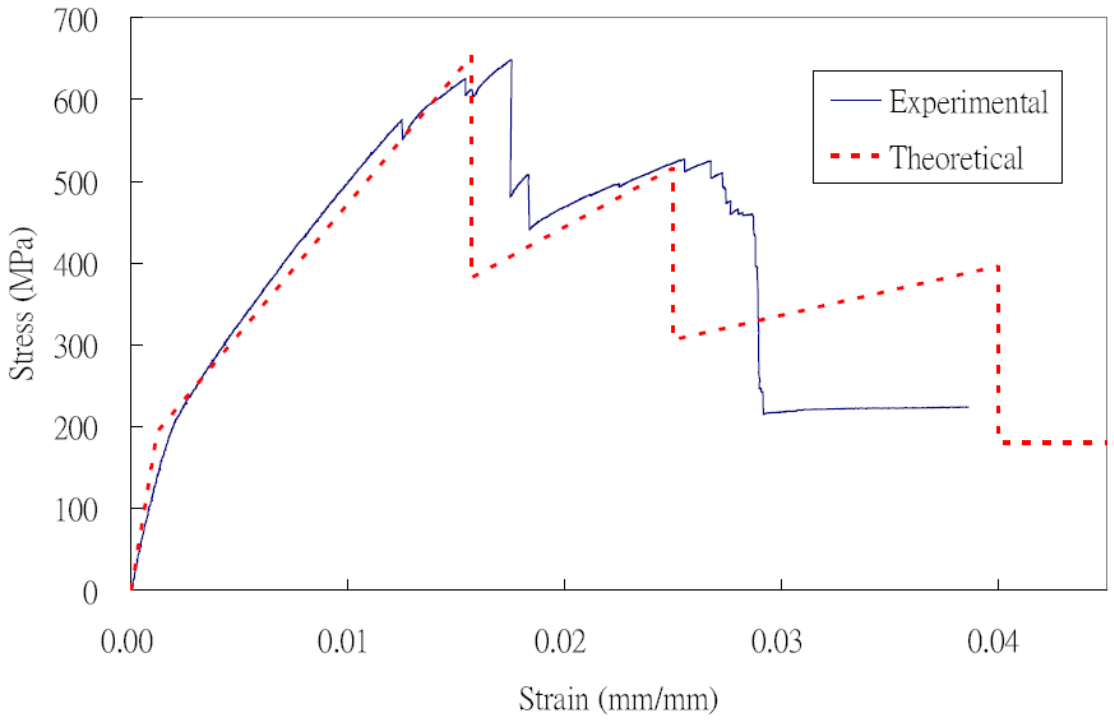

Figure (3-4): Experimental and theoretical results of stress-strain curves by Terry, 2006.

Conclusion 1:

For continuous fiber composite rebar, equation (3-1) and (3-2), i.e. rule-of-mixtures, can be used with good accuracy to calculate E_c and σ_c.

3-3 Short Fiber Composites

In general, the manufacturing process of continuous fibers is more expensive than other forms of reinforcement, and tends to be slow and inflexible. Processing techniques associated with continuous fiber reinforced thermosets composites, such as hand lay-up, filament winding, pultrusion, autoclave and vacuum processing are suitable for short runs

or one-off requirements of high performance, high priced products (Mathews and Rawlings, 1999), but not for high-volume production.

3-3.1 Fiber Length

Fiber length in chopped (short) fiber composites plays an important role in stiffness, strength, and failure mode of these composites. Figure (3-5a) shows a single fiber of length *l* embedded in a matrix and aligned in the direction of loading with two assumptions:

1- the modulus of elasticity of the fiber is greater than that of the matrix, and
2- the bond between the fiber and matrix is perfect.

Then, the applying stress will be transferred from the matrix to the fiber across the interface. Due to different stiffnesses for the matrix and fiber, different tensile strains will be experienced in the region of the fiber ends. At that region, the strain the fiber is less than the strain in the matrix. As a result of this difference, shear stresses will be induced around the fiber ends and in the direction of fiber axis as shown in Figure (3-5b). Generally speaking, fiber-matrix shear strength is relatively low and around 20 MPa (2900 Psi), although it can exceed 50 MPa.

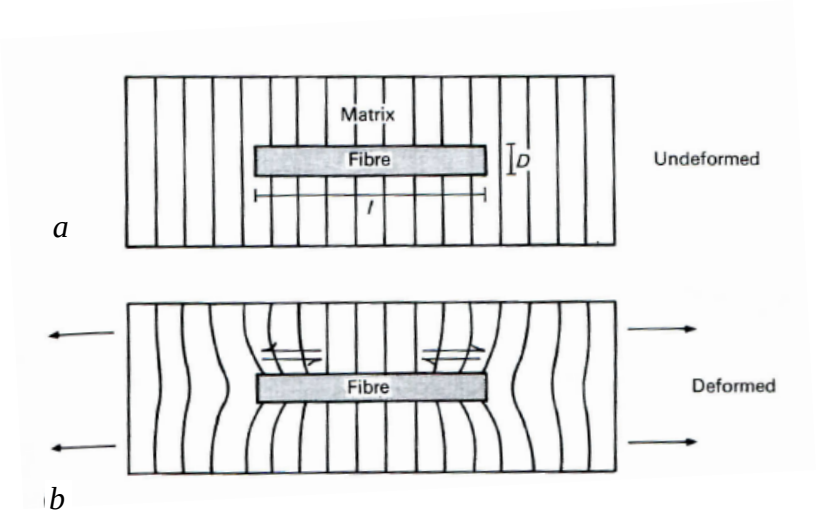

Figure (3-5): Shear stresses induced around short fiber due to variation in strains of matrix and fibers.

Cox (1952) showed theoretically the stress distribution along a fiber aligned parallel to the direction of loading. According to his work,

$$\sigma = \frac{P}{A_f} = E_f \varepsilon_f \left[1 - \frac{\cosh \beta \left(\frac{l}{2} - x \right)}{\cosh \beta \frac{l}{2}} \right] \qquad \text{.....(3-3)}$$

$$\sigma_{\max} = E_f \varepsilon_f \left[1 - \frac{1}{\cosh \beta \frac{l}{2}} \right] \qquad \text{.....(3-4)}$$

where

$$\beta = \frac{1}{r_f} \sqrt{\frac{2G_m}{E_f \ln \left(\frac{R}{r_f} \right)}} = \sqrt{\frac{8G_m}{E_f D^2 \log_e \left(\frac{2R}{D} \right)}} \qquad \text{.....(3-5)}$$

x : distance measured from mid-length of the fiber,

l : length of the fiber,

G_m : Shear modulus of the matrix,

E_f : fiber elastic modulus,

ε_f : strain in the fiber,

D : fiber diameter,

$2R$: mean center-to-center distance between fibers (to be defined later)

and the shear stress is defined in equation (3-6) and (3-7). Figure (3-6) shows the stress distribution based on this work

$$\tau = E_f \varepsilon_f \sqrt{\frac{G_m}{2E_f \ln\left(\frac{R}{r}\right)}} \frac{\sinh\beta\left(\frac{l}{2} - x\right)}{\cosh\beta\frac{l}{2}} \qquad \text{.....(3-6)}$$

$$\tau_{\max} = E_f \varepsilon_f \sqrt{\frac{G_m}{2E_f \ln\left(\frac{R}{r}\right)}} \tanh\beta\frac{l}{2} \qquad \text{.....(3-7)}$$

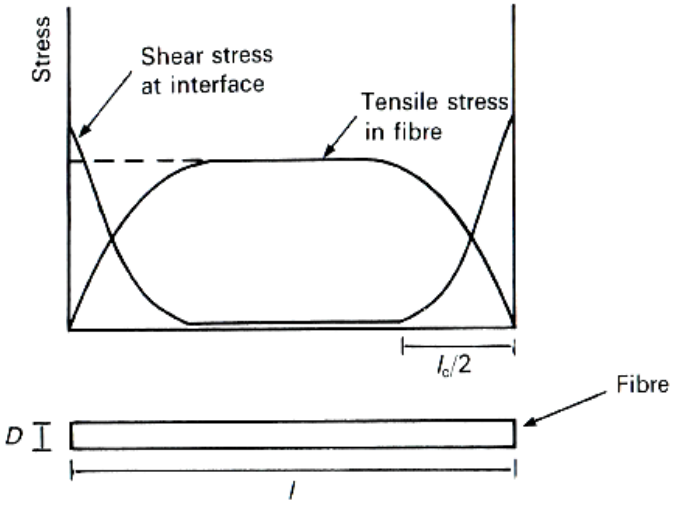

Figure (3-6): Tensile and shear stresses distributions at the interface of the fiber.

A very important term known as *critical fiber length*, l_c should be taken into consideration and this term is defined as the minimum fiber length which will allow tensile failure, and eventually fracture stress, of the fiber rather than shear failure of the interface (Mathews and Rawlings, 2007). Some common values for critical fiber length, l_c are: for Epoxy resin and carbon fiber, l_c equals 0.2 mm for polyester resin and glass fiber, l_c equals 0.5 mm and polypropylene resin and glass fiber, l_c equals 1.8 mm.

If tensile force in the fiber is $\sigma_f = \frac{\pi D^2}{4}$ and the shear force at the interface $\frac{\tau \pi D l_c}{2}$, then by equating these two terms we can calculate critical fiber length as

$$l_c = \frac{\sigma_f D}{2\tau} \qquad \text{.....(3-8)}$$

where

τ: : shear strength of the fiber-matrix interface or of the matrix itself, whichever is lower. The shear strength for epoxy resin is around 29 MPa.

It should be noted that σ_f is the tensile strength of the fiber in the longitudinal direction throughout this work. If we perform a simple equilibrium analysis close to the end of short fiber, we will end up with the following equation

$$\sigma_f = 4\tau \frac{(l/2 - x)}{D} \qquad \text{.....(3-9)}$$

There are three cases for fiber length

- $l < l_c$

  the maximum stress that will occur in the center of the fiber will never be sufficient to be break the fiber and pull-out failure will occur, and the maximum stress will be $\sigma_f = \frac{2\tau l}{D}$. The average stress $\bar{\sigma}_f$, which can be calculated as the area under the stress-fiber length graph divided by the fiber length, will be $\bar{\sigma}_f = \frac{\tau l}{D}$.

- $l = l_c$

  the maximum stress just reaches the fracture/ultimate stress $\hat{\sigma}_f$ of the fiber and will be $\sigma_f = \hat{\sigma}_f = \frac{2\tau l_c}{D}$, and the average stress can be calculated as $\bar{\sigma}_f = \frac{\tau l_c}{D}$

- $l > l_c$

  the maximum stress will cover the central portion of the fiber and will be $\sigma_f = \sigma_f = \frac{2\tau l_c}{D}$. The average stress is calculated as $\bar{\sigma}_f = \left[1 - \left(\frac{l_c}{2l}\right)\right]\bar{\sigma}_f$. Figure (3-7) shows the equations as a ratio of $\frac{\bar{\sigma}_f}{\sigma_f}$ vs. fiber length.

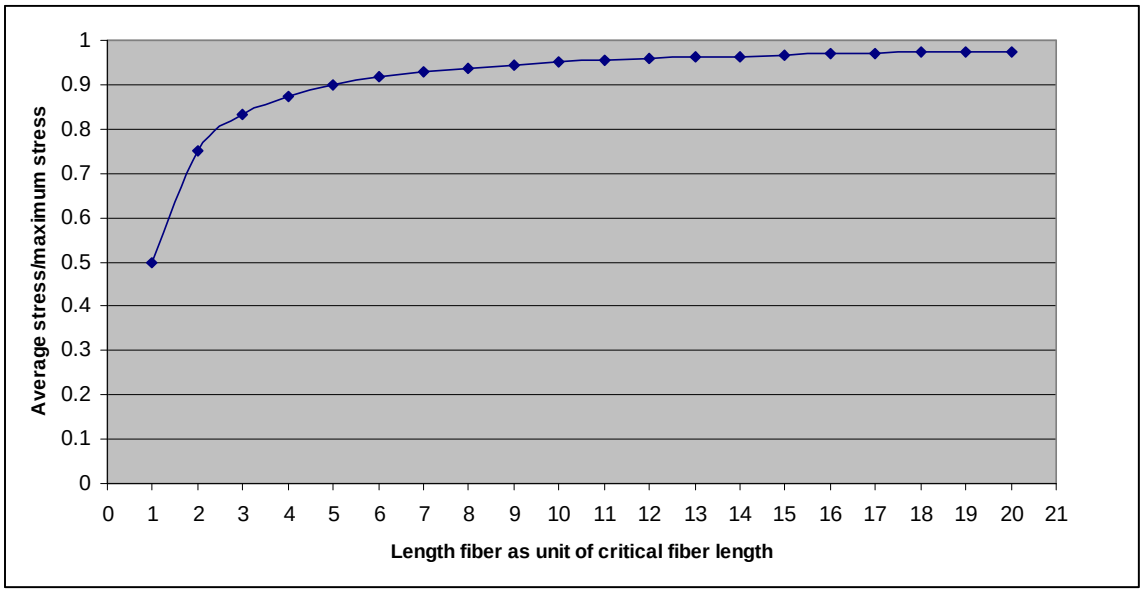

Figure (3-7): Fiber length to critical fiber critical fiber length ratio versus fiber average stress to maximum fiber stress ratio.

A very important observation can be drawn from the above figure, that once the fiber length is 5 times the critical fiber length, 90% of the fracture stress is reached. The three fiber length cases are shown in Figure (3-8) (Mathews and Rawlings, 2007). In this study, the chopped fiber length will be chosen to be more than 8 times the critical fiber length.

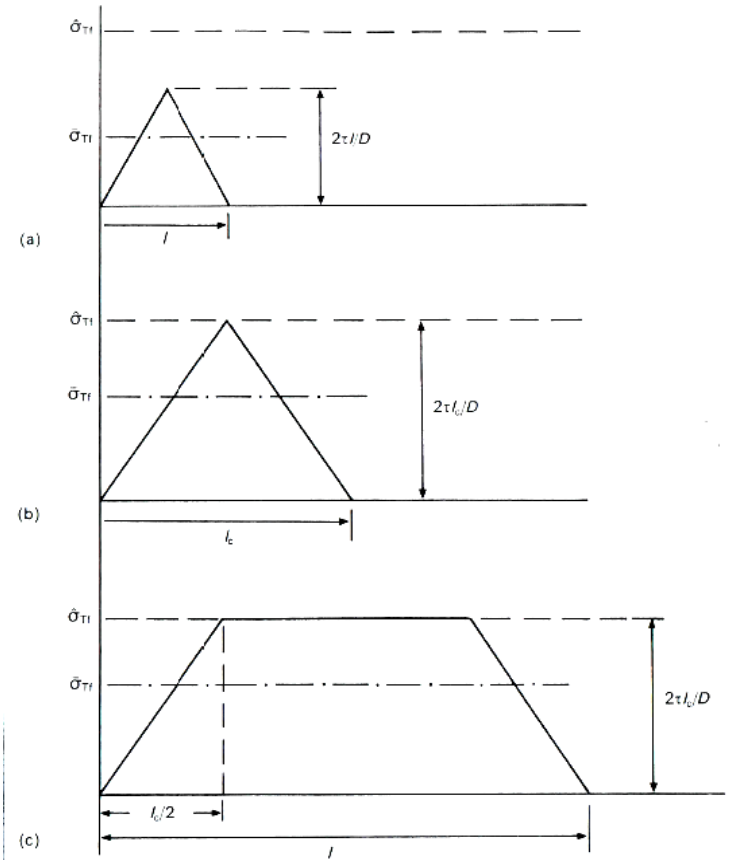

Figure (3-8): Tensile stress distribution in short fibers (a) $l < l_c$ (b) $l = l_c$ (c) $l > l_c$.

3-3.2 Fiber Orientation

Another important factor that has a major effect on the properties of the composite mixture is fiber orientation. Fiber orientation contributes to the physical properties of the composite such as stiffness and strength.

3-4 Modified Rule of Mixtures

In order to take into account the effects of short fiber length and orientation, the modified rule of mixtures set has been used for randomly dispersed chopped fiber composites. This set consists of two equations, one for stiffness/modulus of elasticity, and the other one is used to calculate the strength of the composite.

3-4.1 Stiffness Modified Rule of Mixtures

$$E_c = \eta_{LE} \cdot \eta_{OE} \cdot E_f \cdot v_f + E_m(1 - v_v) \quad \text{.....(3-10)}$$

or

$$E_c = \eta_{LE} \cdot \eta_{OE} \cdot E_{f.} v_f + E_m v_m \quad \text{.....(3-11)}$$

where

$E_{c.}$: modulus of elasticity of the composite in the longitudinal direction,

$E_{f.}$: modulus of elasticity of continuous fiber,

$E_{m.}$: modulus of elasticity of the matrix,

η_{LE} : Fiber length efficiency factor,

η_{OE} : Fiber orientation efficiency factor,

3-4-1.1 Fiber Length Efficiency Factor

If all fibers are aligned in the direction of applied load, i.e. ignoring the effect of fiber orientation, η_{OE} =1 then equation (3-11) becomes

$$E_c = \eta_{LE} \cdot E_{f.} v_f + E_m v_m \quad \text{.....(3-12)}$$

If $E_{f.} >> E_m$ then equation (3-12) becomes

$$E_{(\text{short})} = \eta_{LE} E_{(\text{continuous})} \quad \text{.....(3-13)}$$

For continuous fibers, η_{LE} =1.

For short, equal-length fibers, η_{LE} may be calculated using equation (3-14).

$$\eta_{LE} = 1 - \frac{\tanh(\beta l/2)}{\beta l/2} \qquad \text{.....(3-14)}$$

where, again, β is defined in equation (3-5) as:

$$\beta = \frac{1}{r_f}\sqrt{\frac{2G_m}{E_f \ln\left(\frac{R}{r_f}\right)}} = \sqrt{\frac{8G_m}{E_f D^2 \log_e\left(\frac{2R}{D}\right)}}$$

again;

G_m : Shear modulus of the matrix,

E_f : fiber elastic modulus,

D : fiber diameter.

$2R$: mean center-to-center distance between fibers can be calculated $\frac{R}{r_f} = \sqrt{\frac{K_R}{v_f}}$.

The numerical value of factor K_R depends on fiber geometrical packing. For square packing fibers, this factor equals to $\pi/4$, and for hexagonally packed fiber this factor is calculated to be $\frac{\pi}{2\sqrt{2}}$ (Pan, 1993). Figure (3-9) shows these two fiber packing forms.

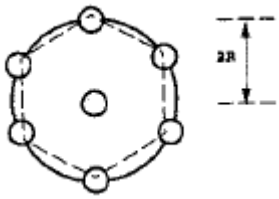

fiber with nearest hexagonally - packed neighbors

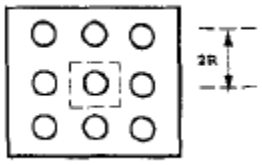

fiber with nearest square-packed neighbors

Figure (3-9): Different geometrical packing configurations.

Fiber diameters are different for fiber types. For example, for Glass fibers (E-Glass and S-Glass) the diameter is 16.5 μm; for Aramid (Kevlar-29, 49, and 149) the diameter is 12 μm; and for Carbon in general, fiber diameter is 10 μm (Somboonsong, 1997).

Theoretical values of η_{LE} for several fiber lengths and types, calculated using equation (3-13) are given in table (3-3) which has been taken from Hull (1981)

Table (3-3): Theoretical fiber length efficiency factor for different fiber lengths and fiber volume fractions.

Material	Fiber length l(mm)	Fiber diameter D (μm)	Volume fraction v_f	η_{LE}
Carbon-epoxy	0.1	8	0.3	0.20
	1.0	8	0.3	0.89
	10.0	8	0.3	0.99
Glass-nylon	0.1	10	0.3	0.21
	1.0	10	0.3	0.89
	10.0	10	0.3	0.99

3-4.1.2 Work Justification 2

Experimental results by Dingle, (1974) for aligned discontinuous carbon fiber/epoxy composites have shown good agreement with the theoretical predictions. Table (3-4) shows that experimental length efficiency factors η_{LE} are slightly less than the theoretical efficiency factors given in Table (3-3) for similar length fibers.

Table (3-4): Experimental fiber length efficiency factor for continuous aligned fiber composites.

Fiber length, l (mm)	Volume fraction, v_f	Theoretical E_c for continuous fibers (GPa)	Experimental E_c for discontinuous fibers (GPa)	η_{LE}
1	0.49	194	155	0.80
4	0.32	128	112	0.87
6	0.42	167	141	0.84

Conclusion 2:

For uniformly aligned short fiber composites, the modified rule of mixtures with fiber lengths and fiber volume fractions listed in Tables (3-3) and (3-4) can be used with good accuracy to calculated E_c.

To account for the possibility of a distribution of fibers with different lengths l_i, the fiber length efficiency factor can be modified as.

$$\eta_{LE} = \frac{1}{v_f}\sum_i v_i\left[1-\frac{\tanh(\beta l_i/2)}{(\beta l_i/2)}\right] \qquad \text{.....(3-15)}$$

3-4.1.3 Fiber Orientation Efficiency Factor

Fiber orientation efficiency factor η_{OE} has been calculated based on fibers that have different orientation distributions with respect to a reference axis. For aligned chopped fibers, η_{OE}=1. Krenchel (1964) ignored the transverse deformation of fibers and introduced η_{OE} as

$$\eta_{OE} = \sum_n a_n \cos^4\phi_n \qquad \text{.....(3-16)}$$

where a_n is the fraction of fibers with orientation angle ϕ_n with respect to the reference axis. The sum of values of a_n must be 1. i.e. $\sum_n a_n = 1$, and if four groups of fibers exist, each with same number of fibers, then $a_1 = a_2 = a_3 = a_4 = 1/4$, and if the have the

following orientation angles: $\phi_1 = 0°, \phi_2 = 45°, \phi_1 = 90°, \phi_1 = -45°$, then after substitution into (3-17),

$$\eta_{OE} = \frac{1}{4}(1) + \frac{1}{4}(1/4) + \frac{1}{4}(0) + \frac{1}{4}(1/4) = \frac{3}{8} \qquad \text{.....(3-17)}$$

then the modified rule of mixtures can be written as;

$$E_c = \left(\frac{3}{8}\right) \cdot \eta_{LE} \cdot E_f . v_f + E_m v_m \qquad \text{.....(3-18)}$$

Table (3-5) shows η_{OE} for simple fiber orientation distributions assuming elastic deformation of the matrix and fibers, and equality of strains (Krenchel, 1964).

Table (3-5): Fiber orientation efficiency factor for several system configurations.

Orientation of fibers	η_{OE}
Aligned-longitudinal	1
Aligned-transverse	0
Random in-plane (2-D)	3/8 = 0.375
Three-dimensional random	0.5

3-4.1.4 Work Justification 3

Experimental results by Owens/Corning Fiberglass Corporation (Weng and Sun, 1979) for a randomly-oriented glass fiber/polyester resin and chopped fiber composite for a two dimensional case has shown good agreement with the modified rule of mixtures as shown in the figure below, with given fiber/resin data: E_m= 7.03 GPa, E_f= 72.4 GPa, l= 2.54 mm.

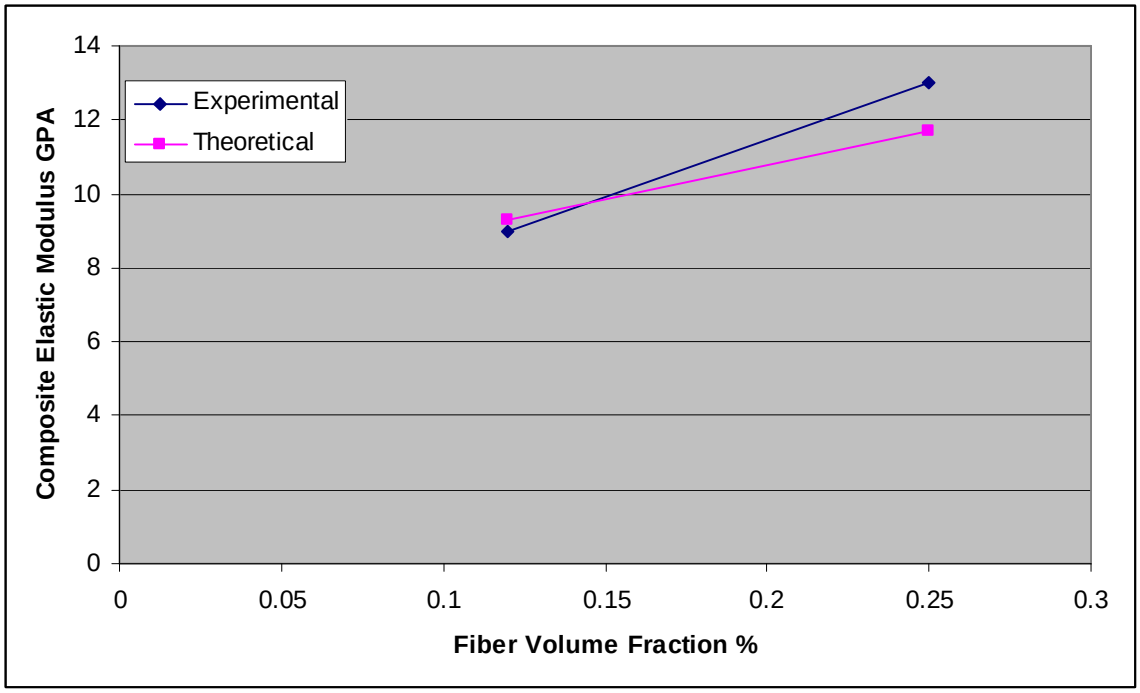

Figure (3-10): Experimental and theoretical data by Owens/Corning Fiberglass Corporation.

Also, a good agreement was found between the experimental work by Manera (1977) and the theoretical results from the modified rule of mixtures, as shown in Figure (3-11).

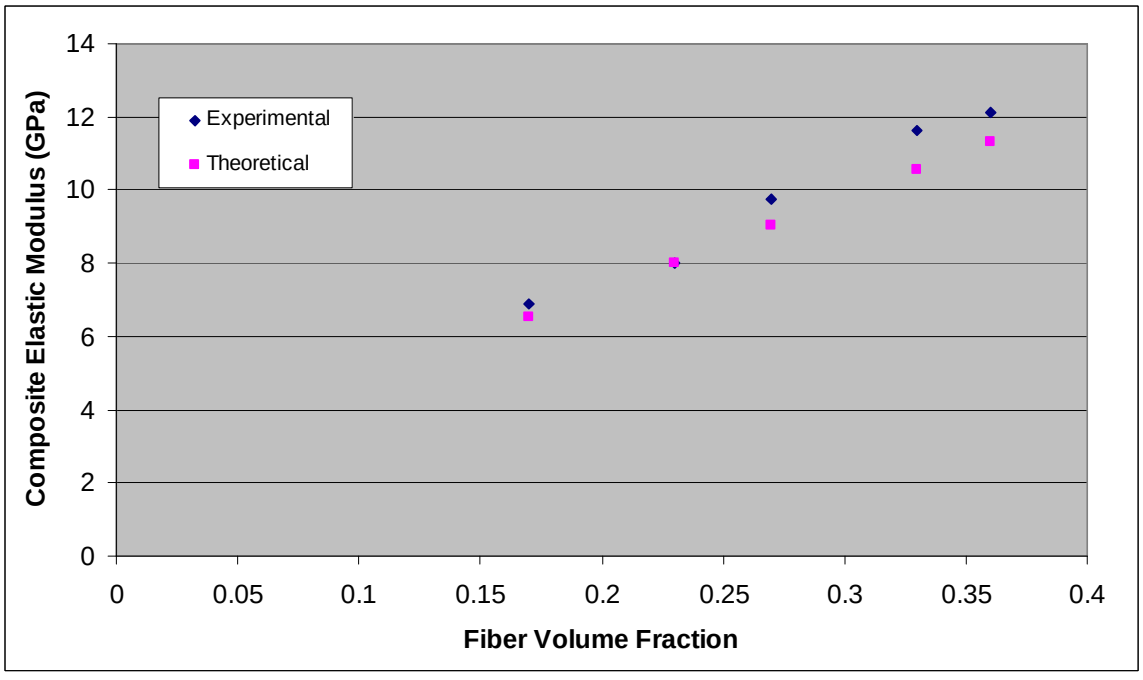

Figure (3-11): Experimental and theoretical data by Manera (1977).

Another example of good agreement between the theoretical and experimental data has been observed in a recent study by Andersons, Sparnins, and Joffe (2006) as can been seen in Figure (3-12). They used flax fiber mats (FFM) as reinforcement and Polypropylene PP and modified Polypropylene (PPM) as resin.

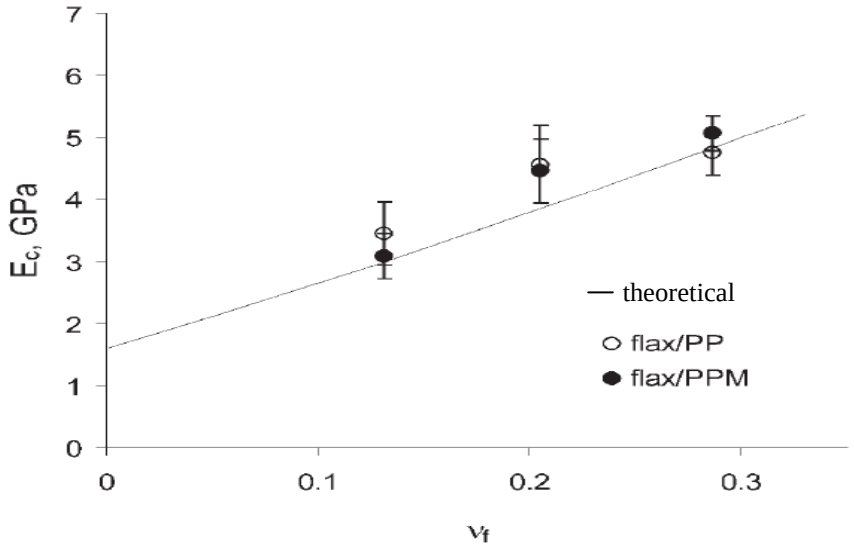

Figure (3-12): Experimental and theoretical data by Andersons et al. (2006).

To verify the validity of the theoretical work, additional experimental data by Thomason and Vlug (1996) has been compared with the results of the theoretical equations. Thomason and Vlug used a random, in-plane (2-D), short glass fiber reinforced polypropylene composite as shown in Figure (3-13). It is very clear from the experimental data that the effect of fiber length is negligible once it is beyond the fiber critical length, which agrees with the theoretical model.

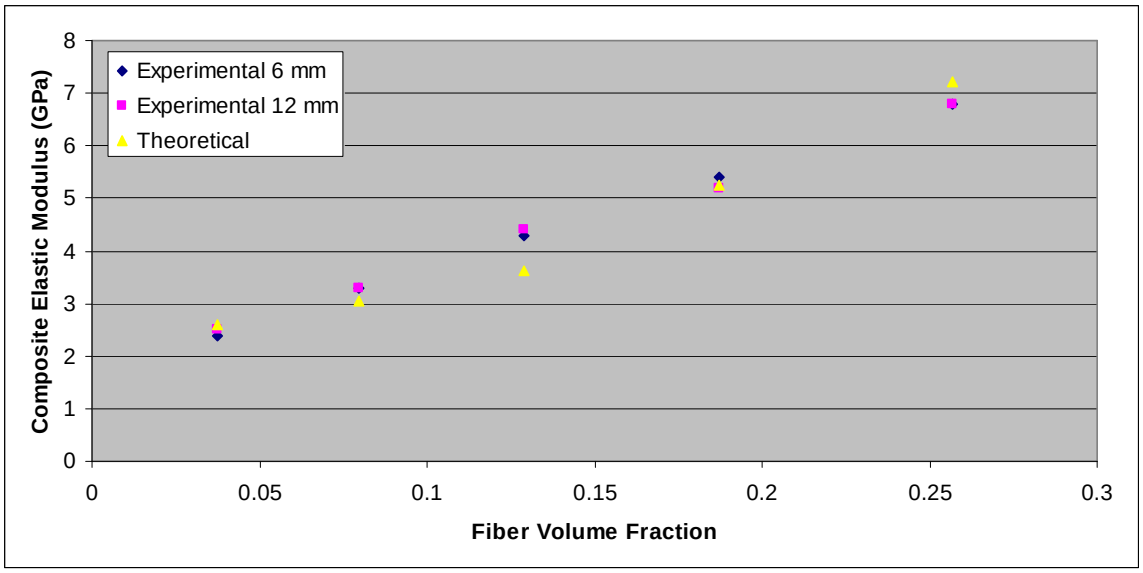

Figure (3-13): Experimental and theoretical data by Thomason and Vlug (1996).

Conclusion 3:

For 2-D in-plane randomly dispersed short fiber composites up to 35% fiber volume fraction, the modified rule of mixtures can be used with good accuracy to calculate E_c.

3-4.2 Strength Modified Rule of Mixtures

Although strength theory for short fiber reinforced composites (SFC) is still under development, the modified rule of mixtures for strength has shown good agreement with experimental data. The ultimate strength of reinforced composite polymer σ_{uc} for aligned fibers can be predicated (Kelly and Tyson, 1965) as

$$\sigma_{uc} = \sum_i \left[\frac{\tau l_i v_{fi}}{D} \right] + \sum_j \left[\sigma_{fj} v_{fj} \left(1 - \frac{l_c}{2l_j} \right) \right] + \left(1 - v_f \right) \sigma_m \qquad \text{.....(3-19)}$$

This equation is referred as the Kelly-Tyson prediction. The first summation is the contribution of fibers shorter than critical fiber length (subcritical), and the second summation takes into account fibers longer than the critical fiber length (supercritical). The fiber length efficiency factor η_{LS} can be defined and calculated using the following equation

$$\eta_{LS} = \begin{cases} 1 - \dfrac{l_c}{2l} & l \geq l_c \\ \dfrac{l}{2l_c} & l < l_c \end{cases} \qquad \text{.....(3-20)}$$

which can be written in one single equation accounting for different length short fiber distributions as

$$\eta_{LS} = \frac{1}{v_f}\left[\sum_i \frac{l_i v_i}{2l_c} + \sum_j v_i\left(1 - \frac{l_c}{2l_j}\right)\right] \qquad \text{.....(3-21)}$$

recall that $l_c = \dfrac{\sigma_f D}{2\tau}$

The same previous argument can be used once again, where the first summation accounts for the contribution from all fibers shorter than the critical length, and the second summation incorporates the strength distribution from fibers whose lengths are greater than or equal to fiber critical length. If we use just one length of chopped fibers (uniform fiber length), then the strength of a short fiber composite (SFC) can be written after adding a factor to account for in-plane (2-D) randomness;

$$\sigma_{cu} = \eta_s \cdot \sigma_f \cdot v_f + \left(1 - v_f\right)\sigma_m \qquad \text{.....(3-22)}$$

where:

σ_f : fiber strength,

σ_m : matrix strength at fiber failure strain,

η_s : fiber efficiency factor.

For linear elastic constituents, $\sigma_m = \frac{\sigma_f \cdot E_m}{E_f}$. Fiber efficiency factor η_s, can be decomposed into two components as follows: $\eta_s = \eta_{LS} \cdot \eta_{OS}$, where fiber length efficiency factor η_{LS} and fiber orientation efficiency factor η_{OS} have similar interpretations as for modulus calculations.

$$\sigma_{cu} = \eta_{LS} \cdot \eta_{OS} \cdot \sigma_f \cdot v_f + (1 - v_f)\sigma_m \qquad \text{.....(3-23)}$$

For random in plane (2-D) short fiber composites with fiber length greater than 5 times the critical fiber length $l > 5l_c$, the effect of fiber length efficiency factor η_{LS} could be ignored. Figure (3-14) shows fiber length efficiency factor η_{LS} versus fiber length according to equations (3-16) and (3-22) (Rosenthal, 1992)

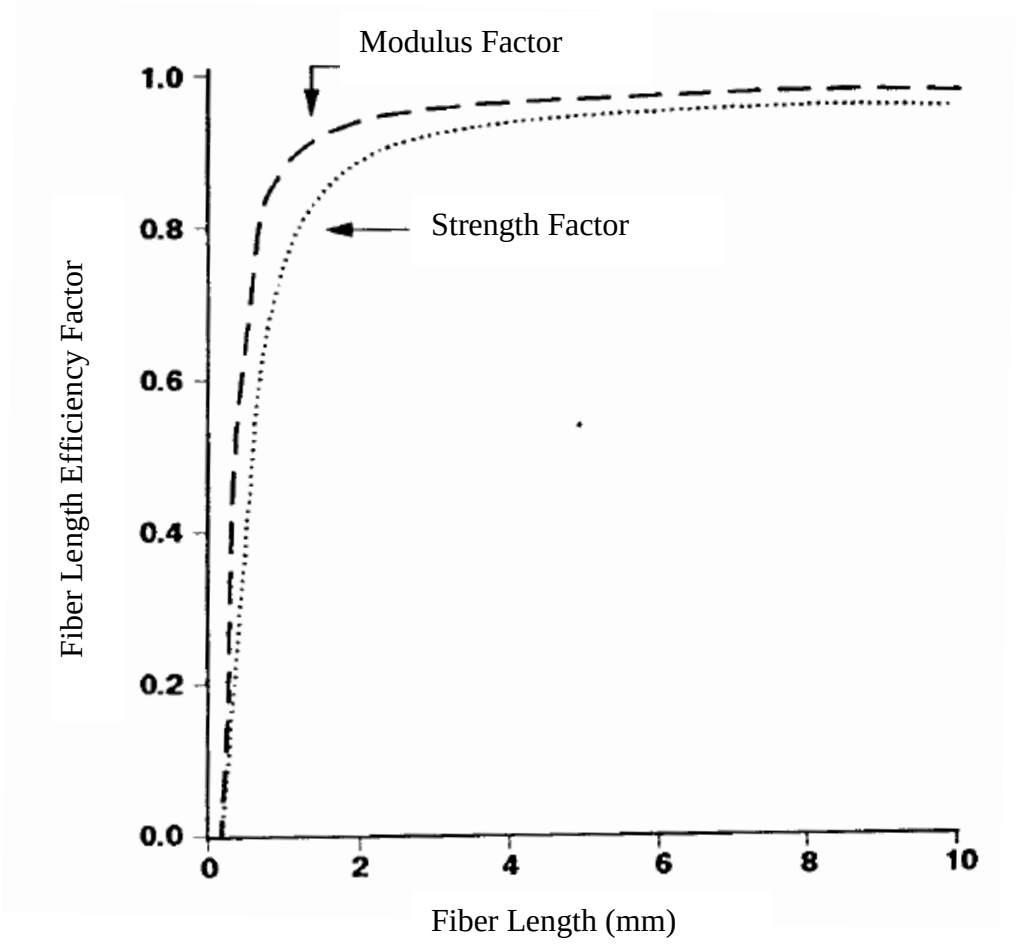

Figure (3-14): Fiber length efficiency factor versus fiber length for both stiffness and strength (Rosenthal, 1992).

When the length of critical fiber length is negligible in comparison to average fiber length, then composite strength is

$$\sigma_{cu} = \eta_{OS} v_f \sigma_f + (1 - v_f)\sigma_m \qquad \text{.....(3-24)}$$

Chou (1992) has published an equation to calculate η_{OS} for random in-plane laminates containing fiber of uniform length greater than critical fiber length, l_c

$$\eta_{OS} = \frac{8}{3\pi}\left(2 + \beta^2\right)\sqrt{1-\beta^2} \times \left[\cos^{-1}\beta - \frac{1}{2}\beta \log\left(\frac{1+\sqrt{1-\beta^2}}{1-\sqrt{1-\beta^2}}\right)\right] \qquad \text{.....(3-25)}$$

This equation can be represented graphically as show in Figure (3-15) where the product of βl is the width of a 'critical zone". Chou recommended a range between 0.2-0.25 for η_{OS}

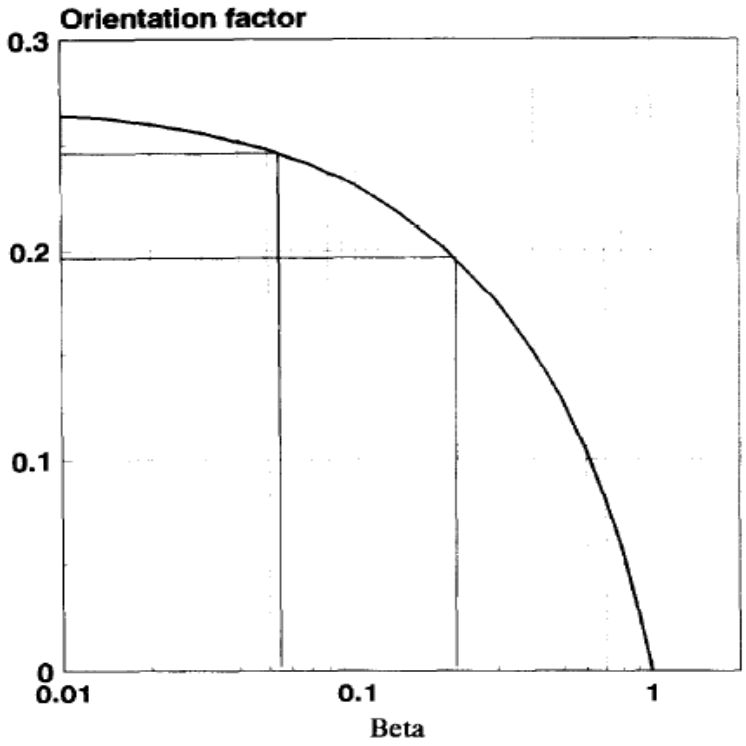

Figure (3-15): Fiber Orientation factor as a function of β.

3-4.3 Work Justification 4

The only experimental work available to study the effect of in-plane (2-D) randomly dispersed chopped fibers on the strength of composites was conducted by Thomason, Vlug, Kirkor and Schipper (1996). They used glass fiber-reinforced polypropylene composites. A single value for η_{OS} = 0.2 was used for different fiber concentration/fractions. Figure (3-16) shows the excellent correlation between experimental results and the theoretical, the modified rule of mixtures or the Kelly-Tyson prediction.

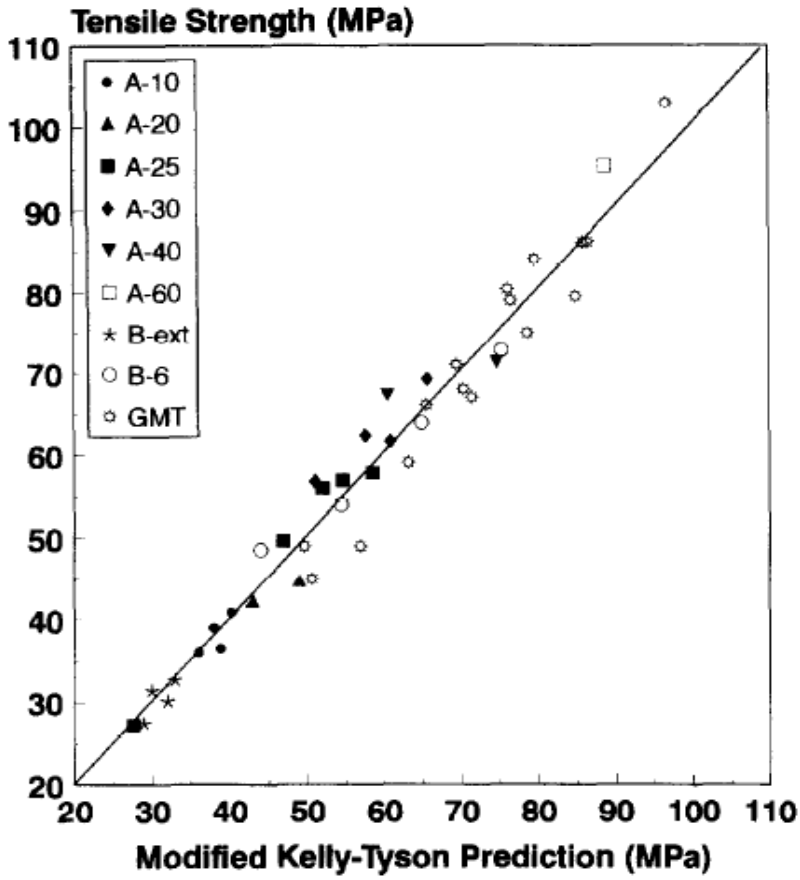

Figure (3-16): Correlation between theoretical and experimental data based on Thomason, Vlug, Kirkor and Schipper (1996).

Conclusion 4:

For 2-D in-plane randomly dispersed short fiber composites, the modified rule of mixtures can be used with good accuracy to calculate σ_{cu}.

3-5 What are Random in-plane (2-D) Short Fiber Composites?

If the short fibers are dispersed randomly in a way the composite material will have isotropic properties in the plane of the layer, but properties are very different normal to that plane, then the composite is referred to as a 2-D or in-plane randomly oriented/dispersed composite as shown in Figure (3-17).

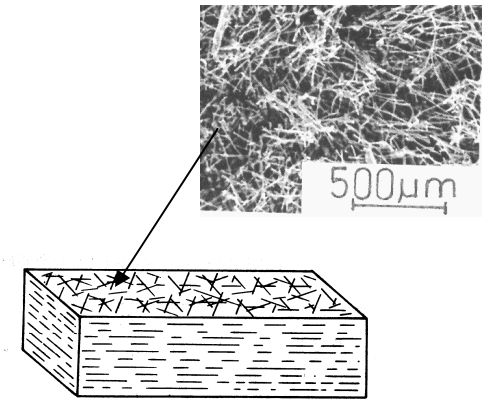

Figure (3-17): In-plane of the layer (top) and normal to the plane of the layer (sides)

The reasons that in-plane (2-D) randomly dispersed short fibers are assumed are:

- The thickness of the layers of the H-DFRP rebar are very small and thus can be considered in plane
- In the presence of shear and tensile stresses, fibers tend to rotate and align in the direction of shear and extensional flow. If we keep increasing these stresses, the fibers will align more in the direction of flow.

3-6 Curvature of Fibers

The fiber mean stiffness modulus $\tilde{E}_f$ with allowance for curvature, based on a continuous sinusoidal curvature (Bažant, 1965) is

$$\tilde{\tilde{E}}_f = \frac{E_f}{1+\kappa v_f \frac{C^2}{l^2}\frac{E_f}{G_{xz}}} \qquad \text{.....(3-26)}$$

where

κ : $\frac{\pi^2}{2}$

C : amplitude of the sinusoid

G_{xz} : shear modulus of fibers and can be calculated as $G_{xz} = \frac{E_f}{2(1+\nu)}$

ν : Poisson's ratio of fibers

l : fiber length of 1/2 sinusoidal wave

Then, the rule of mixture becomes;

$$E_c = E_m v_m + \tilde{\tilde{E}}_f v_f \qquad \text{.....(3-27)}$$

and the modified rule of mixture becomes

$$E_c = E_m v_m + \eta_{LE}\eta_{LE}\,\tilde{\tilde{E}}_f v_f \qquad \text{.....(3-28)}$$

The assumptions in deriving equation (3-22) are:

1- The fiber curvature is relatively small ($C<l/4$)
2- The wavelength is sufficiently long compared to fiber diameter
3- The fibers are closely spaced.
4- The fibers have a much higher modulus than the matrix.
5- Deformations are small.
6- The matrix and the fibers are linearly elastic.

Equation (3-27) can be written in term of the whole stiffness modulus of the fiber reinforced plastic composite rather than the fiber mean stiffness modulus (Tarnopol'skil, Portnov, and Zhigun, 1967) as

$$E_c = \frac{E_{cp}}{1 + \frac{f^2}{2}\frac{E_{cp}}{G_{xzp}}} \qquad \text{.....(3-29)}$$

where

E_c : stiffness modulus of the fiber reinforced plastic composite,

E_{cp} : stiffness modulus of the material with perfectly straight fibers,

G_{xzp} : shear modulus of ideally reinforced material,

$f = C\frac{\pi\kappa}{l}$ is the degree of curvature, and

κ : the number of half-waves on the base l

Since the fiber orientation factor represents the fraction of fiber volume close to parallel with the loading direction that contributes to that specific mechanical property (Thomason, Wug, Schipper and Krikort, 1996) and since the assumption is in-plane (2D) randomly dispersed chopped fibers for the reasons mentioned in Section 3.5, the effect of fiber curvature can be ignored

Chapter Four

Models and Calculations

Two models of D-H-FRP rebars are proposed in this research. In this chapter we will show the scheme of each rebar and the materials used. Also, the stress-strain curves for the materials are identified, and the objective function and set of constraints for each proposed rebar are listed to ensure that the desirable characteristics are satisfied and maintained. Since moment curvature plays an important role in this work, the procedure to construct this crucial curve has been mentioned.

4.1 Proposed Rebar Model One

This model consists of three different types of fibers and steel. The scheme, from core to out side layer, is as follows:

1- steel with volume fraction of 20%.
2- continuous Kevlar-49 fiber layer.
3- randomly dispersed chopped SM-Carbon fiber layer.
4- randomly dispersed chopped IM-Carbon fiber layer.

Figure (4-1) shows the cross section of this proposed rebar and materials used. The reasons of using steel grade 60 with small volume fraction are:

- The stiffness of steel is high which would give positive contribution to the composite total stiffness.

- Using a small volume fraction of steel in the core of the rebar can be easily protected from water by FRP fibers and resin.
- The low price of steel compared to fibers.

The reason for using IM-Carbon and SM-Carbon as chopped fibers is:

- The stiffness moduli of these two types of fibers are higher than that of Kevlar-49. Even after the stiffness reduction associated with chopped fibers, a great deal of stiffness remains.

The reasons for arranging the carbon chopped fiber layers on the first two outside layers are:

1- to reduce the effect of the chopped fiber curvature effect.
2- to eliminate the creation of shock waves inside the rebar, having a less adverse effect on the ultimate stress-strain behavior of the rebar (Terry, 2006).
3- When carbon fibers are allocated on the outside layers, they will protect steel from alkaline attack in the cementitious environment.

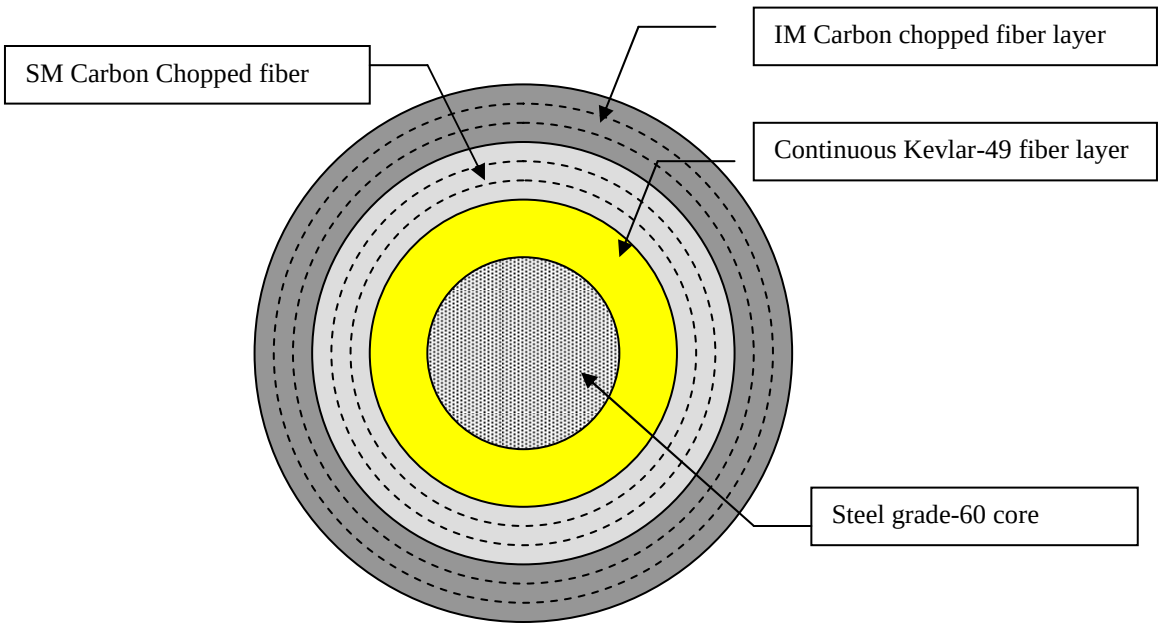

Figure (4-1): A cross sectional area of proposed rebar model 1 (not to scale).

4.2 Proposed Rebar Model Two

This model consists of four different types of fibers with no steel. The scheme, from core to outside layer, is as follows:

1- continuous E-Glass fiber core
2- continuous Kevlar-49 fiber layer
3- randomly dispersed chopped SM-Carbon fiber layer
4- randomly dispersed chopped IM-Carbon fiber layer

Figure (4-2) shows the cross sectional area of this proposed rebar and the materials used. The reason for using IM-Carbon fibers, despite its high price, is because of its high stiffness. The reason of using IM-Carbon and SM-Carbon as chopped fibers is:

- The stiffness moduli of these two types of fibers are higher than that of Kevlar-49 and glass fibers.

The reasons for arranging the carbon chopped fiber layers on the first two outside layers are:

1- to reduce the effect of chopped fiber curvature effect.
2- to eliminate the creation of shock waves inside the rebar, having less adverse effects on the ultimate stress-strain behavior of the rebar.
3- When carbon fibers are allocated in the outside layers, they will protect glass fibers from alkaline attack in the cementitious environment.

It is worth to note that the choice of these types of different fibers is primarily driven by the need to satisfy the ductility requirement.

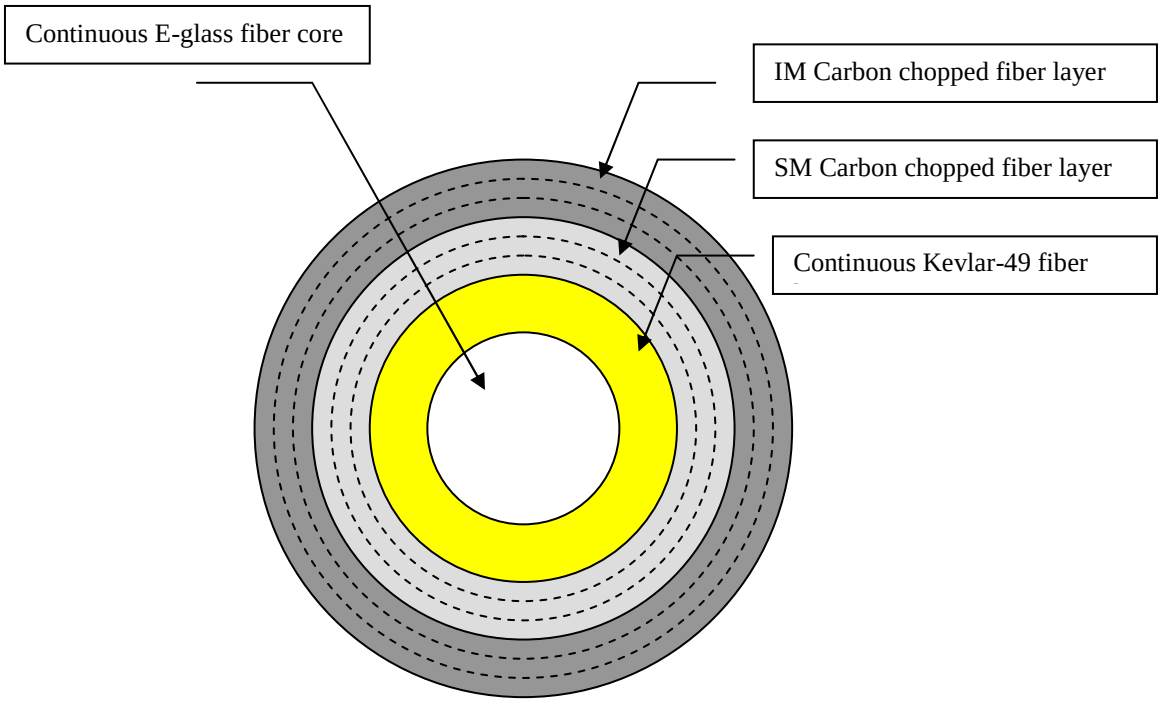

Figure (4-2): A cross sectional area of proposed rebar model 2 (not to scale).

4-3 Moment-Curvature Relationship

One of the most important steps in this work is to construct moment curvature curves for different concrete sections reinforced with the proposed rebars. In order to accomplish this step, stress-strain curves are needed for concrete, steel, and D-H-FRP rebars.

4-3.1 Concrete Stress-Strain Curve

To model the concrete stress-strain relationship, a modified Hognestad's second degree parabola with a linear tail (Kent and Parker, 1971) has been used, as shown in Figure (4-3a), while Figure (4-3b) shows the original Hognestad's model.

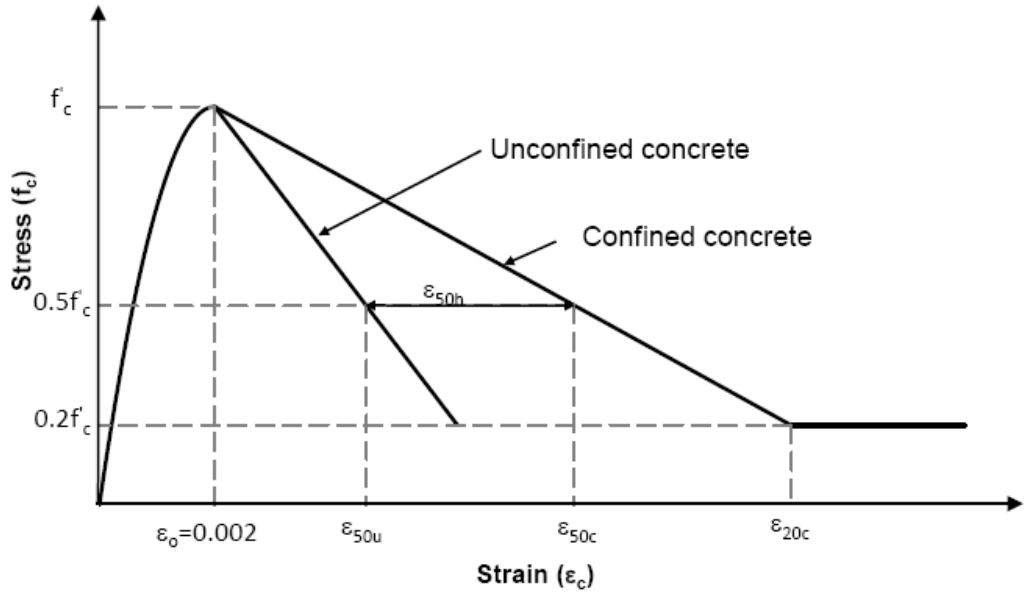

Figure (4-3a): Proposed stress-strain model for confined and unconfined concrete, (Kent and Park 1971).

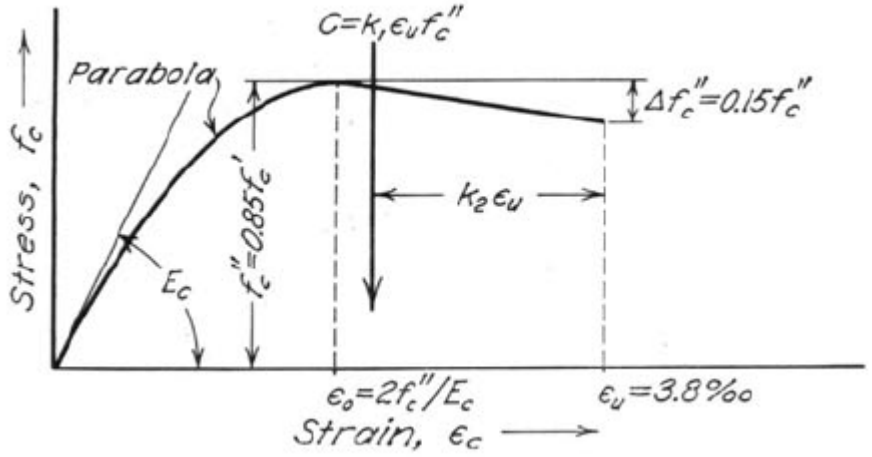

Figure (4-3b): Original Hognestad stress-strain curve for concrete in compression (Hognestad, 1951)

- **Region 1 (Parabola)**

$0 \le \varepsilon_c \le \varepsilon_o$

$$f_c = f_c'\left[2\left(\frac{\varepsilon_c}{\varepsilon_o}\right)-\left(\frac{\varepsilon_c}{\varepsilon_o}\right)^2\right] \qquad \text{.....(4-1)}$$

- **Region 2 (linear tail)**

$$\varepsilon_o \le \varepsilon_c$$

$$f_c = f_c'\left[1 - Z\left(\varepsilon_c - \varepsilon_o\right)\right] \qquad \text{.....(4-2)}$$

where $Z = \dfrac{0.5}{\varepsilon_{50u} - \varepsilon_c}$. ε_{50u} is the strain corresponding to the stress equal to 50% of the maximum concrete strength for unconfined concrete. Z typically taken as:

Z = 150 for unconfined reinforced concrete and,
Z = 50 for confined reinforced concrete.

Here we should clarify that the concrete compressive strength f_c' used in this work is taken as 4500 psi for a bridge deck application and 5500 psi for beams/girders. The reason for avoiding low values for concrete compressive strength is: ***the ductility of the concrete section reinforced with FRP composites comes from a sequence of fiber failures, and because the tensile strength of fibers is high, to maintain ductility, the concrete cannot crush before the sequence of fiber failures occurs***.

4-3.2 Steel Reinforcement Stress-Strain Curve

Since conventional steel has been used in proposed rebar 1, the stress-strain curve needs to be identified. For evaluation purposes of the proposed rebar models, a comparison between the steel rebars and the proposed FRP rebars have been done. For both steel grade 40 and grade 60, Figure (4-4) shows stress-strain relationship and the following equations have been assumed and used:

If $\varepsilon_s \le \varepsilon_y$ then; $f_s = E_s \cdot \varepsilon_s$

If $\varepsilon_y \le \varepsilon_s \le \varepsilon_{sh}$ then; $f_s = f_y$

If $\varepsilon_y \le \varepsilon_s \le \varepsilon_{sh}$ then $f_s = f_y + (f_{su} - f_y)\left[2\xi - \xi^2\right]$

If $\varepsilon_{sh} \le \varepsilon_s$ then; $f_s = f_{su}$

where

f_s : stress in steel reinforcement,

f_y : yielding stress (σ_y),

f_{su} : ultimate stress in steel, and

ξ : ration defined as $\dfrac{\varepsilon_s - \varepsilon_{sh}}{\varepsilon_{su} - \varepsilon_{sh}}$

ε_s : strain in steel reinforcement,

ε_y : yielding strain of steel,

ε_y = 40/29000 for steel grade 40 and 60/29000 for steel grade 60

ε_{sh}: strain hardening of steel (Chen and Duan, 1999),

$$\varepsilon_{sh} = \begin{cases} 14\varepsilon_y & \text{for steel Grade 40} \\ 5\varepsilon_y & \text{for steel Grade 60} \end{cases} \qquad \text{.....(4-3)}$$

ε_{su} : strain corresponds to ultimate stress in steel (Chen and Duan, 1999),

$$\varepsilon_{su} = \begin{cases} 0.14 + \varepsilon_{sh} & \text{for steel Grade 40} \\ 0.12 & \text{for steel Grade 60} \end{cases} \qquad \text{.....(4-4)}$$

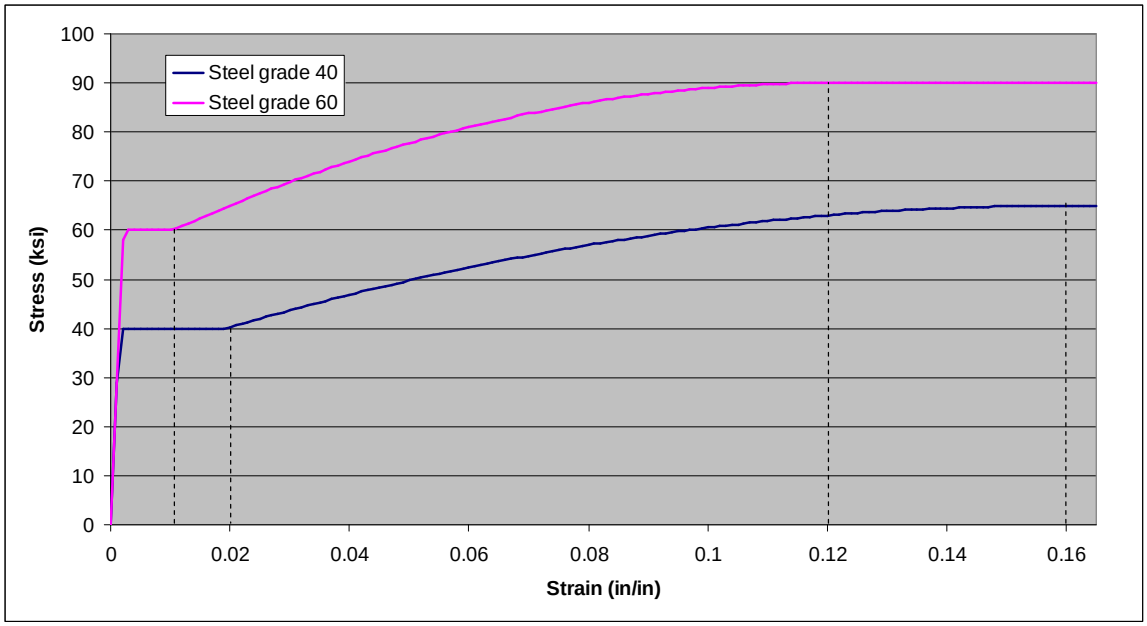

Figure (4-4): Typical stress-strain curves for steel grade 60 and grade 40.

4-3.3 Fibers Stress-Strain Curve

The two major problems in using FRP rebar are costs and lack of ductility. The second one can be observed clearly from the stress-strain curves, which are straight lines, as shown in Figure (4-5). The mechanical properties of each type of fiber used in modeling the proposed FRP rebars are shown in Table (4-1).

Table (4-1): Mechanical properties of the materials used in the proposed FRP rebars

	Stiffness GPa (ksi)	Strength MPa (ksi)	Ultimate Strain mm/mm (in/in)	Fiber diameter mm (in)
HM-Carbon	903 (131000)	2700 (395)	0.003	10 (0.4)
IM-Carbon fibers	650 (95000)	3037.5 (441)	0.0045	10 (0.4)
SM-Carbon fibers	230 (34000)	3570 (518)	0.015	10 (0.4)
Kevlar-49 fibers	125 (18130) 102 (14790)	3125 (460) 2550 (370)	0.025	12 (0.5)
E-glass fibers	74 (10733)	3256 (472)	0.044	16.5 (0.7)
Steel grade 60	200 (29007)	400 (60)	0.00207	N/A
Epoxy resin	3.5 (510)	-	0.06	N/A

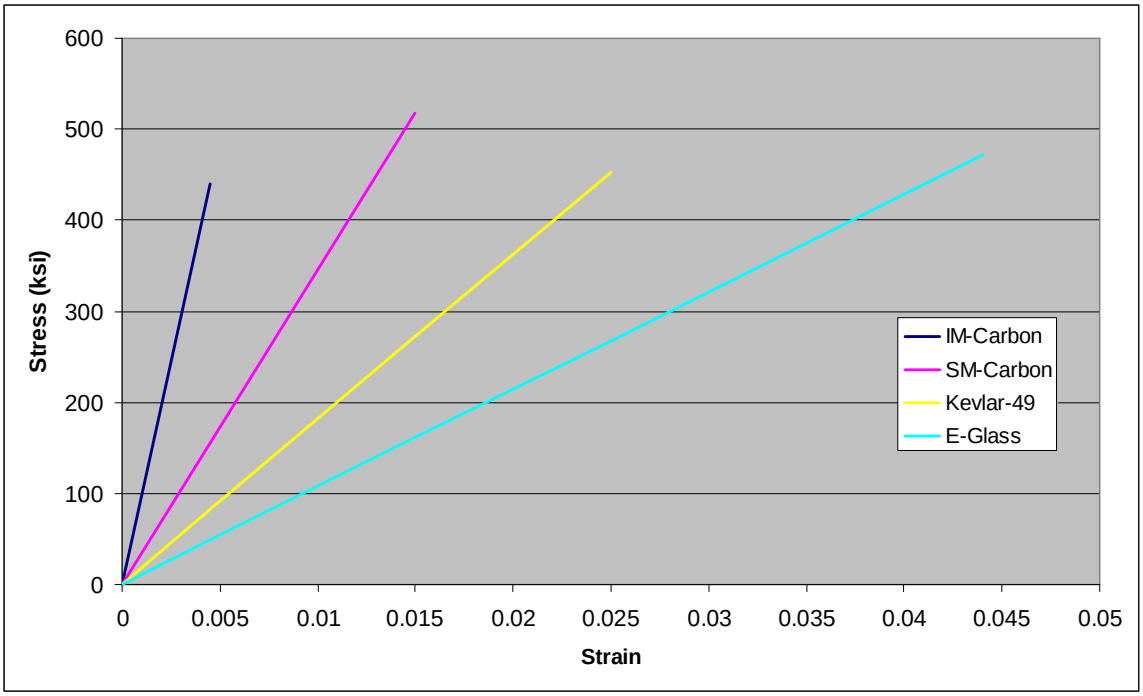

Figure (4-5): Stress-strain diagram for the fibers used in this study.

4-3.3.1 Proposed D-H-FRP Rebar 1 Stress-Strain Curve

Figure (4-6) is a typical stress-strain curve for proposed rebar 1. The general equations that govern stresses as s function of strains are:

$$\text{If } 0 \le \varepsilon_{\text{FRP}} \le \varepsilon_y \qquad \text{then; } \sigma_{\text{comp1}} = E_{\text{FRP1}} \cdot \varepsilon_{\text{FRP}}$$

$$\text{If } \varepsilon_y \le \varepsilon_{\text{FRP}} \le \varepsilon_{\text{IM-Carbon}} \qquad \text{then; } \sigma_{\text{comp2}} = E_{\text{FRP2}} \cdot \varepsilon_{\text{FRP}} + \sigma_y v_{\text{Steel}}$$

$$\text{If } \varepsilon_{\text{IM-Carbon}} \le \varepsilon_{\text{FRP}} \le \varepsilon_{\text{SM-Carbon}} \qquad \text{then; } \sigma_{\text{comp3}} = E_{\text{FRP3}} \cdot \varepsilon_{\text{FRP}} + \sigma_y \cdot v_{\text{Steel}}$$

$$\text{If } \varepsilon_{\text{SM-Carbon}} \le \varepsilon_{\text{FRP}} \le \varepsilon_{\text{Kevlar-49}} \qquad \text{then; } \sigma_{\text{comp4}} = E_{FRP4} \cdot \varepsilon_{FRP} + \sigma_y v_{\text{Steel}}$$

$$\text{If } \varepsilon_{\text{Kevlar-49}} \le \varepsilon_{FRP} \le \varepsilon_{su} \qquad \text{then; } \sigma_{\text{comp5}} = \sigma_y v_{\text{Steel}}$$

Where:

$$E_{\text{FRP1}} = E_{\text{IM-Carbon}} v_{\text{IM-Carbon}} + E_{\text{SM-Carbon}} v_{\text{SM-Carbon}} + E_{\text{Kevlar-49}} v_{\text{Kevlar-49}} + E_{\text{resin}} v_{\text{resin}} + E_s v_{\text{Steel}} \qquad \text{.....(4-5)}$$

$$E_{FRP2} = E_{IM-Carbon} v_{IM-Carbon} + E_{SM-Carbon} v_{SM-Carbon} + E_{Kevlar-49} v_{Kevlar-49} + E_{resin} v_{resin} \quad \text{.....(4-6)}$$

$$E_{FRP3} = E_{SM-Carbon} v_{SM-Carbon} + E_{Kevlar-49} v_{Kevlar-49} + E_{resin} v_{resin} \quad \text{.....(4-7)}$$

$$E_{FRP4} = E_{Kevlar-49} v_{Kevlar-49} + E_{resin} v_{resin} \quad \text{.....(4-8)}$$

and

ε_{FRP} : ultimate strain in FRP rebar

ε_{y} : yielding strain in steel

ε_{su} : ultimate strain in steel

$\varepsilon_{IM-Carbon}$: ultimate strain IM-Carbon fibers

$\varepsilon_{SM-Carbon}$: ultimate strain SM-Carbon fibers

$\varepsilon_{Kevlar-49}$: ultimate strain in Kevlar-49 fibers

v_{Steel} : volume fraction of steel

$v_{IM-Carbon}$: volume fraction of IM-Carbon fibers

$v_{SM-Carbon}$: volume fraction of SM-Carbon fibers

$v_{Kevlar-49}$: volume fraction of Kevlar-49 fibers

v_{resin} : volume fraction of resin (v_m)

$E_{IM-Carbon}$: modulus of elasticity of IM-Carbon fiber layer

$E_{SM-Carbon}$: modulus of elasticity of SM-Carbon fiber layer

$E_{Kevlar-49}$: modulus of elasticity of Kevlar-49 fibers

E_s : modulus of elasticity of steel

The maximum value that σ_{comp1} can reach is when steel starts yielding, the maximum value that σ_{comp2} can reach is when IM-Carbon fibers start breaking, the maximum value that σ_{comp3} can reach is when SM-Carbon fibers start breaking, and the maximum value that σ_{comp4} can reach is when Kevlar-49 fibers start breaking as shown in Figure (4-6). σ_{comp5} is the stress when there is steel only.

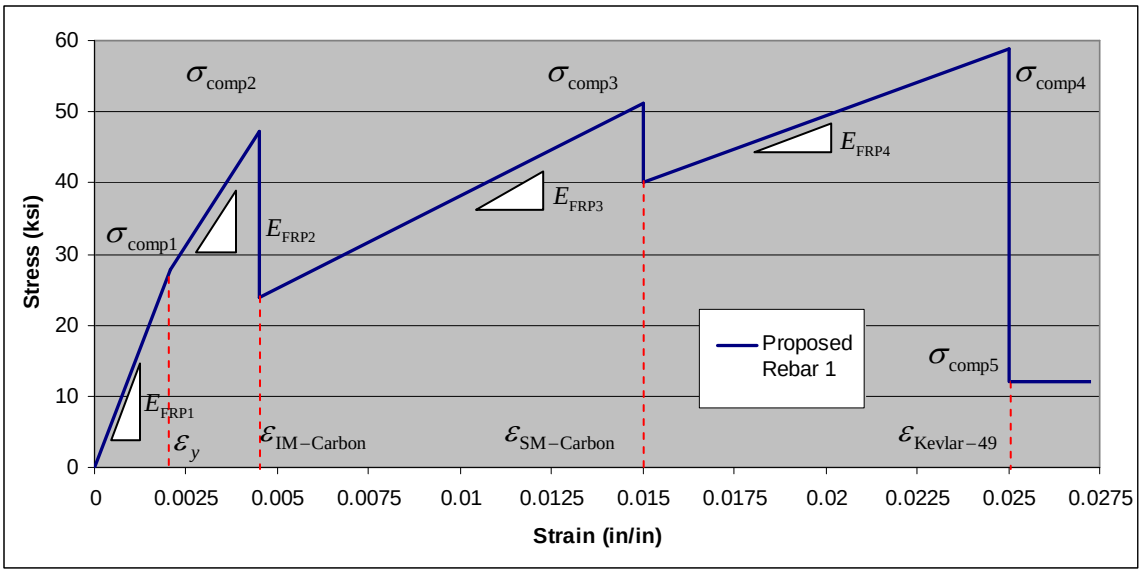

Figure (4-6): A typical stress-strain curve for proposed rebar 1 of 20% steel and 80% FRP.

4-3.3.2 Proposed D-H-FRP Rebar 2 Stress-Strain Curve

Figure (4-7) is a typical stress-strain curve of proposed rebar 2. The general equations that govern stresses as a function of strains are:

$$\text{If } 0 \le \varepsilon_{FRP} \le \varepsilon_{IM-Carbon} \quad \text{then; } \sigma_{comp1} = E_{FRP1} \cdot \varepsilon_{FRP}$$

$$\text{If } \varepsilon_{IM-Carbon} \le \varepsilon_{FRP} \le \varepsilon_{SM-Carbon} \quad \text{then; } \sigma_{comp2} = E_{FRP2} \cdot \varepsilon_{FRP}$$

$$\text{If } \varepsilon_{SM-Carbon} \le \varepsilon_{FRP} \le \varepsilon_{Kevlar\text{-}49} \quad \text{then; } \sigma_{comp3} = E_{FRP3} \cdot \varepsilon_{FRP}$$

$$\text{If } \varepsilon_{Kevlar\text{-}49} \le \varepsilon_{FRP} \le \varepsilon_{E\text{-}Glass} \quad \text{then; } \sigma_{comp4} = E_{FRP4} \cdot \varepsilon_{FRP}$$

Where:

$$E_{FRP1} = E_{IM-Carbon}\nu_{IM-Carbon} + E_{SM-Carbon}\nu_{SM-Carbon} + E_{Kevlar\text{-}49}\nu_{Kevlar\text{-}49} + E_{E\text{-}Glass}\nu_{E\text{-}Glass} + E_{resin}\nu_{resin} \quad \text{.....(4-9)}$$

$$E_{FRP2} = E_{SM-Carbon}\nu_{SM-Carbon} + E_{Kevlar\text{-}49}\nu_{Kevlar\text{-}49} + E_{E\text{-}Glass}\nu_{E\text{-}Glass} + E_{resin}\nu_{resin} \quad \text{.....(4-10)}$$

$$E_{FRP3} = E_{Kevlar\text{-}49}\nu_{Kevlar\text{-}49} + E_{E\text{-}Glass}\nu_{E\text{-}Glass} + E_{resin}\nu_{resin} \quad \text{.....(4-11)}$$

$$E_{FRP4} = E_{E\text{-}Glass}\nu_{E\text{-}Glass} + E_{resin}\nu_{resin} \quad \text{.....(4-12)}$$

and

$\varepsilon_{\text{E-Glass}}$: ultimate strain in E-Glass fibers

$v_{\text{E-Glass}}$: volume fraction of E-Glass fibers

$E_{\text{E-Glass}}$: modulus of elasticity of E-Glass fiber

The maximum value that σ_{comp1} can reach is when IM-Carbon fibers start breaking, the maximum value that σ_{comp2} can reach is when SM-Carbon fibers start breaking, the maximum value that σ_{comp3} can reach is when Kevlar-49 fibers start breaking, and the maximum value that σ_{comp4} can reach is when E-Glass fibers start breaking as shown in Figure (4-7).

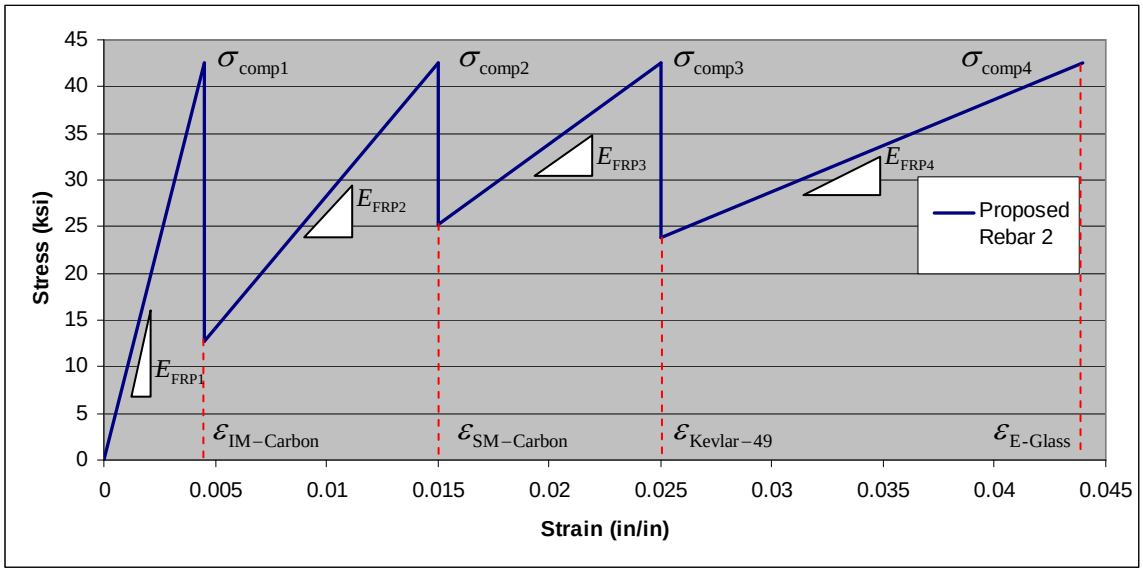

Figure (4-7): A typical stress-strain curve for proposed rebar 2 of 100% FRP.

4-4 Model of Reinforced Concrete Section in Flexure (beyond cracking)

The five basic assumptions in flexure theory are:

1- sections perpendicular to the axis of bending which are plane before bending remain plane after bending.
2- The strain in the reinforcement is equal to the strain in the concrete at the same level.
3- The compressive stress-strain relationship for concrete has been assumed to follow the Modified Hognestad's model
4- The tensile strength of concrete is not neglected and contributes in flexural strength calculations.
5- Concrete fails when the compressive strain reaches 0.003, which is the limiting value in this study.

Figure (4-8) shows the reinforced concrete section, strain and stress distributions.

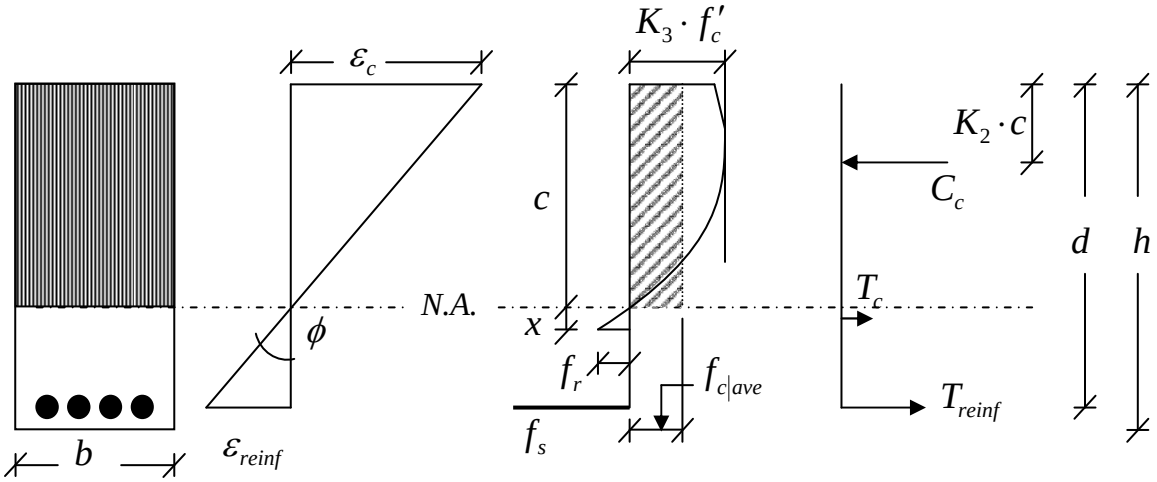

Figure (4-8): (a) beam cross-section. (b) strain distribution. (c) stress distribution (d) force diagram

For equilibrium

$$T_{\text{reinf}} + T_c = C_c$$

where

T_{reinf} : tensile force in reinforcement = $A_{\text{reinforcement}} \cdot f_{\text{reinforcement}}$

T_c : tensile force in concrete = $\frac{1}{2} \cdot f_r \cdot b \cdot x$

C_c : compressive force in concrete = area of stress block × width of beam section

$$C_c = K_1(K_3 \cdot f_c') \qquad \text{.....(4-13)}$$

K_1 : ratio of the average compressive stress to the maximum stress = $\frac{f_{c|ave}}{K_3 \cdot f_c'}$, the most common number for K_1 is 1.

K_2 : ratio of the distance between the extreme compression fiber and the resultant of the compressive force to the depth of the neutral axis, c

K_3 : ratio of the maximum stress f_c'', in the compression zone of a beam to the cylinder strength, f_c'

f_r : modulus of rupture = $7.5\sqrt{f_c'(psi)}$

$$x = \frac{\varepsilon_r}{\varepsilon_c} c \qquad \text{.....(4-14)}$$

where

c : distance from top of compression fiber to the neutral axis (N.A.),

ε_c : concrete strain in top compression fiber,

ε_r : limiting concrete cracking strain; $\varepsilon_r = \frac{f_r}{E_c}$ (linear in tension).

4-4.1 Determining Concrete Strength Parameters K_1, and K_2

When $0 \le \varepsilon_{cu} \le \varepsilon_o$,

$$K_1 = \frac{f_{c|ave}}{K_3 \cdot f_c'} = \eta - \frac{1}{3}\eta^2 \qquad \text{.....(4-15)}$$

$$K_2 = \frac{1/3 - (1/12)\eta}{1 - (1/3)\eta} \qquad \text{.....(4-16)}$$

when $\varepsilon_{cu} > \varepsilon_o$,

$$K_1 = \frac{1}{\varepsilon_c}\left[\varepsilon_c - \frac{\varepsilon_o}{3} - \frac{Z}{2}(\varepsilon_c - \varepsilon_o)^2\right] \qquad \text{.....(4-17)}$$

$$K_2 = 1 - \frac{1}{c_3}\left[\frac{5}{12}c_1\varepsilon_o + c_4\left(c_1 + \frac{c_2}{2\varepsilon_c}\right) + c_3\left(c_1 + \frac{c_2}{2\varepsilon_c}\right)\right] \qquad \text{.....(4-18)}$$

where $\eta = \frac{\varepsilon_{cu}}{\varepsilon_o}$; $c_1 = \frac{\varepsilon_o}{\varepsilon_c}$; $c_2 = \varepsilon_c - \varepsilon_o$; $c_3 = \frac{1}{2}Z c_2^2$; $c_4 = c_2 - Z c_2^2$; $c_5 = \varepsilon_c - \frac{1}{3}\varepsilon_o - c_3$

4-4.2 Moment (M) and Curvature (ϕ) Calculations

Since the Modified Hognestad's model can be used on the onset of concrete cracking, the moment capacity up to cracking shall be calculated based on the elastic section as follows:

$$M_{cr} = \frac{f_r I_g}{y_t} \qquad \text{.....(4-19)}$$

where

M_{cr} : Cracking moment,

f_r : modulus of rapture = $7.5\sqrt{f_c'}$,

I_g : moment of inertia of the concrete section,

y_t : distance from centroid to extreme tension fiber.

After concrete cracks, the resisting moment can be calculated by taking the summation of moments around the centroid of the reinforcement:

$$M = C_c\left(d - K_2\, c\right) - T_c(d - c - \frac{2}{3}x) \qquad \text{.....(4-20)}$$

and the corresponding curvature ϕ can be calculated as

$$\phi = \frac{\varepsilon_c}{c} \qquad \text{.....(4-21)}$$

4-5 Rebar Optimization

An objective of this study is to develop a low cost D-H-FRP rebar. In order to achieve this goal, an objective function and a set of constraints have been set up for each proposed rebar. The prices and mechanical properties of the fiber types used are widely variable in the market. For the purpose of comparison between different materials, specific cost *sc*, which is defined as ratio of price of fiber C_f multiplied by fiber density ρ_f to steel price C_s multiplied by steel density ρ_f. as shown in equation (4-22). Table (4-2) shows specific costs of the materials used in this work and their corresponding densities (Terry, 2006, Bank, 2006).

$$sc = \frac{C_f\, \rho_f}{C_s\, \rho_s} \qquad \text{.....(4-22)}$$

Table (4-2): Specific costs and densities of different materials assumed in this work.

Material	Specific cost (*sc*)	Density (gr/cm^3)
HM-Carbon fibers	120	1.76
IM-Carbon fibers	70.00	1.76
SM-Carbon fibers	6.00	1.76
Kevlar-49 fibers	8.00	1.45
E-Glass	1.00	2.56
Steel Grade 60	1.00	7.8
Epoxy Resin	1.5	1.05

4-5.1 Objective Function

The objective function is simply the multiplication of the volume fraction of each type of fibers by its corresponding relative price. The result will be the total relative price which means how many times are the proposed rebar is more expensive than steel for the same cross-sectional area and the same length.

4-5.2 Types of Constraints

For both proposed D-H-FRP rebars, there are seven types of constraints.

1. *Volume fraction constraints*: volume fractions should be satisfied at all times. Volume fraction could refer to the overall volume fraction or a partial volume fraction for a specified material. For example, the volume fraction of all materials should equal to 1.0, while the volume fraction of resin for continuous fibers could be set to 0.1 (the percentage of resin to continuous fibers will be around 50/50 which is a common ratio in FRP composites). Similarly, the volume fraction of steel could be set to 0.2 (see Section 4-1), while the volume fraction of IM-Carbon, SM-Carbon, Kevlar-49, and E-glass fibers should be greater than zero. Constraints I, II, and IX are volume fraction constraints.
2. *Failure pattern constraint*: this constraint describes how D-H-FRP rebar should fail. When the first fiber type fails, the remaining fiber types and resin should be able to carry the applied load. If the second fiber type fails, the remaining fiber

types and resin should be able to carry the load, and so on so forth, until the last material fails. Constraint (III) is failure pattern constraint.

3. *Ductility constraint*: if the ductility index is higher than 3.0, the FRP rebar will be considered ductile and this is one of the objectives of this work (to be discussed later in this chapter). Constraint (IV) is a ductility constraint.
4. *Design moment constraint*: the moment at which the first type of fibers breaks, which in this case is IM-Carbon, will be used as the design moment. The breakage will happen due to the material reaching its failure strain. This constraint means that the moment capacity of the cross section is greater or equal to the applied moment $\phi M_n \geq M_u$. Constraint (V) is a design moment constraint.
5. *Reliability index constraint*: this will be discussed in detail later in Chapter 5. Constraint (VI) is reliability index constraint.
6. *Efficiency constraint*: it desirable to have concrete crushing and failure in the last remaining fiber type occur simultaneously. However, the chances to have zero feasible solutions from the optimization process for this condition are extremely high. By reducing the desirable failure strain to 85% of the fiber ultimate failure strain, a feasible solution will be reached. That is, the concrete crushes when the strain in the last rebar material is 85% of its failure strain. One more important characteristic for having the efficiency constraint satisfied is the final moment-curvature diagram will be more uniform in that the multiple peaks are closer in value to each other. Constraint (VII) is an efficiency constraint.
7. *Deflection constraint*: for beams/girders in buildings, the deflection should not exceed the maximum limit stated in ACI-318 specifications. Constraint (VII) is a deflection constraint.

Table (4-3) shows the design variables although some preliminary design had been made to narrow the solution's range. Also, uniformity of concrete compression strength was a goal for each type of design member.

Table (4-3): List of design variables.

Symbol	description	Starting values	Ending values
$v_{\text{IM–Carbon}}$	volume fraction of IM-Carbon fibers	0.01	0.5
$v_{\text{SM–Carbon}}$	volume fraction of SM-Carbon fibers	0.01	0.5
$v_{\text{Kevlar-49}}$	volume fraction of Kevlar-49 fibers	0.01	0.5
$v_{\text{E-Glass}}$	volume fraction of E-Glass fibers	0.01	0.5
v_{resin}	volume fraction of resin	≥ 0.1	
A_{FRP}	reinforcement area	0.1	6
f_c'	concrete compressive strength	4500, 5000 5500	
b	width of the designing member	12	20
d	depth of the designing member	20	38
ϕ	flexural reduction factor	0.9	0.7

4-5.3 Proposed D-H-FRP rebar model 1

Objective Function: Minimize:

$$Z = sc_{\text{IM-Carbon}} v_{\text{IM-Carbon}} + sc_{\text{SM-Carbon}} v_{\text{SM-Carbon}} + sc_{\text{Kevlar-49}} v_{\text{Kevlar-49}} + sc_{\text{Steel}} v_{\text{Steel}} + sc_{\text{resin}} v_{\text{resin}} \quad \text{.....(4-23)}$$

Subjected to

$$\begin{aligned}
&\text{(I)} && v_{\text{IM-Carbon}} + v_{\text{SM-Carbon}} + v_{\text{Kevlar-49}} + v_{\text{steel}} + v_{\text{resin}} = 1 \\
&\text{(II)} && v_{\text{resin}} \geq 0.1 \\
&\text{(III)} && \sigma_{\text{comp2}} \leq \sigma_{\text{comp3}} \leq \sigma_{\text{comp4}} \\
&\text{(IV)} && \mu_{\phi} = \frac{1}{2}\left(\frac{E_{\text{total}}}{E_{\text{elastic}}} + 1\right) \geq 3.0 \\
&\text{(V)} && M_n \geq \frac{M_u}{\phi}\ ^{1} \text{ at } \varepsilon_{\text{IM-Carbon}}\big|_{\text{Ultimate}} \\
&\text{(VI)} && \beta_{\text{T}} \geq 3.5 \\
&\text{(VII)} && \varepsilon_{\text{Kevlar-49}} \geq 0.85\varepsilon_{\text{Kevlar-49}}\big|_{\text{Ultimate}} \\
&\text{(VIII)} && \Delta \leq \frac{L}{360} \text{ (for beams)} \\
&\text{(IX)} && v_{\text{steel}} = 0.2\ ;\ v_{\text{IM-Carbon}} > 0\ ;\ v_{\text{SM-Carbon}} > 0\ ;\ v_{\text{Kevlar-49}} > 0
\end{aligned} \quad \text{.....(4-24)}$$

where:

$$\sigma_{\text{comp2}} = \left(E_{\text{IM-Carbon}} v_{\text{IM-Carbon}} + E_{\text{SM-Carbon}} v_{\text{SM-Carbon}} + E_{\text{Kevlar-49}} v_{\text{Kevlar-49}}\right)\varepsilon_{\text{IM-Carbon}} + \sigma_y v_{\text{steel}} \quad \text{.....(4-25)}$$

$$\sigma_{\text{comp3}} = \left(E_{\text{SM-Carbon}} v_{\text{SM-Carbon}} + E_{\text{Kevlar-49}} v_{\text{Kevlar-49}}\right)\varepsilon_{\text{SM-Carbon}} + \sigma_y v_{\text{steel}} \quad \text{.....(4.26)}$$

$$\sigma_{\text{comp4}} = \left(E_{\text{Kevlar-49}} v_{\text{Kevlar-49}}\right)\varepsilon_{\text{Kevlar-49}} + \sigma_y v_{\text{steel}} \quad \text{.....(4-27)}$$

[1] within ± 1%.

4-5.4 Proposed D-H-FRP rebar model 2

Objective Function: Minimize

$$Z = sc_{\text{IM-Carbon}} v_{\text{IM-Carbon}} + sc_{\text{SM-Carbon}} v_{\text{SM-Carbon}} + sc_{\text{Kevlar-49}} v_{\text{Kevlar-49}} + sc_{\text{E-Glass}} v_{\text{E-Glass}} + sc_{\text{resin}} v_{\text{resin}} \quad \text{.....(4-28)}$$

Subjected to

$$\begin{aligned}
&\text{(I)} && v_{\text{IM-Carbon}} + v_{\text{SM-Carbon}} + v_{\text{Kevlar-49}} + v_{\text{E-Glass}} + v_{\text{resin}} = 1 \\
&\text{(II)} && v_{\text{resin}} \geq 0.1 \\
&\text{(III)} && \sigma_{\text{comp1}} \leq \sigma_{\text{comp2}} \leq \sigma_{\text{comp3}} \leq \sigma_{\text{comp4}} \\
&\text{(IV)} && \mu_{\phi} = \frac{1}{2}\left(\frac{E_{\text{total}}}{E_{\text{elastic}}} + 1\right) \geq 3.0 \\
&\text{(V)} && M_n \geq \frac{M_u}{\phi}\ ^{1} \text{ at } \varepsilon_{\text{IM-Carbon}}\big|_{\text{Ultimate}} \\
&\text{(VI)} && \beta_{\text{T}} \geq 3.5 \\
&\text{(VII)} && \varepsilon_{\text{E-Glass}} \geq 0.85\varepsilon_{\text{E-Glass}}\big|_{\text{Ultimate}} \\
&\text{(VIII)} && \Delta \leq \frac{L}{360} \text{ (for beams)} \\
&\text{(IX)} && v_{\text{IM-Carbon}} > 0\,;\ v_{\text{SM-Carbon}} > 0\,;\ v_{\text{Kevlar-49}} > 0\,;\ v_{\text{E-Glass}} > 0
\end{aligned} \quad \text{.....(4-29)}$$

where

$$\sigma_{\text{comp1}} = \left(E_{\text{IM-Carbon}} v_{\text{IM-Carbon}} + E_{\text{SM-Carbon}} v_{\text{SM-Carbon}} + E_{\text{Kevlar-49}} v_{\text{Kevlar-49}} + E_{\text{E-Glass}} v_{\text{E-Glass}}\right) \times \varepsilon_{\text{IM-Carbon}} \quad \text{.....(4-30)}$$

$$\sigma_{\text{comp2}} = \left(E_{\text{SM-Carbon}} v_{\text{SM-Carbon}} + E_{\text{Kevlar-49}} v_{\text{Kevlar-49}} + E_{\text{E-Glass}} v_{\text{E-Glass}}\right)\varepsilon_{\text{SM-Carbon}} \quad \text{.....(4-31)}$$

$$\sigma_{\text{comp3}} = \left(E_{\text{Kevlar-49}} v_{\text{Kevlar-49}} + E_{\text{E-Glass}} v_{\text{E-Glass}}\right)\varepsilon_{\text{Kevlar-49}} \quad \text{.....(4-32)}$$

$$\sigma_{\text{comp4}} = \left(E_{\text{E-Glass}} v_{\text{E-Glass}}\right)\varepsilon_{\text{E-Glass}} \quad \text{.....(4-33)}$$

[1] within ± 1%.

4-6 Ductility

Ductility can be defined as an increase in deformation without an increase in capacity. Excessive deformations give warning to the occupants that failure of the structure is expected to happen. Carbon, Aramid, and Glass fibers have very high tensile strength; however, they are undesirable since no ductility is evident due to their linear elastic properties. In order to over come this problem, an "artificial" technique of using multi-layers of different polymer fiber properties is suggested with the condition that after the failure of the first layer, the remaining layer or layers should have the capability of carrying the load until we reach the desired ductility. For concrete beam members reinforced with FRP rebars, ductility index μ will be used to evaluate ductility. Most common ductility indices are given in terms of one of these three: curvatures, rotations, or deflections $\mu_\phi = \frac{\phi_u}{\phi_y}$, $\mu_\theta = \frac{\theta_u}{\theta_y}$, $\mu_\Delta = \frac{\Delta_u}{\Delta_y}$ or respectively. The subscript y stands for yielding, and subscript u stands for ultimate. However, since FRP rebars do not yield, the conventional definition of ductility cannot be used.

For non-yielding materials, Naaman and Jeong (1995) proposed a new definition to calculate ductility index in terms of the ratio of the total energy to the elastic energy based on perfectly elasto-plastic behavior. The energy terms were obtained from the area under the load deflection curves as follows:

$$\mu = \frac{\Delta u}{\Delta y} = \frac{1}{2}\left(\frac{E_{\text{total}}}{E_{\text{elastic}}} + 1\right) \qquad \text{.....(4-34)}$$

where

E_{total} : the total energy computed as the area under the load deflection curve.

E_{elastic} : the elastic energy which is part of the total energy.

Figure (4-9) below shows these terms

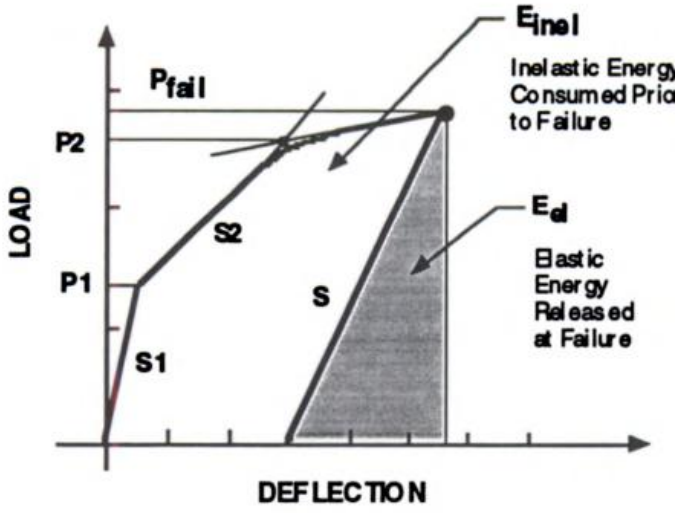

Figure (4-9): Load-deflection curve with more than one slope (Naaman and Jeong, 1995).

In this work, however, ductility index will be calculated from the moment curvature curve proposed by Naaman and Jeong (1995) using the following equation:

$$\mu_\phi = \frac{\phi u}{\phi y} = \frac{1}{2}\left(\frac{E_{\text{total}}}{E_{\text{elastic}}} + 1\right) \qquad \text{.....(4-35)}$$

Maghsoudi and Bengar (2010) found that ductility index of 3.0 is an acceptable lower bound for reinforced concrete continuous beams strengthened with carbon fiber reinforced polymer CFRP sheets. On the other hand, Shin, Kang, Ahn, and Kim (2010) sought a ductility index of 3.0 and above for a double reinforced beam and 2.0 and above for singly reinforced beam reinforced with conventional steel and ultra high strength concrete. In this work, the minimum acceptable ductility index has been set to 3.0. See Figure (8-2) in section 8-2.2 and observation # 2 from the same section.

4-7 FRP Rebar Bonding to Concrete

FRP bars with a sand-coated exterior have been shown to develop a satisfactory bond to concrete (Bank, 2006). Quayyum, (2010) studied the behavior and failure modes of FRP rebars with different type of surfaces. Using a braided layer of FRP material is another method to develop such bond (Somboonsong, 1998), but it is 10 times more expensive than pultrusion. Throughout this work it is assumed that the exterior layer is sand-coated for bonding and bond is adequate. Figure (4-10) shows different surface textures of FRP rebars.

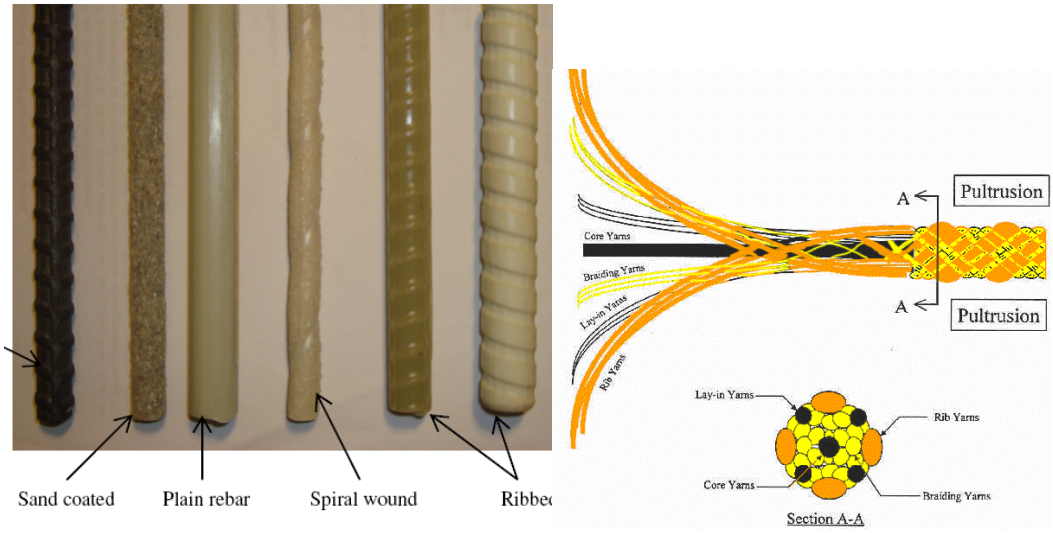

Figure (4-10): Different types of commercial available FRP rebar and braided FRP rebar (Quayyum, 2010) (Somboonsong, 1998)

Chapter Five

Structural Reliability

For good design of structures and their components, a number of aspects like strength, performance, safety, serviceability, and durability should be satisfied. A desirable level of reliability of the structure should be reached in order to account for uncertainties. Sources of uncertainties are applied loads (*S*) and resistance/capacity parameters (*R*). Uncertainties in structural resistance/capacity include mechanical properties of the materials, and geometry of the structure. In civil engineering, however uncertainties are accounted for by using a probabilistic evaluation of reliability. All uncertain parameters should identified and quantified using the aid of random variables (RV)s.

In civil engineering, due to direct involvement with the public, acceptable levels of capacity adequacy, or of risk of failure, are required. An unreliable structure is in a state which it does not fulfill design requirements related to its function and desirable performance. Failure may entail a collapse of the structure, a deficiency in structural resistance, or unfulfilled service demands of the structure, i.e. excessive deformations, excessive vibrations, etc. Structures usually have a number of possible failure scenarios. For most of the structures it is impossible to examine all possible failure modes. Therefore, representative failure scenarios have to be chosen. The analysis usually includes an estimation of structural reliability with respect to specified failure modes. All modes must be treated separately. Thus, reliability of a structure is the probability that the system will not reach a specified failure mode related to a specified limit state during a specified period of time (Lutomirska and Nowak. 2009).

5-1 Common Statistical Parameters

In order to describe a random variable, the probability distribution that best fits that random variable must be identified, as well as the parameters of that distribution. These parameters are generally mean value, variance/standard deviation, and bias factor.

- Mean

The mean μ or expected value of *X*, is a measure of central tendency in the data. The mean can be calculated by taking the first central moment. For continuous random variables with *probability density function* PDF $f_X(x)$, the mean can be calculated as

$$E(X) = \mu_X = \int_{-\infty}^{\infty} x\, f_X(x)dx \qquad \text{.....(5-1)}$$

and for discrete random variables with *probability mass function* $p_X(x_i)$

$$E(X) = \mu_X = \sum_{\text{all } x_i} x_i\, p_X(x_i) \qquad \text{.....(5-2)}$$

- Variance

The variance σ^2 of *X*, is a measure of spread in the data about the mean. The variance can be calculated by taking the second central moment. For continuous random variables, the variance can be calculated as

$$\text{Var}(X) = \int_{-\infty}^{\infty} (x - \mu_X)^2\, f_X(x)dx \qquad \text{.....(5-3)}$$

and for discrete random variables

$$\mathrm{Var}(X) = \sum_{\text{all } x_i} (x_i - \mu_X)^2 \, p_X(x_i) \qquad \text{.....(5-4)}$$

- Standard Deviation

The standard deviation σ of a random variable is the square root of the variance.

- Bias Factor

The bias factor λ of a random variable X, can be calculated as

$$\text{Bias factor} = \lambda = \frac{\text{Mean Value}}{\text{Nominal Value}} = \frac{\mu_X}{N_X} \qquad \text{.....(5-5)}$$

- Coefficient of Variation

The coefficient of variation c.o.v or δ of a random variable X, is simply the standard deviation divided by the mean.

$$\delta = \text{c.o.v} = \frac{\sigma}{\mu} \qquad \text{.....(5-6)}$$

Some structural reliability references use the symbol V for the coefficient of variation.

5-2 Probability Distributions

Some commonly used probability distributions in structural reliability are: Normal, Log-Normal, Gamma, and some kind of extreme value such as the Type I Extreme Value Distribution (Gumbel).

5-2.1 Normal Distribution

The normal distribution (Gaussian distribution) is the most commonly used probability distribution in civil engineering. The PDF of this distribution can be expressed as

$$f_X(x) = \frac{1}{\sigma_x\sqrt{2\pi}}\exp\left[-\frac{1}{2}\left(\frac{x-\mu_X}{\sigma_X}\right)^2\right],\ -\infty < x < \infty \qquad \text{.....(5-7)}$$

the corresponding cumulative distribution function CDF can be expressed as

$$F_X(x) = \int_{-\infty}^{x}\frac{1}{\sigma_x\sqrt{2\pi}}\exp\left[-\frac{1}{2}\left(\frac{x-\mu_X}{\sigma_X}\right)^2\right]dx \qquad \text{.....(5-8)}$$

a special form of normal distribution is when the mean equals 0 and the standard deviation equals 1. This form is known as the *standard normal distribution*. The PDF and CDF of a standard normal distribution are $\phi(s)$, and $\Phi(s)$ respectively. The transformation variable S can be calculated as

$$\frac{S-0}{1} = \frac{X-\mu_X}{\sigma_X} \Rightarrow S = \frac{X-\mu_X}{\sigma_X} \qquad \text{.....(5-9)}$$

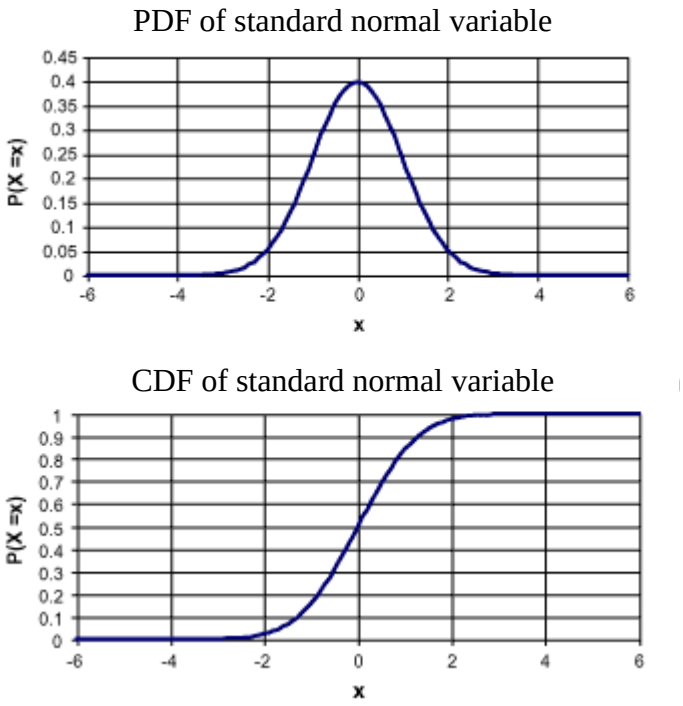

Figure (5-1): Typical shapes of PDF and CDF for a normal distribution.

5-2.2 Log-Normal Distribution

If a random variable has a lognormal distribution, then its natural logarithm has a normal distribution. This distribution is very useful in engineering applications where a random variable cannot have negative values due to the physical nature of the problem. The PDF of a lognormal variable is giving by

$$f_X(x) = \frac{1}{\sqrt{2\pi}\,\zeta_X\, x}\exp\left[-\frac{1}{2}\left(\frac{\ln x - \lambda_x}{\zeta_x}\right)^2\right],\ 0 \le x < \infty \qquad \text{.....(5-10)}$$

where λ_x and ζ_x are the parameters of lognormal distribution

It can be proven that λ_x and ζ_x can be related to the mean μ_x and the standard deviation σ_x, respectively as shown in equation (5-11) and (5-12)

$$\lambda_x = E(\ln x) = \ln \mu_x - \frac{1}{2}\zeta_x^2 \qquad \text{.....(5-11)}$$

$$\zeta_x^2 = \mathrm{Var}(\ln x) = \ln\left[1 + \left(\frac{\sigma_x}{\mu_x}\right)^2\right] = \ln\left(1 + \delta_x^2\right) \qquad \text{.....(5-12)}$$

Note to distinguish between the lognormal parameter λ_x and bias factor λ.

This type of distribution has been suggested for the yield strength of steel and for calculating moment capacity of a cross-sectional area of a structural member (Melchers, 1999) although other distributions could be used for this physical property.

5-2.3 The Type I Extreme Value Distribution (Gumbel)

In many engineering applications, the extreme values of random variables are of special interest. The CDF and PDF forms of type I of the distribution of largest value, known as Gumbel, can be expressed in equations (5-13) and (5-14) respectively

$$F_{X_n}(x_n) = \exp\left[-e^{-\alpha_n(y_n - u_n)}\right] \qquad \text{.....(5-13)}$$

$$f_{X_n}(x_n) = \alpha_n e^{-\alpha_n(y_n - u_n)} \exp\left[-e^{-\alpha_n(y_n - u_n)}\right], \quad -\infty < x_n < \infty \qquad \text{.....(5-14)}$$

where α_n and u_n are parameters of the distribution and are related to the mean and standard deviation as shown

$$\alpha_n = \frac{1}{\sqrt{6}}\left(\frac{\pi}{\sigma_{X_n}}\right), \text{ and } u_n = \mu_{X_n} - \frac{0.5772}{\alpha_n}$$

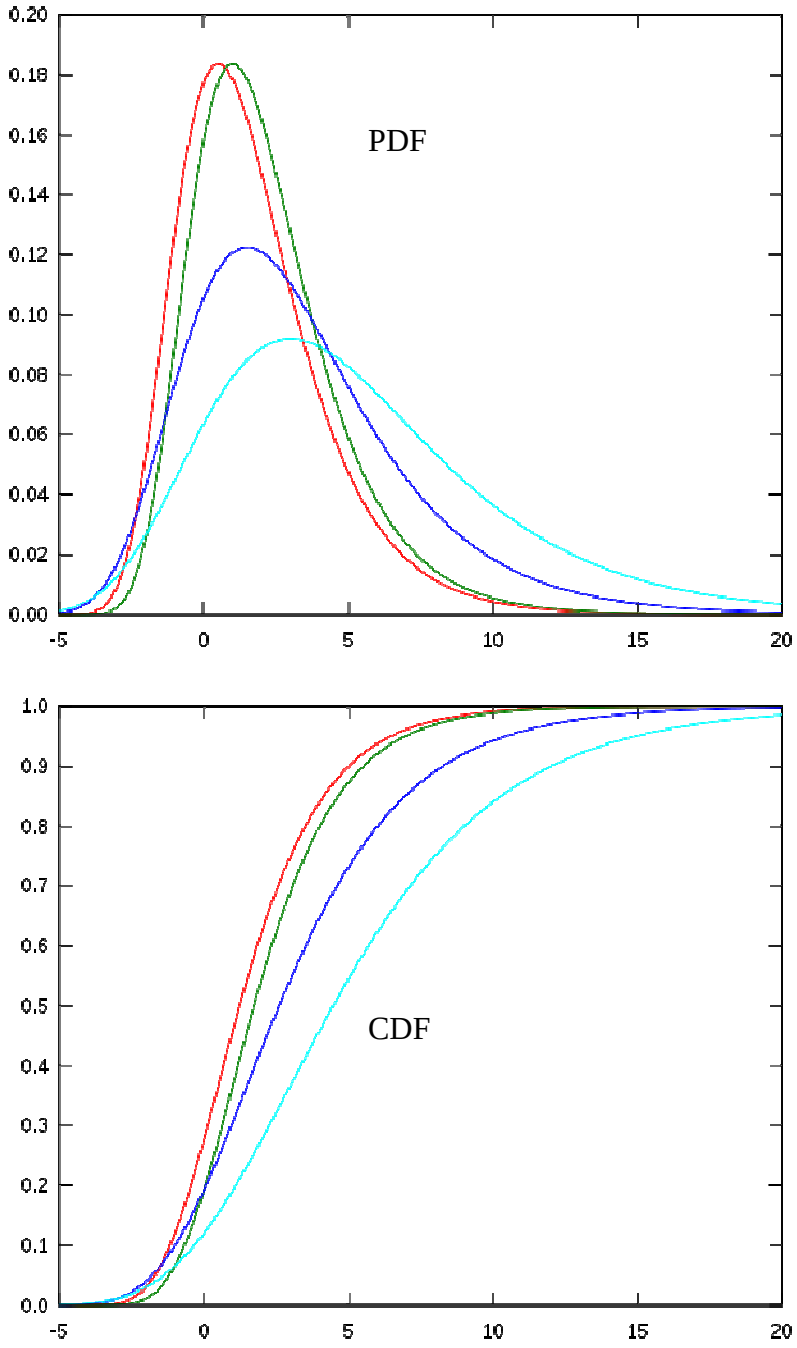

Figure (5-2): Typical shapes of PDF and CDF of Type I Extreme value distribution (Gumbel) for different values.

In this work the Type I Extreme Value Distribution (Gumbel) has been used to model the live load when present.

Tables (5-1) and (5-2), at the end of the chapter, show the statistical properties of resistance and load RVs used in this work which are adopted from Nowak and Collins (2000), Nowak and Szerszen (2003), Eamon and Rais-Rohani (2008), Ellingwood, MacGroger, Galambos, and Cornell (1980), Melchers (1999), Nowak (1999), Lutomirska (2009), and finally Mertz, Kulicki, Prucz, Clancy, and Nowak (2007).

5-3 The Concept of Reliability-Based Design

Figure (5-3) shows a case of two continuous variables resistance/capacity R and load S and their corresponding PDF $f_R(r)$ and $f_S(s)$, respectively. The shaded area, which is the area of overlap of the two curves, represents the probability of failure. In order to achieve an increasingly safe design, this area should be minimized by narrowing the shape of the curves and the two curves should be shifted away from each other. The nominal resistance R_N is usually k_R fractions of standard deviation σ_R below the mean value. The nominal load S_N is usually k_S fractions of standard deviation σ_S above the mean value.

$$R_N = \mu_R - k_R\sigma_R \qquad \text{.....(5-15)}$$

$$S_N = \mu_S + k_S\sigma_S \qquad \text{.....(5-16)}$$

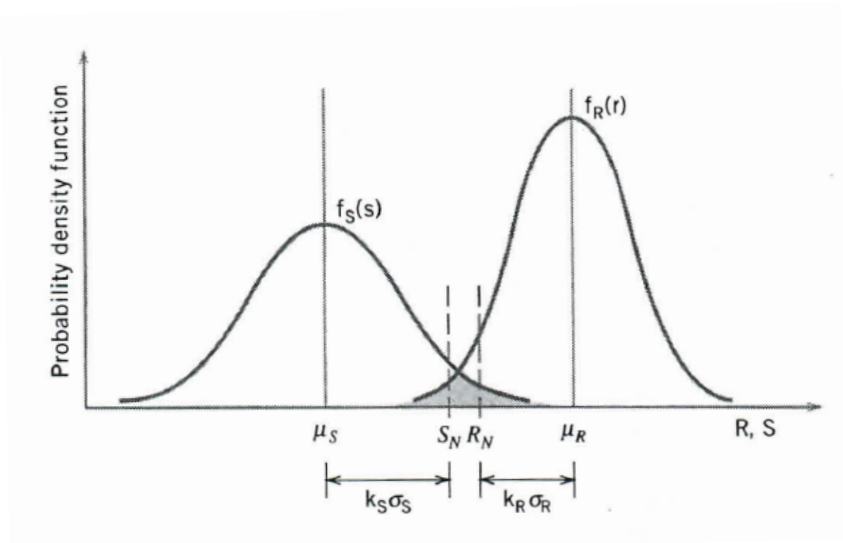

Figure (5-3): The concept of safe design and failure probability (Haldar and Mahadevan, 1999).

5-4 Limit State Function

When the limit state function g(x), as a function of RVs (x), is set to zero, it defines the boundary between safe/desirable and unsafe/undesirable of the specific structural performance state measured. Limit states could be in terms of ultimate capacity, serviceability, fatigue, or any other criteria which can be quantified. If all loads are incorporated into one single variable (S) and the resistance of the structure is incorporated into one single variable (R) then, the limit state function takes the form of the following equation:

$$g(R,S) = R - S \qquad \text{.....(5-17)}$$

The probability of the safe/desired performance of a structure which is equal to the safety margin (p_s) and the probability of an unsafe/undesired performance of a structure which is equal to the probability of failure (p_f) can be related to each other by $p_f + p_s = 1.0$. Figure (5-4) shows the limit state function of two random variables R and S.

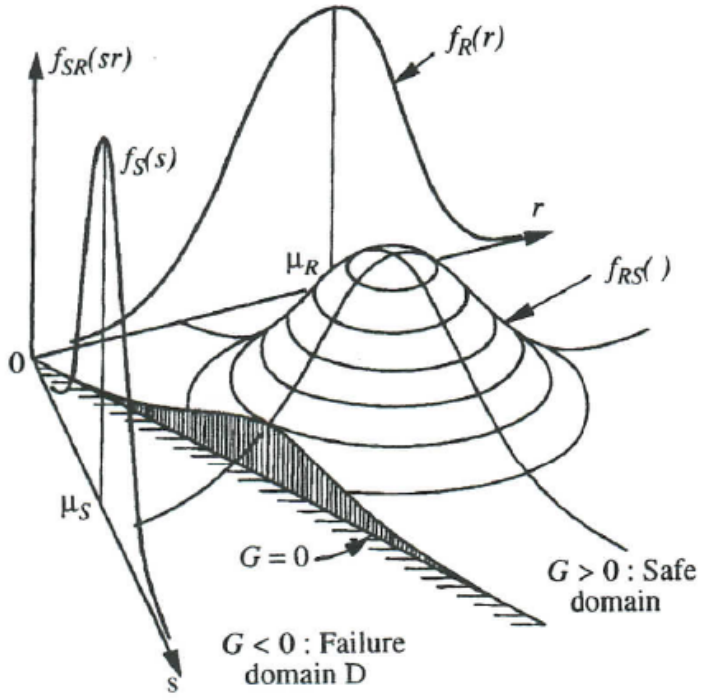

Figure (5-4): Limit state function g(x) of two continuous random variables (Melchers, 1999).

The probability of failure (p_f) can be calculated in terms of the PDF of two random variables, capacity/resistance (R) and the load (S); the joint probability distribution of all random variables; or the CDF of capacity/resistance and PDF of the load. Equation (5-18) shows the last case when R and S are independent random variables.

$$p_f = P(R - S \le 0) = \int_0^{\infty} F_R(x)\, f_s(x) dx \qquad 0 < x_n < \infty \qquad \text{.....(5-18)}$$

5-5 Reliability Index

Reliability index, β, can be defined as the shortest distance from the origin to the limit state function in a system of reduced variables coordinates (Hasofer and Lind, 1974). Using Lagrange Multipliers or analytic geometry we can calculate the shortest distance

from a line $ax + by + k = 0$ and the origin as $\frac{k}{\sqrt{a^2 + b^2}}$. Then, if g(x) is the simple linear limit state given by equation (5-17) above, and *R* and *S* are normally distributed and uncorrelated

$$\beta = \frac{\mu_R - \mu_S}{\sqrt{\sigma_S^2 + \sigma_S^2}} \qquad \text{.....(5-19)}$$

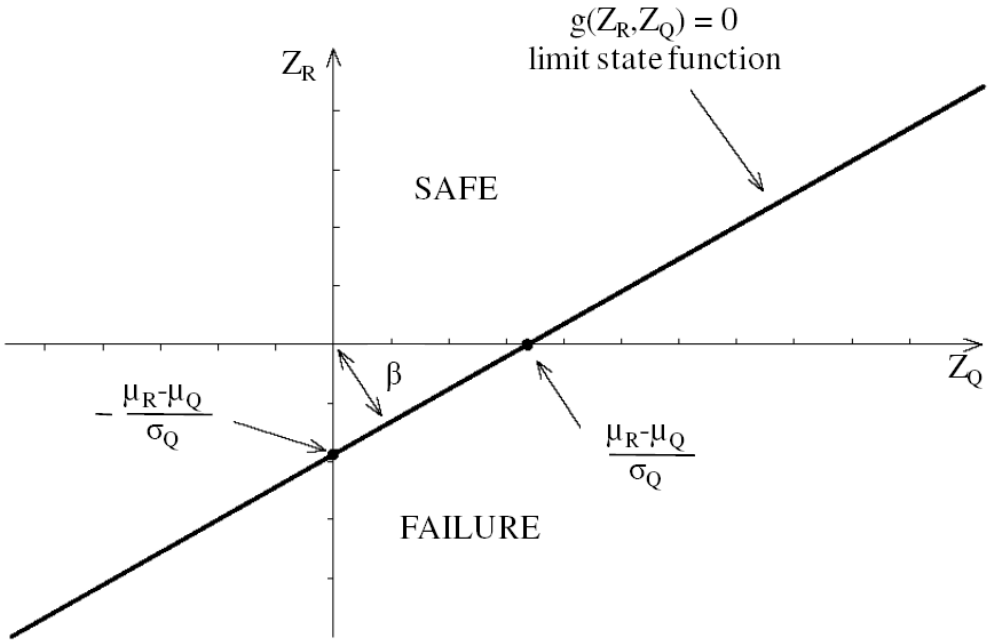

Figure (5-5): Reliability index (Nowak and Collins, 2000)[1].

If *R* and *S* are correlated then the reliability index β can be calculates as (Harr, 1997)

$$\beta = \frac{\mu_R - \mu_S}{\sqrt{\sigma_S^2 + \sigma_S^2 - 2\rho\sigma_S\sigma_R}} \qquad \text{.....(5-20)}$$

In reduced coordinates, all variables should expressed in dimensionless terms using the following standard normal transformation equations:

[1] In this dissertation, *S* is equivalent to *Q* in the reference.

$$Z_R = \frac{R - \mu_R}{\sigma_R} \qquad \text{.....(5-21)}$$

$$Z_S = \frac{R - \mu_S}{\sigma_S} \qquad \text{.....(5-22)}$$

The probability of failure (p_f) can be calculated in terms of reliability index β, and the standard normal distribution function Φ, using the following formula .

$$p_f = \Phi(-\beta) \qquad \text{.....(5-23)}$$

This equation can give exact results if the β calculated represents a true measure of reliability. Otherwise it provides only an approximation. In this research this equation has been used to calculate the reliability index.

5-6 Monte-Carlo Simulation Technique

Monte Carlo simulation technique is the most commonly used technique in simulation. In this method, the computer generates a set of numbers that simulates a phenomenon without conducting real experiments. This theoretical simulation is called numerical or computer experimentation (Lutomirska, 2009). In this dissertation, Monte Carlo simulation has been used to calculate the probability of failure and eventually the reliability index β by following these steps:

1- Define the problem in terms of all random variables.
2- Quantify the probabilistic characteristics of all random variables in terms of PDFs and the corresponding parameters.
3- Identify the limit state function $g(x)$ in terms of all random variables
4- Generate random numbers u_i between 0 and 1 for each random variable. In Visual Basic for Application VBA, this function can be performed using command RND.

5- The numbers generated from above will be entered into the appropriate CDF. For normal and log-normal distributions, the standard normal random number is calculated using the equation

$$s_i = \Phi^{-1}(u_i) \qquad \text{.....(5-24)}$$

In Visual Basic for Application VBA, this function can be performed using command

WorksheetFunction.NormSInv(ui) for normal distribution, and
WorksheetFunction.LogInv(ui) for log-normal distribution.

Then the value s_i will be transformed to a normal or lognormal variant using the following transformation equation

$z_i = s_i \sigma_X + \mu_X$ for normal distribution, or
$z_i = s_i \xi_X + \lambda_X$ for log-normal distribution

6- substitute z_i in their corresponding distributions in the limit state function.

7- calculate the probability of failure using the equation.

$$p_f = \frac{\text{number of failures}}{\text{total number of simulations}} = \frac{\text{number of times g(x) < 0}}{\text{total number of simulated g()}}$$

.....(5-25)

or

$$p_f = \frac{1}{N}\sum_{j=1}^{N} I\left[g(\hat{\boldsymbol{x}}_j) \le 0\right] \qquad \text{.....(5-26)}$$

where $I[\ ]$ is an indicator, which equals to 1 if [ ] is 'true' and 0 if [ ] is 'false', and $g(\hat{\boldsymbol{x}}_j)$ is the limit state function of the j^{th} vector of random observations. The symbol ^ means 'generated' not 'true'.

5-7 Moment Capacity in Terms of Random Variables

If concrete tensile force is ignored, which plays a minor role in section resistance, an expression of the moment capacity of the concrete reinforced cross section in terms of random variables which represents R in the limit state function g(x) can be developed. For proposed rebar 1, the resistance moment in terms of random variables is

$$M_c = \left[d_e - K_2 \frac{\left(v_{f_1} + v_{f_2} + v_{f_3} + v_m\right)A_T}{K_1 \cdot f_c' \cdot b} \left\{\left(v_{f_1}E_{f_1} + v_{f_2}E_{f_2} + v_{f_3}E_{f_3} + v_m E_m\right)\varepsilon_{f_1} + v_s \cdot f_y\right\}\right]$$
$$K_1 \cdot f_c' \cdot b \left[\frac{\left(v_{f_1} + v_{f_2} + v_{f_3} + v_m\right)A_T}{K_1 \cdot f_c' \cdot b} \left\{\left(v_{f_1}E_{f_1} + v_{f_2}E_{f_2} + v_{f_3}E_{f_3} + v_m E_m\right)\varepsilon_{f_1} + v_s \cdot f_y\right\}\right]$$

.....(5-27)

For proposed rebar 2 the resistance moment in terms of random variables is

$$M_c = \left[d_e - K_2 \frac{\varepsilon_{f_1}}{K_1 \cdot f_c' \cdot b} \left(v_{f_1}E_{f_1} + v_{f_2}E_{f_2} + v_{f_3}E_{f_3} + v_{f_4}E_{f_4} + v_m E_m\right)\left(v_{f_1} + v_{f_2} + v_{f_3}\right.\right.$$
$$\left.\left. + v_{f_4} + v_m\right)A_T \right] K_1 \cdot f_c' \cdot b \left[\frac{\varepsilon_{f_1}}{K_1 \cdot f_c' \cdot b} \left(v_{f_1}E_{f_1} + v_{f_2}E_{f_2} + v_{f_3}E_{f_3} + v_{f_4}E_{f_4}\right)\left(v_{f_1} + v_{f_2} + v_{f_3} + v_{f_4}\right)A_T \right]$$

.....(5-28)

where

v_{f_1} : volume fraction of IM-Carbon fiber layer

v_{f_2} : volume fraction of SM-Carbon fiber layer

v_{f_3} : volume fraction of Kevlar-49 fiber

v_{f_4} : volume fraction of E-glass fiber

v_s : volume fraction of steel

v_m : volume fraction of matrix/resin

E_{f_1} : young's modulus of IM-Carbon fiber layer

E_{f_2} : Young's modulus of SM-Carbon fiber layer

E_{f_3} : Young's modulus of Kevlar-49 fiber

E_{f_4} : Young's modulus of E-glass fiber

E_m : Young's modulus of matrix/resin

f_y : Yield stress of steel grade 60

d_e : Effective depth of reinforcement

f_c' : Compressive strength of concrete

ε_{f_1} : Failure strain of IM-Carbon fiber

A_T :Total area of reinforcements

K_1, K_2 : Hognastd's coefficients (constants)

b : Width of the cross section (for bridge deck it is constant and equal to 1, but for beams/girders it is a RV)

in both cases the units of M_c is (k-in). 200,000 cycles were used for all Monte-Carlo simulations. It has been observed that increasing the number of simulations did not change the solution.

Table (5-1): Resistance Random Variables.

	Description	Distribution Type	δ = c.o.v	Bias Factor (λ)
$v_{\text{IM−Carbon}}$	Volume fraction of IM-Carbon layer	Normal Distribution	0.05	1.0
$v_{\text{SM−Carbon}}$	Volume fraction of SM-Carbon layer	Normal Distribution	0.05	1.0
$v_{\text{Kevlar-49}}$	Volume fraction of Kevlar-49	Normal Distribution	0.05	1.0
$v_{E-Glass}$	Volume fraction of E-Glass	Normal Distribution	0.05	1.0
v_{Steel}	Volume fraction of steel	Normal Distribution	0.05	1.0
v_{resin}	Volume fraction of resin	Normal Distribution	0.05	1.0
$E_{\text{IM−Carbon}}$	Modulus of elasticity of Carbon-IM	Normal Distribution	0.045	1.0
$E_{\text{SM−Carbon}}$	Modulus of elasticity of Carbon-SM	Normal Distribution	0.045	1.0
$E_{\text{Kevlar-49}}$	Modulus of elasticity of Kevlar-49	Normal Distribution	0.045	1.0
$E_{E-glass}$	Modulus of elasticity of E-glass	Normal Distribution	0.045	1.0
E_{resin}	Modulus of elasticity of resin	Normal Distribution	0.045	1.0
σ_y	Yielding strength of steel	Lognormal Distribution	0.065	1.145
ε_{C_IM}	Strain failure of Carbon-IM	Normal Distribution	0.05	N/A[1]
f_c'	Compressive strength of concrete f_c' = 4500 psi (Bridge deck cast-in-place) …….. f_c' = 5500 psi (Beam/Girder cast-in-place) …….	Normal Distribution	0.042 0.05	1.14 1.14
d	Effective depth of the reinforced cross sectional Slab cast-in-place (bridge deck) …… Beam/Girder cast-in-place …….	Normal Distribution	 0.12 0.04	 0.92 0.99
b	Width of the reinforced cross section Beam/Girder	Normal Distribution	0.04	1.01

Table (5-2): Load Random Variables

[1] The mean value will be calculated from the factory supplier value "0.0045" according to $\varepsilon_{C\_IM} = \mu_{C\_IM} - 2\sigma_{C-IM}$ (2 standard deviation below the mean).

	Description	Distribution Type	c.o.v	Bias Factor (λ)
Bridge Deck				
DL own	Dead load of own slab weight (lb/ft^2)	Normal Distribution	0.1	1.05
DL FWS	Dead load of Asphalt future wearing surface (lb/ft^2)	Normal Distribution	0.25	1.0
DL par	Dead load of parapet (lb/ft^2)	Normal Distribution	0.1	1.05
LL-DT	Axel load of two 16 kips spaced at 6 feet	Gumbel Distribution	0.12	1.2
Beam/Girder				
DL	Dead load of the member (own weight + imposed)	Normal Distribution	0.1	1.0
LL	Live load on the member (based on 50-year live load)	Gumbel Distribution	0.23	N/A[1]

[1] A mean value will be used directly.

Chapter six

Design and Analysis of Structural Components

In this chapter the proposed chopped fiber D-H-FRP rebar reinforcements will be used in designing two structural components: a concrete bridge deck slab, and a concrete simply supported beam.

6-1 Bridge Deck

Figure (6-1) shows a typical 1-ft cross section of concrete bridge deck slab of thickness *h*. The cross section usual consists of

1- asphalt *future wearing surface FWS* of 2.5 inch. This is a non-structural component.
2- *integrated wearing surface IWS* of 0.5 inches. This is a non-structural component.
3- top cover C_{top}. AASHTO-LRFD *Bridge design Specifications* (2010) requires a minimum top cover of 2.5 inches for concrete that is exposed to deicing salt. The top cover may be decreased to 1.5 inch when epoxy-coated reinforcement is used. However, a clear top cover of 1.0 inch has been used on two FRP-reinforced bridge decks built in Wisconsin (Berg et al., 2006; Bank et al., 2006). In this work, the top cover is similarly set to 1.00 inch since a non corrodible and salt resistant reinforcement is being used.
4- top reinforcing bars. Reinforcing bars will be #6 for proposed rebar 1 and #7 for proposed rebar 2.

5- bottom reinforcing bars. Reinforcing bars will be #6 for proposed rebar 1 and #7 for proposed rebar 2[1].

6- bottom cover C_{bottom} which is usually 1 inch for an 8 inch-slab deck and 1.5 inches for an 8.5 inch-slab deck. In this work, the bottom cover is set to 1.00 inch.

The thickness of the concrete bridge deck slab is usually between 8-10 inches that includes the *IWS* and excludes the *FWS*. However, in this work the thickness *h* includes 8 inches of structural components including 0.5 of *IWS* non-structural component. Non-structural component means the specific component does not contribute to the structural strength of the member or cross section and should be treated and added as a dead load only.

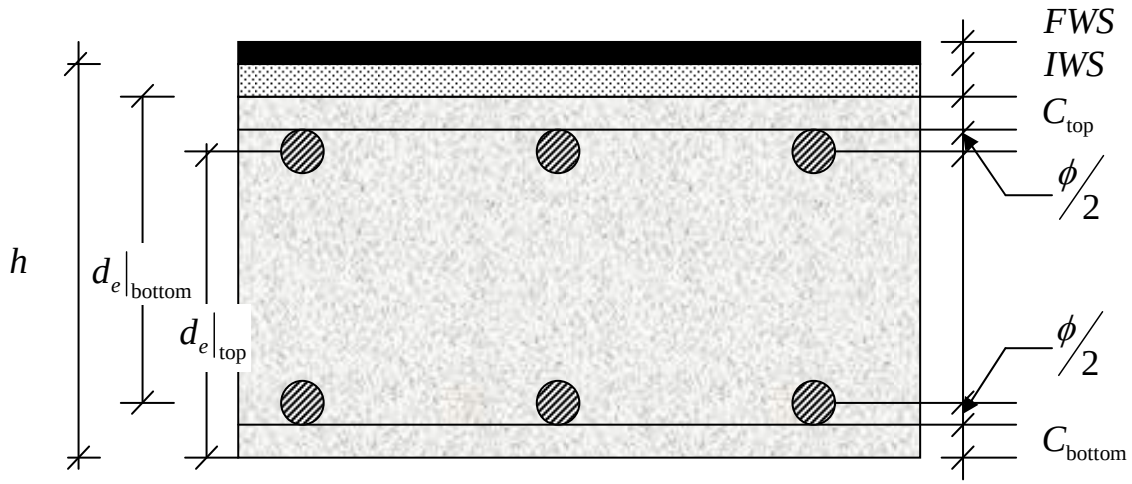

Figure (6-1): A typical 1 ft cross section of concrete bridge deck slab.

Where the effective depths are calculated using the following equations:

$$d_e\big|_{bottom} = h - \frac{\phi}{2} - C_{bottom} - IWS \qquad \text{.....(6-1)}$$

$$d_e\big|_{top} = h - \frac{\phi}{2} - C_{top} - IWS \qquad \text{.....(6-2)}$$

[1] These two sizes and very common bar sizes in concrete bridge deck design.

Table (6-1) shows the dimensions used throughout this work and the type of components whether there are structural or non-structural.

Table (6-1): Assumed dimensions for the concrete bridge deck slab.

Component type	description	Dimension (in)	Rebar type
Non-structural	Asphalt future wearing surface FEW	0.25	
	Integrated wearing surface IWS	0.5	
Structural	Overall depth	8.0	
	Top cover	1.0	
	Rebar diameter ϕ	0.75 0.875	for #6 for #7
	Bottom cover	1.00	
Effective depths	$d_e\|_{\text{bottom}}$	6.0625 6.125	for #7 for #6
	$d_e\|_{\text{top}}$	6.0625 6.125	for #7 for #6

The AASHTO-LRFD Specifications (2010) allow five methods of deck design. These methods are:

1- The equivalent strip method,
2- The empirical design method.
3- The yield-line method which is excellent for extreme-event limit states,
4- The refined method using finite element method or finite strip methods,
5- The grillage method.

In this study, the AASHTO equivalent strip method will be used to perform the bridge deck analysis and design. A five-bay bridge deck with two 4.5 ft cantilevers, one at each end, will be considered for design as shown in Figure (6-2). Different girder spacing S will be used: 6, 8, 9, 10, and 12 ft. The bridge deck has concrete compressive strength f_c' of 4500 psi.

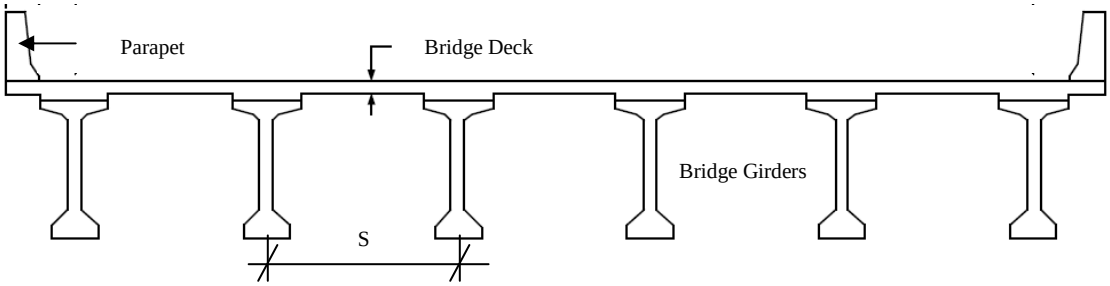

Figure (6-2): Five-bay bridge deck used in this work

6-1.1 Loads to Consider

- ***Dead Loads***

Three different components of dead load are considered in this work as shown in Figure (6-3):

1- The deck self weight (Q_{DC}) of thickness 8 inches plus 0.5 inch *IWS* of density γ_{con} = 0.145 k/ft^3 which covers the entire deck and will be considered as uniform distributed load

2- Asphalt future wearing surface (Q_{DW}) of thickness 2.5 inches and density $\gamma_{asphalt}$ = 0.140 k/ft^3 which covers the deck up to the two inside end parapets and will be considered as uniform distributed load

3- Parapet loads (Q_{DC}) close to the ends of the deck and will be considered as concentrated loads although it can be expressed as uniformly distributed load of 0.457 k/ft

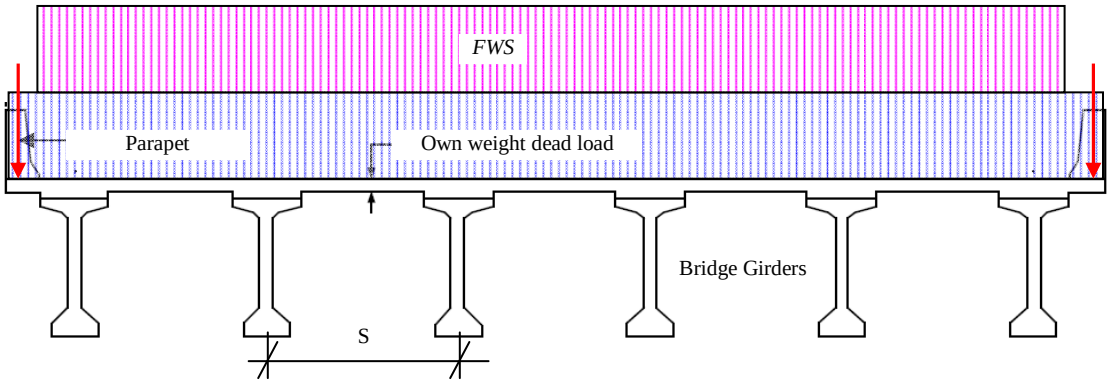

Figure (6-3): The three types of dead load considered in analyzing and designing the concrete bridge deck slab.

To analyze a bridge deck, the following steps are used:

1- Consider one unit width along the deck.
2- Place a uniformly distributed load of 1 k/ft over the entire bridge deck to represent the dead load of self weight.
3- Perform structural analysis to develop the moment diagram.
4- Place a uniformly distributed load of 1 k/ft over the entire bridge deck except where the parapets are to represent the dead load of asphalt future wearing surface.
5- Perform structural analysis to develop the moment diagram.
6- Place a concentrated load of 1 k on each side of the bridge deck where the centers of gravity of the parapets pass through.
7- Perform structural analysis to perform the moment diagram.
8- Multiply the ordinates from unit loading by real loading values.

Appendix (A) shows the analysis of the bridge deck for different girder spacing (S) and for different load types with values of 1 k/ft and 1 k. The moment diagrams were constructed using SAP2000 software (CSI, 1984).

- ***Live loads***

Two 16 kip wheel loads spaced 6 feet (LL) apart will be multiplied by the multiple presence factor of 1.2 since the number of design lanes considered is 1.0, which is the dominate case for the concrete bridge deck slab. Figure (6-4) shows a typical HL-93 truck axle load.

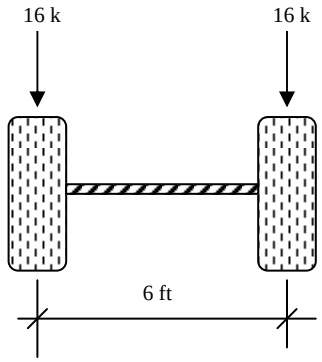

Figure (6-4): Typical HL-93 truck axel load to be used in bridge deck design.

- ***Impact load/ Dynamic effect***

In order to account for impact factor (IM), the live load should be multiplied by 1.33.

6-1.2 Design Limit State

The general expression in the AASHTO-LRFD *Bridge Specifications* (2010) that must be satisfied is given as

$$\sum \eta_i \gamma_i Q_i \le \phi R_n \qquad \text{.....(6-3)}$$

where

Q_i : force effect,

R_n : nominal resistance,

η_i : modification factor,

γ_i : statistically based load factor applied to the force effects, and

ϕ : statistically based load factor applied to the nominal resistance[1]

in the specifications, however, there are four types of limit states: strength, service, extreme events, and fatigue. In this study we will consider one strength limit state, specifically, Strength limit state I, which can be expressed by the following equation

$$\phi R_n = \gamma_p Q_{DC} + \gamma_p Q_{DW} + 1.75 Q_{LL+IM} \quad \text{.....(6-4)}$$

The load factors for the permanent loads, γ_p can be taken from Table (6-2). The factors are chosen to generate the highest load effect.

Table (6-2) Part from AASHTO-LRFD Bridge Specifications for load factors

Type of load	Load Factor	
	Maximum	Minimum
DC : component and attachments	1.25	0.90
DW: Wearing surface and utilities	1.5	0.65

6-1.3 Influence Function

The influence function represents the load effect at a point in the structure as a unit load moves along a path or over a surface. In case of a one-dimensional problem, this function is called an influence line. According to Barker and Puckett (2006), Two critical sections located at 40% and 50% of the first interior bay for positive moments are expected to be maxima, section (1-1) and (2-2) respectively, and one critical section located at the inner support of the first interior bay for negative moment is expected to be the maximum section (3-3), as shown in Figure (6-5).

[1] For conventional steel, this value is 0.9.

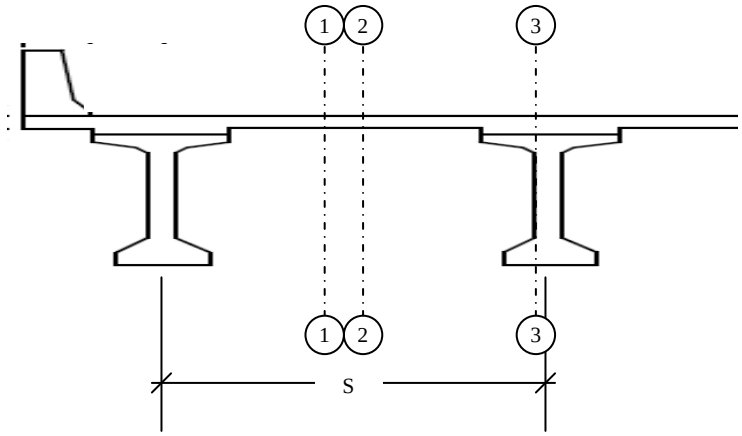

Figure (6-5): Locations where maximum positive and negative moments expected.

The influence functions for the three critical sections for the bridge deck considered are shown in Figure (6-6). This is a very crucial step since the analysis and design will be based on the constructed influence functions.

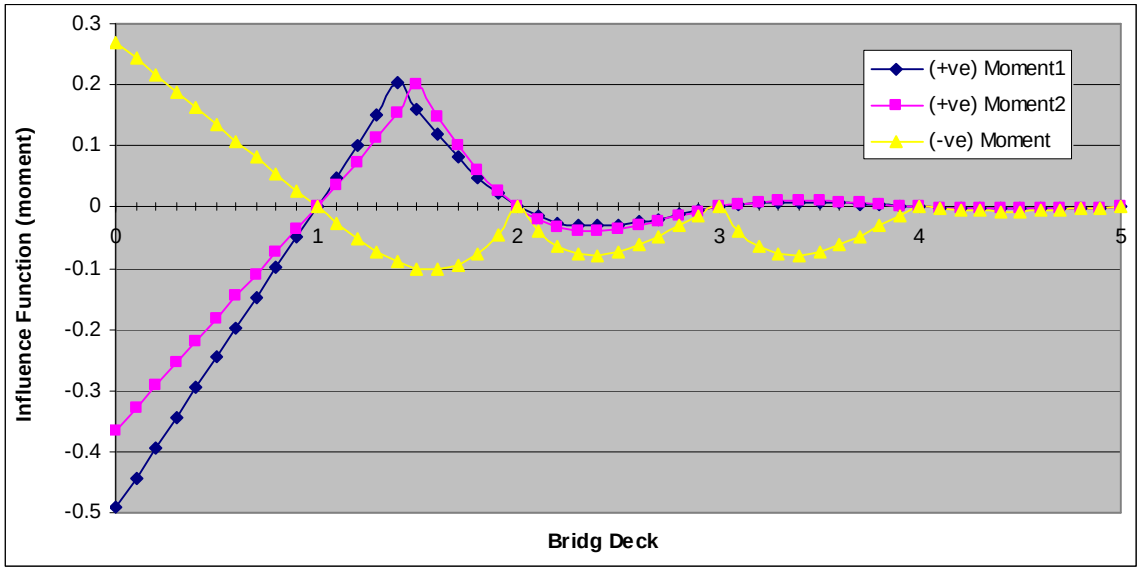

Figure (6-6): Influence function for bridge deck at sections (1-1), (2-2), and (3-3)

6-1.4 The Equivalent Strip Method

In this method, the deck slab may be considered as a one-way slab system since the aspect ratio, which is panel length divided by panel width, is large.

According to AASHTO-LRFD (2010) the strip width SW in inches for an interior panel can be calculated as

$$M^{+}: \mathrm{SW} = 26.0 + 6.6S \quad \text{.....(6-5)}$$

$$M^{-}: \mathrm{SW} = 48 + 3.0S \quad \text{.....(6-6)}$$

where *S* is the girder spacing of the bridge in feet. This method of design can be summarized as follows:

1- Construct the influence function for the critical sections mentioned earlier
2- Place the HL-93 truck axle load on the critical section then multiply moment values by 16 k. Figure (6-7) shows the expected locations for maximum positive and negative moments for a 9-ft girder spacing.
3- Multiply the above moments by girder spacing and divide by the strip width SW.

Finally, to get the required nominal capacity, use equation 6-4 as follows

$$R_n = \frac{\gamma_p Q_{DC} + \gamma_p Q_{DW} + 1.75 Q_{LL+IM}}{\phi}$$

Table (6-3) shows the maximum expected positive and negative moments at the three candidate sections induced from dead load components, while Table (6-4) shows the maximum expected positive and negative moments at the same sections induced from the HL-93 truck axle load.

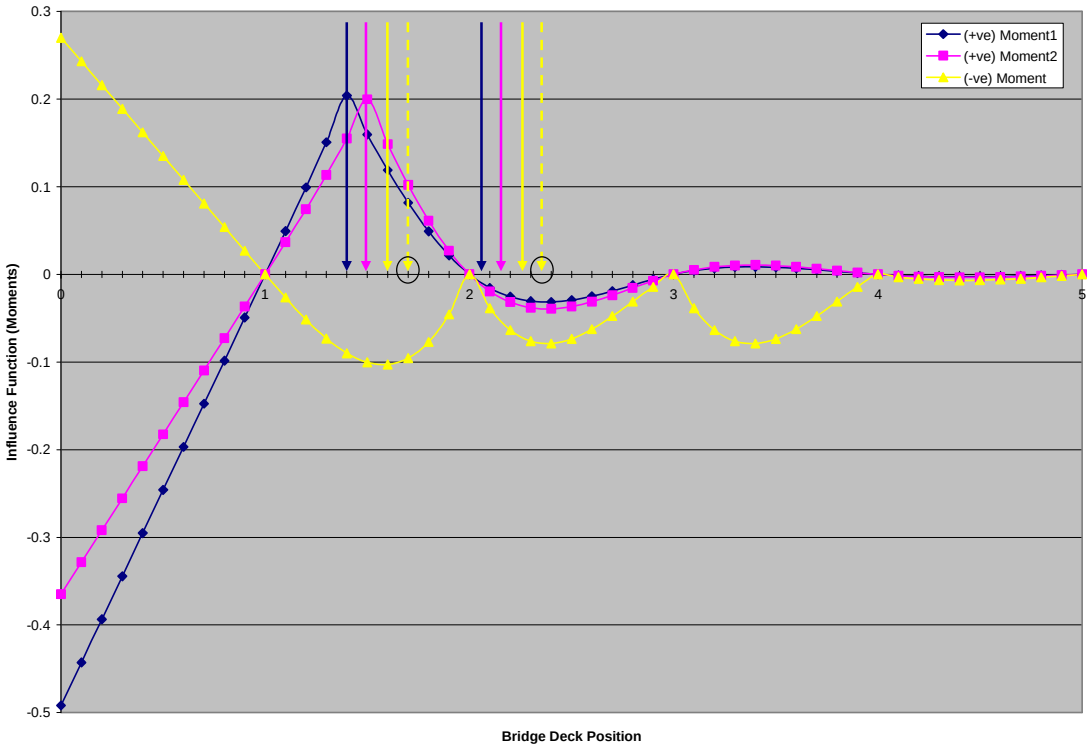

Figure (6-7): Expected locations for (+) and (–) moments for 9-ft girder spacing on the influence function diagram.

Table (6-3): Positive and negative moments for the three different dead load components at the three candidate sections.

	Unfactored moments (k-ft) from dead load bridge deck analysis		
	Self weight dead load	Asphalt FWS dead load	Parapet dead load
S = 6 ft			
Section 1-1	-0.217	0.00725	-0.877
Section 2-2	-0.112	0.02059	-0.65351
Section 3-3	-0.114	-0.07134	0.44786
S = 8 ft			
Section 1-1	-0.006	0.07018	-0.87287
Section 2-2	0.0863	0.079025	-0.65351
Section 3-3	-0.397	-0.15631	0.457
S = 9 ft			
Section 1-1	0.1164	0.10846	-0.87287
Section 2-2	0.216	0.11542	-0.64894
Section 3-3	-0.5694	-0.20793	0.457
S = 10 ft			
Section 1-1	0.262	0.15109	-0.87287
Section 2-2	0.3395	0.15515	-0.64894
Section 3-3	-0.7634	-0.26593	0.457
S = 12 ft			
Section 1-1	0.6	0.25172	-0.87287
Section 2-2	0.64	0.24766	-0.64894
Section 3-3	-1.2	-0.4002	0.46157

Table (6-4): Positive and negative moments for the live load at the three candidate sections.

	Unfactored moments (k-ft) from HL-93 truck axle load from bridge deck analysis including multiple presence factor and impact factor.		
	Section 1-1	Section 2-2	Section 3-3
S = 6 ft	4.80	4.60	-4.85
S = 8 ft	5.70	5.60	-6.14
S = 9 ft	6.25	5.64	-6.36
S = 10 ft	6.70	6.00	-6.50
S = 12 ft	7.89	7.00	-6.95

6-2 Simply Supported Beam

A second case of regular simply supported beam for a building was studied as well. For a reinforced concrete girder/beam, moment and deflection limit states will be considered.

6-2.1 Strength Requirements

According to ACI-318, the basic requirement for strength may be expressed as follows:

Design Strength ≥ Required Strength

The required moment strength M_u can be expressed as function of dead load moment M_{DL} and live load moment M_{LL} as

$$M_u = 1.2M_{DL} + 1.6M_{LL} \quad \text{.....(6-7)}$$

The design moment strength M_r can be expressed as function of nominal moment capacity M_n as

$$M_r = \phi M_n \quad \text{.....(6-8)}$$

for a simply supported beam/ girder shown in Figure (6-8), the maximum moment is located at the center of the beam and can be calculated as function of length of the beam L and uniformly distributed load w in force/length unit as $M = \frac{wL^2}{8}$. Table (6-5) shows the factored moments induced from dead and live uniformly distributed loads.

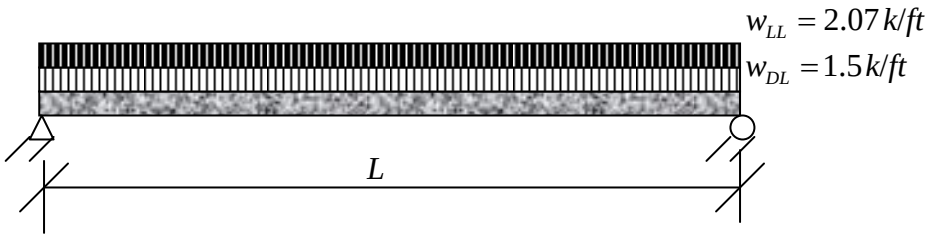

Figure (6-8): Simply supported reinforced concrete beam/girder with length L subjected to uniformly distributed dead and live loads

Table (6-5): Maximum moments at the center of the simple beam induced from uniformly distributed dead and live loads.

	Service moments (k-in)		Factored moments (k-in)	
	Dead load	Live load	Dead load	Live load
L = 20 ft	900	1242	1080	1987.2
L = 25 ft	1406	1940	1687	3105
L = 30 ft	2025	2794	2430	4471

6-3 Deflection

Due to the lower modulus of chopped fiber layers and glass fibers relative to steel rebars, deflections in proposed FRP rebar 1 and FRP rebar 2 reinforced beams will be larger than those for equivalent reinforcement ratios of steel reinforced beams. Similar to the case of steel reinforced concrete members, deflection should be determined under service loads and the corresponding applied service load moment will be M_a. In order to calculate deflections, gross and cracked moment of inertias I_g and I_{cr} respectively, should be calculated first. From elementary studies, the gross moment of inertia for rectangular cross section can be calculated as $I_g = \frac{bh^3}{12}$ where b is the width of the beam, and h is the

height of the section. For singly reinforced beams, cracked moment of inertia I_{cr} can be calculated in accordance with ACI-440, or ACI 318 as :

$$I_{cr} = \frac{bd^3}{3}k^3 + \eta_f A_f d^2(1-k)^2 \qquad \text{.....(6-9)}$$

where d is the effective depth, A_f is the area of reinforcement and k is calculated as

$$k = \sqrt{(\rho_f \eta_f)^2 + 2\rho_f \eta_f} - \rho_f \eta_f , \qquad \text{.....(6-10)}$$

$\eta_f = \frac{E_f}{E_c}$ modular ratio between FRP reinforcement and concrete[1], and

$\rho_f = \frac{A_f}{bd}$ FRP reinforcement ratio for rectangular beam.

Also, the effective moment of inertia can be calculated using an empirical equation proposed by Branson (1965, 1977) with a simple modification based on Gao et al. (1998) by introducing a reduction factor, β_d to take the account of lower stiffness of the rebar and associated bonding problems. The philosophy behind using I_e is that under service load the effective moment of inertia varies between I_g and I_{cr}. Thus, effective moment of inertia I_e can be determined as

$$I_e = \left(\frac{M_{cr}}{M_a}\right)^3 \beta_d I_g + \left[1 - \left(\frac{M_{cr}}{M_a}\right)^3\right] I_{cr} \le I_g \qquad \text{.....(6-11)}$$

[1] For proposed rebar 1 with 20% steel, E_f is average of the first two line in stress-strain curve. The first line is before steel yields and the second line is after steel yield.

where M_{cr} is the cracking moment, and is calculated as $M_{cr} = \frac{f_r I_g}{y_t}$ where f_r is the modulus of rupture and can be calculated as $f_r = 7.5\sqrt{f_c'}$ and y_t is the distance from centroid to extreme tension fiber and is equal to $h/2$. M_a is the service load moment.

The above equation is valid only when $M_a > M_{cr}$ because when $M_a < M_{cr}$ the beam remains uncracked. The reduction factor β_d can be calculated according ACI-440.1R (2003) as

$$\beta_d = \alpha_b \left[\frac{E_f}{E_s} + 1 \right] \qquad \text{.....(6-12a)}$$

where the coefficient α_b in the above equation is a bond-dependent coefficient. ACI-440 suggests the use of α_b = 0.5 for types of bars for which this value is not known. The reduction factor β_d can also be calculated according ACI-440.1R (2006) as

$$\beta_d = \frac{1}{5}\left(\frac{\rho_f}{\rho_{fb}} \right) \leq 1.0 \qquad \text{.....(6-12b)}$$

where ρ_f is the FRP reinforcement ratio and ρ_{fb} is the balanced FRP reinforcement ratio. The reduction factor (β_d) is around 0.6 (Bank, 2006) (Bischoff, 2007), and (GangaRao et al., 2006). Bischoff (2007) conducted a comprehensive work to calculate deflection and evaluate the existing two equations in ACI-440 (2003) and (2006). He suggested two new equations to calculate β_d. In this work, this reduction factor will be calculated using Bischoff's new equation which works for all cross sections.

$$\beta_d = 3.3\frac{I_{cr}}{I_g} \qquad \text{.....(6-13)}$$

For a simply supported beam, the maximum deflection Δ at the midspan of the beam can be calculated using the following equation

$$\Delta = \frac{5}{48}\frac{M_{\max} L^2}{E_c I_e} \qquad \text{.....(6-14)}$$

where $M_{\max} = \frac{w_a L^2}{8}$ is the moment at the midspan of the beam

According to ACI-318, the maximum permissible computed deflections for different cases and explanations are shown in Table (6-6). Alternatively, both ACI-318 and ACI-440 provide minimum thickness of reinforced concrete flexural members as function of length of the member as shown in Table (6-7) and Table (6-8), respectively.

Table (6-6): Maximum permissible computed deflections (ACI-318).

Type of member	Deflection to be considered	Deflection limitation
Flat roofs not supporting or attached to non-structural elements likely to be damaged by large deflections	Immediate deflection due to live load	L/180
Floors not supporting or attached to nonstructural elements likely to be damaged by large deflections	Immediate deflection due to live load	L/360
Roofs or floors construction supporting or attached to nonstructural elements likely to be damaged by large deflections	That part of the total deflection occurring after attachment of nonstructural elements (sum of the long-term deflection due to all sustained loads and the immediate deflection due to any additional live load.	L/480
Roofs or floors construction supporting or attached to nonstructural elements not likely to be damaged by large deflections		L/240

Table (6-7): Minimum thickness of nonprestressed beams or one-way slabs unless deflections are calculated[1].

	Minimum thickness, h			
	Simply supported	One end continuous	Both ends continuous	Cantilever
Member	Members not supporting or attached to partitions or other construction likely to be damaged by large deflections			
Sold one-way slab	*l*/20	*l*/24	*l*/28	*l*/10
Beams or ribbed one-way slabs	*l*/16	*l*/18.5	*l*/21	*l*/8

Table (6-8): Minimum thickness of FRP-reinforced flexural members.

	Support Conditions			
	Simply supported	One end continuous	Both ends continuous	Cantilever
Sold one-way slab	*l*/13	*l*/17	*l*/22	*l*/5.5
Beams	*l*/10	*l*/12	*l*/16	*l*/4

[1] using f_y = 60 ksi

Chapter Seven

Calculations and Results

In order to perform Reliability Based Design Optimization RBDO to determine optimum rebar materials, first the penalties of using: chopped fibers, and random dispersion of these fibers must be considered. Also, the length of short fibers must be checked to ensure that the failure of chopped fibers will be breakage and not slippage. Finally, the tensile stress in chopped fiber composite layers σ_c will be compared with the ultimate tensile strength of the composite σ_{cu}. The ultimate tensile strength of the composite should never be exceeded. All theories have been discussed in previous chapters.

7-1 Critical Fiber Length l_c Calculations

The chopped fiber length should be at least 8 times the critical fiber length l_c where, $l_c = \frac{\sigma_f D}{2\tau_m}$. Table (7-1) shows the calculated critical fiber length l_c and used fiber length.

Table (7-1): Critical fiber length l_c vs. used values.

Fiber Type	Tensile strength MPa (ksi)	Shear strength Epoxy Resin τ_m	l_c (mm)	8 l_c (mm)	Used Length (mm)
IM-Carbon	3037.5 (441)	29 MPa	0.524	4.18	6
SM-Carbon	3570 (518)	29 MPa	0.616	4.92	6

7-2 Fiber Length Efficiency Factor Calculation

7-2.1 Effect on Modulus of Elasticity

The governing equation for fiber length efficiency factor for short, equal-length fibers, η_{LE} was mentioned in Chapter Three. For purpose of clarification, we will rewrite equation (3-3).

$$\eta_{LE} = 1 - \frac{\tanh(\beta l/2)}{\beta l/2}$$

where $\beta = \frac{1}{r_f}\sqrt{\frac{2G_m}{E_f \ln\left(\frac{R}{r_f}\right)}} = \sqrt{\frac{8G_m}{E_f D^2 \log_e\left(\frac{2R}{D}\right)}}$, $\frac{R}{r_f} = \sqrt{\frac{K_R}{v_f}}$.

and $G_m = \frac{E_m}{2(1+\nu_m)}$

The definition of all symbols can be found in Chapter three, section 3-6-1.1. Table (7-2) shows the fiber length, *l*, properties, fiber length efficiency factor, and the corresponding reduction factors. For IM-Carbon fiber, $E_f = 650$ GPa ($E_f = 95000$ ksi) and for SM-Carbon fiber $E_f = 230$ GPa ($E_f = 34000$ ksi). The Carbon fiber diameter is assumed to be 0.01 mm, while the volume fraction of chopped carbon fiber in the first two outer layers is 35%; the Poisson's ratio of the matrix (resin) is taken as ν_m = 0.39; and modulus of elasticity is E_m = 3.5 GPa (508 ksi).

Table (7-2): Fiber length and the corresponding fiber length efficiency factor and associated reduction.

	l (mm)	Square Packing	Hexagon Packing	Square Packing	Hexagon Packing
		η_{LE}	η_{LE}	% reduction	% reduction
IM- Carbon	6	0.98	0.98	2%	2%
Fiber $E_f = 650\,\text{GPa}$	8	0.99	0.98	1%	2%
($E_f = 95000\,\text{ksi}$)	10	0.99	0.99	1%	1%
SM- Carbon	6	0.99	0.99	1%	1%
Fiber $E_f = 230\,\text{GPa}$	8	0.99	0.99	1%	1%
($E_f = 34000\,\text{ksi}$)	10	0.99	0.99	1%	1%

Figure (7-1) and (7-2) show fiber length efficiency factors for different fiber length and different fiber types.

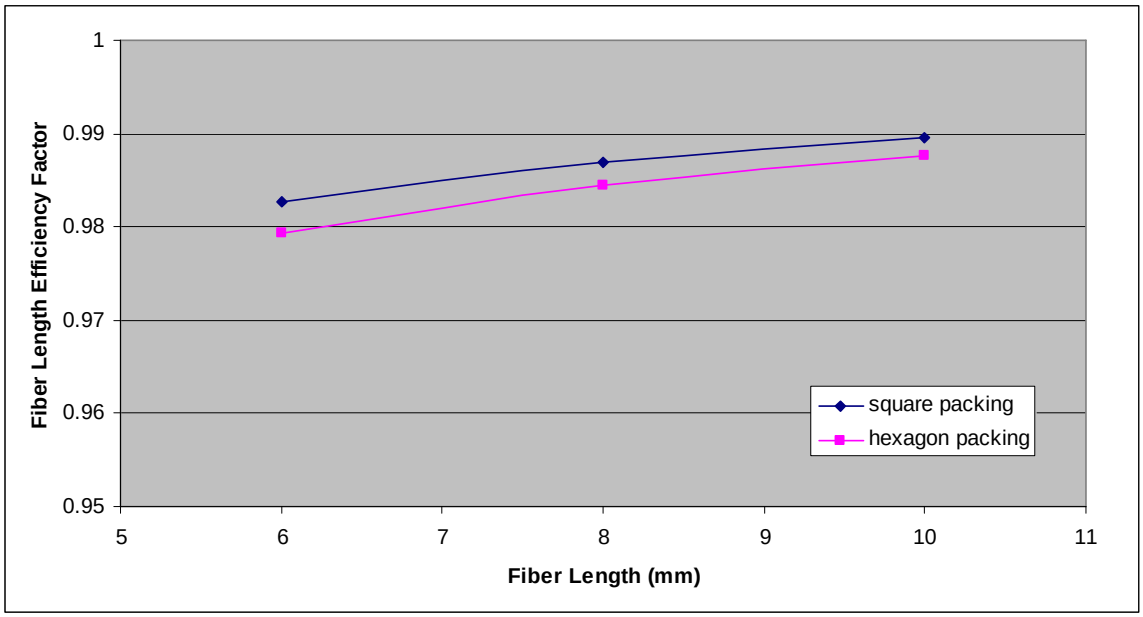

Figure (7-1): Fiber length and the corresponding fiber length efficiency factor for IM-Carbon fiber $E_f = 650\,\text{GPa}$ ($E_f = 95000\,\text{ksi}$).

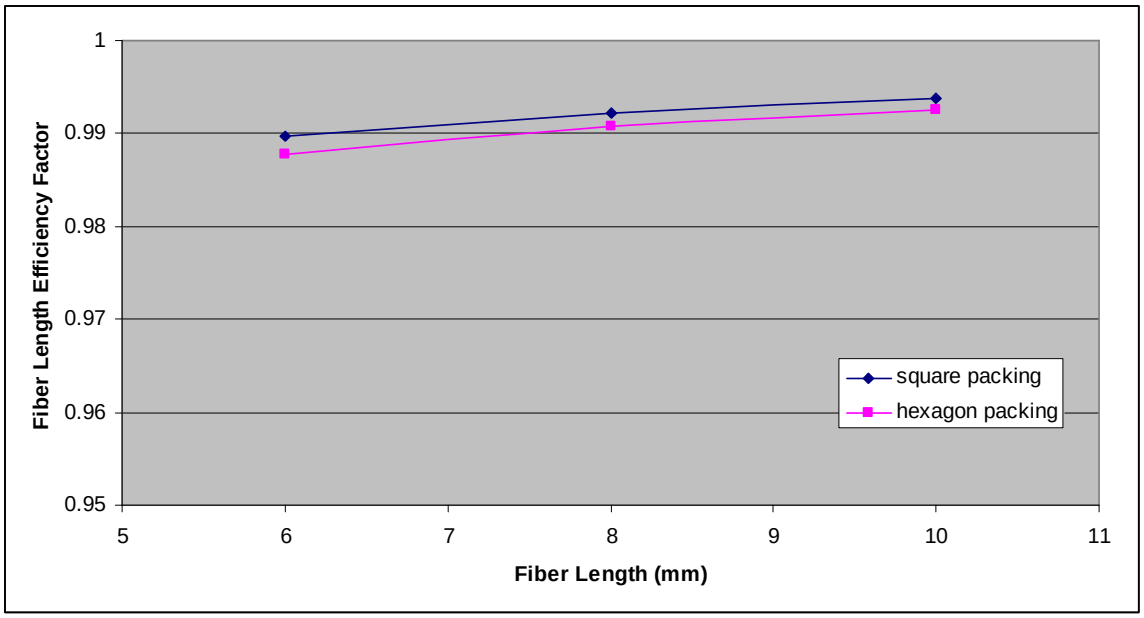

Figure (7-2): Fiber length and the corresponding fiber length efficiency factor for SM-Carbon fiber $E_f = 230\,\text{GPa}$ ($E_f = 34000\,\text{ksi}$).

Through out this work, **an equal length chopped fiber of 6 mm will be used**. Table (7-3) shows the new values of E_f and composite material modulus E_c after deducting penalties for using chopped fibers.

Table (7-3a): Carbon fibers reduced moduli of elasticity due to fiber length efficiency factor.

Fiber Type	Initial E_f	η_{LE} used	New E_f
IM-Carbon fiber	650 GPa (95000 ksi)	0.98	634.5 GPa (92035 ksi)
SM-Carbon fiber	230 GPa (34000 ksi)	0.99	226 GPa (32780 ksi)

Table (7-3b): Composites of carbon fiber layers reduced moduli of elasticity due to fiber length efficiency factor.

Fiber Type	New E_f	E_m	E_c
IM-Carbon fiber layer	634.5 GPa (92035 ksi)	3.5 GPa (508 ksi)	224 GPa (32500 ksi)
SM-Carbon fiber layer	226 GPa (32780 ksi)	3.5 GPa (508 ksi)	81 GPa (11803 ksi)

7-2.2 Effect on Composite Ultimate Strength

For composite material ultimate strength σ_{cu}, fiber length efficiency factor η_{LS} will be taken as 0.95 (see Chapter 3, section (3-4.2)).

7-3 Fiber Orientation Efficiency Factor Calculation

7-3.1 Effect on Modulus of Elasticity

Fiber orientation efficiency factor η_{OE} will be taken as $\frac{3}{8}$ (see Chapter 3, section 3-4.1.3) and the results are shown in Table (7-4).

Table (7-4): Carbon fiber modulus of elasticity after deducting the effect of randomness of dispersed chopped fibers.

Fiber Type	Old E_f	E_m	New E_f Final	New E_c Final
IM-Carbon fiber	634.5 GPa (92035 ksi)	3.5 GPa (508 ksi)	238 GPa (34513 ksi)	85.5 GPa (12410 ksi)
SM-Carbon fiber	226 GPa (32780 ksi)	3.5 GPa (508 ksi)	85 GPa (12293 ksi)	32 GPa (4633 ksi)

7-3.2 Effect on Composite Ultimate strength

For composite ultimate strength, fiber orientation efficiency factor η_{OS} will be taken as 0.2 (see Chapter 3, section (3-4.2)).

7-4 Composite Ultimate Stress Calculations

For the above results to be valid, the composite ultimate stress should not be exceeded. The potential problem comes from the first two outside layers which are made of

randomly dispersed chopped fibers. Table (7-5) represents the worst case scenario for these two layers. i.e.; the height stresses could be generated on these two layers (See Appendix B for stresses and Tables 7-11 to 7-14 for volume fraction).

Table (7-5): Maximum stresses reached for proposed rebar 1 and 2 and stresses on each layers and the corresponding stresses on chopped fiber layers

	Proposed Rebar 1		Proposed Rebar 2	
	IM-Carbon layer	SM-Carbon layer	IM-Carbon layer	SM-Carbon layer
Stress (ksi)	50	60	43	47
Volume fraction	0.44	0.21	0.54	0.25
Stress on layer (ksi)	**24.5**	**14.6**	**30.125**	**17.4**

.

Recall equation (3-22) from Chapter 3, and specifically, the modified rule of mixtures for stresses, after substituting η_{LS} = 0.95, and η_{OS} = 0.2:

$$\sigma_{cu} = 0.95 \times 0.2 \times \cdot \sigma_f \cdot v_f + (1 - v_f)\sigma_m \qquad \text{.....(7-1)}$$

and again, σ_f is fiber strength, σ_m matrix the strength at fiber failure strain, and v_f is the volume fraction of fiber in the composite. Table (7-6) shows the resulting ultimate stresses that the composite layers can resist.

Table (7-6): Strength of the composite materials made of chopped fibers.

	σ_f (ksi)	σ_m (ksi)	v_f =1- v_m	v_m	σ_{cu} (ksi)
IM-Carbon layer	441	2.3	0.35	0.65	**30.8**
SM-Carbon layer	518	7.6	0.35	0.65	**39.4**

7-5 Optimizing Proposed Rebars

Figures (7-3) and (7-4) show the flowcharts to conduct a Reliability Based Design Optimization (RBDO) of the proposed rebar 1 and rebar 2, respectively. Tables (7-7) and (7-8) show the optimized constituents of proposed rebars 1 and 2 respectively, for the bridge deck. Tables (7-9) and (7-10) show the optimized constituents of proposed rebars 1 and 2 for the building beam/girder, while Table (7-11) shows the total volume fractions of the constituents of the proposed D-H-FRP rebars. Appendix B shows stress-strain curves for the optimized D-H-FRP rebars, while Appendix C shows moment-curvature graphs for concrete sections reinforced with optimized D-H-FRP rebars.

All constrains are within three or four nested loops. These Four or five nested loops are to generate the area of reinforcement and volume fractions of the fibers starting with minimum values up to the maximum values. For each total volume fraction set:

- The total volume fraction should be 1.0. If this constraint is satisfied,
- The corresponding stress-strain diagram should be determined and should follow the failure pattern mentioned earlier. If this constraint is satisfied,
- Moment-curvature values should be determined to check the value of the moment capacity, M_n, that corresponds to the first fiber type failure. This value should be equal to applied moment Mu/ϕ. If this constraint is satisfied,
- From Moment-curvature values check ductility. If this constraint is satisfied,
- Deflection should be checked and should be less than the code value. If this constraint is satisfied,
- Conduct Monte-Carlo simulation and calculate β, If this constraint is satisfied,
- Calculate the corresponding relative price and choose the smallest.

The reason of using this method in optimization is to avoid the first and/or second derivates associated with other methods since the constraints are not mathematical functions besides, dealing up to 5 or six 6 nested loops with known upper and lower limits for each one make the solution easy and although sometimes it is time consuming.

Appendix D shows an example of an optimization example with 2 nested loops in VBA Language. Tables (5-1) and (5-2) show the resistance and load random variables, respectively.

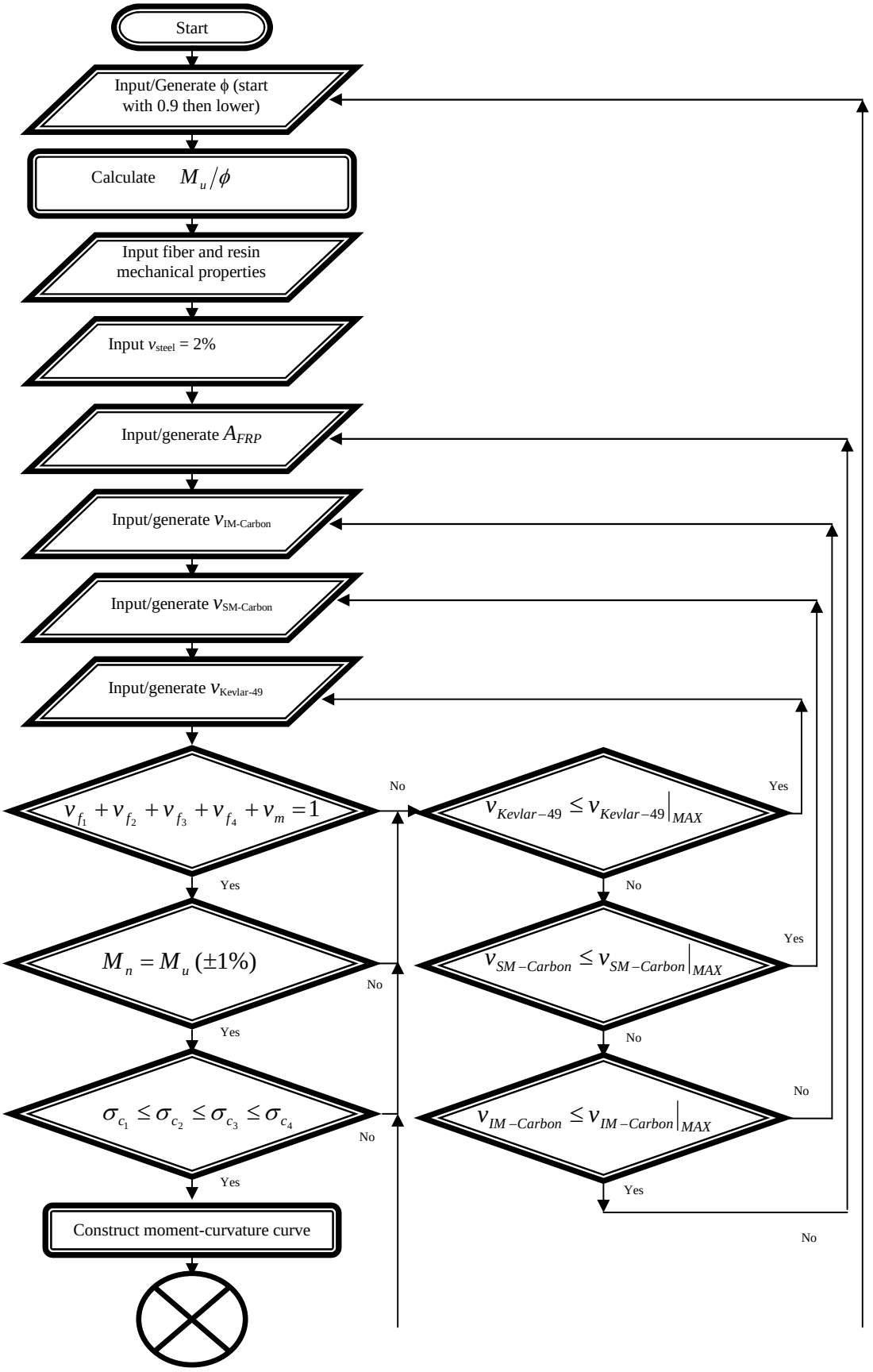
Start
Input/Generate ϕ (start with 0.9 then lower)
Calculate M_u/ϕ
Input fiber and resin mechanical properties
Input v_{steel} = 2%
Input/generate A_{FRP}
Input/generate $v_{IM\text{-}Carbon}$
Input/generate $v_{SM\text{-}Carbon}$
Input/generate $v_{Kevlar\text{-}49}$
$v_{f_1} + v_{f_2} + v_{f_3} + v_{f_4} + v_m = 1$
No
$v_{Kevlar-49} \le v_{Kevlar-49}|_{MAX}$
Yes
Yes
No
$M_n = M_u\,(\pm 1\%)$
No
$v_{SM-Carbon} \le v_{SM-Carbon}|_{MAX}$
Yes
Yes
No
$\sigma_{c_1} \le \sigma_{c_2} \le \sigma_{c_3} \le \sigma_{c_4}$
No
$v_{IM-Carbon} \le v_{IM-Carbon}|_{MAX}$
No
Yes
Yes
No
Construct moment-curvature curve

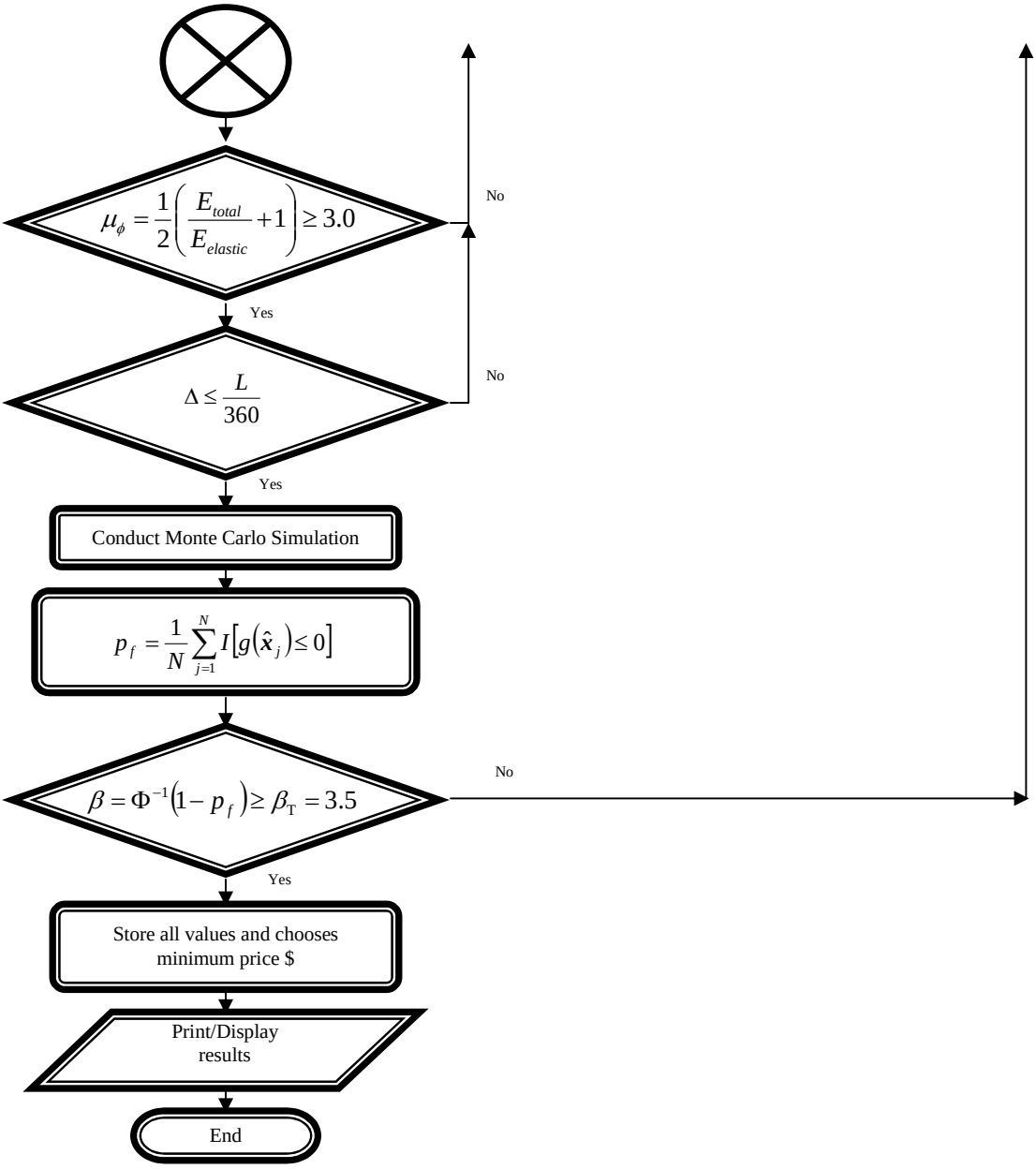

Figure (7-3): Flowchart to conduct RBDO for proposed rebar 1 for building beam/girder.

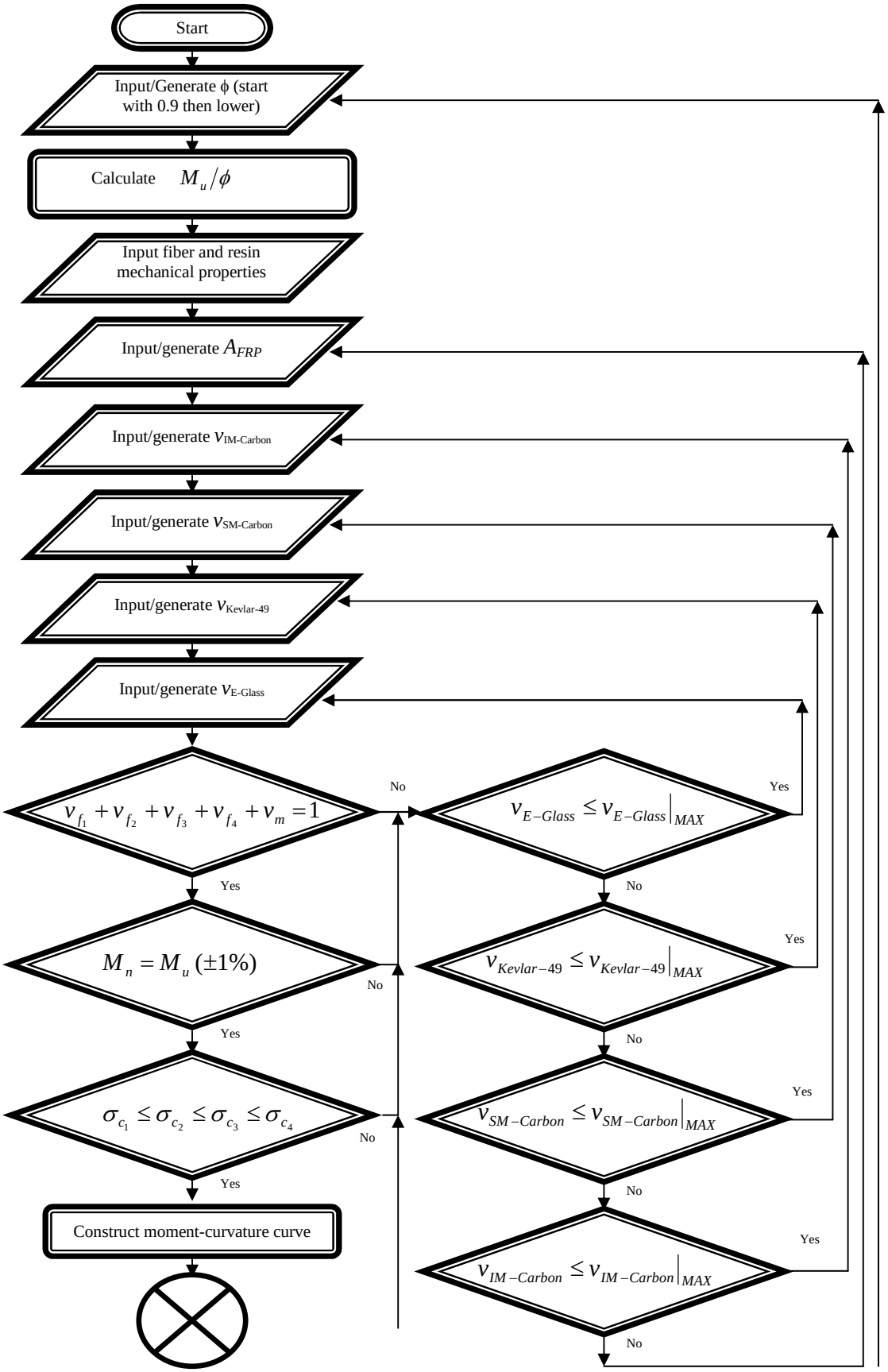
Start
Input/Generate ϕ (start with 0.9 then lower)
Calculate M_u/ϕ
Input fiber and resin mechanical properties
Input/generate A_{FRP}
Input/generate $v_{IM\text{-}Carbon}$
Input/generate $v_{SM\text{-}Carbon}$
Input/generate $v_{Kevlar\text{-}49}$
Input/generate $v_{E\text{-}Glass}$
$v_{f_1}+v_{f_2}+v_{f_3}+v_{f_4}+v_m=1$
No
Yes
$v_{E-Glass} \le v_{E-Glass}|_{MAX}$
Yes
No
$M_n = M_u(\pm 1\%)$
No
Yes
$v_{Kevlar-49} \le v_{Kevlar-49}|_{MAX}$
Yes
No
$\sigma_{c_1} \le \sigma_{c_2} \le \sigma_{c_3} \le \sigma_{c_4}$
No
Yes
$v_{SM-Carbon} \le v_{SM-Carbon}|_{MAX}$
Yes
No
Construct moment-curvature curve
$v_{IM-Carbon} \le v_{IM-Carbon}|_{MAX}$
Yes
No

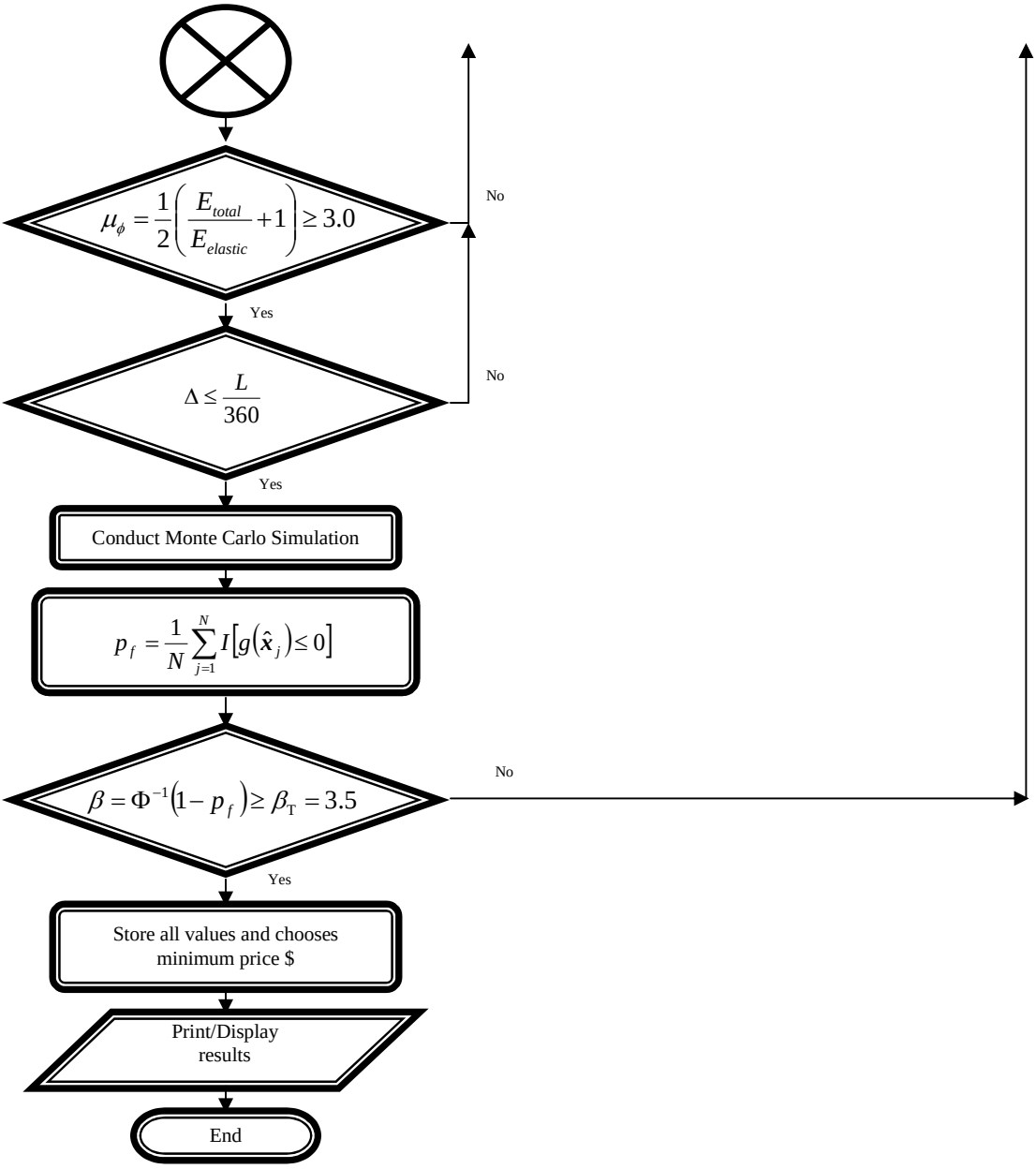

Figure (7-4): Flowchart to conduct RBDO for proposed rebar 2 for building beam/girder.

Table (7-7a): Characteristics of concrete section reinforced with proposed rebar 1 for bridge deck

S=	β	ϕ	Δ (Ductility)	ε (rebar strain at ultimate strain failure in concrete)	Relative cost	A FRP (in2)
6 ft						
+ve moment	**3.7**	**0.9**	**3.0**	**0.025**	**12.12**	**0.38**
-ve moment	**3.5**	**0.9**	**3.2**	**0.0248**	**12.46**	**0.43**
9 ft						
+ve moment	**3.5**	**0.9**	**3.71**	**0.024**	**11.89**	**0.53**
-ve moment	**3.66**	**0.9**	**3.48**	**0.0213**	**11.76**	**0.61**
12 ft						
+ve moment	**3.6**	**0.9**	**4.35**	**0.0215**	**12.00**	**0.74**
-ve moment	**3.6**	**0.9**	**4.34**	**0.0219**	**11.83**	**0.72**

Table (7-7b): Optimized constituents of proposed rebar 1 for bridge deck

S=	v_{C_IM} layer[1]	v_{C_SM} layer[2]	v_{K-49}	v_{Steel}	v_{resin}	A FRP	Moment Mn (k-in)
6 ft							
+ve moment	**0.425**	**0.125**	**0.155**	**0.2**	**0.095**	**0.38**	**105**
-ve moment	**0.41**	**0.15**	**0.135**	**0.2**	**0.105**	**0.43**	**111**
9 ft							
+ve moment	**0.42**	**0.16**	**0.11**	**0.2**	**0.11**	**0.53**	**139**
-ve moment	**0.42**	**0.15**	**0.12**	**0.2**	**0.11**	**0.61**	**160**
12 ft							
+ve moment	**0.44**	**0.17**	**0.09**	**0.2**	**0.10**	**0.74**	**188**
-ve moment	**0.43**	**0.18**	**0.09**	**0.2**	**0.10**	**0.72**	**184/**

[1] 65% resin and 35% chopped carbon Intermediate modulus of this layer.
[2] 65% resin and 35% chopped carbon small modulus of this layer

Table (7-8a): Characteristics of concrete section reinforced with proposed rebar 2 for bridge deck.

S= \	β	ϕ	Δ (Ductility)	ε (rebar strain at ultimate strain failure in concrete)	Relative cost	A FRP (in2)
6 ft						
+ve moment	**3.52**	**0.895**	**6.10**	**0.0375**	**13.89**	**0.43**
-ve moment	**3.50**	**0.9**	**7.53**	**0.0398**	**14.12**	**0.48**
8 ft						
+ve moment	**3.67**	**0.89**	**8.66**	**0.0395**	**13.88**	**0.54**
-ve moment	**3.53**	**0.875**	**10.52**	**0.0387**	**14.12**	**0.66**
9 ft						
+ve moment	**3.54**	**0.885**	**10.46**	**0.0397**	**14.14**	**0.62**
-ve moment	**3.50**	**0.87**	**10.88**	**0.0376**	**14.14**	**0.69**
10 ft						
+ve moment	**3.50**	**0.87**	**10.88**	**0.0376**	**14.14**	**0.69**
-ve moment	**3.51**	**0.90**	**11.00**	**0.0374**	**14.14**	**0.70**
12 ft						
+ve moment	N/A	N/A	N/A	N/A	N/A	N/A
-ve moment	N/A	N/A	N/A	N/A	N/A	N/A

Table (7-8b): Optimized constituents of proposed rebar 2 for bridge deck.

S= \	v_{C_IM} layer[1]	v_{C_SM} layer[2]	v_{K-49}	v_{Glass}	v_{resin}	A FRP	Moment Mn (k-in)
6 ft							
+ve moment	**0.53**	**0.23**	**0.04**	**0.1**	**0.10**	**0.43**	**100**
-ve moment	**0.54**	**0.23**	**0.04**	**0.08**	**0.11**	**0.48**	**112**
8 ft							
+ve moment	**0.53**	**0.24**	**0.04**	**0.07**	**0.12**	**0.54**	**128**
-ve moment	**0.54**	**0.24**	**0.04**	**0.06**	**0.12**	**0.66**	**152**
9 ft							
+ve moment	**0.54**	**0.25**	**0.04**	**0.06**	**0.11**	**0.62**	**142**
-ve moment	**0.54**	**0.25**	**0.04**	**0.06**	**0.11**	**0.69**	**162**
10 ft							
+ve moment	**0.54**	**0.25**	**0.04**	**0.06**	**0.11**	**0.69**	**163**
-ve moment	**0.54**	**0.25**	**0.04**	**0.06**	**0.11**	**0.70**	**165**
12 ft							
+ve moment	N/A	N/A	N/A	N/A	N/A	N/A	N/A
-ve moment	N/A	N/A	N/A	N/A	N/A	N/A	N/A

[1] 65% resin and 35% chopped carbon Intermediate modulus of this layer
[2] 65% resin and 35% chopped carbon small modulus of this layer

Table (7-9a): Characteristics of concrete section reinforced with proposed rebar 1 for building Beam/Girder.

L= \	β	ϕ	Δ (Ductility)	ε (rebar strain at ultimate strain failure in concrete)	Relative cost	b (in)	d (in)
20 ft							
+ve moment	**3.50**	**0.85**	**4.72**	**0.0213**	**11.07**	**13**	**22.5**
25 ft							
+ve moment	**3.5**	**0.82**	**5.01**	**0.022**	**11.2**	**14**	**27.5**
30 ft							
+ve moment	**3.5**	**0.82**	**5.5**	**0.0213**	**11.2**	**16**	**32.5**

Table (7-9b): Optimized constituents of proposed rebar 1 for building Beam/Girder.

L= \	v_{C_IM} layer[1]	v_{C_SM} layer[2]	v_{K-49}	v_{Steel}	v_{resin}	A frp	Moment Mn (k-in)
20 ft							
+ve moment	**0.4**	**0.21**	**0.08**	**0.2**	**0.11**	**4.0**	**3615**
25 ft							
+ve moment	**0.41**	**0.19**	**0.07**	**0.2**	**0.13**	**4.46**	**5885**
30 ft							
+ve moment	**0.41**	**0.19**	**0.07**	**0.2**	**0.13**	**7.2**	**8460**

[1] 65% resin and 35% chopped carbon Intermediate modulus of this layer
[2] 65% resin and 35% chopped carbon small modulus of this layer

Table (7-10a): Characteristics of concrete section reinforced with proposed rebar 2 for building Beam/Girder.

L= \	β	ϕ	Δ (Ductility)	ε (rebar strain at ultimate strain failure in concrete)	Relative $/bar	b (in)	d (in)
20 ft							
+ve moment	**3.50**	**0.82**	**10.8**	**0.0378**	**14.11**	**14**	**24.5**
25 ft							
+ve moment	**3.51**	**0.837**	**10.7**	**0.0383**	**14.11**	**14.5**	**30.5**
30 ft							
+ve moment	**3.5**	**0.837**	**10.9**	**0.0376**	**14.11**	**16**	**34**

Table (7-10b): Optimized constituents of proposed rebar 2 for building Beam/Girder

L= \	v_{C_IM} layer[1]	v_{C_SM} layer[2]	v_{K-49}	v_{Glass}	v_{resin}	A frp	Moment Mn (k-in)
20 ft							
+ve moment	**0.54**	**0.25**	**0.04**	**0.06**	**0.11**	**3.93**	**3740**
25 ft							
+ve moment	**0.54**	**0.25**	**0.04**	**0.06**	**0.11**	**4.95**	**5710**
30 ft							
+ve moment	**0.54**	**0.25**	**0.04**	**0.06**	**0.11**	**6.3**	**8294**

[1] 65% resin and 35% chopped carbon Intermediate modulus of this layer
[2] 65% resin and 35% chopped carbon small modulus of this layer

Table (7-11): Total volume fractions of the constituents of the proposed D-H-FRP rebars.

	proposed rebar 1 for bridge deck				
	v_{C_IM}	v_{C_SM}	v_{K-49}	v_{Steel}	v_{resin}
6 ft					
+ve moment	0.14875	0.04375	0.155	0.2	0.4525
-ve moment	0.1435	0.0525	0.135	0.2	0.469
9 ft					
+ve moment	0.147	0.056	0.11	0.2	0.487
-ve moment	0.147	0.0525	0.12	0.2	0.4805
12 ft					
+ve moment	0.154	0.0595	0.09	0.2	0.4965
-ve moment	0.1505	0.063	0.09	0.2	0.4965
	proposed rebar 2 for bridge deck				
	v_{C_IM}	v_{C_SM}	v_{K-49}	v_{Glass}	v_{resin}
6 ft					
+ve moment	0.1855	0.0805	0.04	0.1	0.594
-ve moment	0.189	0.0805	0.04	0.08	0.6105
8 ft					0
+ve moment	0.1855	0.084	0.04	0.07	0.6205
-ve moment	0.189	0.084	0.04	0.06	0.627
9 ft					0
+ve moment	0.189	0.0875	0.04	0.06	0.6235
-ve moment	0.189	0.0875	0.04	0.06	0.6235
10 ft					
+ve moment	0.189	0.0875	0.04	0.06	0.6235
-ve moment	0.189	0.0875	0.04	0.06	0.6235
	proposed rebar 1 building Beam/Girder				
	v_{C_IM}	v_{C_SM}	v_{K-49}	v_{Steel}	v_{resin}
20 ft					
+ve moment	0.14	0.0735	0.08	0.2	0.5065
25 ft					
+ve moment	0.1435	0.0665	0.07	0.2	0.52
30 ft					
+ve moment	0.1435	0.0665	0.07	0.2	0.52
	proposed rebar 2 building Beam/Girder				
	v_{C_IM}	v_{C_SM}	v_{K-49}	v_{Glass}	v_{resin}
20 ft					
+ve moment	0.189	0.0875	0.04	0.06	0.6235
25 ft					
+ve moment	0.189	0.0875	0.04	0.06	0.6235
30 ft					
+ve moment	0.189	0.0875	0.04	0.06	0.6235

7-6 Optimum Volume Fractions

In order to determine the optimum volume fraction for each proposed rebar, Table 4-3 is suggested to be used for initial values.

7-6.1 Volume Fraction Bridge Deck

Based on Tables (7-7b) and (7-8b), the volume fraction shown in Table (7-12) could be assumed as the optimum volume fractions of fibers to be used in bridge deck reinforcement. It is important to note that the $v_{IM-Carbon}$ and $v_{SM-Carbon}$ layers consist of 35% fiber and 65% resin.

Table (7-12): Suggested volume fractions for proposed rebars used in bridge deck.

	Proposed D-H-FRP rebar 1	Proposed D-H-FRP rebar 2
$v_{IM-Carbon}$ layer	42%	54%
$v_{SM-Carbon}$ layer	17%	25%
$v_{Kevlar-49}$ layer	11%	4%
$v_{E-glass}$ layer	-	6%
v_{steel} layer	20%	-
v_{resin}	10%	11%

7-6.2 Volume Fractions for Building Beam/Girders

Based on Tables (7-9b) and (7-10b), the volume fractions shown in Table (7-13) are the optimum volume fractions of fibers to be used in building Beam/Girder reinforcement. It is important to note that the $v_{IM-Carbon}$ layer and $v_{SM-Carbon}$ layer consists of 35% fiber and 65% resin.

Table (7-13): Suggested volume fractions for proposed rebars used in beams/girders.

	Proposed D-H-FRP rebar 1	Proposed D-H-FRP rebar 2
$v_{IM-Carbon}$ layer	41%	54%
$v_{SM-Carbon}$ layer	20%	25%
$v_{Kevlar-49}$ layer	8%	4%
$v_{E-glass}$ layer	-	6%
v_{steel} layer	20%	-
v_{resin}	11%	11%

7-6.3 All Purpose Final Volume Fractions

Based on the average of Tables (7-12) and (7-13), the volume fractions shown in Table (7-14) could be assumed as the optimum volume fraction of fibers to be used for all-purpose reinforcement (Bridge deck and/or Beam/Girder).

Table (7-14): Suggested volume fraction for proposed rebars used in all purposes.

	Proposed D-H-FRP rebar 1	Proposed D-H-FRP rebar 2
$v_{IM-Carbon}$ layer	42%	54%
$v_{SM-Carbon}$ layer	18%	25%
$v_{Kevlar-49}$ layer	10%	4%
$v_{E-glass}$ layer	-	6%
v_{steel} layer	20%	-
v_{resin}	10%	11%

7-7 Deflection of Beam/Girders

The immediate live-load deflection Δ_{iL} can be computed using equation (7-2) (MacGregor and White, 2011)

$$\Delta_{iL} = \Delta_{iL+D} - \Delta_{iD} \qquad \text{.....(7-2)}$$

where Δ_{iL+D} is the immediate live and dead-load deflection and Δ_{iD} is the immediate dead-load deflection. In calculating Δ_{iD}, the cracked moment of inertia should be used because when the live load is removed, the beam will not return to its dead-load deflection as it is now cracked. Table (7-15) shows a summary of the calculated deflections, while Table (7-16) shows the minimum thickness according to ACI-440 and ACI-318 and those used in this calculation. In the same table, it can be seen that thickness of the cross section reinforced with rebar 1 is 10% less than the minimum design value in ACI-440. The reason behind that is rebar 1 is not totally FRP material, but has 20% steel.

Table (7-15): Deflection in inches for both proposed rebars for different span lengths and maximum permissible deflections.

Rebar 1: 20% Steel	Δ (inch)	Controlling limit			Δ (inch)	Rebar 2: 100% FRP
		L/180	L/240	L/360		
L=20 ft	0.62	1.33	1.00	0.66	0.59	L=20 ft
L=25 ft	0.75	1.67	1.25	0.83	0.74	L=25 ft
L=30 ft	1.00	2.00	1.5	1.00	0.91	L=30 ft

Table (7-16): Minimum thickness of FRP-reinforced flexural members.

	Thickness of cross section reinforced with Rebar 1 (in)	Thickness of cross section reinforced with Rebar 2 (in)	Minimum required thickness (in)	
			ACI-440	ACI-318
L= 20 ft	25	27	24	15
L = 25 ft	30	33	30	18.7
L = 30 ft	32.5	36.5	36	22.5

Finally, a graphical presentation of beam deflection is given in Figure (7-5). These beams have the same moment capacity and use the minimum thickness recommended by the appropriate corresponding code. i.e.; for sections reinforced with FRP reinforcements, the thicknesses used are 24, 30, and 36 inches, respectively, as required by ACI-440 for FRP rebar, and for sections reinforced with steel reinforcement, the thicknesses used are 15, 18.7, and 22.5 inches, respectively, as required by ACI-318, and are designated (I). For comparison, all-steel sections but with thicknesses equal to those of the FRP sections are designated (II).

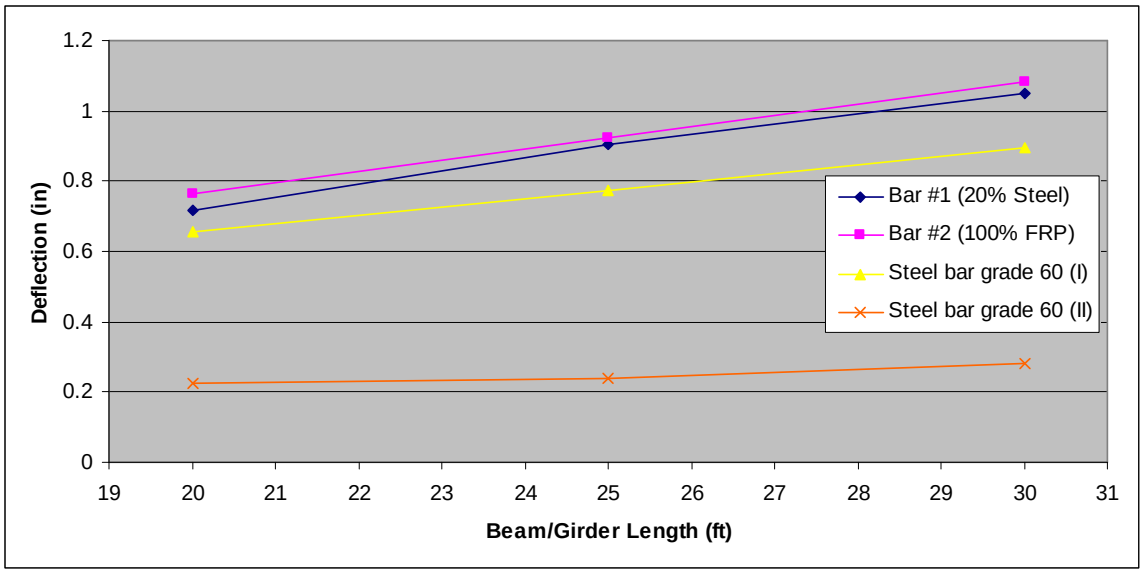

Figure (7-5): Deflection based on minimum beam/girder thickness in ACI-440 and ACI 318 for different reinforcements.

7-8 Balanced FRP Reinforcement Ratio (ρ_{fb})

By definition, balanced FRP reinforcement ratio ρ_{fb} is the case where concrete crushes by reaching a failure strain of 0.003 and the first fiber breaks by reaching its ultimate failure strain ε_{fu_1}. From the fundamentals of reinforced concrete design, we can show that the ρ_{fb} can be determined as

$$\rho_{fb} = 0.85\beta_1 \frac{f'_c}{\sigma_f}\left(\frac{\varepsilon_{cu}}{\varepsilon_{cu} + \varepsilon_{fu_1}}\right) \qquad \text{.....(7-3)}$$

this can be rewritten as

$$\rho_{fb} = 0.85\beta_1 \frac{f'_c}{\sigma_{fu}}\left(\frac{\varepsilon_{cu} E_f}{\varepsilon_{cu} E_f + \sigma_{fu}}\right) \qquad \text{.....(7-4)}$$

where

$$\beta_1 = \begin{cases} 0.85 & f_c' \le 4000\,\text{psi} \\ 1.05 - 0.05\dfrac{f_c'}{1000} & 4000 < f_c' \le 8000\,\text{psi} \\ 0.65 & f_c' > 8000\,\text{psi} \end{cases} \qquad \text{.....(7-5)}$$

E_f is the modulus of elasticity of the bar when first fiber breaks off.

- Proposed Rebar 1: 20 % Steel

  For proposed rebar 1 which is 20% steel and 80% FRP, the modulus can be calculating by taking the second slope from stress-strain curve. The ultimate stress in the FRP rebar is where IM-carbon breaks after steel yields.

$$E_f = E_{IM-\text{Carbon}} v_{IM-\text{Carbon}} + E_{SM-\text{Carbon}} v_{SM-\text{Carbon}} + E_{\text{Kevlar-49}} v_{\text{Kevlar-49}} + E_{\text{resin}} v_{\text{resin}} \qquad \text{.....(7-6)}$$

$$\sigma_{fu} = E_f \cdot \varepsilon_{fu_1} + \sigma_y v_s \qquad \text{.....(7-7)}$$

- Proposed Rebar 2: 100 % FRP

  For proposed rebar 2 which is 100% FRP, the modulus can be calculating by taking the first modulus from the stress-strain curve. The ultimate stress in the FRP rebar is where IM-carbon breaks.

$$E_f = E_{IM-\text{Carbon}} v_{IM-\text{Carbon}} + E_{SM-\text{Carbon}} v_{SM-\text{Carbon}} + E_{\text{Kevlar}} v_{\text{Kevlar}} + E_{\text{Glass}} v_{\text{Glass}} + E_{\text{resin}} v_{\text{resin}} \qquad \text{.....(7-8)}$$

$$\sigma_{fu} = E_f \cdot \varepsilon_{fu_1} \qquad \text{.....(7-9)}$$

Table (7-17) shows values of ρ_f and ρ_{fb} for both proposed rebars and for different spans.

Table (7-17): Reinforcement ratios and balanced reinforcement ratios for proposed rebars for different span lengths.

	Rebar 1: 20% Steel			Rebar 2: 100% FRP			100% steel bars		
	L=20	L=25	L=30	L=20	L=25	L=30	L=20	L=25	L=30
E_f (ksi)	7118	7002	7001.7	9282	9282	9282	29000		
σ_{fu} (ksi)	45.17	44.64	44.64	42.06	42.06	42.06			
ρ_f	0.0136	0.0142	0.0138	0.0115	0.0112	0.0116	0.024	0.02	0.021
ρ_{fb}	0.026	0.026	0.026	0.034	0.034	0.034	0.032		

From the table above we can observe clearly that the reinforcement ratio of the cross sections reinforced with FRP (ρ_f) is less than the balanced ratio. This means that all beams are under-reinforced. From Tables (7-7) to (7-10), the average strains in D-H-FRP reinforcement when the strain in the concrete is 0.003 are: 0.022 in/in for proposed rebar 1 and 0.038 for proposed rebar 2 as shown in Table (7-18), while the yield strain of steel grade 60 is 0.00207. According to ACI-318, the flexural reduction factor ϕ is equal to 0.9 when the strain in the concrete is 0.003 and the strain in steel reinforcement is 0.005.

Table (7-18): Strain in D-H-FRP rebars when concrete strain is 0.003.

Proposed Rebar 1		Proposed Rebar 2	
s (Bridge Deck)	Strain in FRP rebar	s (Bridge Deck)	Strain in FRP rebar
6 ft : +ve moment	0.025	6 ft : +ve moment	0.0375
6 ft : -ve moment	0.0248	6 ft : -ve moment	0.0398
9 ft : +ve moment	0.024	8 ft : +ve moment	0.0395
9 ft : -ve moment	0.0213	8 ft : -ve moment	0.0387
12 ft : +ve moment	0.0215	9 ft : +ve moment	0.0397
12 ft : -ve moment	0.0219	9 ft : -ve moment	0.0376
		10 ft : +ve moment	0.0376
		10 ft : -ve moment	0.0374
Proposed Rebar 1		Proposed Rebar 2	
L (Beam/Girder)		L (Beam/Girder)	
20 ft : +ve moment	0.0213	20 ft : +ve moment	0.0378
25 ft : +ve moment	0.022	25 ft : +ve moment	0.0383
30 ft : +ve moment	0.0213	30 ft : +ve moment	0.0376

7-9 Continuous FRP Rebar

7-9.1 Two-Material Continuous FRP Rebar

For comparison, a continuous scheme similar in materials to that one used by Somboonsong (1997) was investigated. This model consists of two types of continuous fibers: carbon P55 and Kevlar-49. The percentage of fiber is 56%, while epoxy resin is 44%. For the 56% fiber content, 28% of that is carbon and 28% is Kevlar. The modulus of elasticity of P55 carbon fiber is 400 GPa, the modulus of Kevlar-49 fiber is 102 GPa, and the modulus of epoxy resin is 3.5 GPa.

After performing the reliability analysis, it was observed that the flexural reduction factor ϕ for a bridge deck using this bar was 0.82 and for building beams/girders, ϕ was 0.74. The flexural reduction factor ϕ in beams/girders is smaller than that for bridge decks because the c.o.v. of live load for buildings is 0.23, while the c.o.v. of traffic load on bridges is 0.12, causing the building case to have a higher failure probability and thus requiring a lower resistance factor, just as with chopped FRP rebar.

Tables (7-19a,b) and (7-20a,b) show the data used and the results generated using this data.

Table (7-19a): Characteristics of concrete section reinforced continuous FRP for bridge deck.

S=	β	ϕ	Δ (Ductility)	ε (rebar strain at ultimate strain failure in concrete)	Relative cost
9 ft					
+ve moment	3.54	0.82	3.01	0.024	17.41
-ve moment	3.63	0.81	3.02	0.022	17.41
10 ft					
+ve moment	3.51	0.82	3.01	0.0225	16.9
-ve moment	3.52	0.82	3.00	0.0218	16.9
12 ft					
+ve moment	3.53	0.825	3.00	0.02	16.9
-ve moment	3.58	0.82	3.00	0.0201	16.9

Table (7-19b): Constituents of continuous FRP rebar for bridge deck.

S=	v_{C_IM}	v_{K-49}	v_{resin}	A FRP (in^2)	Moment M_n (k-in)
9 ft					
+ve moment	0.29	0.29	0.42	0.26	151
-ve moment	0.29	0.29	0.42	0.30	172
10 ft					
+ve moment	0.28	0.28	0.44	0.30	171
-ve moment	0.28	0.28	0.44	0.312	181
12 ft					
+ve moment	0.28	0.28	0.44	0.365	205
-ve moment	0.28	0.28	0.44	0.35	202

Table (7-20a): Characteristics of concrete section reinforced with continuous FRP rebar building Beam/Girder.

L=	β	ϕ	Δ (Ductility)	ε (rebar strain at ultimate strain failure in concrete)	Relative cost
20 ft					
+ve moment	3.5	0.74	3.0	0.0214	17.41
25 ft					
+ve moment	3.53	0.74	3.0	0.0217	17.41
30 ft					
+ve moment	3.58	0.74	3.0	0.0218	17.41

Table (7-20b) : Constituents of continuous FRP rebar for building Beam/Girder.

L=	v_{C_IM}	v_{K-49}	v_{resin}	A FRP (in^2)	Moment M_n (k-in)
20 ft					
+ve moment	0.29	0.29	0.42	1.9	4132
25 ft					
+ve moment	0.29	0.29	0.42	2.4	6485
30 ft					
+ve moment	0.29	0.29	0.42	2.87	9230

For the four-material proposed chopped FRP rebars, the flexural reduction factor ϕ was 0.9 for bridge decks and 0.83 for building beam/girders. The change in reduction factor is primarily a function of the number of materials rather than material type (i.e. chopped or continuous). Bars with fewer materials have a higher failure probability. This is because stress (and thus moment) at failure is governed by the proportional sum of the elastic moduli of the constituent materials, per equation (3.2a). With only two materials present in the bar, a random low sample for modulus for one material may significantly effect bar capacity. However, when more materials are present, capacity is less affected by a single low modulus.

7-9.2 Three-Material Continuous FRP Rebar

Using three different types of continuous fibers improves the flexural reduction factor for beams/girders over that of the two-material case, but a drawback is that the size of the concrete cross section must be increased in depth significantly. The flexural reduction factor (ϕ) was found to be 0.79 which lies in the middle of results for the 4-material chopped fiber rebar and the 2-material continuous fiber rebar, as shown in Figure (7-4).

It was found that the three different material continuous fiber rebars cannot be practically used in all concrete bridge deck spans due to the larger depth required to meet the desired moment. In order to increase the moment capacity of the cross section such that it is adequate, the amount of reinforcement or volume fractions of fibers must be increased. However, increasing the reinforcement changes the failure mode from ductile

to brittle i.e.; concrete crushes before the desired ductility or strain is reached in the FRP rebar.

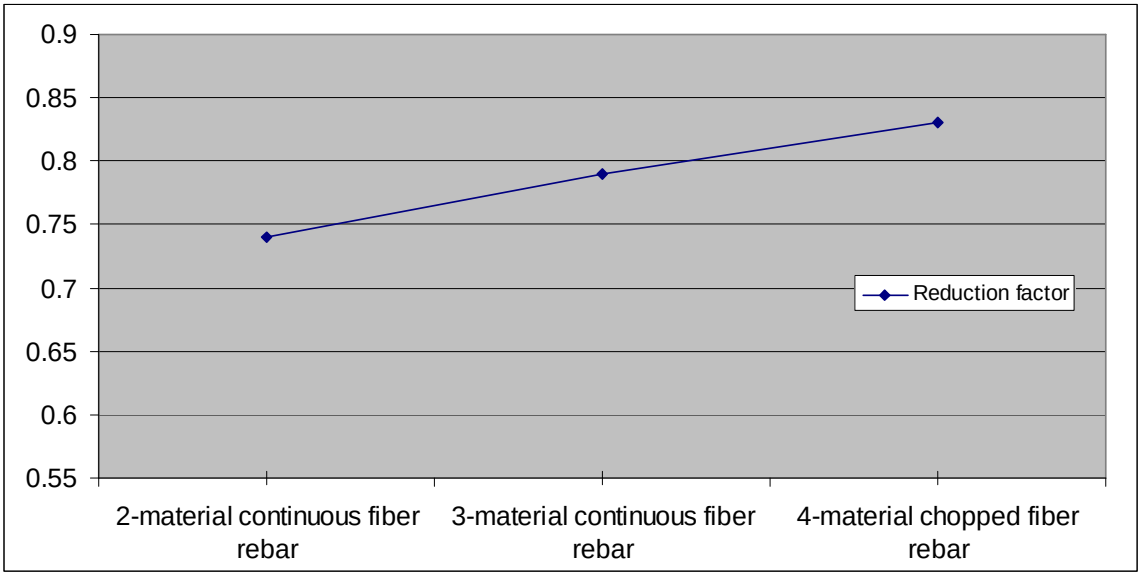

Figure (7-6): ϕ for different number of materials used in D-H-FRP rebars.

7-9.3 Four-Material Continuous FRP Rebar

In general, for the ductility and efficiency constraints to be satisfied, it is desirable to make the cross section wide and deep. It was found that the four different material continuous fiber bar considered is not viable in beams/girders nor in bridge decks, for the following reason: carbon fibers have the highest modulus of elasticity and lowest failure strains among other structural types of fibers. The carbon fibers used have an average modulus of elasticity 4-9 times greater than modulus of elasticity of Kevlar fibers and an average modulus of elasticity 8-12 times greater than modulus of elasticity of glass fibers. Because moment at failure is a function of the modulus of the materials in the bar, once the high-E carbon fibers fail, the remaining materials have insufficient modulus to maintain the moment, violating the failure pattern constraint. In chopped fiber, on the other hand, due to the reductions of modulus of elasticity of the materials, the differences in modulus among the materials are not as great, allowing for the remaining material to carry the moment after the first material (carbon) fails.

In general, the strength of D-H-FRP rebars is smaller than steel bars due to the imposed failure pattern constraint which requires the last fiber to break to maintain the load when all other fibers fail. As a result of this, more reinforcement and/or deeper sections will be needed. A wider section can be used to decrease the stress on the concrete so the fibers can reach the desired strain without crushing the concrete.

Chapter Eight

Discussion

In this chapter, we will discuss the results from Chapter 8. The discussion will cover the effect of randomly dispersed short fibers, and the optimized FRP rebars used in the reinforced concrete section. Steel will be a base for comparison in many cases to evaluate the performance of the proposed rebars.

8-1 Chopped Fibers Performance

8-1.1 Fiber Length

The effect of using chopped fibers has very a small effect on the original modulus of elasticity. The reduction is about 1% if a 6 mm fiber length is used and a smaller reduction if longer chopped fibers are used. The effect using chopped fibers on ultimate strength is more significant than that of modulus of elasticity. A loss of almost 5% is experienced when a 6 mm fiber length is used.

8-1.2 Fiber Randomness Dispersion

The factor that has the most impact on reduction in elasticity is randomness in orientation of the chopped fibers. This results of a loss of 5/8 (62.5%) of its original value of the modulus of elasticity of the fiber (See Section 3-4.1.3). This factor cannot be changed or reduced if randomly dispersed chopped fibers are used. The impact of random dispersion is higher on composite ultimate strength, which is reduced by 80% of the original

strength of the fibers. However, this effect does not play a noticeable role in the proposed rebars since the chopped fiber composite layers will fail by reaching the ultimate failure strain before the composites reach the ultimate strength. i.e.; the stress in the composite layer, σ_c, will be less than ultimate tensile strength of the composite σ_{cu}, as discussed in Chapter 7, Section 7-4.

8-2 Proposed Rebars Relative Performance

A comparison with conventional steel bars, grade 60 and grade 40, will be performed. Two types of comparison have been done using: stress-strain curves and moment-curvature curves.

8-2.1 Stress-Strain Curves Comparison

Figure (8-1) shows stress-strain curves for the proposed H-D-FRP rebars and conventional steel bars. For the proposed rebars, the volume fractions are based on the building beam/girder with a span of span 20 ft.

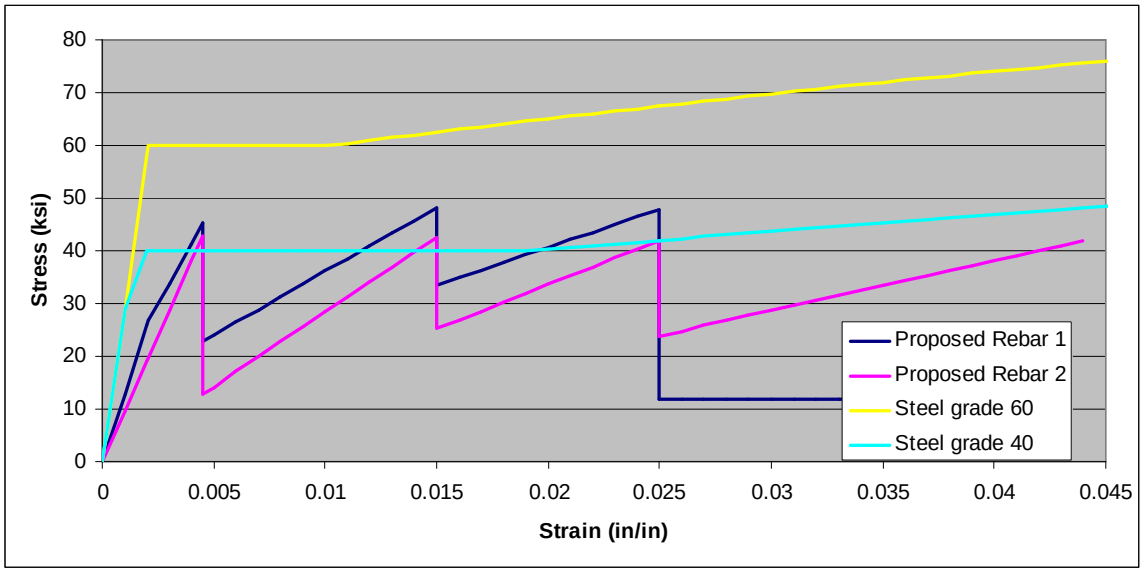

Figure (8-1): Stress-strain curves for proposed rebars and conventional steel bars.

From the above Figure it can be observed that:

1- proposed H-D-FRP rebars strength is greater than that of steel grade 40 and around 75% of yield stress of steel bar grade 60.
2- The stiffness (modulus of elasticity) of the proposed H-D-FRP rebars is around 1/3 of those of steel bars grade 40 and 60.
3- The failure strain of the proposed H-D-FRP rebar 1 and rebar 2 is much beyond the yield strain of steel grade 60 and grade 40. Proposed H-D-FRP rebar 1 has a failure strain around 12 times greater than steel yield strain and proposed H-D-FRP rebar 2 has a failure strain around 21 times greater than the yield strain of steel.

8-2.2 Moment-Curvature Curves Comparison

Figure (8-2) shows the moment-curvature curves for the proposed rebars and conventional steel bars based on the same amount of reinforcement. The material properties and cross-section dimensions are shown in Table (8-1). Appendix (E) shows moment-curvature curves of continuous fiber for some selected works.

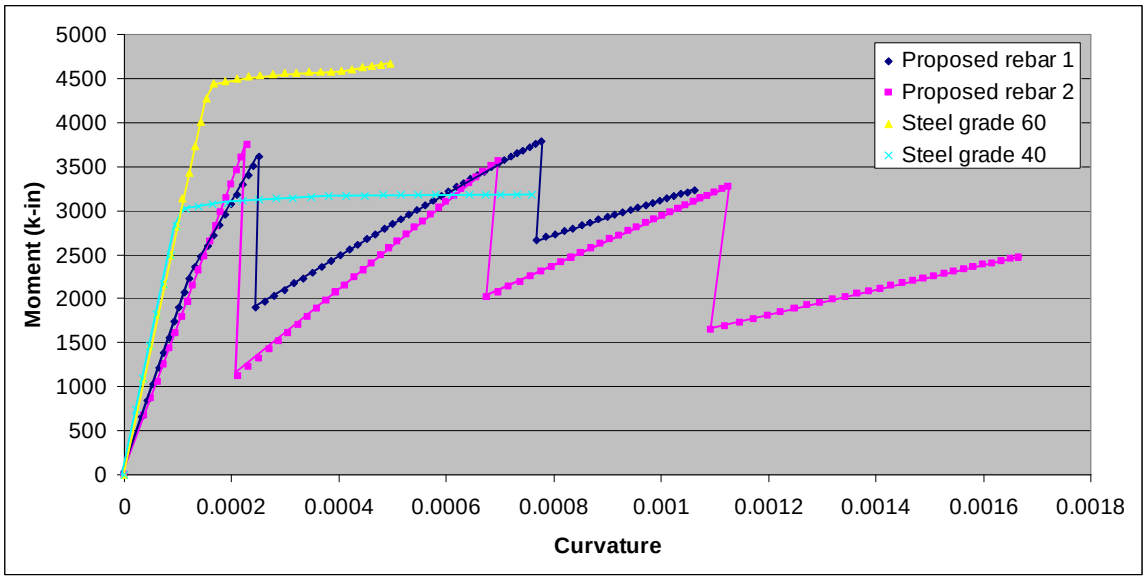

Figure (8-2): Moment-curvature curves for proposed rebars and conventional steel bars.

From the above Figure it can be observed that:

1- The ultimate curvatures of the proposed rebars are higher than those of conventional steel. The reason behind this is that after the steel yields (grade 60), the stress remain constant until it reaches the strain hardening point where the stress in the steel increases dramatically. This will be accompanied by an increase in the strain in the concrete to balance the force from the steel. Close to the strain hardening point, the concrete will crush by reaching the ultimate strain. At this point, the strain in the reinforcement is less than 4 times the yield strain. In the FRP rebar, due to the relatively low modulus of elasticity, in general the stresses in the bar are less than those in the steel (as shown in stress-strain diagrams). After reaching the first fiber material failure strain, the stress in the bar will drop down and less force is present in the concrete needed to balance the reinforcement force, allowing the reinforcement strain to again increase to the second peak on the diagram where the second fiber material breaks by reaching it ultimate strain. By continuing this process, the ultimate strain generated is relatively high. Since curvature is $\phi = \frac{\varepsilon_c}{c} = \frac{\varepsilon_{FRP}}{d-c}$, curvature is proportional to strain in the reinforcement, and similarly high at ultimate failure of the reinforcement. When there is a drop in the stress due fiber failure, the distance from the compression face to neutral axis, *c*, will increase but the shape of stress-strain of the concrete will be narrower according to the Modified Hognestad's model. If the value (*d*-*c*) increases more than the increase in ε_{FRP}, the result will be a decrease in curvature $\phi = \frac{\varepsilon_{FRP}}{d-c}$. This is not the case in conventional steel bars.

2- The concrete cross-sections reinforced with the proposed rebars are generally a little bit bigger than those sections reinforced with conventional steel. The reason behind that is by increasing the depth of the cross section, the moment arm will increase and thus moment capacity of the section will increase since the tensile strength of D-D-FRP rebars are less than those of steel (See Figure (8-1). By increasing the width of the cross section, the stress developed on the concrete will

decease and this will allow to get the desired ductility and strain in the reinforcing bars.

3- In Figures 8-1 and 8-2, the ductility index for the concrete section reinforced with conventional steel grade 60 is 3.2; reinforced with conventional steel grade 40 is 7.2; reinforced with proposed rebar 1 is 4.7; and reinforced with proposed rebar 2 is 10.8.

4- The *design moment capacity* of sections reinforced with the proposed H-D-FRP rebars is less than that of cross-sections reinforced with conventional steel grade 60 (around 80%), but higher than that of sections reinforced with conventional steel grade 40. The design moment capacity is taken as the moment at which the first type of chopped fiber breaks.

5- The slope (i.e. stiffness) of beams designed with H-D-FRP rebars is less than those designed with conventional steel bars.

Table (8-1): Cross-section dimensions and material properties.

	Proposed rebar 1	Proposed rebar 2	Steel grade 60	Steel grade 40
f_c' (psi)	5500	5500	4500	4500
b (in)	13	14	12	12
h (in)	25	27	24	24
d (in)	22.5	24.5	21.5	21.5
A_{FRP} (in2)	4	3.93	4	4

8-3 Deflection Control

Figure (8-3) shows a comparison between the deflection of beams reinforced with the proposed rebars and steel grade 60 for different girder lengths. As mentioned earlier, the proposed rebars always need a bigger cross section and higher concrete compressive strength to reach the desired ductility by reaching the ultimate failure strain without crushing in the concrete. Table (8-2) shows concrete cross section dimensions, amount of reinforcement, and concrete compressive strength.

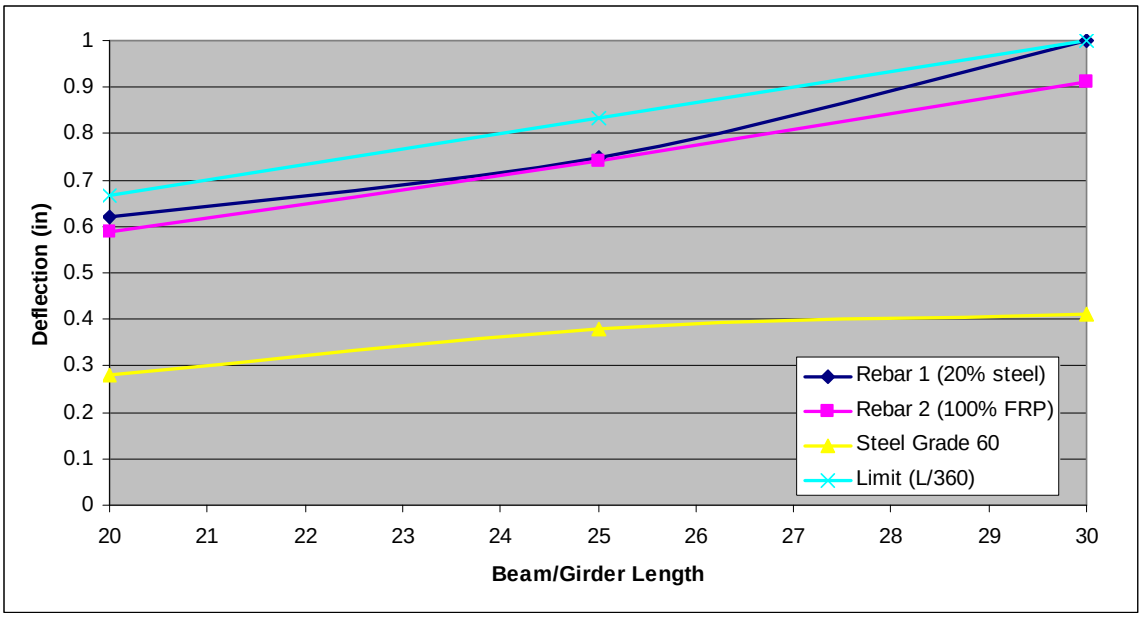

Figure (8-3): Deflection of different types of rebars and limiting values.

Table (8-2): Dimensions and properties used for deflection calculations.

	L = 20 ft		
	Rebar 1 (20% steel)	Rebar 2 (100% FRP)	Steel Grade 60
$A_{reinforcement}$ (in^2)	4	3.93	4
h (in)	25	27	24
d (in)	22.5	24.5	21.5
b (in)	13	14	12
f'_c (psi)	5500	5500	4500
	L =25 ft		
	Rebar 1 (20% steel)	Rebar 2 (100% FRP)	Steel Grade 60
$A_{reinforcement}$ (in^2)	5.46	4.95	5
h (in)	30	33	28
d (in)	27.5	30.5	25.5
b (in)	14	14.5	14
f'_c (psi)	5500	5500	4500
	L =30 ft		
	Rebar 1 (20% steel)	Rebar 2 (100% FRP)	Steel Grade 60
$A_{reinforcement}$ (in^2)	7.2	6.3	6
h (in)	32.5	36.5	30
d (in)	30	34	27.5
b (in)	16	16	14
f'_c (psi)	5500	5500	4500

From Figure (8-3), it is clear that both proposed rebars have very close deflection but the deflection in steel has noticeably less deflection. We also can observe from the same Figure that sections using the proposed rebars can meet the deflection limit specified by ACI-318. From Table (8-2) we can observe that proposed rebar 1 needs more reinforcement but a slightly smaller cross section than proposed rebar 2. We also can observe that steel grade 60 is superior to proposed rebar 1 and 2 when it comes to deflection, and require a smaller cross section.

In order to have deflections in beams reinforced with D-H-FRP rebars equal to that of deflections in beams reinforced with conventional steel bars, the depth of the cross section should be increased.

8-4 Cost, Ductility, and Ultimate Strain

Although cost does not play a major role in the optimization process as much as the constraints, the cost of both proposed rebars are very close as well as the area of reinforcement. The ductility achieved by proposed rebar 2 is almost double or triple those achieved from proposed rebar 1. The reason behind this is that the ultimate failure strain of proposed rebar 2 is higher than that of proposed rebar 1. Consequently, the area under the moment-curvature curve is bigger for proposed rebar 2, as shown in Figure (8-2). At section failure, the percentage of ultimate strain reached by proposed rebar 1 is much higher than that reached by 2. In many occasions, we have reached 100% of the ultimate strain of the fiber (0.025 in/in), while the average ultimate strain reached by proposed rebar 2 is 87% of its ultimate failure strain. The reason behind this is very obvious. It is easier to reach ultimate strain failure of 0.025 in/in before concrete crushes than reach ultimate strain failure of 0.044 in/in. The 0.025 in/in is the ultimate strain of proposed rebar 1 while 0.044 in/in the ultimate strain of proposed rebar 2.

8-5 Cost Comparison

According to Janney, Geiger, and Baitcher (2007), chopped fibers don't have to be dried and need not be wound onto bobbins which is the case for continuous fibers. As a result of this, the cost of chopped fiber to the cost of continuous fiber is estimated at approximately (1:1.6). It has been mentioned earlier that there are three major approaches presented in the literature to continuous fiber D-H-FRP rebar. Figure (8-4) shows a comparison in materials used in these models and the two models considered in this study based on relative and roving form costs.

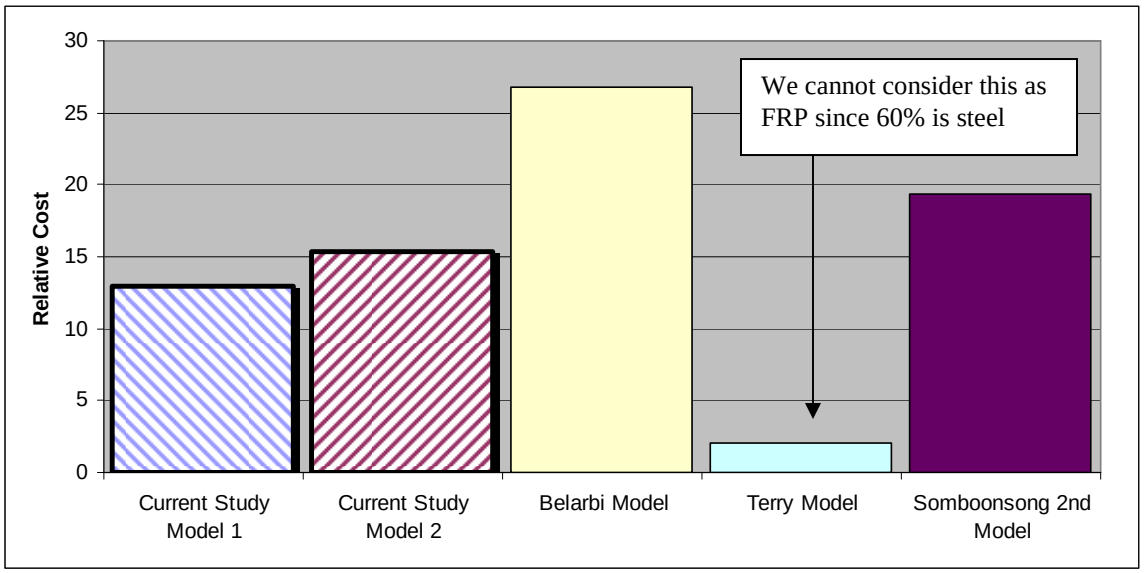

Figure (8-4): Relative costs of different D-H-FRP models.

A few notes should be listed here:

1- Terry's model has around 60% steel, which makes it cheap but may be prone to corrosion since no much fibers and resin to protect the core steel. A sand-coated layer was used in this model.
2- Belarabi's model has the most expensive materials in the market, but no corrosion is expected. Filament winding was used in this model.
3- Somboonsong's 2nd model has no steel and reasonably priced materials. Braiding for the exterior layer was used in this study.

4- The proposed FRP rebars are the cheapest models among all other models.

As these ductile bars are experimental and have yet to be mass-produced, manufacturing costs are not known. However, it is known that the cost of manufacturing chopped-fiber composites is generally less than that of continuous-fiber composites (Mathews and Rawlings, 1999). Thus, additional cost benefits are expected to be realized with the proposed schemes over those shown in Figure 8-4.

8-6 Reliability Indexes of The New Proposed Rebars

Reliability indexes for both proposed rebars for bridge deck and building beams/girder for girder spacing and beam length selected are close to each others and close to the target value β_T =3.5. This is shown clearly in Figures (8-5) to (8-8).

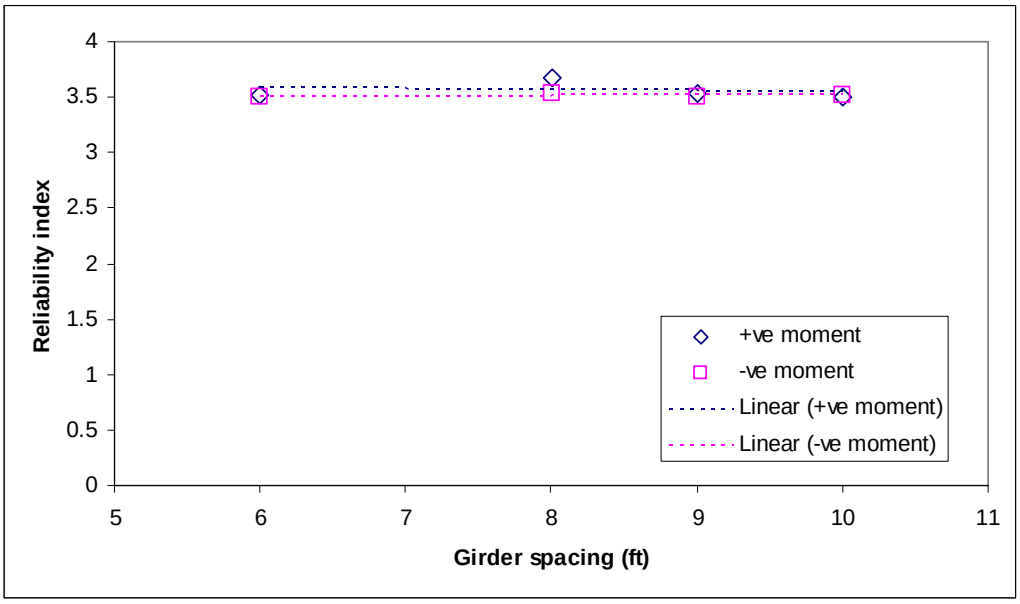

Figure (8-5): Reliability indexes for bridge deck reinforced with D-H-FRP rebar 1, bending limit state.

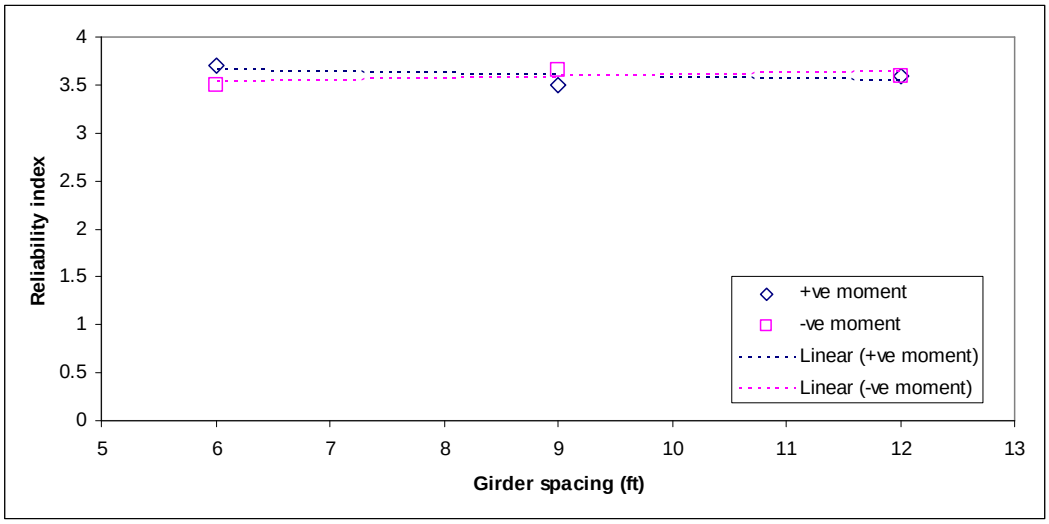

Figure (8-6): Reliability indexes for bridge deck reinforced with D-H-FRP rebar 2, bending limit state.

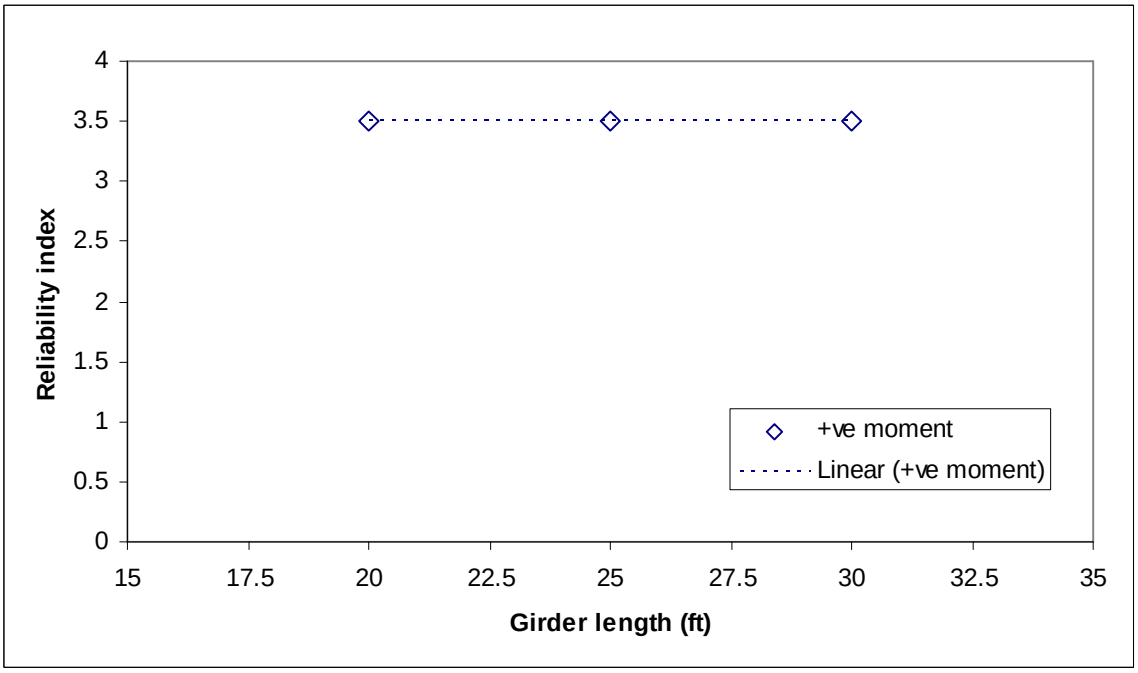

Figure (8-7): Reliability indexes for beam/girder reinforced with D-H-FRP rebar 1, bending limit state.

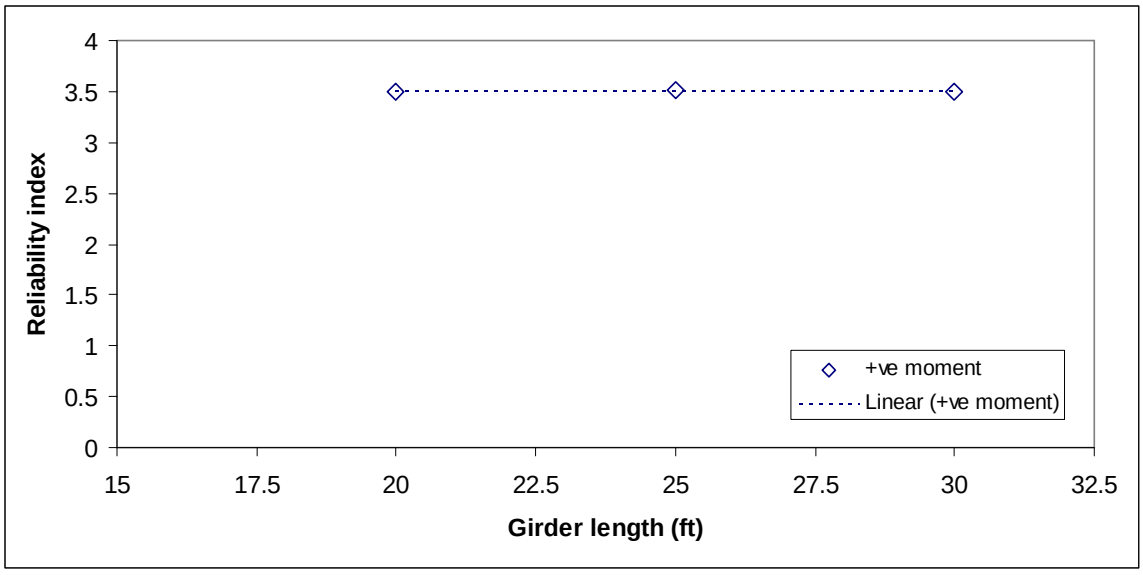

Figure (8-8): Reliability indexes for beam/girder reinforced with D-H-FRP rebar 2, bending limit state.

8-7 Capacity Reduction Factor ϕ

From Tables (7-7) to (7-10), it easy to conclude the Capacity Reduction Factor ϕ for flexure, for design purposes, should be used as shown in Table (8-3).

Table (8-3): Capacity reduction factor for flexure to use in design.

	Capacity Reduction Factor ϕ		
	Proposed D-H-FRP rebar 1	Proposed D-H-FRP rebar 2	Continuous FRP rebar 2 materials
Bridge deck	**0.9**	**0.88**	**0.82**
Beam/Girder	**0.83**	**0.83**	**0.74**

The reason the that flexural reduction factor ϕ for bridge decks is greater than that for building beams/girders comes from the fact the live load coefficient of variation for building beams/girders is double the live load coefficient of variation for bridge decks

The c.o.v for bridge decks is taken 0.12 (Nowak, 1999) and c.o.v for building beams/girders is taken 0.23 (Ellingwood et al., 1980). The lower c.o.v. corresponds to a lower failure probability, or a higher reliability index, requiring less of a reduction factor in bridge decks than in building beams. For simplicity and in order to use one number for each structural component, it is recommended to use:

$\phi = 0.89$ for bridge decks.

$\phi = 0.83$ for building beams/girders.

For conventional steel reinforcement grade 60, according to AASHTO specifications, $\phi = 1$ for bridge decks and $\phi = 0.9$ for building beams/girders. For verification purposes, Mote-Carlo simulation was conducted on a beam reinforced with conventional steel of yield strength equals 60 ksi and concrete of compressive strength equals 4500 psi. The resulting value of reduction factor ϕ was found to be 0.9 and the corresponding β_T was found to 4.0. The reason that ϕ of steel bar is greater than ϕ of FRP rebar comes from many sources like the changes in E of fibers (c.o.v.), changes in volume fractions of fibers (c.o.v.) (although these two reasons play a minor role), and bias factor λ for yield strength which is about 1.14 while bias factor λ for Es of fibers was taken 1.0 since there are a wide variety of E under the same name and no comprehensive study to measure the bias factor.

Chapter Nine

Conclusions and Recommendations

9-1 Conclusions

1- The effect of short fiber length on fiber modulus of elasticity and composite ultimate strength is small.
2- The effect of randomness of chopped fiber orientation on fiber modulus of elasticity and composite ultimate strength is very big.
3- The effect of curvature is small on modulus of elasticity for the proposed schemes, but it could be very high if chopped fibers are mis-sized or mis-positioned.
4- Both proposed rebar 1 and rebar 2, which are built of randomly dispersed chopped fibers, can be used successfully to replace conventional steel reinforcements.
5- The ductility index of proposed rebar 2 is higher than that of proposed rebar 1.
6- Proposed rebar 2 needs a bigger cross sectional area to reach the desirable ductility. This is because of the high failure strain of E-glass fibers (0.044 in/in), which require a higher compressive force in the concrete to balance the force in the reinforcement.
7- Deflection is higher for concrete beams reinforced with the proposed D-H-FRP rebars than concrete beams reinforced with conventional steel.
8- Ductility indices obtained from using the proposed D-H-FRP rebars is higher from those obtained from using conventional steel grade 60[1].
9- The concrete compressive strength used with D-H-FRP rebars should be higher than that used for conventional steel.

[1] Ductility index for conventional steel is between 3.00 and 3.3.

10- The concrete cross section reinforced with D-H-FRP rebar should be bigger than that section reinforced with conventional steel.
11- The composite FRP rebars will not reach ultimate tensile failure before concrete crushing.
12- In general, due to the many constraints imposed on the objective function, there is a small feasible domain for the design variable function. This explains why relative costs do not play a major role; i.e. material volumes had very little room for adjustment.
13- The flexural capacity reduction factor ϕ for the proposed rebars is smaller than those of conventional steel.
14- The initial cost of the new proposed rebars is much higher than the cost of using conventional steel, but they need no maintenance, so long term costs may be lower than that of steel.

9.2 Recommendations for Future Studies

1- A full-scale model of the proposed rebars and concrete bridge deck and beam/girder reinforced with these rebars should be built to experimentally verify the analytical results.
2- Using finite element methods, the proposed rebars can be modeled and tested. A comparison between the theoretical model results and the numerical results generated from FEM should be made to verify the results.
3- Different types of continuous and chopped plastic fibers can be used. For example, a different rebar composed of chopped SM-Carbon fiber, chopped Kevlar-49 fiber, continuous E-glass fibers and limited amount of steel in the core, could give good results.
4- An economical study and comparison between concrete sections reinforced with D-H-FRP rebars and conventional steel bars could show which one is best long term. This is a very important and crucial point.

5- Aligned chopped fibers will improve the performance of fiber reinforced polymer composites.

APPENDICES

APPENDIX A

Moment Diagram for Bridge deck.

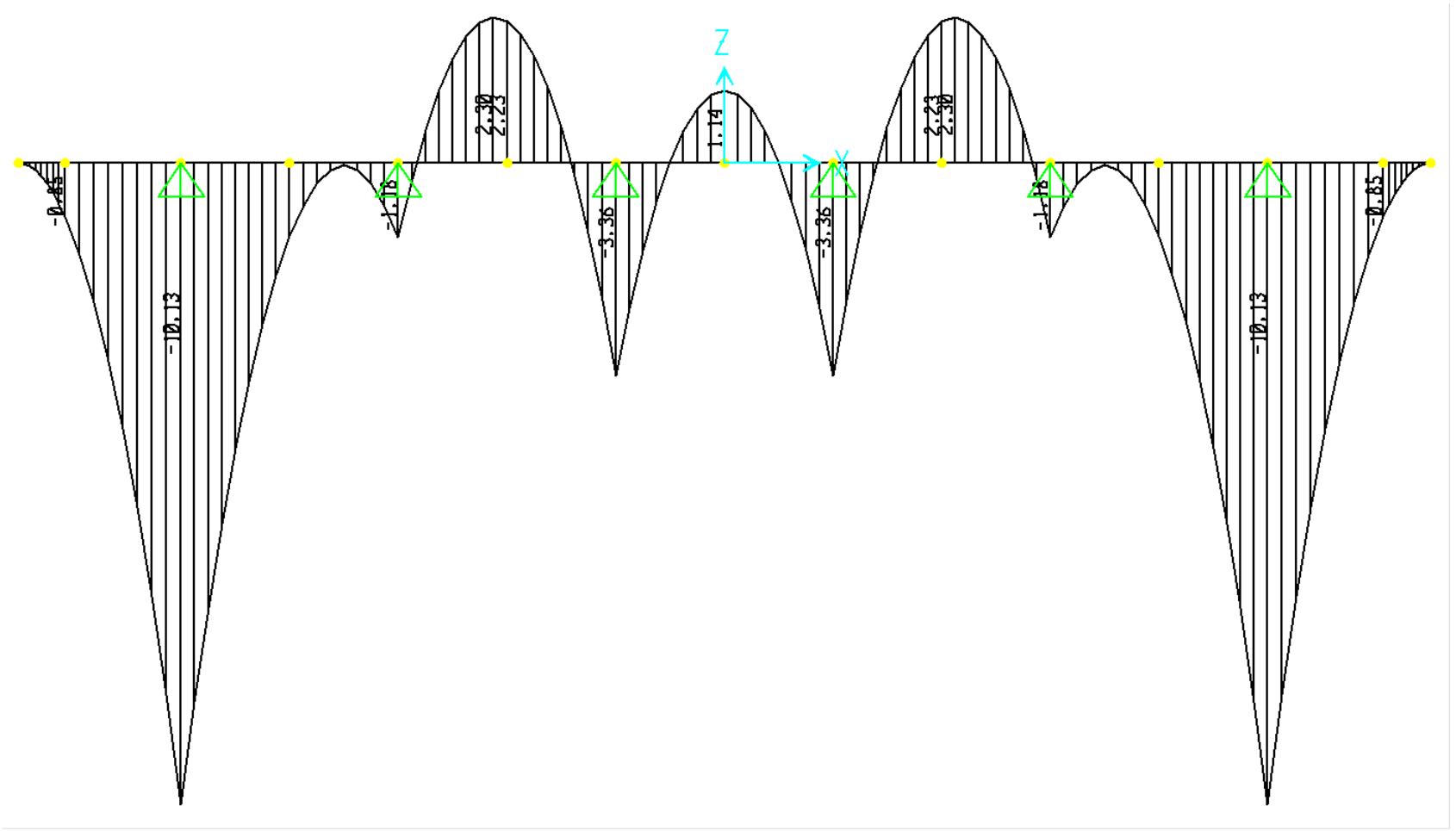

Figure (A-1): Moment diagram due to the deck own weight of 1 k/ft for S = 6 ft

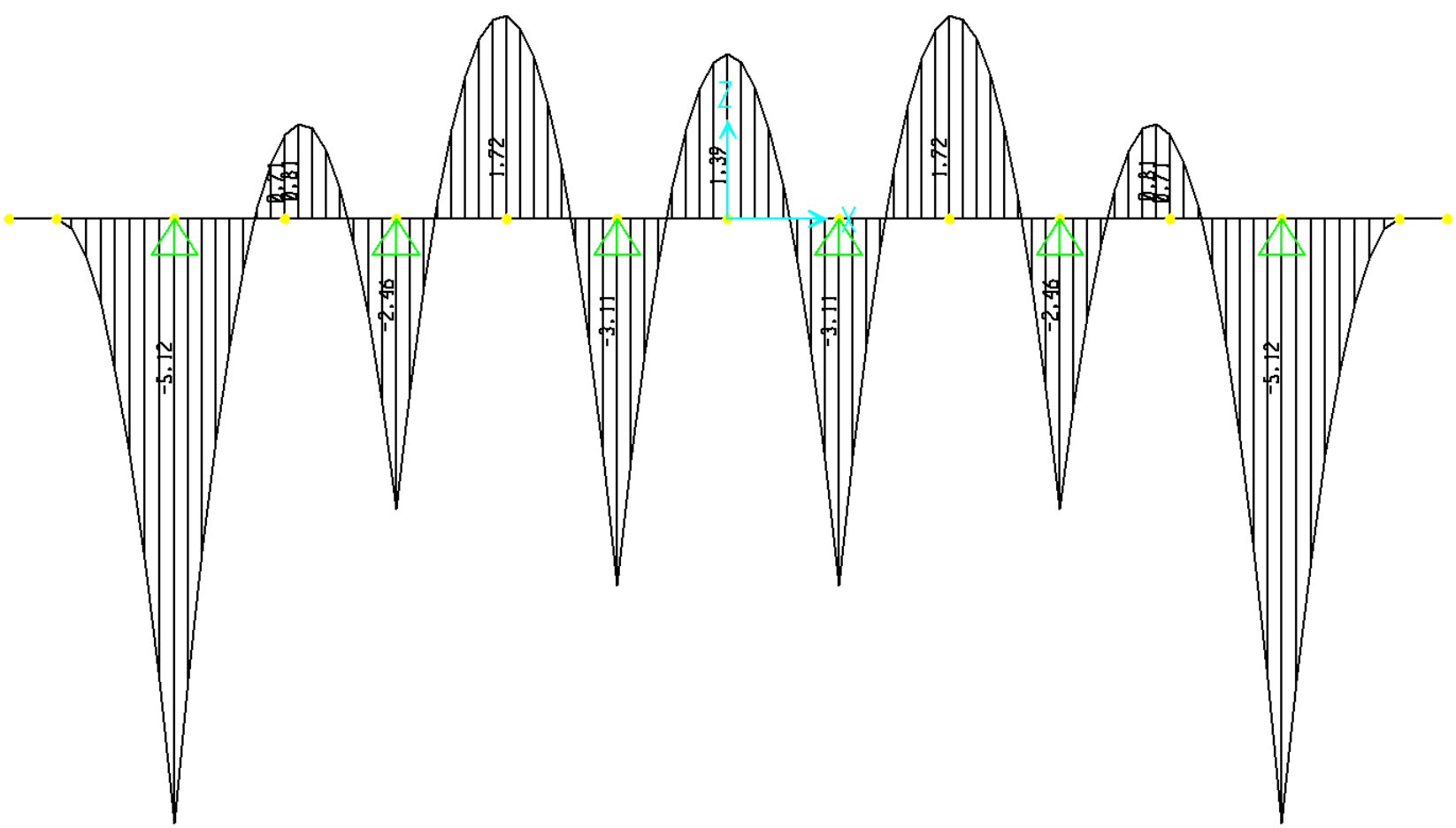

Figure (A-2): Moment diagram due to asphalt future wearing surface of 1 k/ft for S = 6 ft

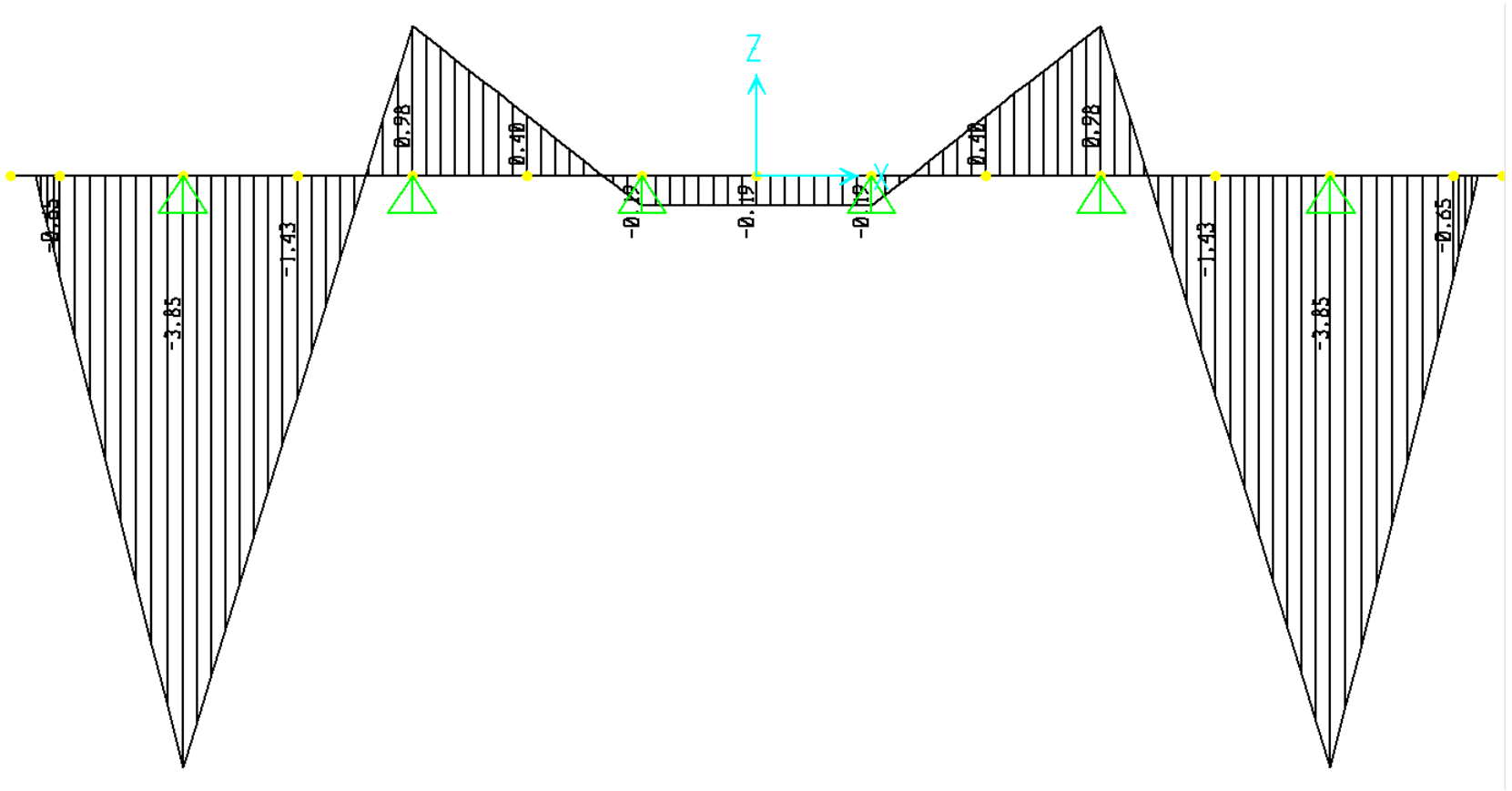

Figure (A-3): Moment diagram due to parapet weight of 1 k for S = 6 ft

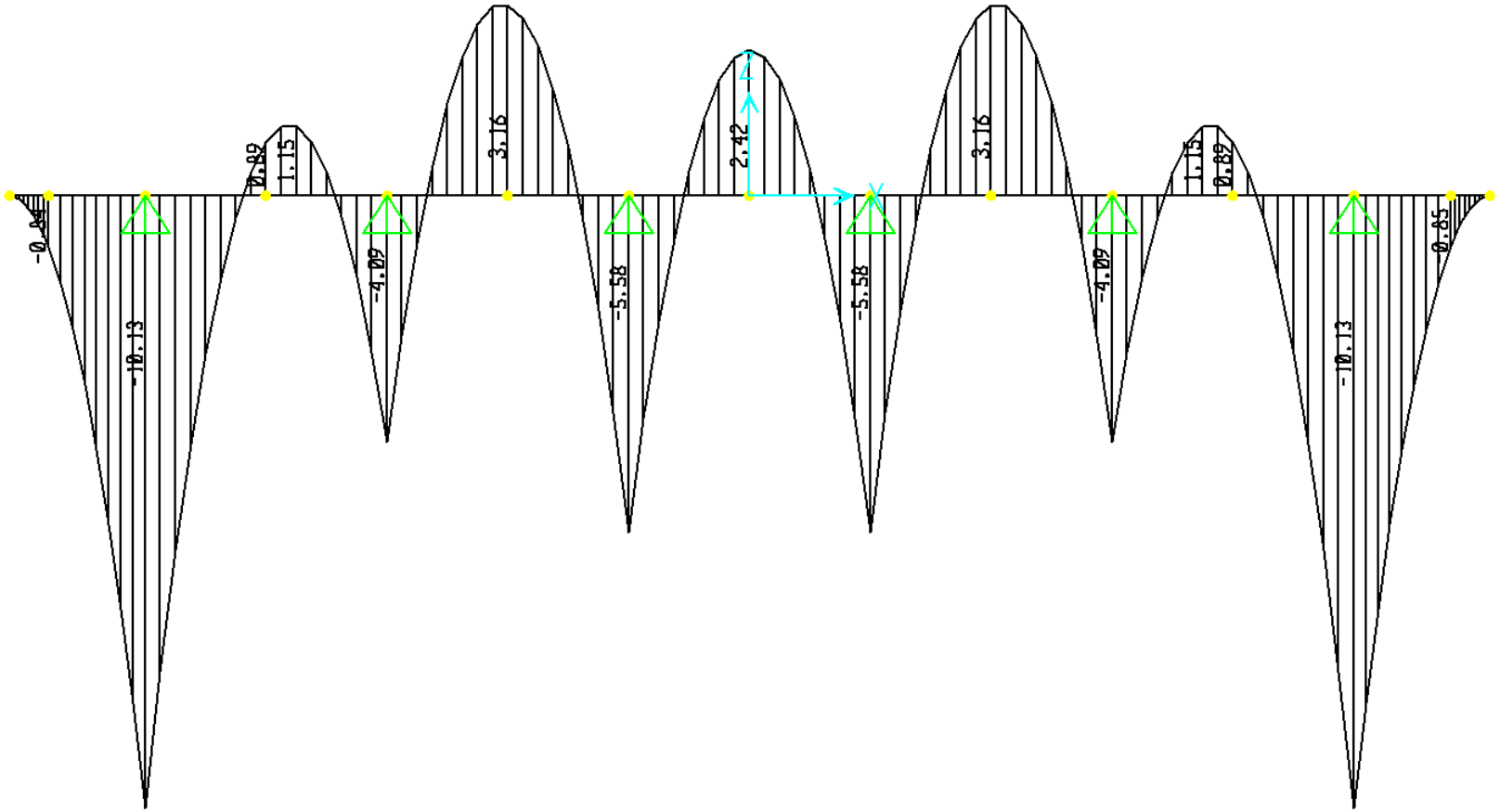

Figure (A-4): Moment diagram due to the deck own weight of 1 k/ft for S = 8 ft

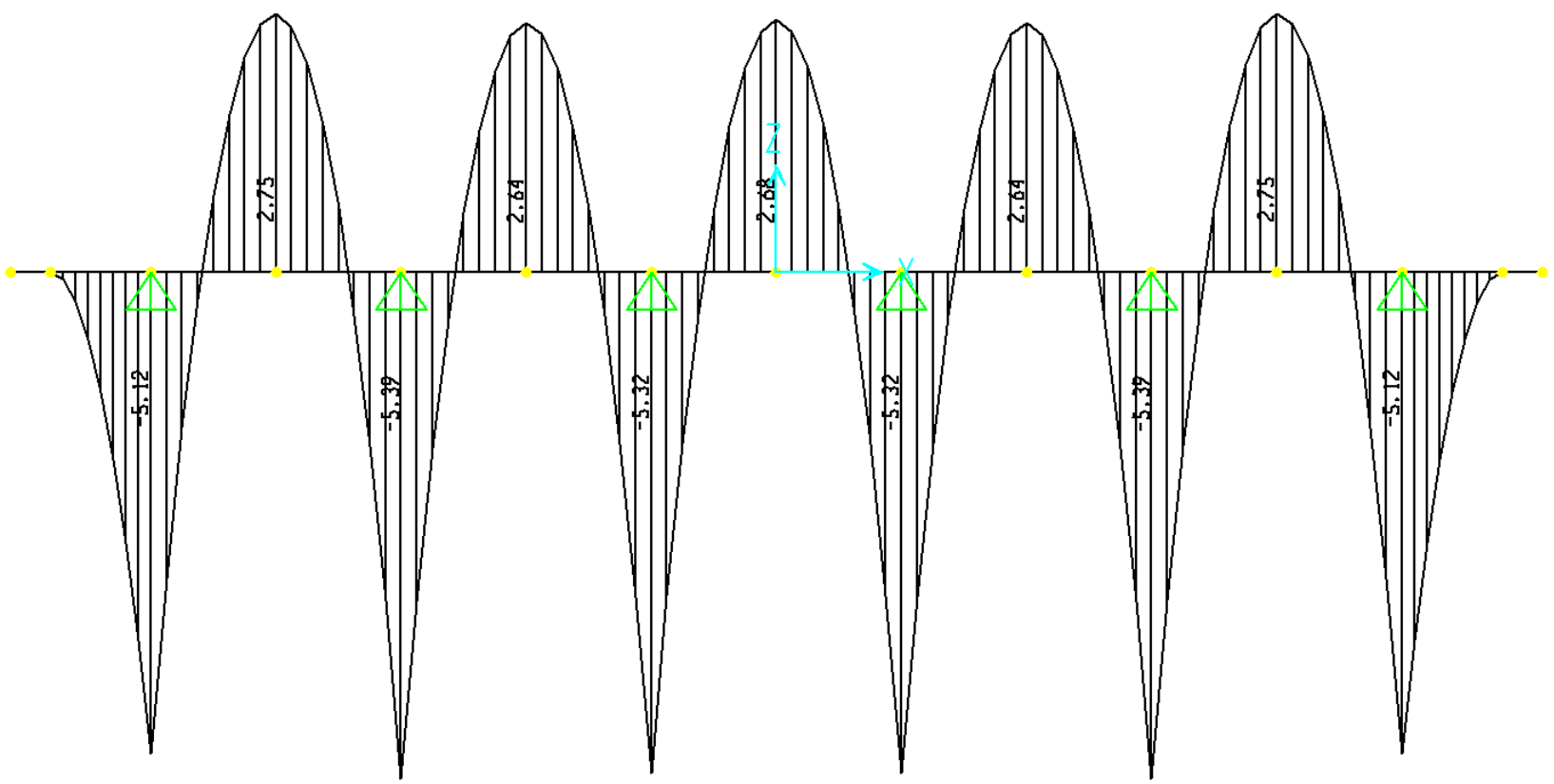

Figure (A-5): Moment diagram due to asphalt future wearing surface of 1 k/ft for S = 8 ft

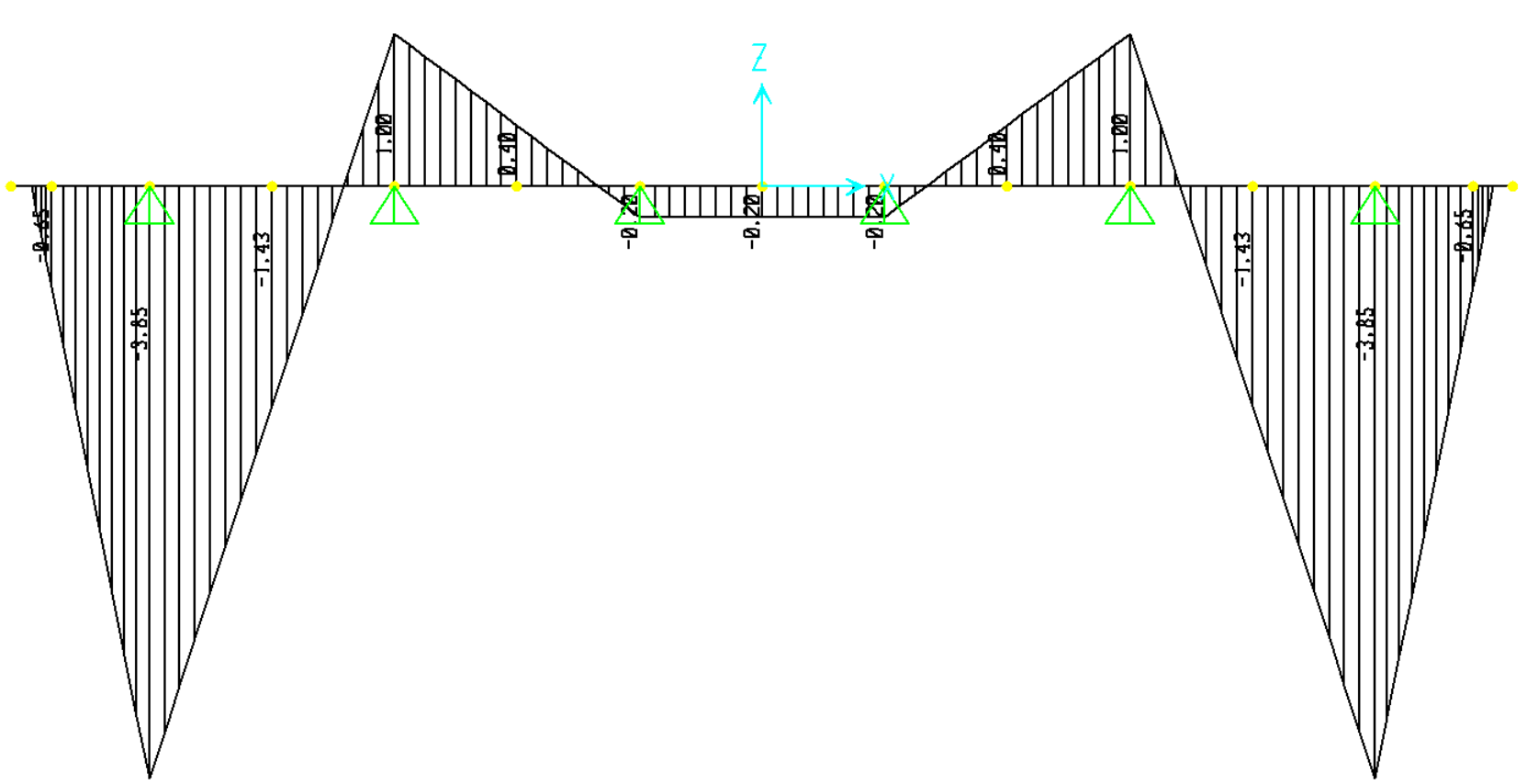

Figure (A-6): Moment diagram due to parapet weight of 1 k for S = 8 ft

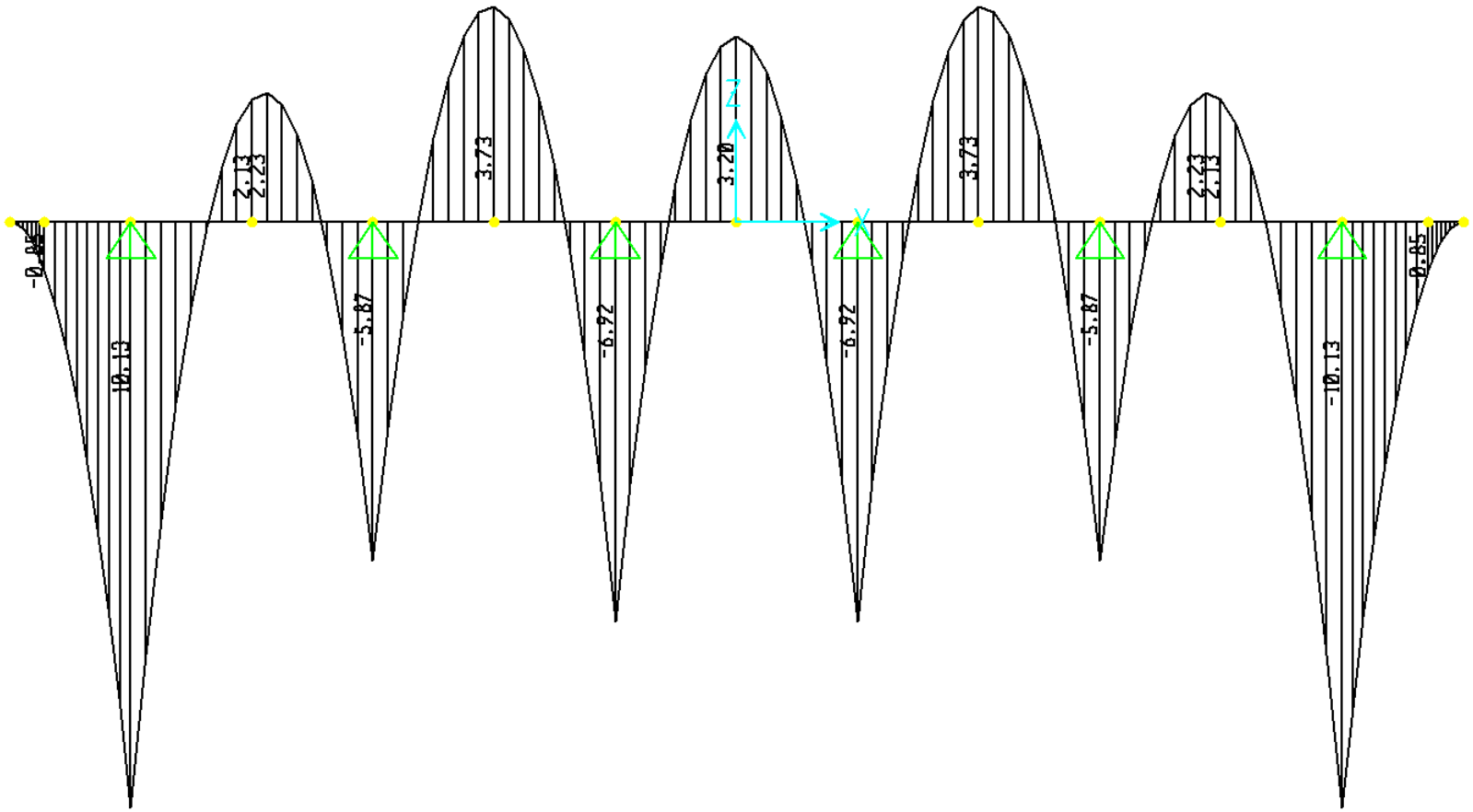

Figure (A-7): Moment diagram due to the deck own weight of 1 k/ft for S = 9 ft

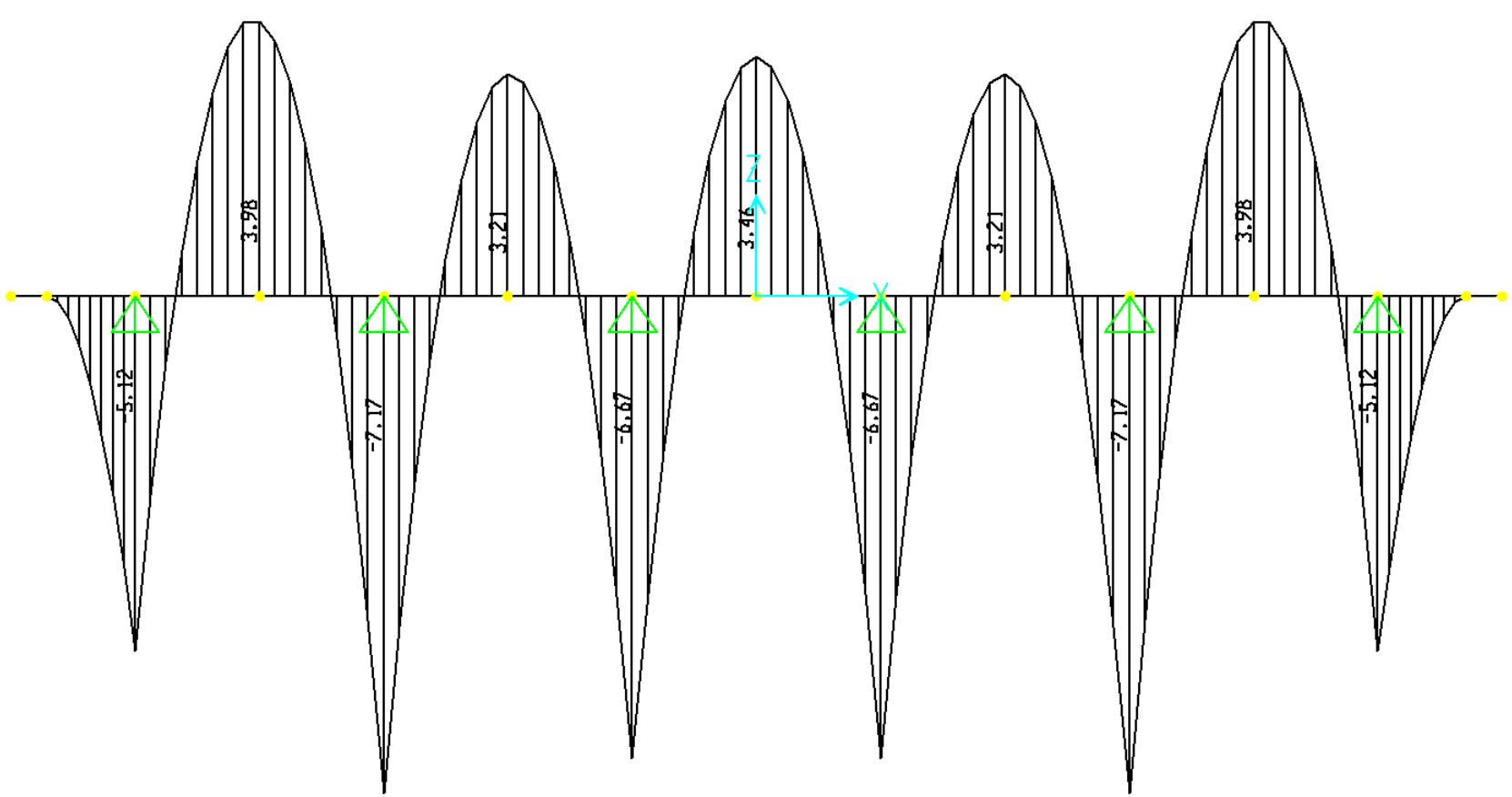

Figure (A-8): Moment diagram due to asphalt future wearing surface of 1 k/ft for S = 9 ft

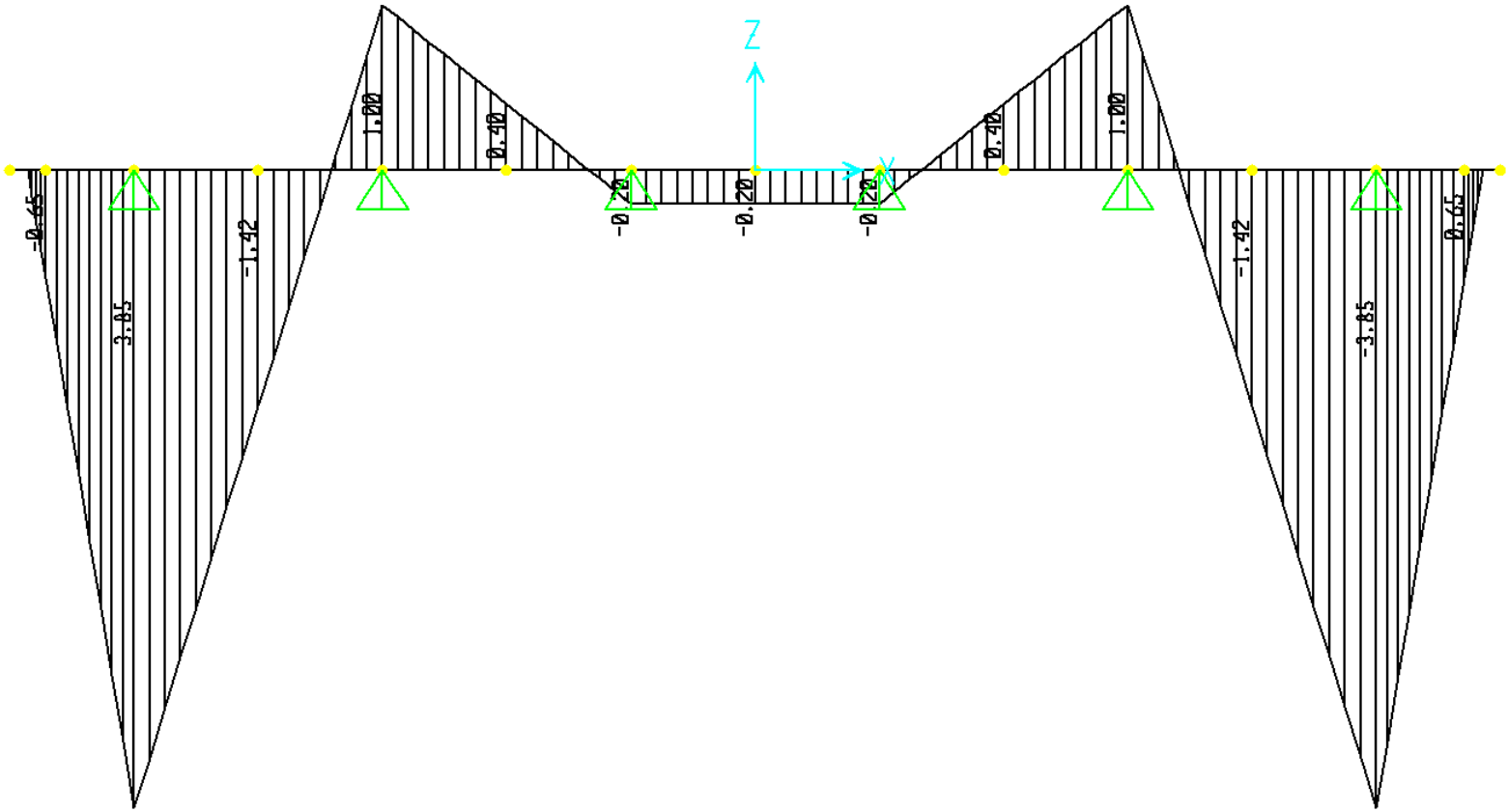

Figure (A-9): Moment diagram due to parapet weight of 1 k for S = 9 ft

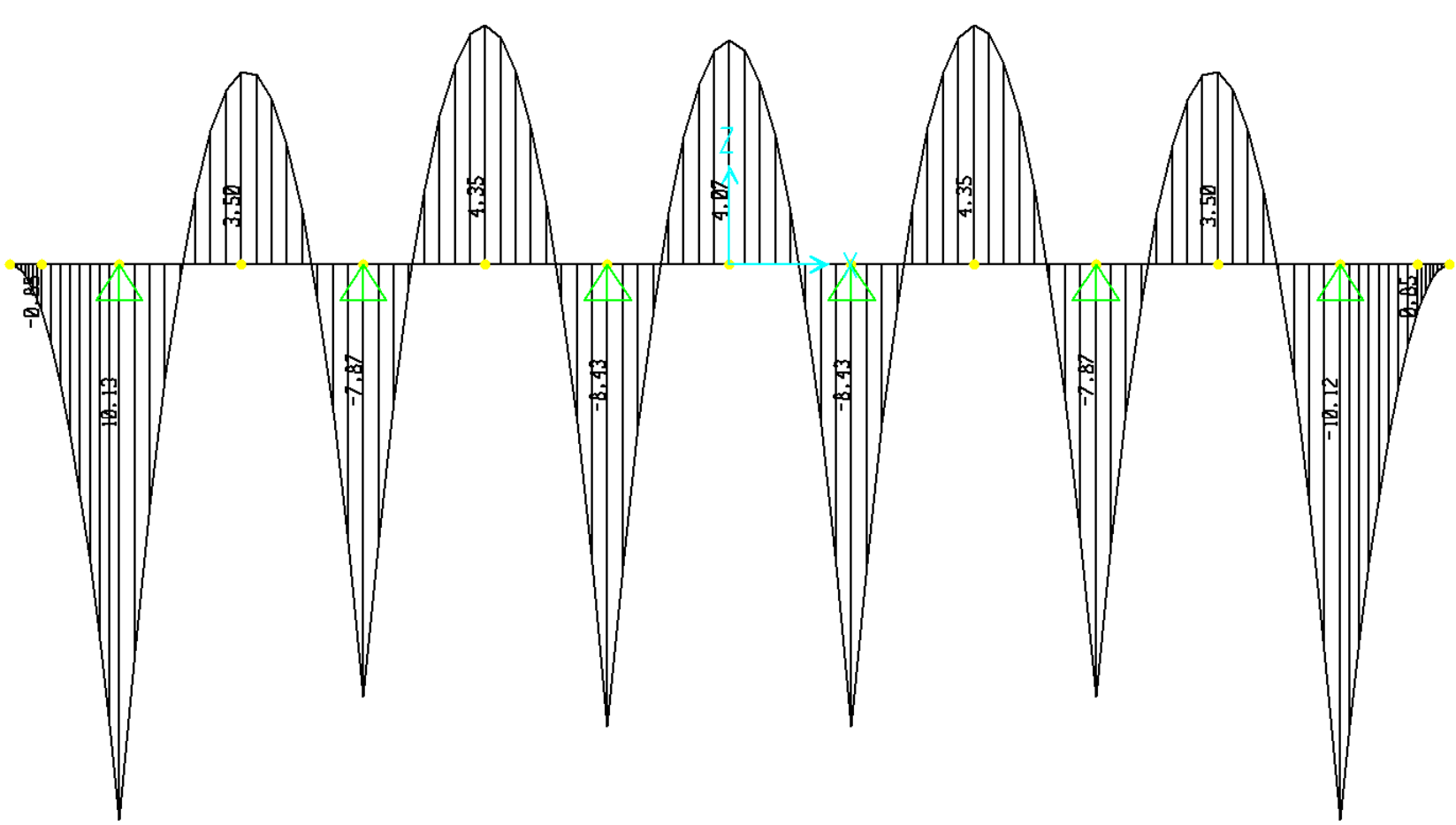

Figure (A-10): Moment diagram due to the deck own weight of 1 k/ft for S = 10 ft

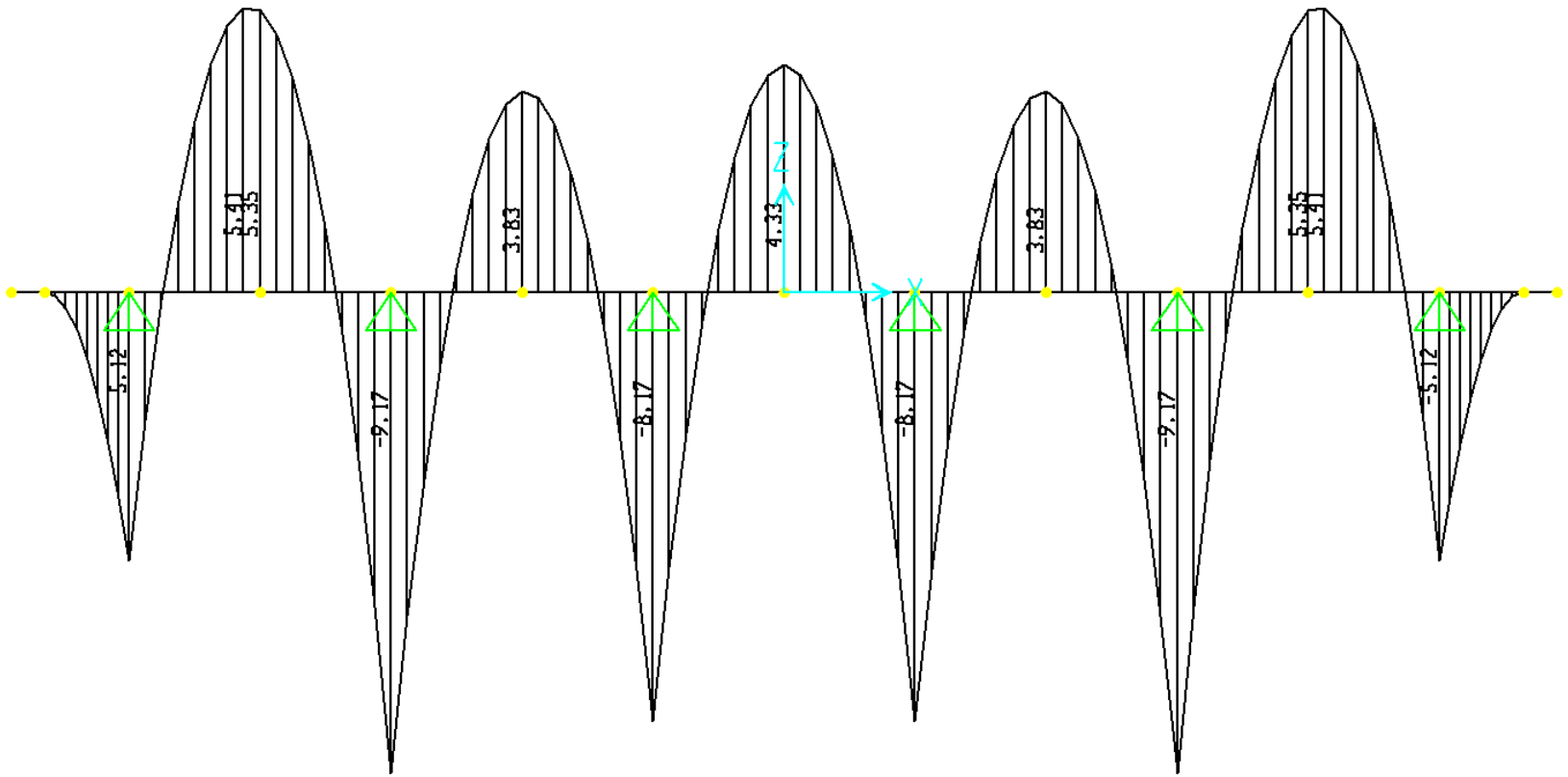

Figure (A-11): Moment diagram due to asphalt future wearing surface of 1 k/ft for S = 10 ft

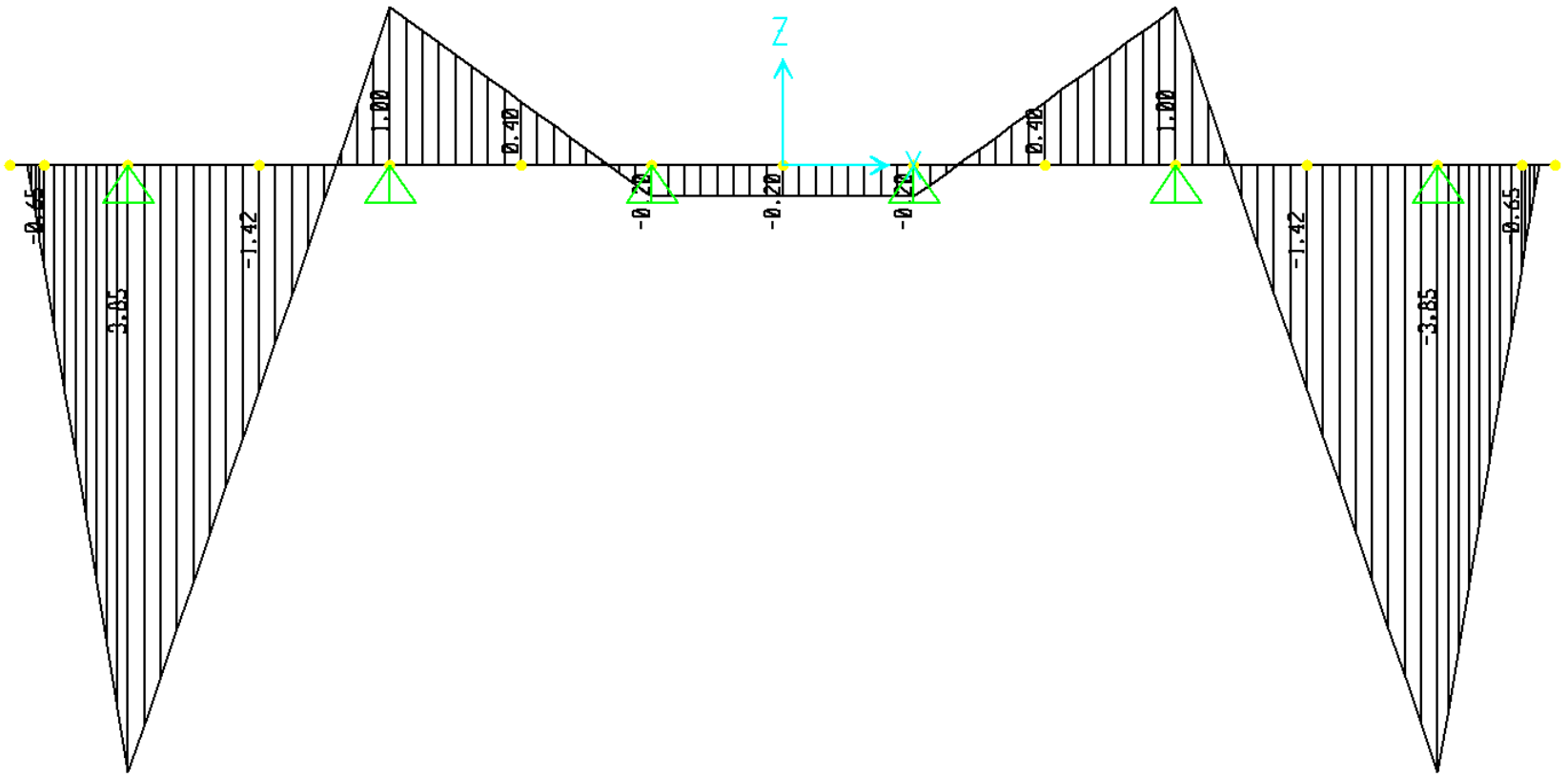

Figure (A-12): Moment diagram due to parapet weight of 1 k for S = 10 ft

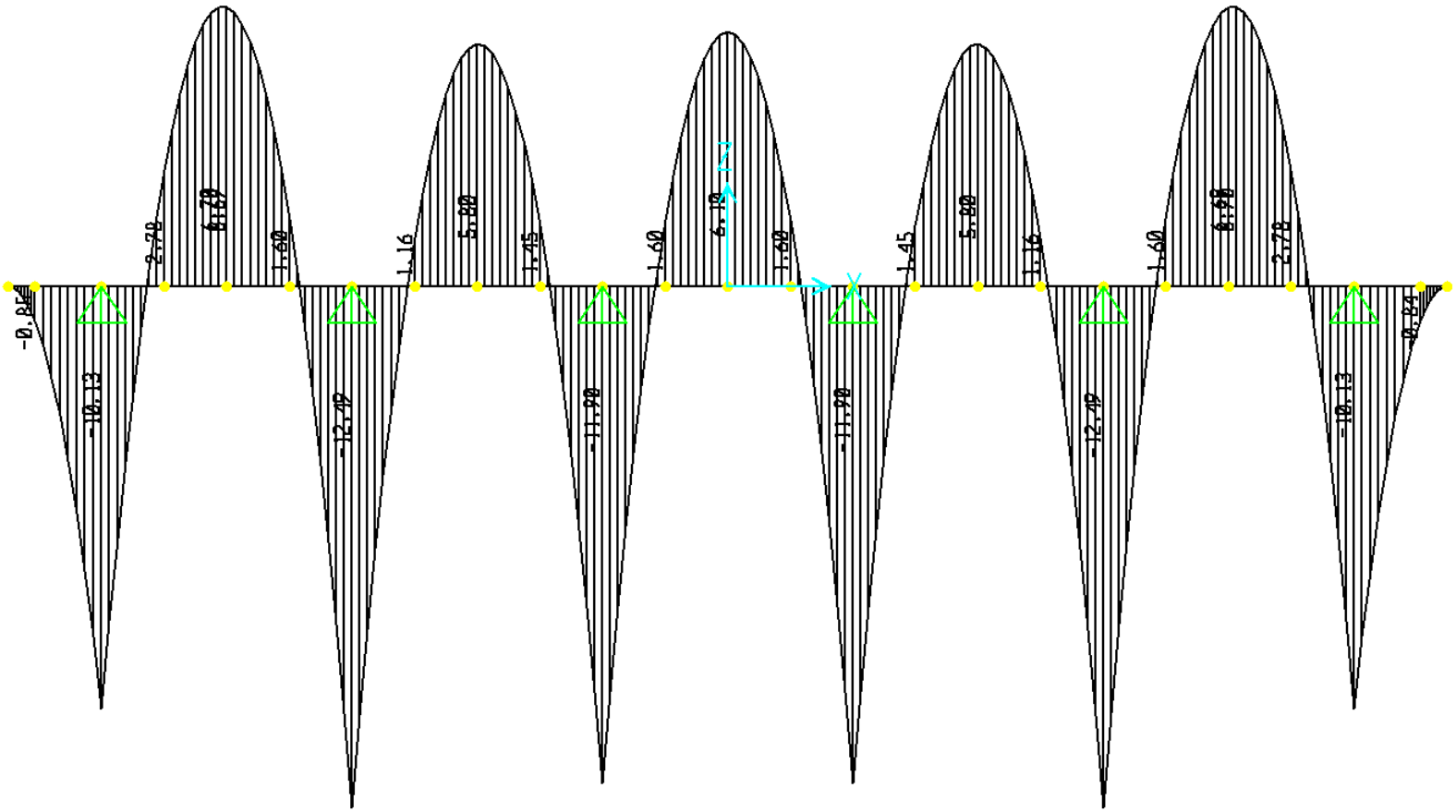

Figure (A-13): Moment diagram due to the deck own weight of 1 k/ft for S = 10 ft

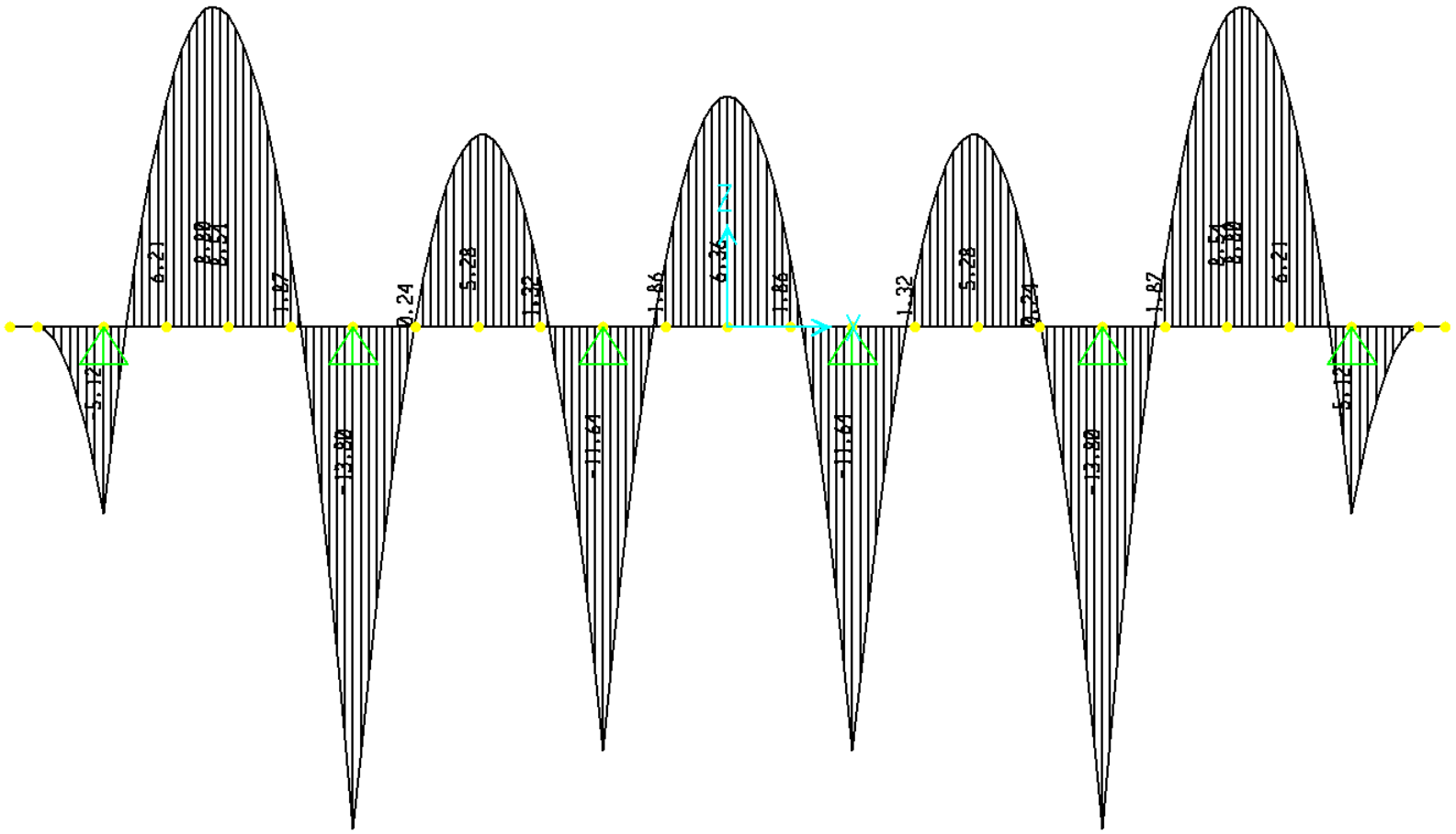

Figure (A-14): Moment diagram due to asphalt future wearing surface of 1 k/ft for S = 12 ft

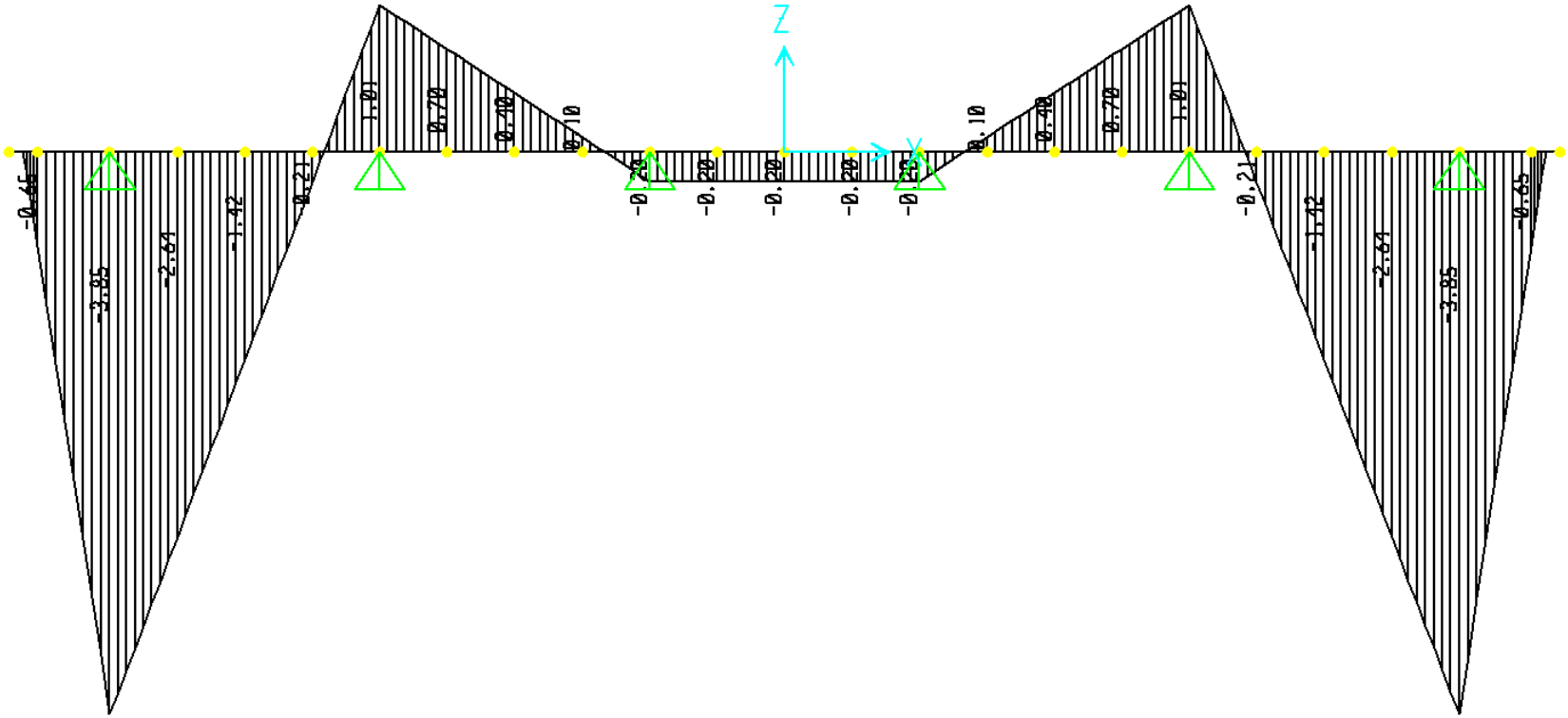

Figure (A-15): Moment diagram due to parapet weight of 1 k for S = 12 ft

APPENDIX B

Stress-Strain Curves

Appendix B shows the stress-strain curves for optimized proposed rebars. The following abbreviation will be used:

For Birder Deck: (Girder spacing in feet, proposed rebar number)

For example, (S9,#2) ≡ (S = 9 ft, proposed rebar 2)

(S8,#1) ≡ (S = 8 ft, proposed rebar 1)

For Birder Deck: (Girder length in feet, proposed rebar number)

For example, (L20,#2) ≡ (L = 20 ft, proposed rebar 2)

(L25,#1) ≡ (L = 8 ft, proposed rebar 1)

1- Bridge Deck

a- Proposed Rebar 1

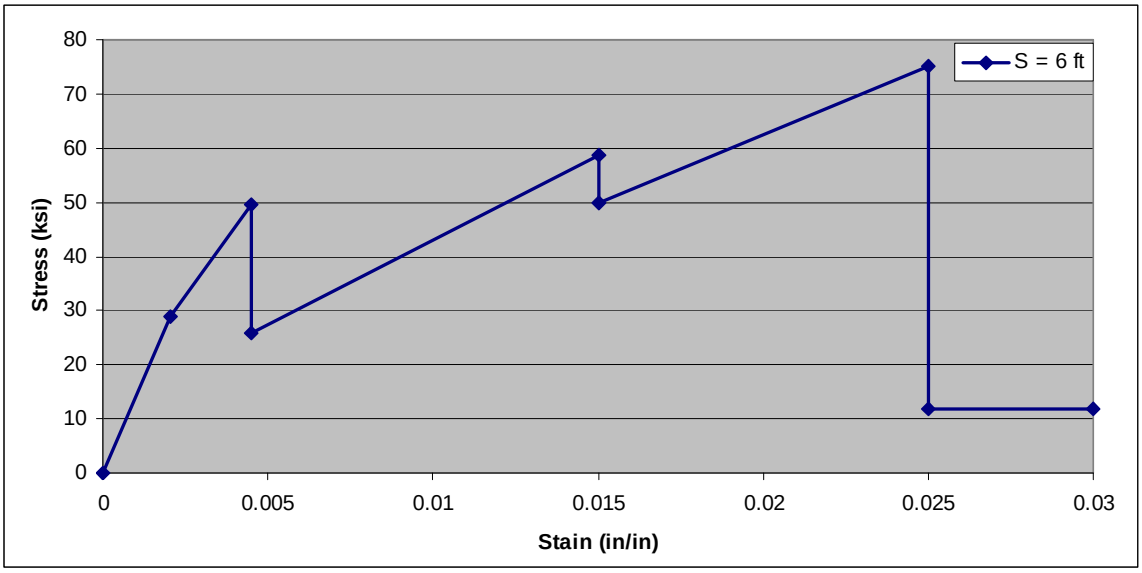

Figure (B-1): Stress-Strain curve for +ve moment of a bridge deck and (S6,#1)

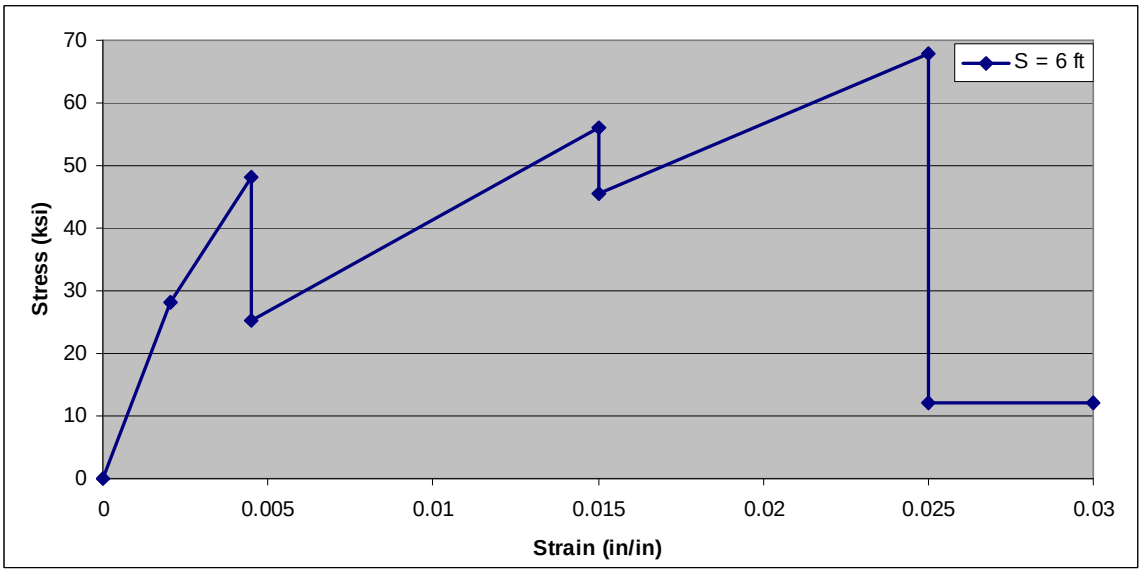

Figure (B-2): Stress-Strain curve for -ve moment of a bridge deck (S6,#1).

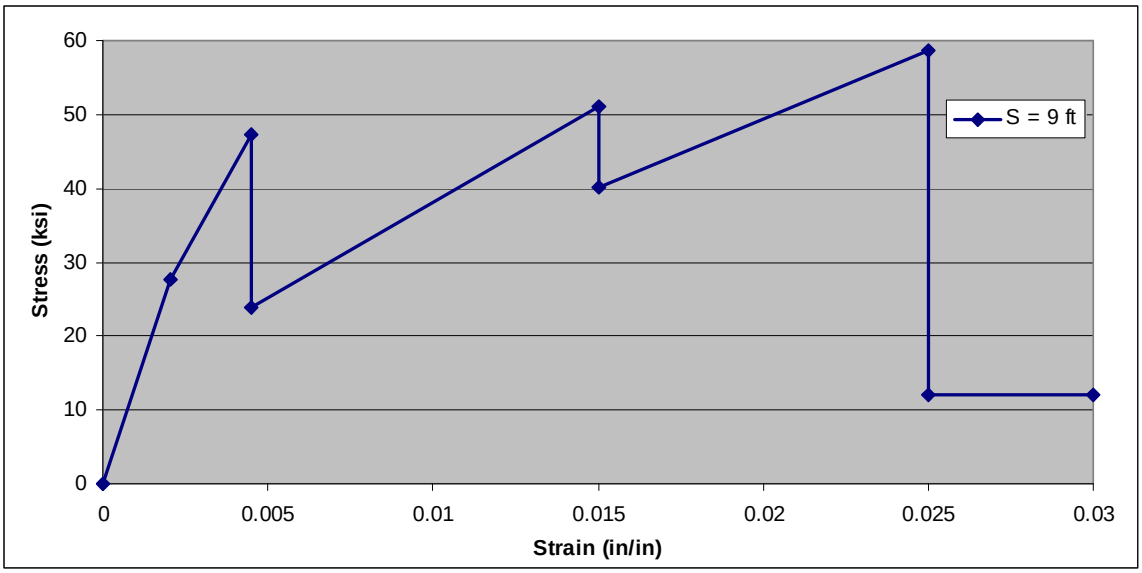

Figure (B-3): Stress-Strain curve for +ve moment of a bridge deck (S9,#1).

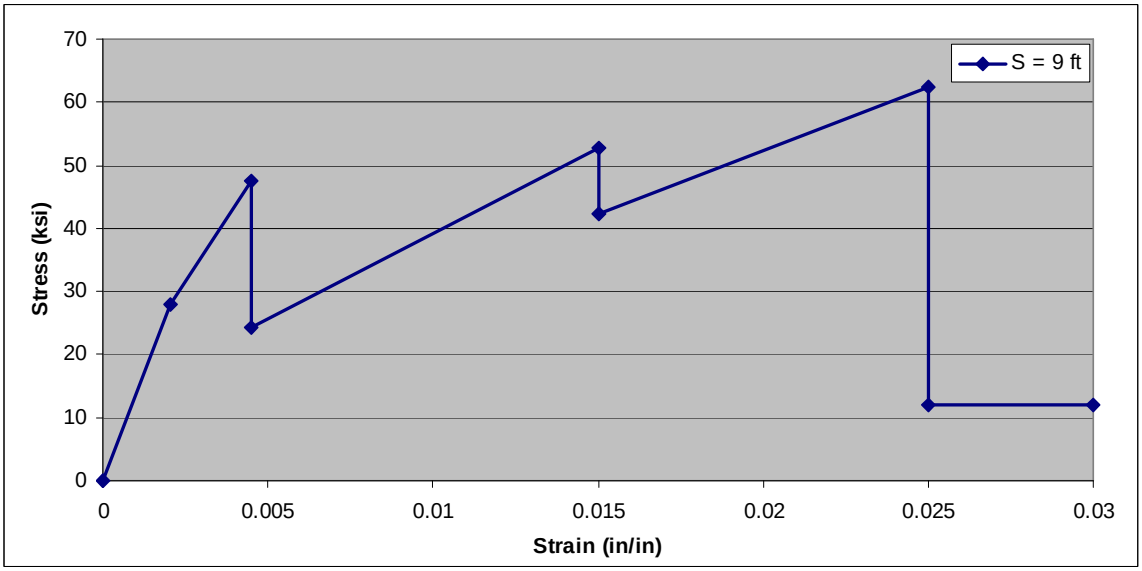

Figure (B-4): Stress-Strain curve for -ve moment of a bridge deck (S9,#1).

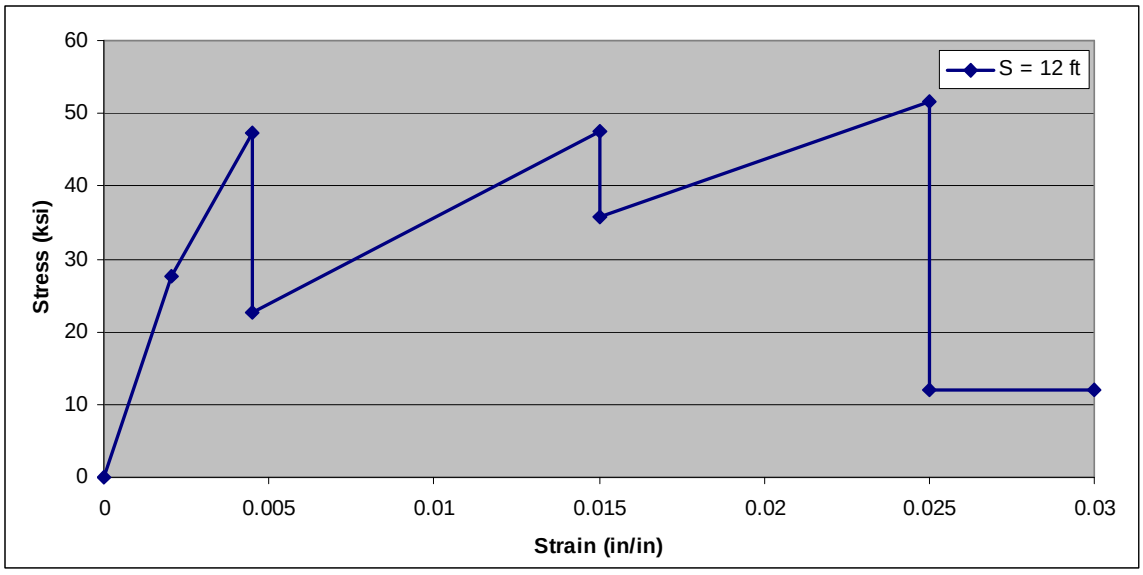

Figure (B-5): Stress-Strain curve for +ve moment of a bridge deck (S12,#1).

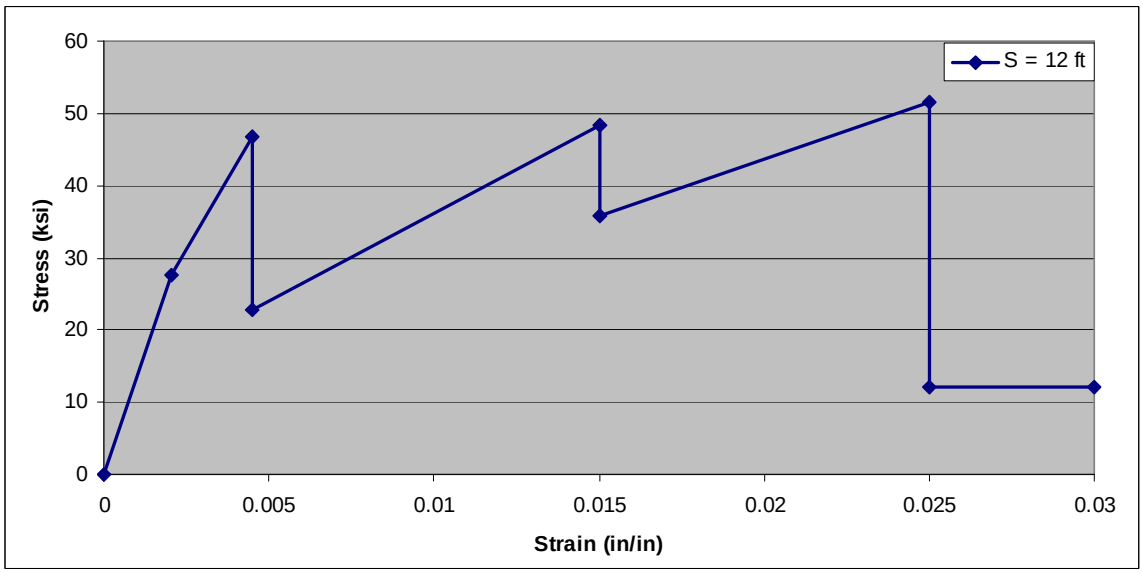

Figure (B-6): Stress-Strain curve for -ve moment of a bridge deck (S12,#1).

b- Proposed Rebar 2

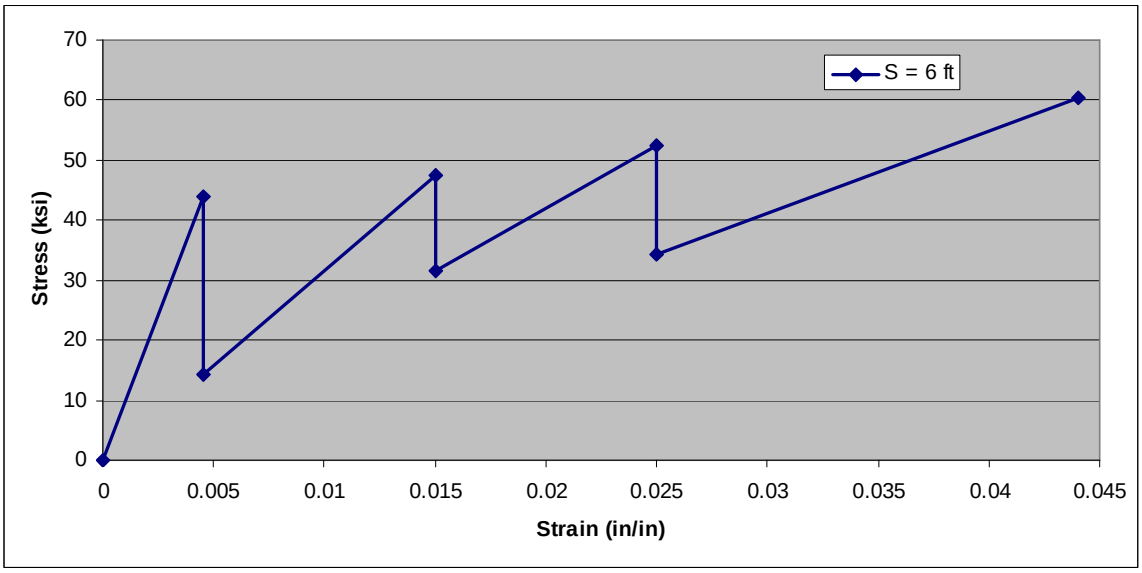

Figure (B-7): Stress-Strain curve for +ve moment of a bridge deck (S6,#2).

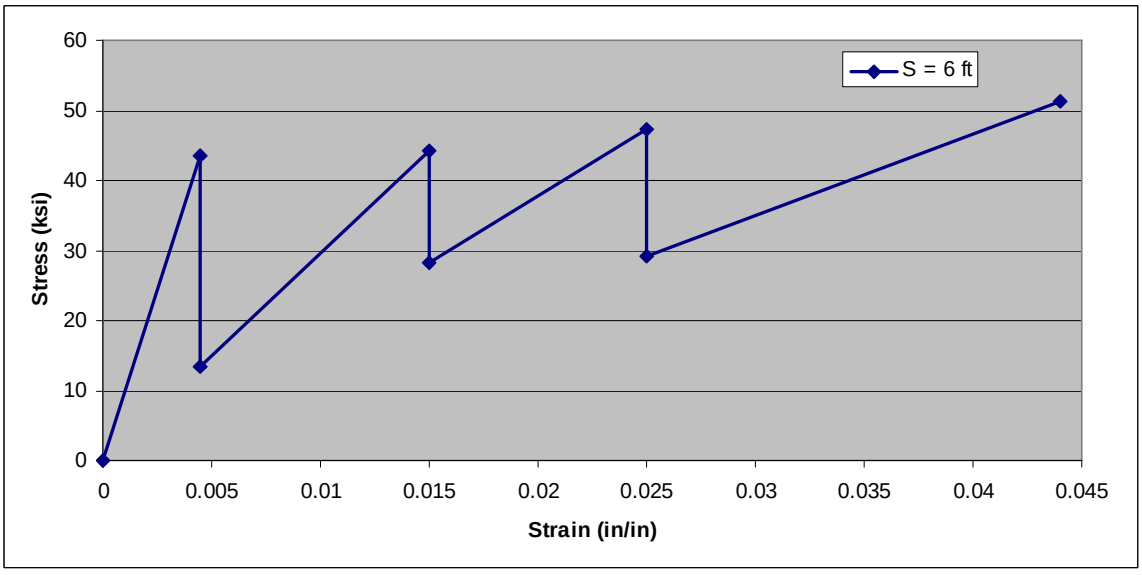

Figure (B-8): Stress-Strain curve for -ve moment of a bridge deck (S6,#2).

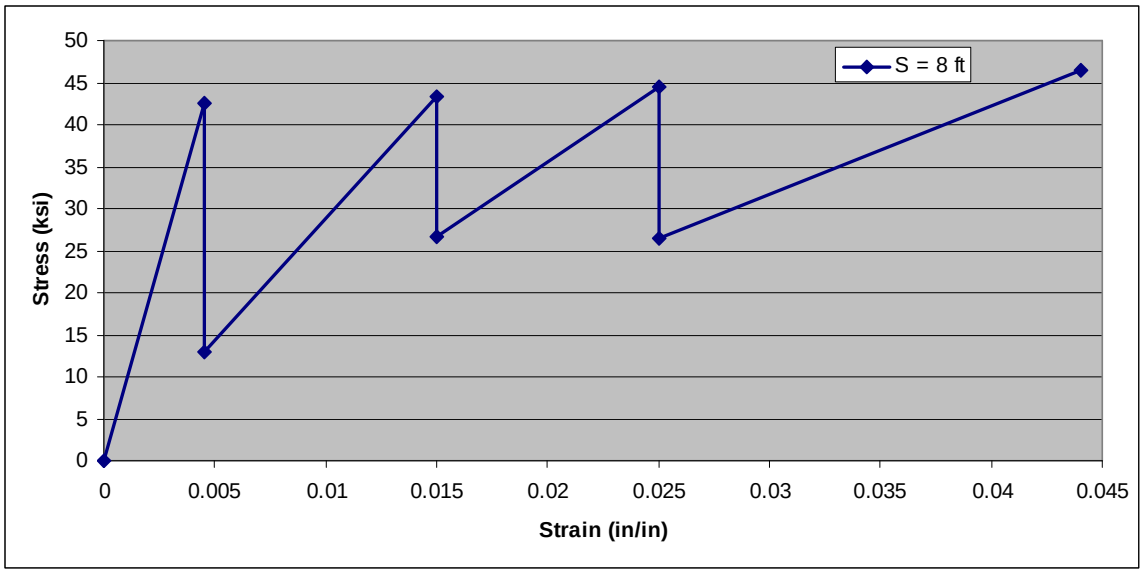

Figure (B-9): Stress-Strain curve for +ve moment of a bridge deck (S8,#2).

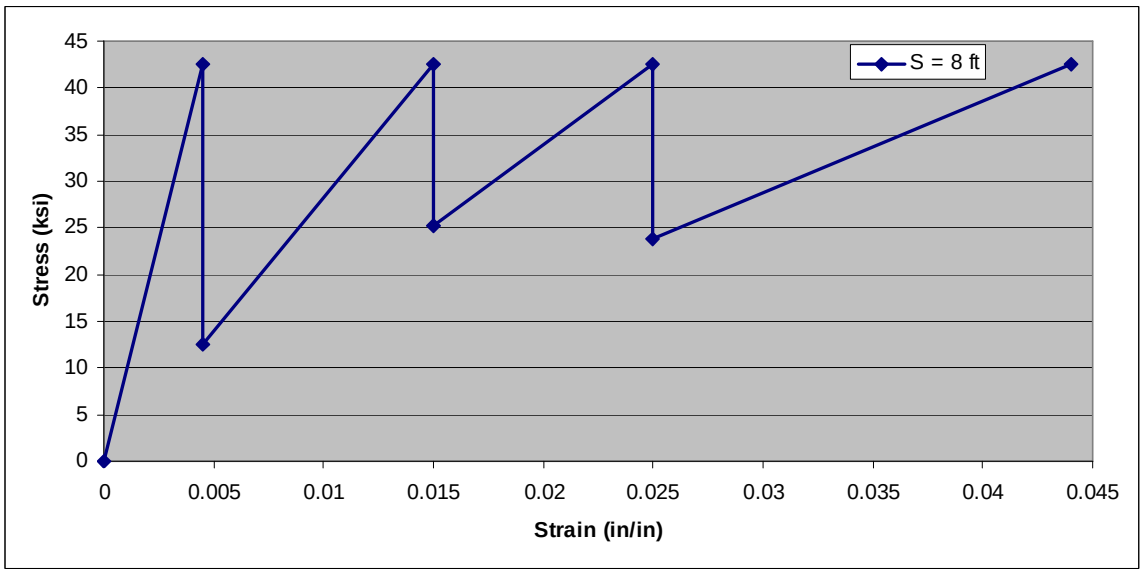

Figure (B-10): Stress-Strain curve for -ve moment of a bridge deck (S8,#2).

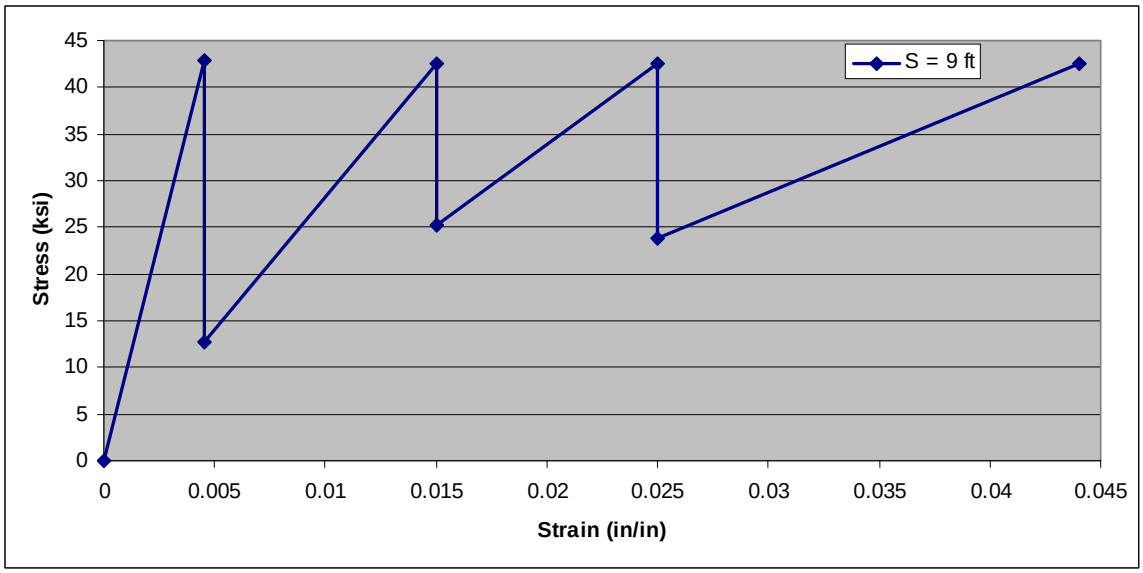

Figure (B-11): Stress-Strain curve for +ve moment of a bridge deck (9,#2).

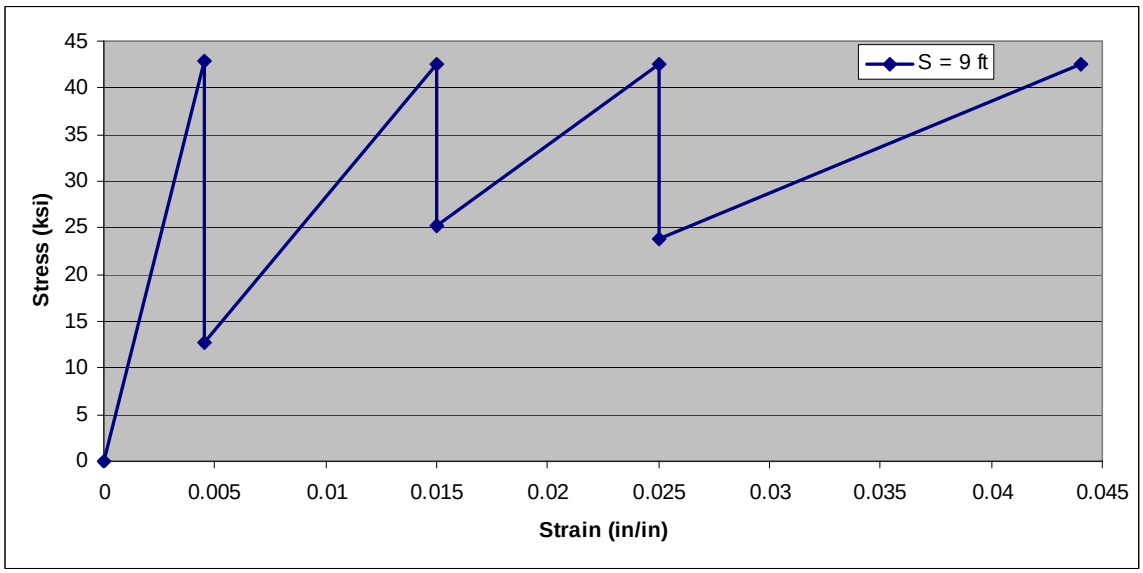

Figure (B-12): Stress-Strain curve for -ve moment of a bridge deck (S9,#2).

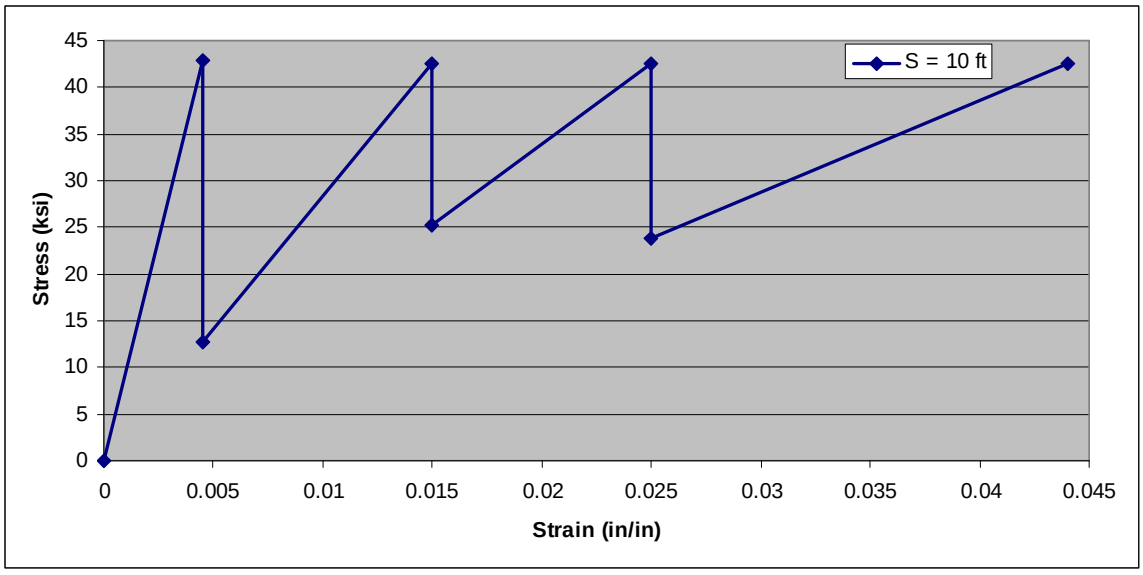

Figure (B-13): Stress-Strain curve for +ve moment of a bridge deck (S10,#2).

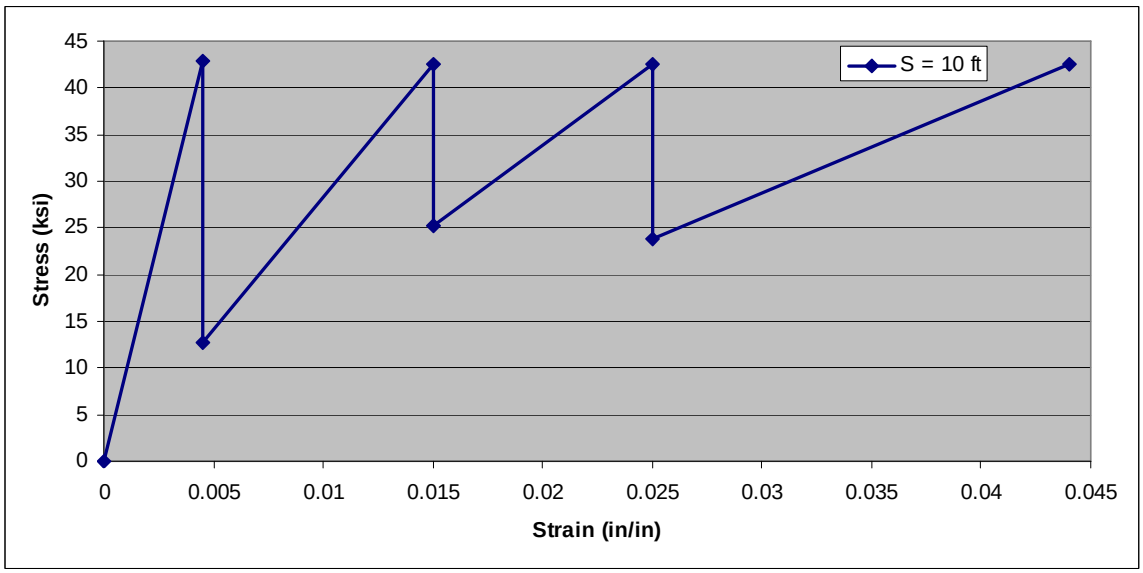

Figure (B-14): Stress-Strain curve for -ve moment of a bridge deck (S10,#2).

2- Building Beam/Girder

a- Proposed Rebar 1

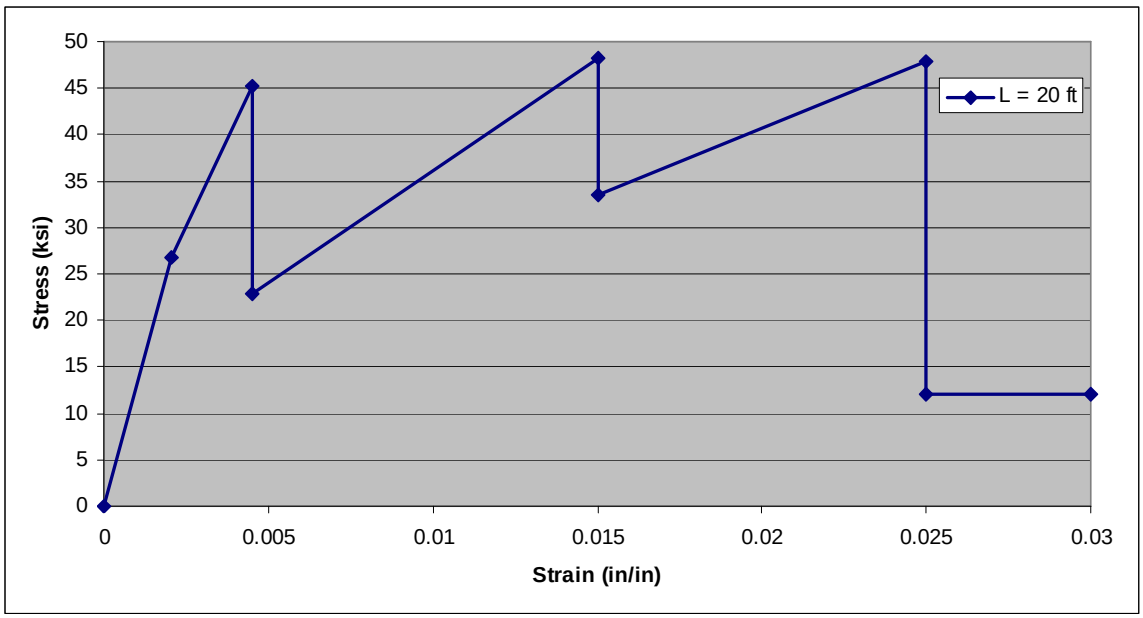

Figure (B-15): Stress-Strain curve for +ve moment of a building beam (L=20,#1).

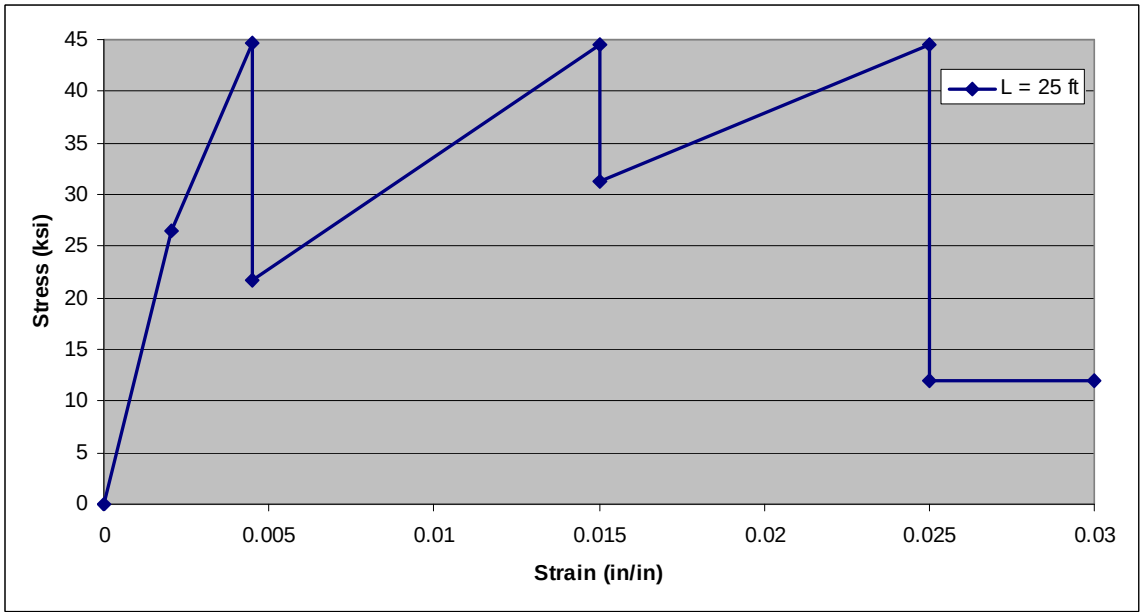

Figure (B-16): Stress-Strain curve for +ve moment of a building beam (L=25,#1).

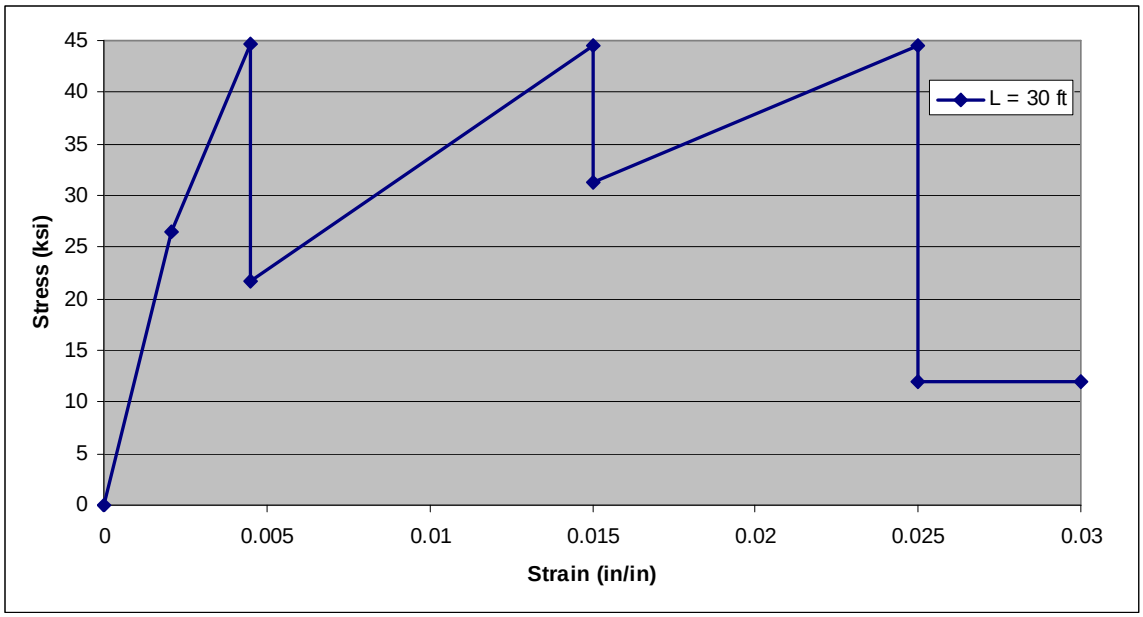

Figure (B-17): Stress-Strain curve for +ve moment of a building beam (L=30,#1).

b- **Proposed Rebar 2**

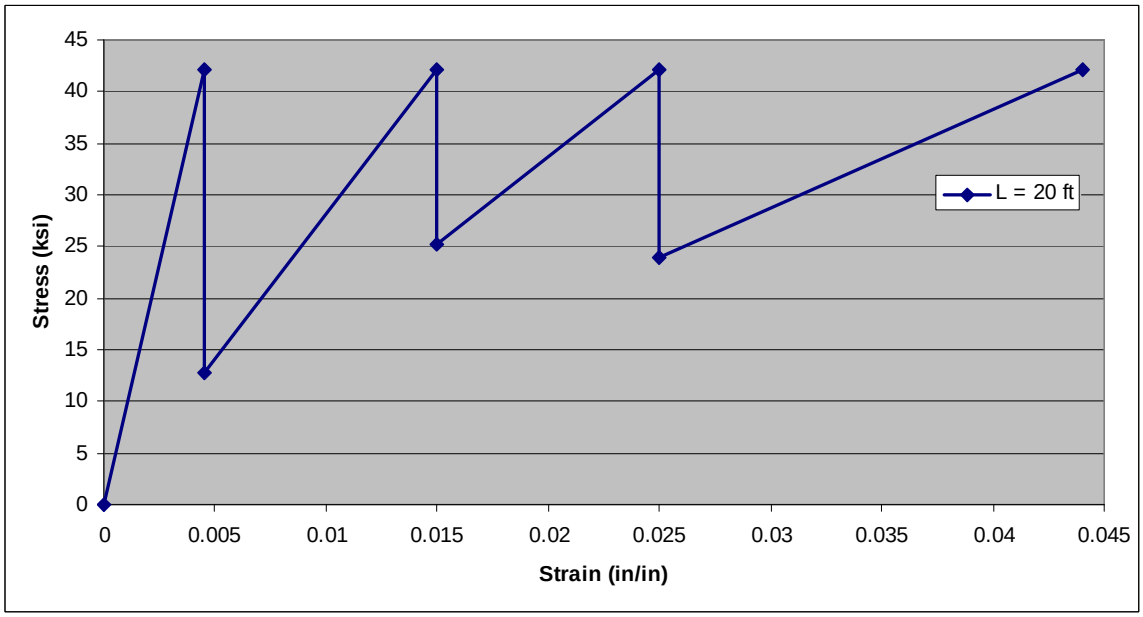

Figure (B-18): Stress-Strain curve for +ve moment of a building beam(L=20,#2).

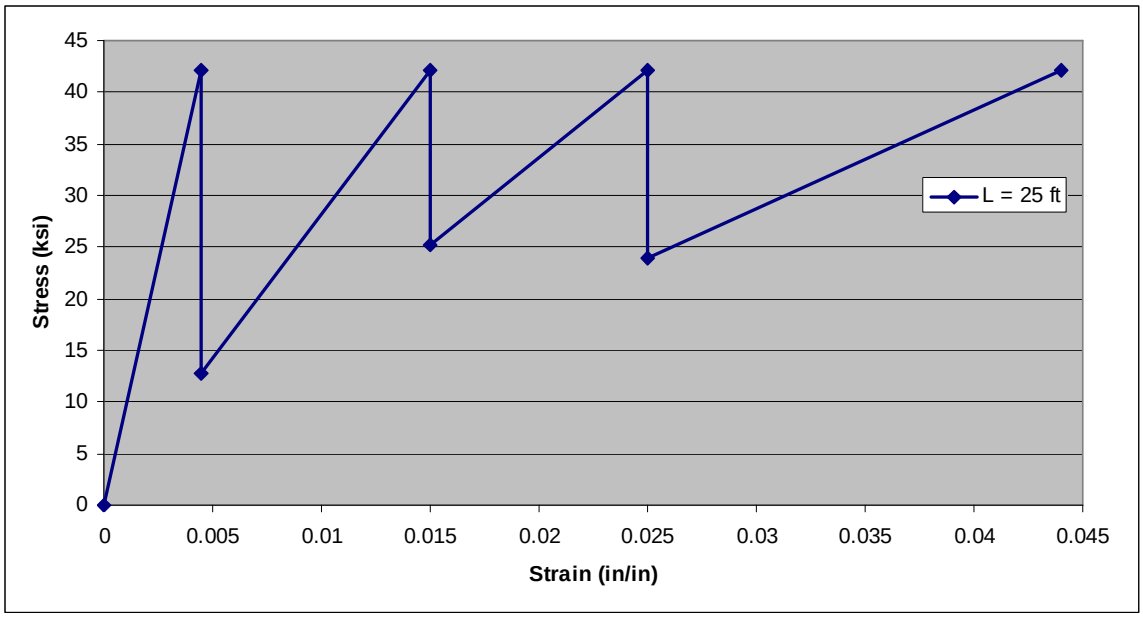

Figure (B-19): Stress-Strain curve for +ve moment of a building beam (L=25,#2).

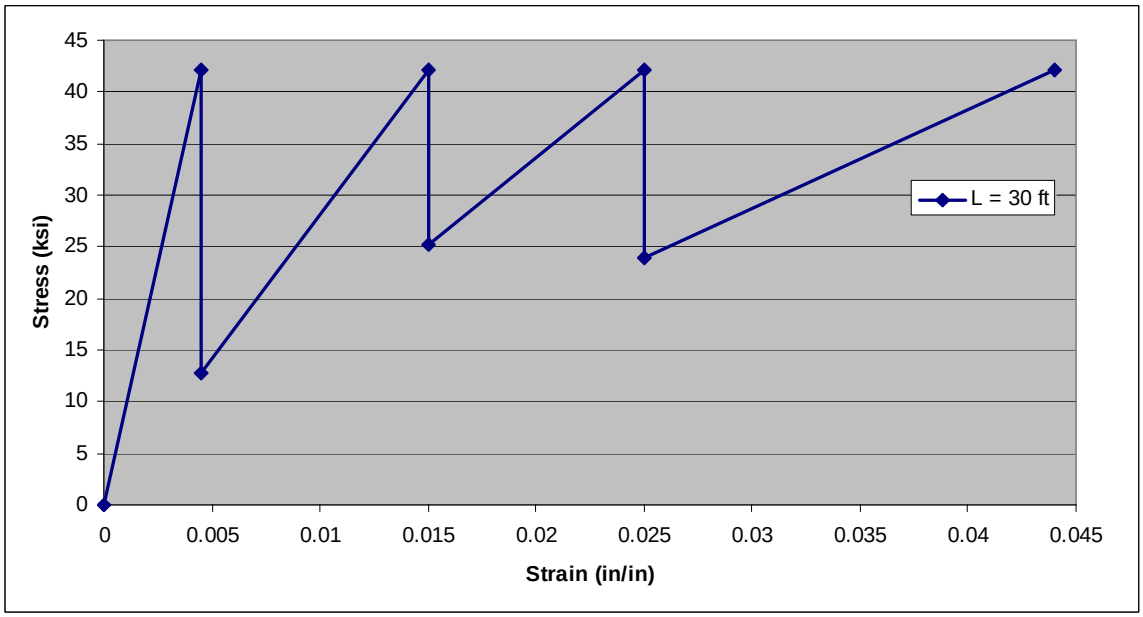

Figure (B-20): Stress-Strain curve for +ve moment of a building beam (L=30,#2).

APPENDIX C

Moment-Curvature Curves

Appendix C shows the moment-curvature curves for optimized proposed rebars reinforcing concrete sections. The following abbreviation will be used:

For Birder Deck: (Girder spacing in feet, proposed rebar number)

For example, (S9,#2) ≡ (S = 9 ft, proposed rebar 2)

(S8,#1) ≡ (S = 8 ft, proposed rebar 1)

For Beam/Girder: (Girder length in feet, proposed rebar number)

For example, (L20,#2) ≡ (L = 20 ft, proposed rebar 2)

(L25,#1) ≡ (L = 8 ft, proposed rebar 1)

1- Bridge Deck

c- Proposed Rebar 1

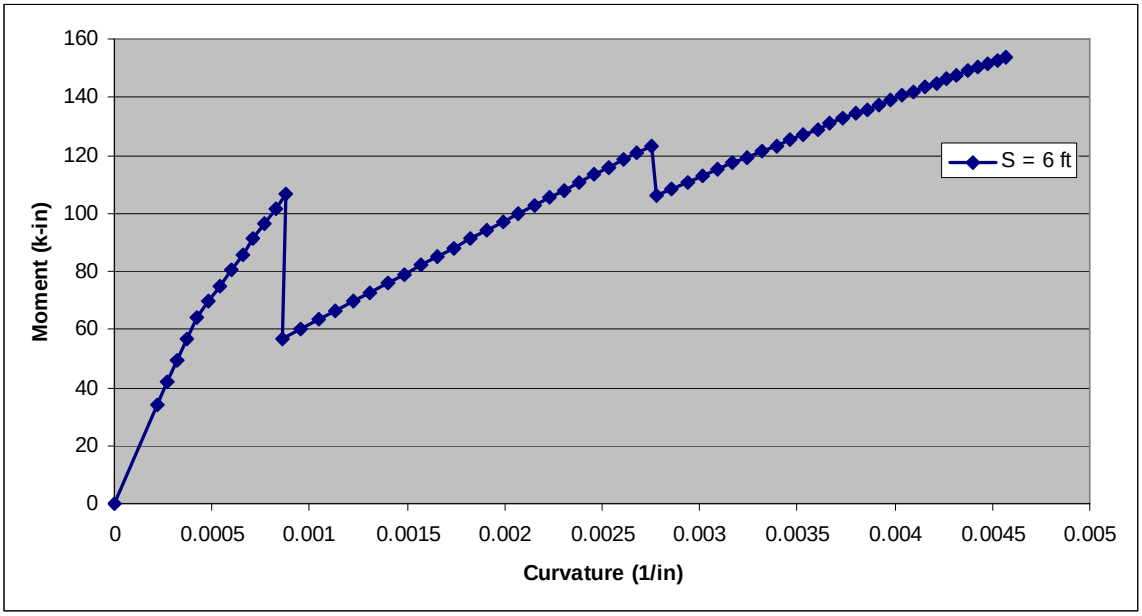

Figure (C-1): Moment-Curvature curve for +ve moment of a bridge deck (S6,#1).

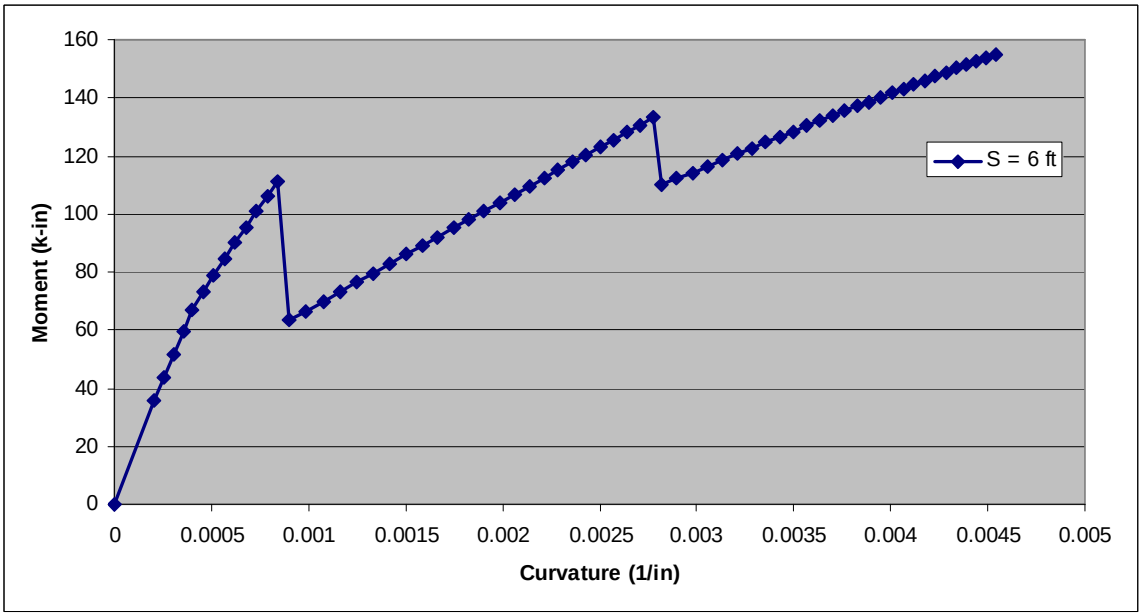

Figure (C-2): Moment-Curvature curve for -ve moment of a bridge deck (S6,#1).

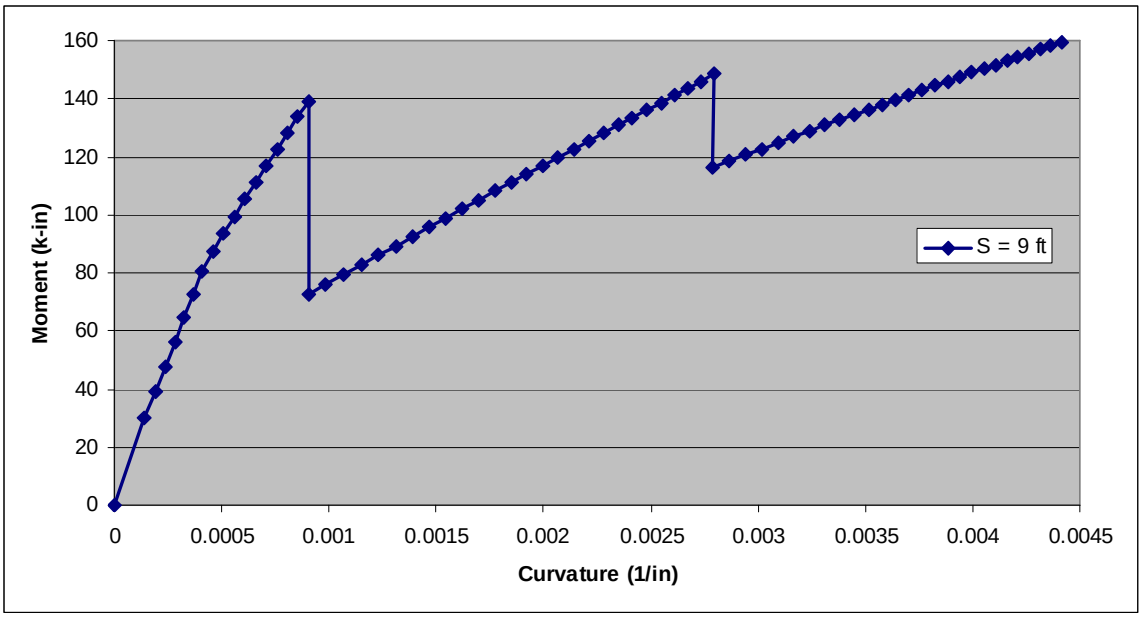

Figure (C-3): Moment-Curvature curve for +ve moment of a bridge deck (S9,#1).

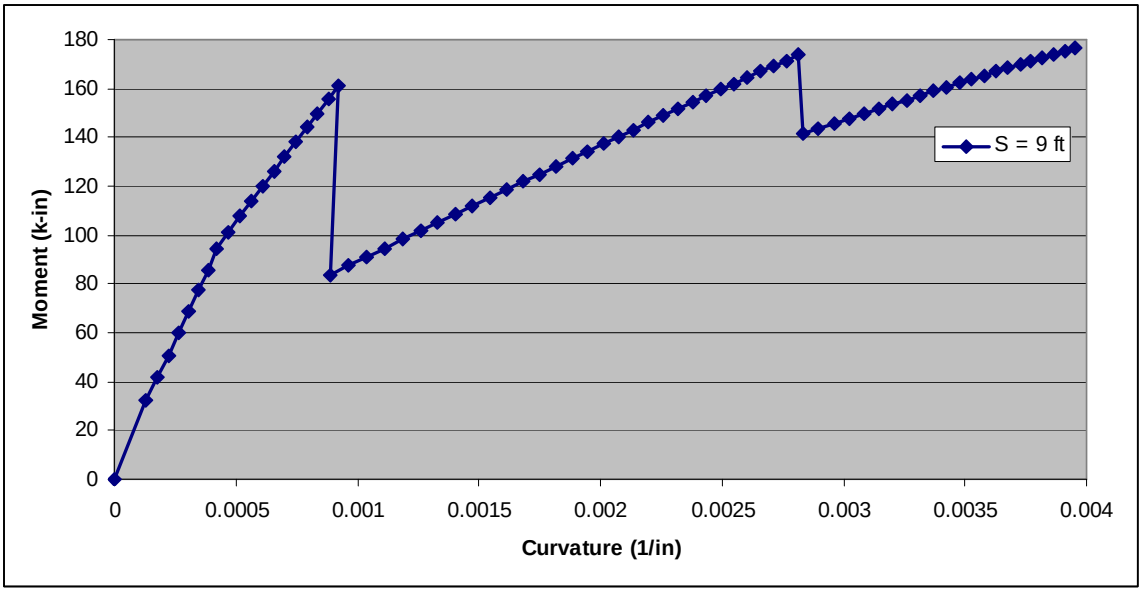

Figure (C-4): Moment-Curvature curve for -ve moment of a bridge deck (S9,#1).

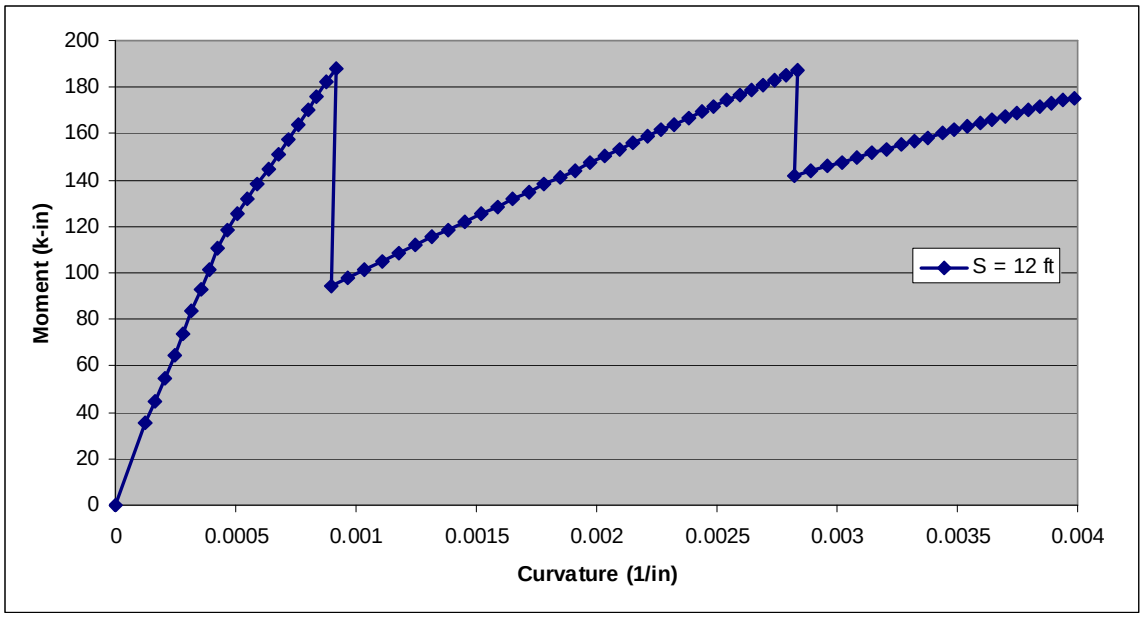

Figure (C-5): Moment-Curvature curve for +ve moment of a bridge deck (S12,#1).

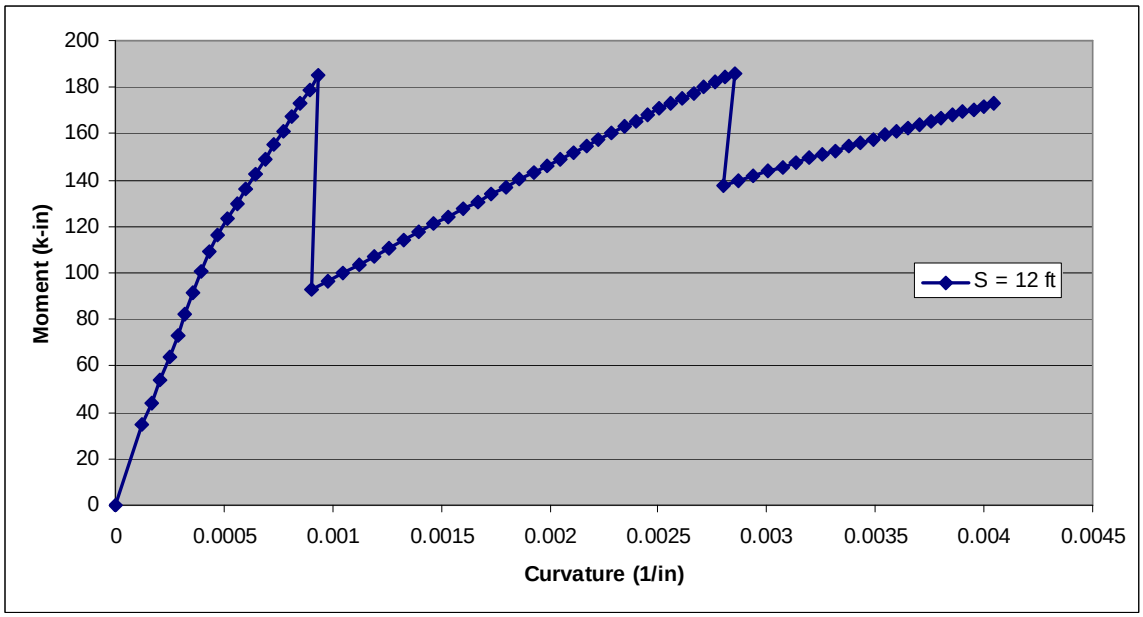

Figure (C-6): Moment-Curvature curve for -ve moment of a bridge deck (S12,#1).

d- **Proposed Rebar 2**

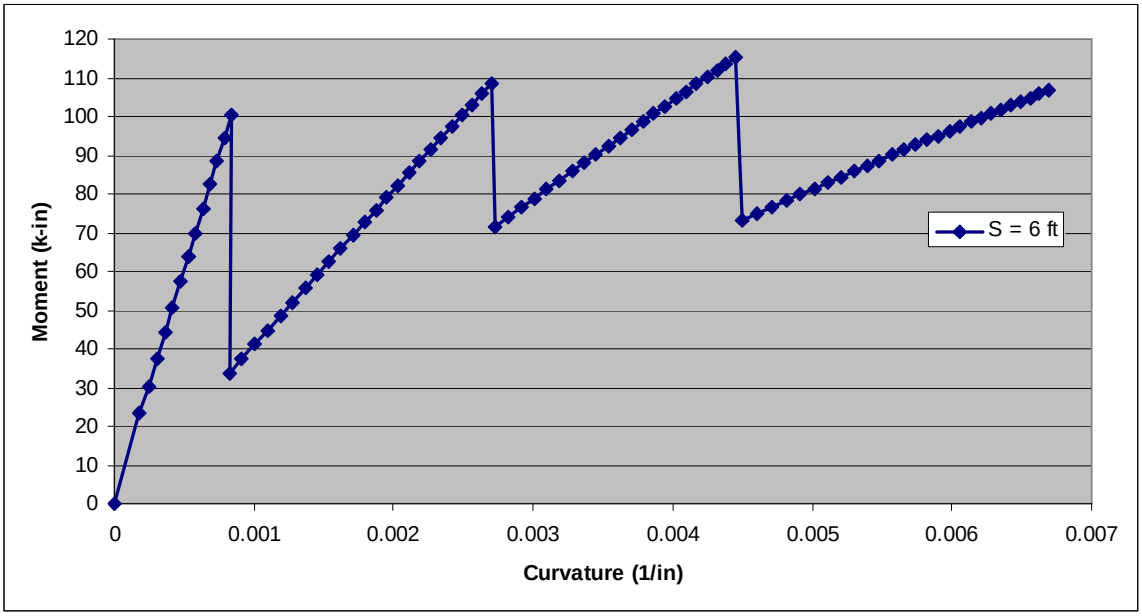

Figure (C-7): Moment-Curvature curve for +ve moment of a bridge deck (S6,#2).

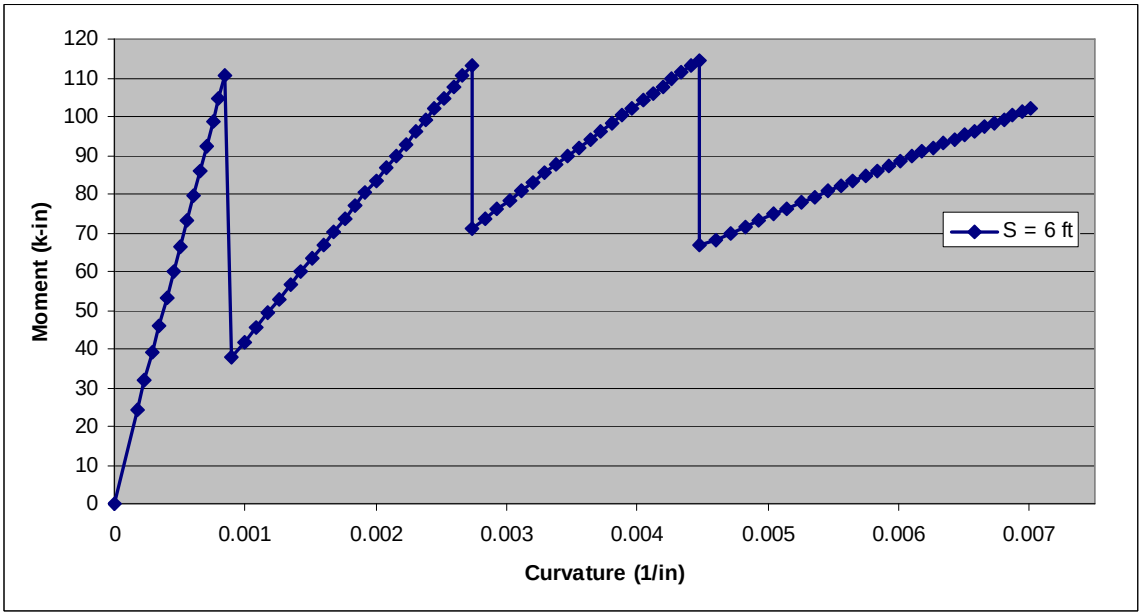

Figure (C-8): Moment-Curvature curve for -ve moment of a bridge deck (S6,#2).

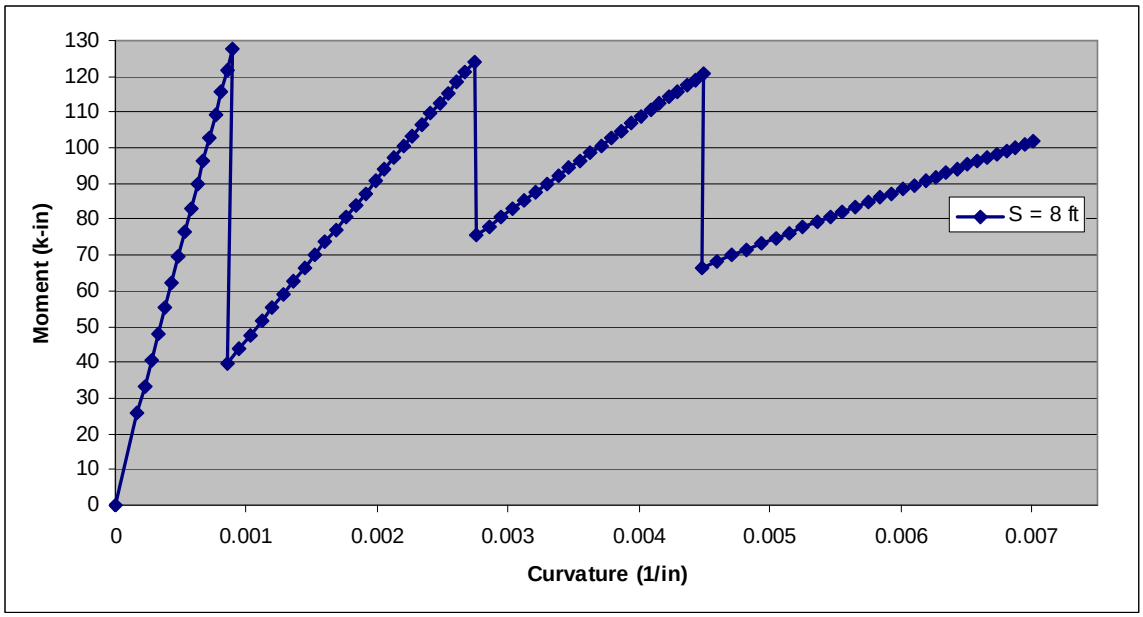

Figure (C-9): Moment-Curvature curve for +ve moment of a bridge deck (S8,#2).

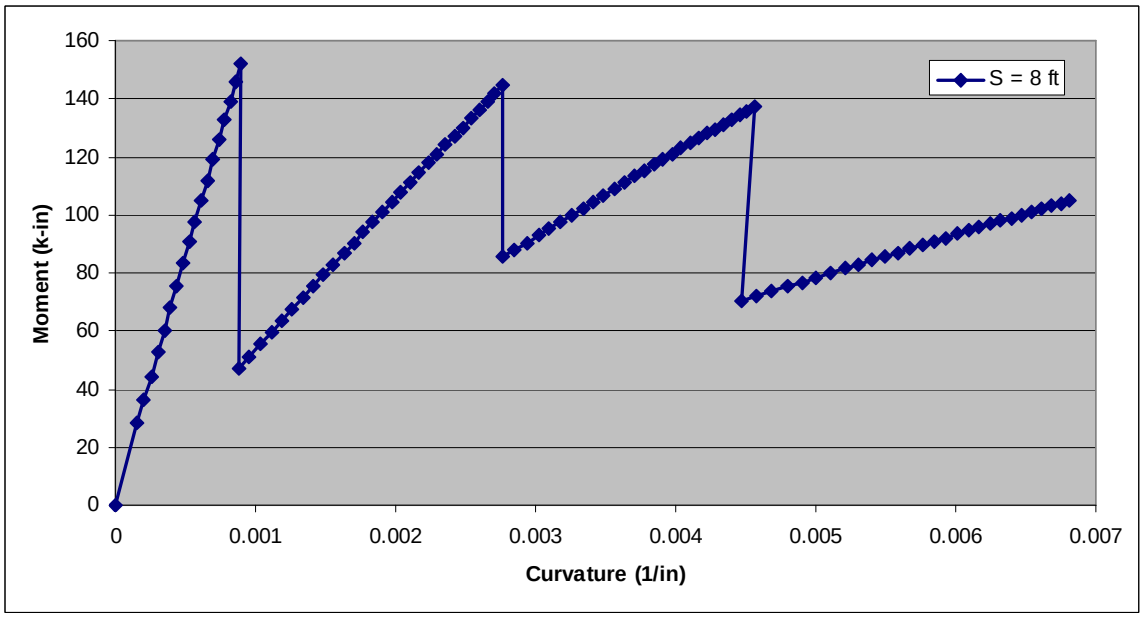

Figure (C-10): Moment-Curvature curve for -ve moment of a bridge deck (S8,#2).

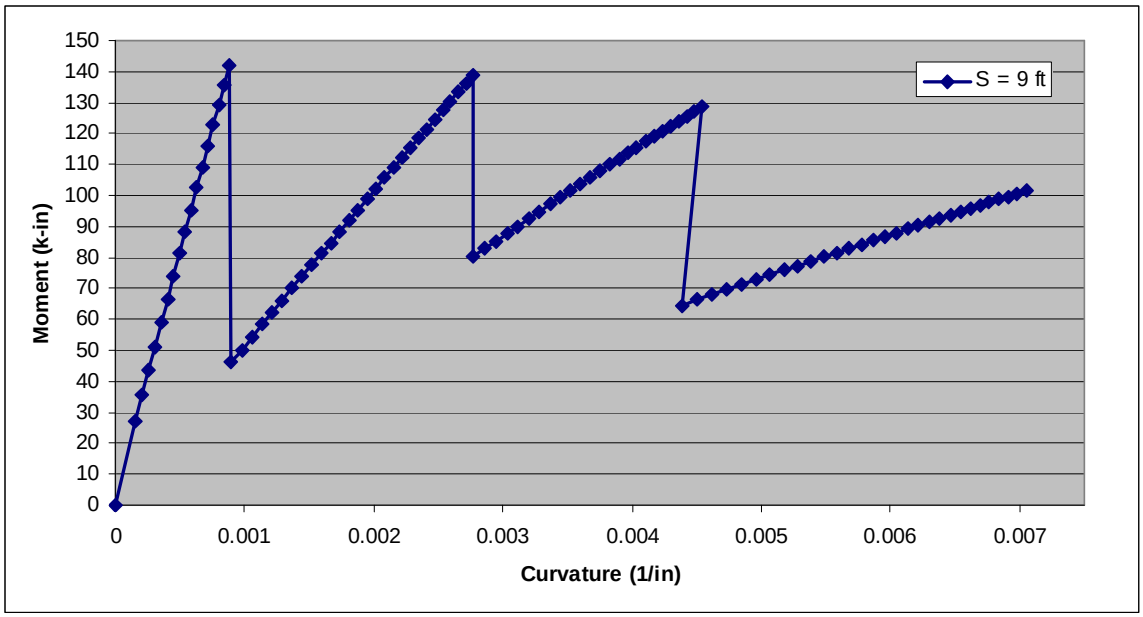

Figure (C-11): Moment-Curvature curve for +ve moment of a bridge deck (S9,#2).

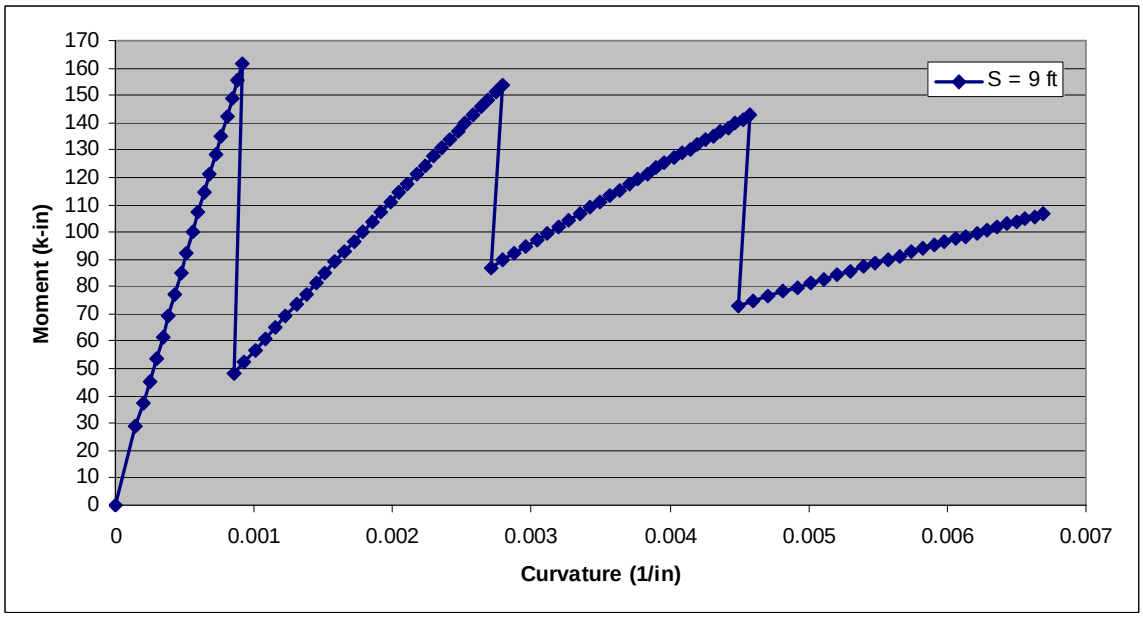

Figure (C-12): Moment-Curvature curve for -ve moment of a bridge deck (S9,#2).

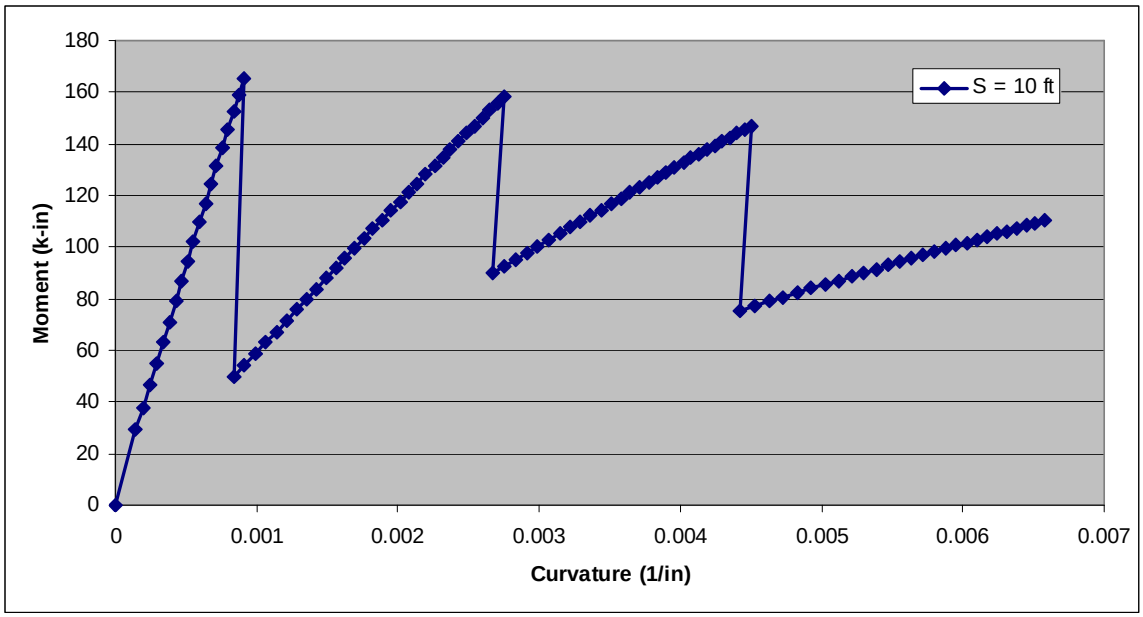

Figure (C-13): Moment-Curvature curve for +ve moment of a bridge deck (S10,#2).

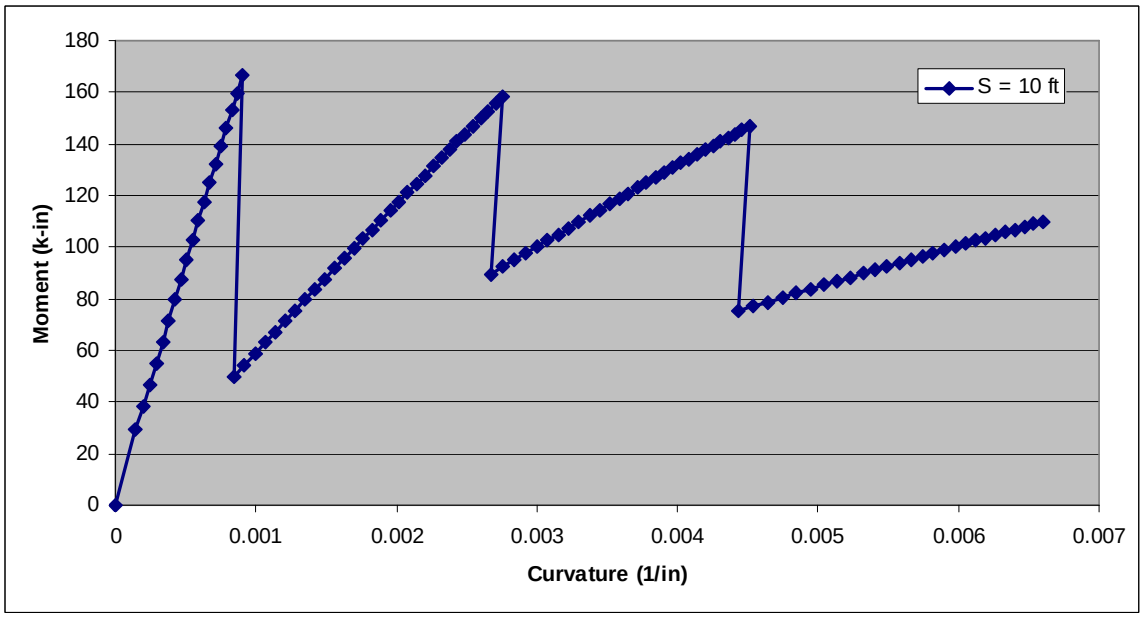

Figure (C-14): Moment-Curvature curve for -ve moment of a bridge deck (S10,#2).

2- Building Beam/Girder

a- Proposed Rebar 1

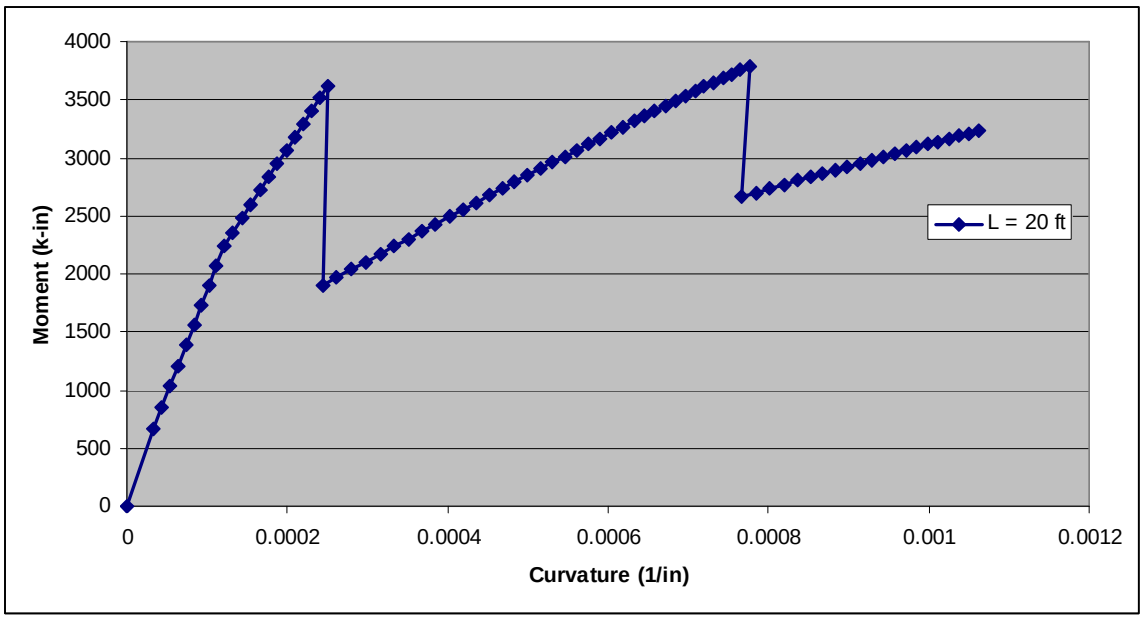

Figure (C-15): Moment-Curvature curve for +ve moment of a building beam (L=20,#1).

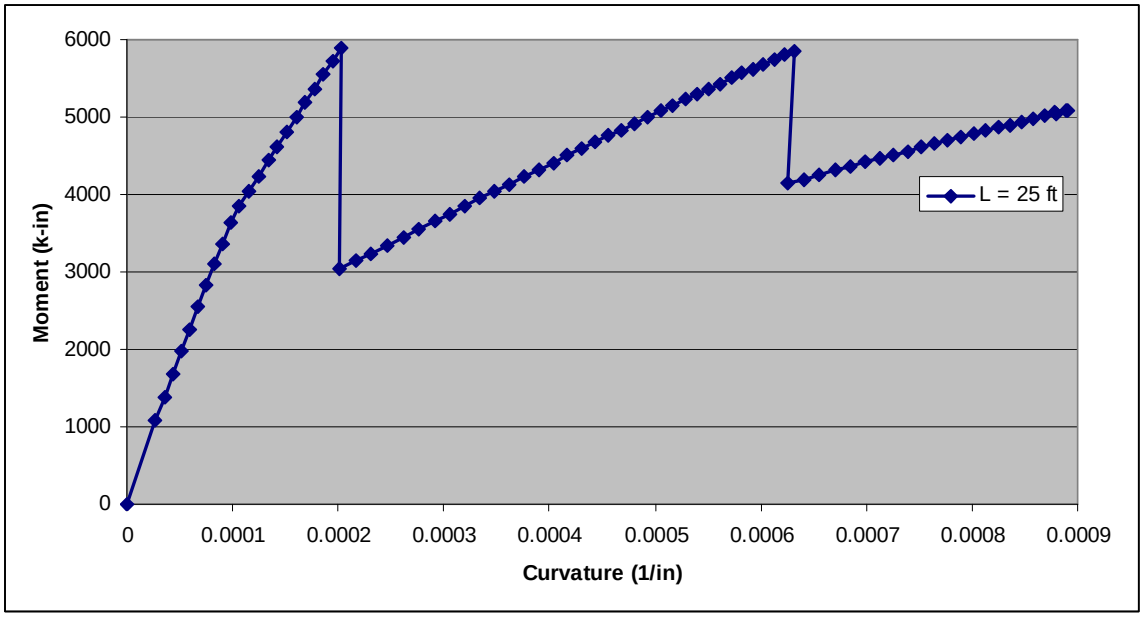

Figure (C-16): Moment-Curvature curve for +ve moment of a building beam (L=25,#1).

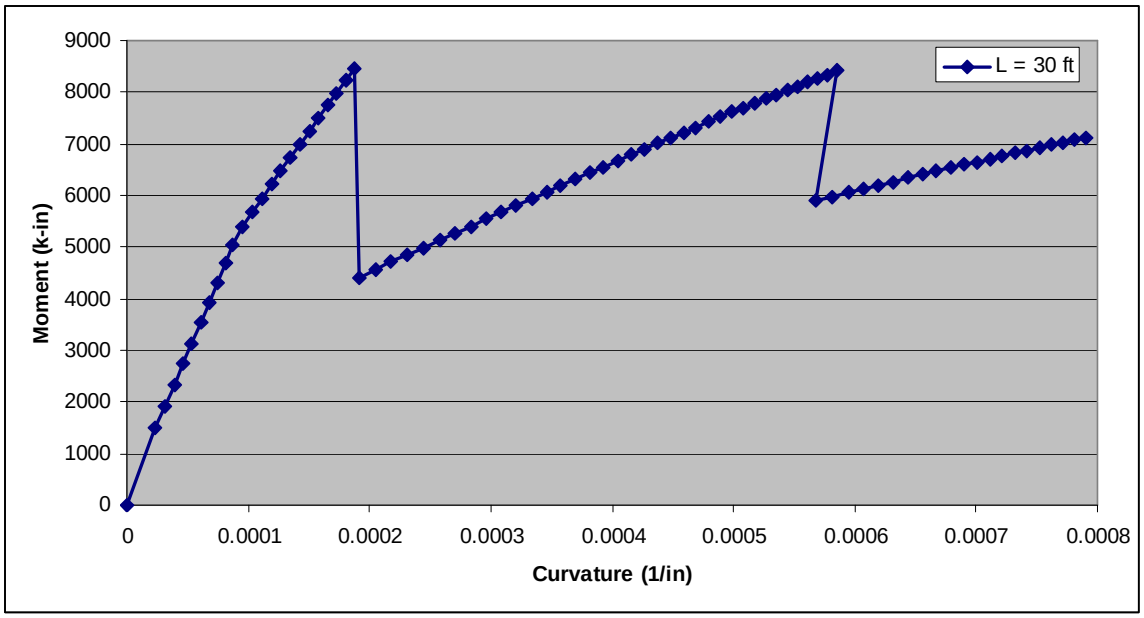

Figure (C-17): Moment-Curvature curve for +ve moment of a building beam (L=30,#1).

b- **Proposed Rebar 2**

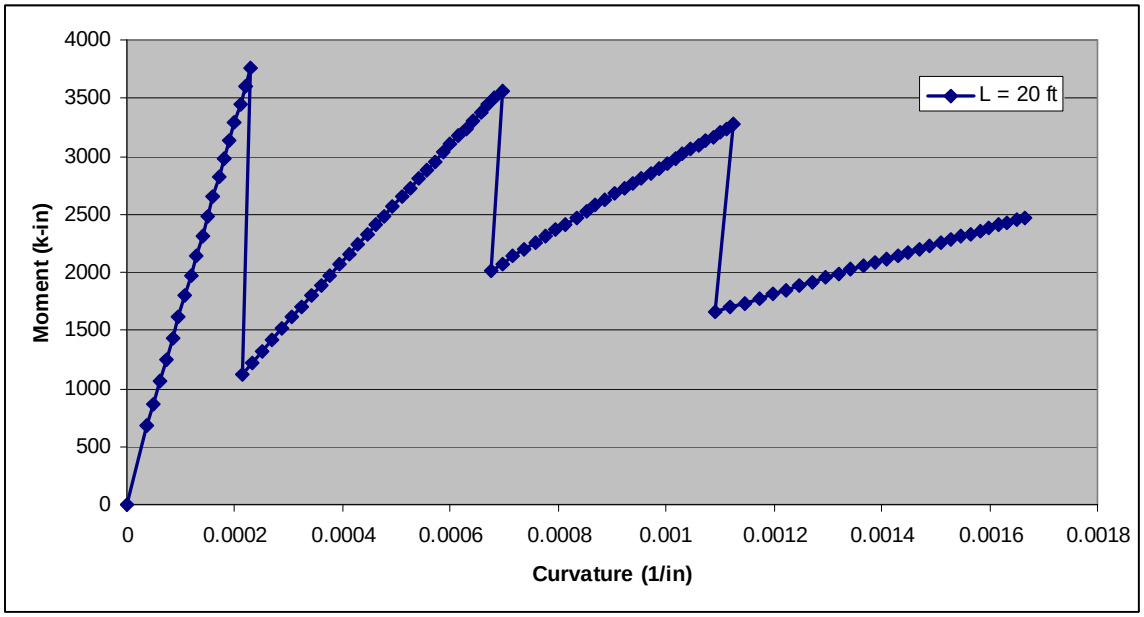

Figure (C-18): Moment-Curvature curve for +ve moment of a building beam (L=20,#2).

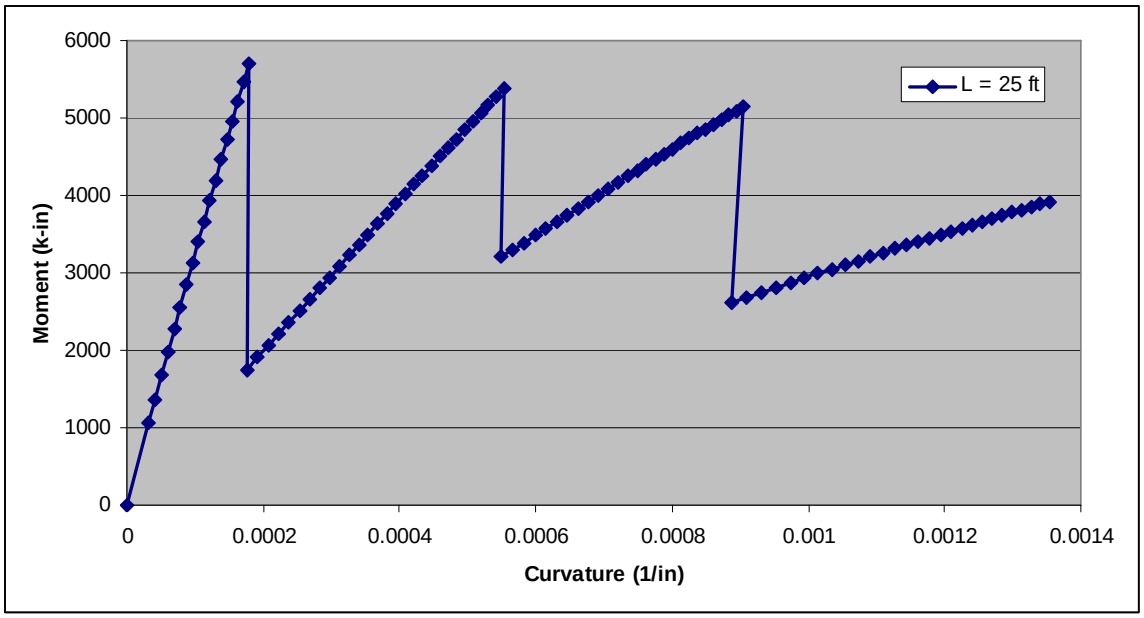

Figure (C-19): Moment-Curvature curve for +ve moment of a building beam (L=25,#2).

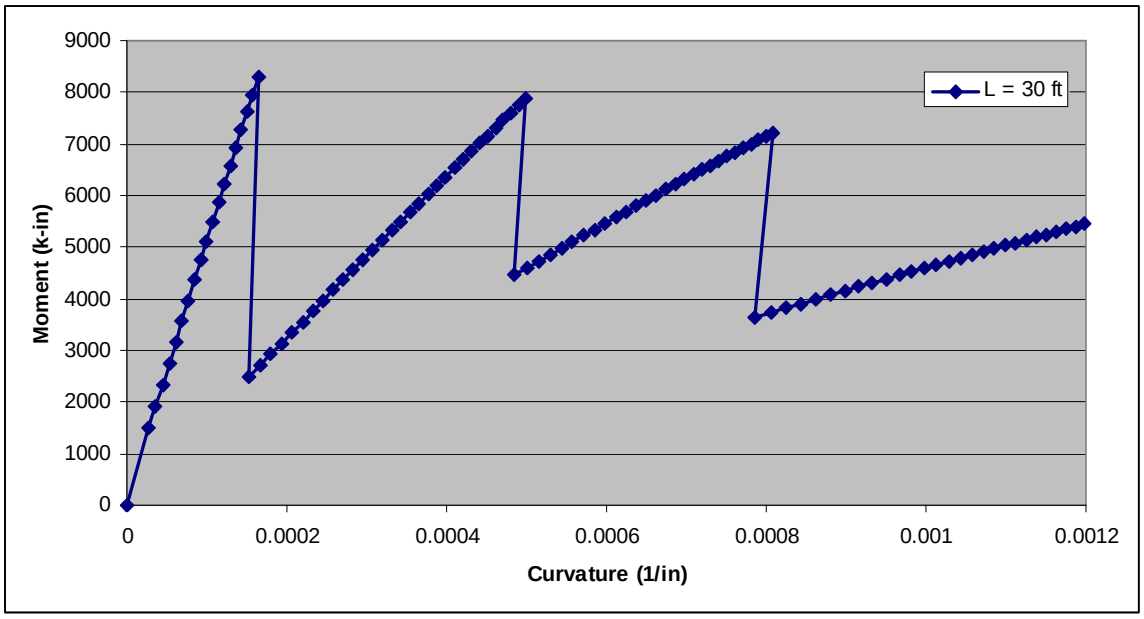

Figure (C-20): Moment-Curvature curve for +ve moment of a building beam (L=30,#2).

APPENDIX D

Optimization Example

For verification of the optimization method used, two example problems with known solutions were solved with the method. The first problem is minimizing a function of two variables with two constraints plus the non-negativity constraints, with exact solution of **X**={0.7647, 1.0588}, and *f*={-4.059}. The proposed technique resulted in a solution of **X**={0.764, 1.059}, and *f*={-4.0588}. The second minimizing a function of two variables with two constraints plus the non-negativity constraints, with exact solution of **X**={ $\sqrt{3}$, $\sqrt{3}$ }, and *f*={-3}. The proposed technique resulted in a solution of **X**={1.732,1.732}, and *f*={-2.99982}.

Example 1

Minimize $f(x,y)=x^2+y^2-2x-4y$

Subjected to

$g_1(x,y)=x+4y-5\le 0$
$g_2(x,y)=2x+3y-6\le 0$
$x\ge 0;\ y\ge 0$

VBA sub-routine

```
Sub nestedloops_()


Mini = 10 ^ 6
For x = 0 To 10 Step 0.001
For y = 0 To 10 Step 0.001

If x + 4 * y - 5 > 0 Then GoTo 10
If 2 * x + 3 * y - 6 > 0 Then GoTo 10

z = x ^ 2 + y ^ 2 - 2 * x - 4 * y

If z > Mini Then GoTo 10

Mini = z
xx = x
yy = y

10 Next y
20 Next x

Cells(2, 1) = xx
Cells(2, 2) = yy
Cells(2, 3) = Mini

End Sub
```

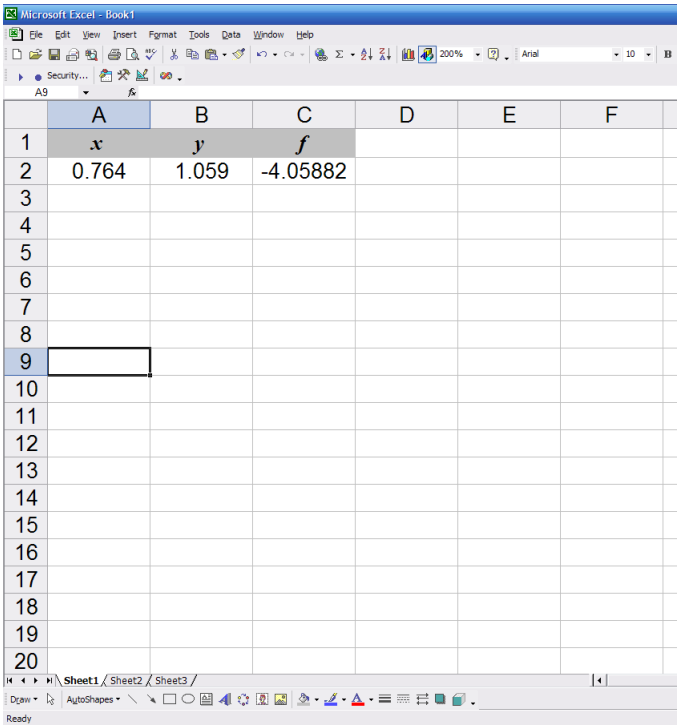

Example 2

Minimize $f(x,y)=x^2+y^2-3xy$

Subjected to

$$g_1(x,y)=\frac{1}{6}x^2+\frac{1}{6}y^2-1\le 0$$

$$x\ge 0;\ y\ge 0$$

VBA sub-routine

```
Sub nestedloops_()

Mini = 10 ^ 6
For x = 0 To 10 Step 0.001
For y = 0 To 10 Step 0.001


If 1 / 6 * x ^ 2 + 1 / 6 * y ^ 2 - 1 > 0 Then GoTo 10

f = x ^ 2 + y ^ 2 - 3 * x * y

If f > Mini Then GoTo 10

Mini = f
xx = x
yy = y


10 Next y
   Next x


Cells(2, 1) = xx
Cells(2, 2) = yy

Cells(2, 4) = Mini

End Sub
```

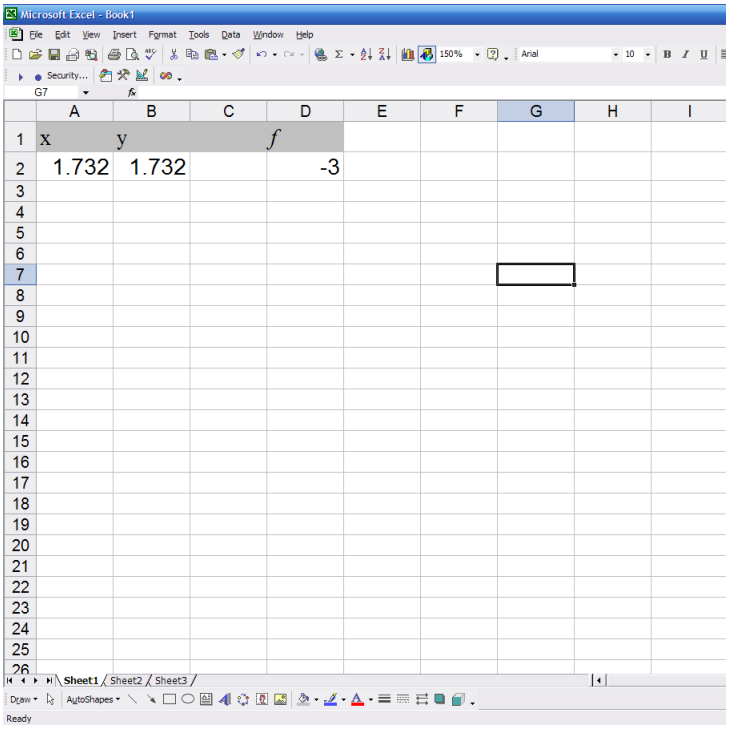

APPENDIX E

Different Moment-Curvature Curves

Terry's Model

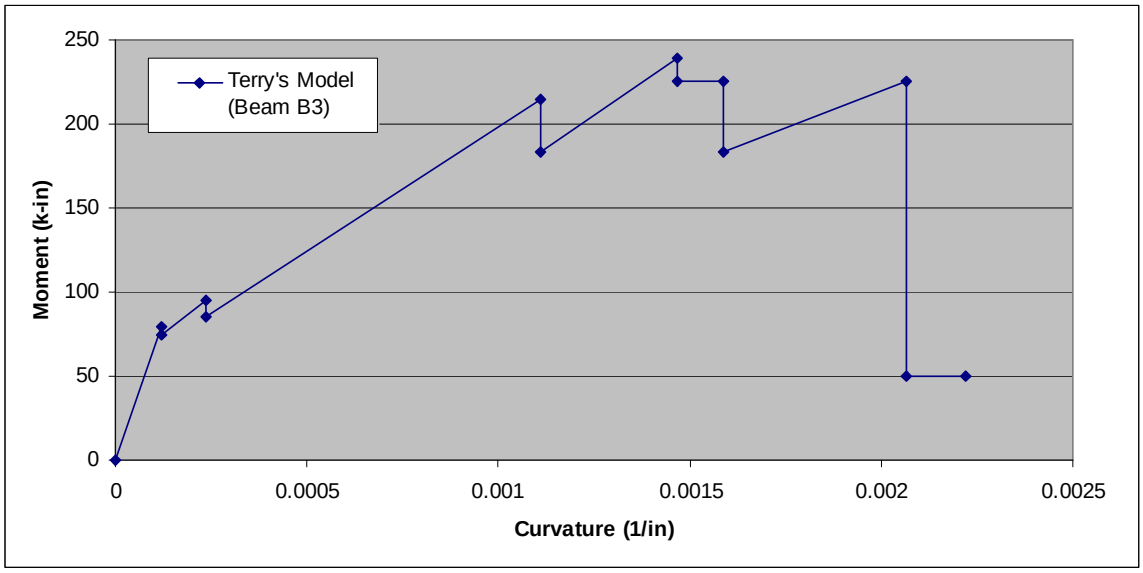

Figure (E-1): Moment-curvature curve for Terry's experimental work.

Somboonsong's Model

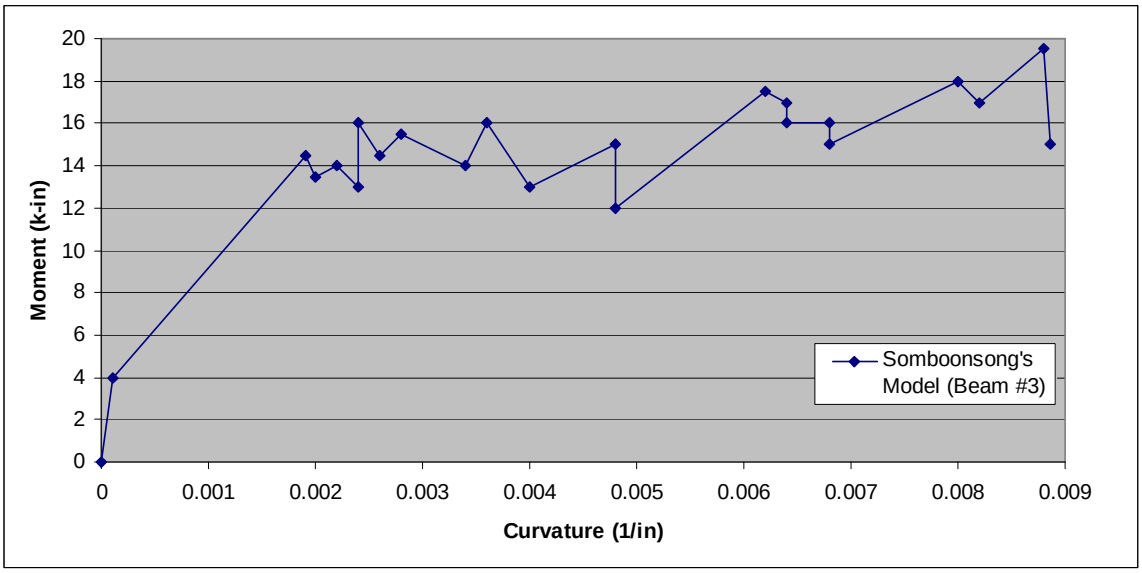

Figure (E-2): Moment-curvature curve for Somboonsong's experimental work.

Belarabi's Model

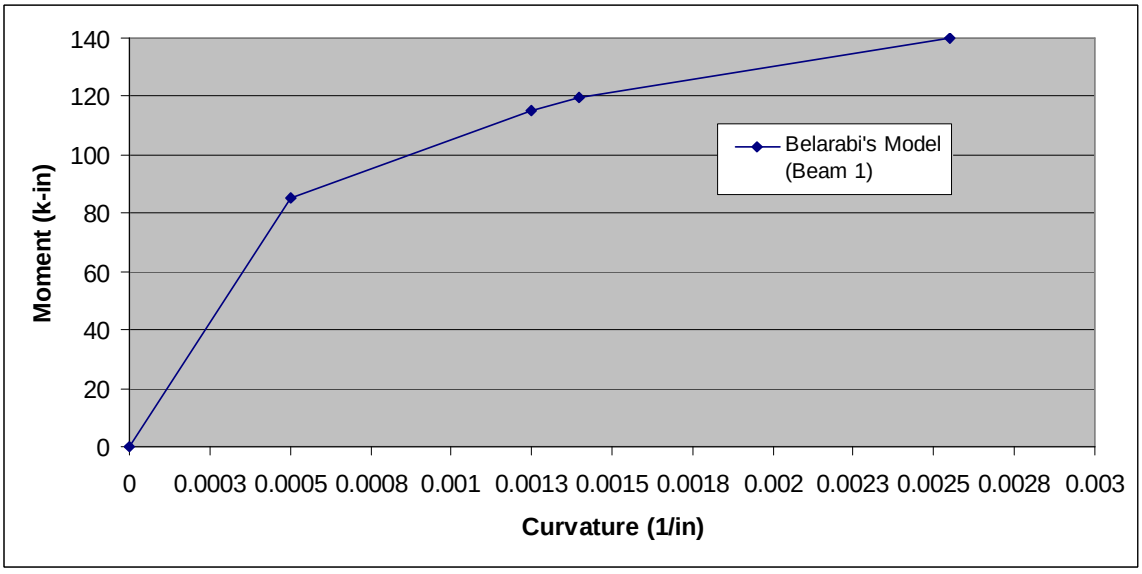

Figure (E-3): Moment-curvature curve for Belarabi's experimental work.

REFERENCES

AASHTO, “LRFD Bridge Specifications and Commentary.” 3rd edition, American Association of State Highway and Transportation Officials, Washington 2010.

AASHTO “LRFD Bridge Design Guide Specifications for GFRP-Reinforced Concrete Bridge Decks and Traffic Railings.” 1st edition, American Association of State Highway and Transportation Officials, Washington 2009

ACI Committee, “Building Code Requirements for Structural Concrete.” ACI 318.08, American Concrete Institute, Farmington Hills, MI, 2008.

ACI Committee, “Guide for Design and Construction of Structural Concrete Reinforced with FRP Bars.” ACI 440.1R-02, American Concrete Institute, Farmington Hills, MI, 2006.

ACI Committee, “Guide for Design and Construction of Structural Concrete Reinforced with FRP Bars.” ACI 440.1R-06, American Concrete Institute, Farmington Hills, MI, 2006.

Agarwal, H., Mozumder, C.K., Renaud, J. E., and Watson, L. T., “An Inverse-Measure-Based Unilevel Architecture for Reliability-Based Design Optimization”, Journal of Structural and Multidisciplinary Optimization, Vol. 33, No. 3, 2007, pp. 217-227.

AISC, “ASD/LRFD Steel Construction Manual.” 13th edition, American Institute of Steel Construction, Chicago, IL 2005.

Andersons, J., Joffe, R., and Sparnins, E., “Stiffness and Strength of Flax Fiber/Polymer Matrix Composites.” Polymer Composites, Vol. 27, No. 2, 2006, pp. 221-229.

Ang, A. H-S and Cornell, C. A. “Reliability Bases of Structural Safety and Design,” Journal of the Structural Division, ASCE, Vol. 100, No. ST9, 1974.

ASCE, “Minimum Design Loads for Buildings and Other Structures.” ASCE/SEI 7-10, American Society of Civil Engineers, 2010.

Atadero, A., Lee, L., and Karbhari, V.M, “Consideration of Material Variability in Reliability Analysis of FRP Strengthened Bridge Decks.” Composite Structures, Vol. 7, 2005, pp. 430-443.

Au, S.K., Ching, J., and Beck, J.L. “Application of Subset Simulation Methods to Reliability Benchmark Problems.” Structural Safety, Vol. 29, No. 3, 2007, pp. 183-193.

Au, S.K. and Beck, J.L. “Estimation of Small Failure Probabilities in High Dimensions by Subset Simulation.” Probabilistic Engineering Mechanics, Vol. 16, No. 4, 2001, pp. 263-277.

Ayyub, B.M., and Chia, Y.C. “Generalized Conditional Expectation for Structural Reliability Assessment.” Structural Safety, Vol. 11, 1992, pp. 131-146.

Ayyub, B.M., and Haldar, A. “Practical Structural Reliability Techniques.” Journal of Structural Engineering, ASCE, Vol. 110, No. 8, 1984, pp. 1707-1724.

Bader, M.G. and Manders, P.W. “The strength of hybrid glass/carbon fiber composites, part I: failure strain enhancement and failure mode.” Journal of Materials Science, Vol. 16, 1981, pp. 2233-2245.

Baker, R.M., and Puckett, J.A. “Design of Highway Bridges: An LRFD Approach.” Wiley; 2 edition, 2006.

Bank, L.C. “Composites for Construction Structural Design with FRP Materials.”, Wiley, 2006.

Bažant, Z,P., “Effect of Curvature of The Reinforcing Fibers on The Moduli of Elasticity and Strength of Composites.” Polymer Mechanics, Vol. 4, No. 2, 1968, pp. 314-321.

Belarbi, A., Chandrashekhara, K., and Watkins, S.E. “Performance Evaluation of Fiber Reinforced Polymer Reinforcing Bar Featuring Ductility and Health Monitoring Capability.” Final Report RTD-99-005. University of Missouri-Rolla, 1999.

Bengar, A.H., Maghsoudi, A.A., “Acceptable Lower Bound of The Ductility Index and Serviceability State of RC Continuous Beams Strengthened with CFRP Sheets.” Scientia Iranica, Vol. 18, No. 1, 2011, pp. 36–44.

Bert, C.W., and Kline, R.A. “Composite-Material Mechanics: Properties of Planar-Random Fiber Composites.” Polymer Composites, Vol. 6, No. 3, 1985, pp.133-141.

Box, M.J. “A New Method of Constrained Optimization and a Comparison with Other Methods.” Computer Journal, Vol. 8, No. 1, 1965, pp. 42-52.

Box, M.J. “A Comparison of Several Current Optimization Methods and The Use of Transformations in Constrained Problems.” Computer Journal, Vol. 9, No. 1, 1966, pp. 67-77.

Branson, D.E., “Instantaneous and Time-Dependant Deflections of Simple and Continuous Reinforced Concrete Beams.” HPR Report No. 7, Part 1, Alabama Highway Department, Bureau of Public Roads, Auburn, AL: Department of

Civil Engineering and Auburn Research Foundation, Auburn University, 1965.

Branson, D.E., “Deformation of Concrete Structures.” New York, McGraw-Hill, 1977.

Brongers, M.P.H., Payer, J.H., Koch, G.H., Thompson, N.G., Virmani, Y.P. “Corrosion Costs and Preventive Strategies in the United States” Publication no. FHWA-RD-01-156, 2002.

Breitung, K. “Asymptotic Approximation for Multinormal Integral.” Journal of Engineering Mechanics, ASCE, Vol. 110, No. 3, 1984, pp. 357-366.

Bucher, C.G., and Bourgund, U., “A Fast and Efficient Response Surface Approach for Structural Reliability Problem.” Structural Safety, Vol. 11, No. 4, 1992, pp. 57-66.

Bunsell, A.R. and Harris, B. “Hybrid Carbon and Glass Fiber Composites.” Composites, Vol. 5, 1974, pp. 157-164.

Cauchy, A.L. "Méthode générale pour la résolution des systèmes d'équations simultanées", C.R. Acad. Sci., Paris, Vol. 25, 1847, pp. 536–538.

Chen, S.H., Kang, H.Y., and Lee, H.T. “A Study of Generalized Reduced Gradient Method with Different Search Direction.” Measurement of Management Journal (China), ISSN 1812-8572, Vol. 1, no. 1, 2004, pp. 25-38.

Chen, W.F. and Duan, L. “Bridge Design Handbook.” CRC Press, First Edition, 1999.

Cheney, E.W., and Goldstein, A.A., “Newton’s Method of Constrained Optimization and Tchebycheff Approximation.” Numerische Mathematik, Vol. 1, pp. 253-268, 1959.

Chin, W.K., Lee, Y.D., and Liu, H.T. “Effects of Fiber and Orientation Distribution on Elastic Modulus of Short Fiber Reinforced Thermoplastics.” Polymer Composites, Vol. 9, No. 1, 1988, pp. 37-35.

Chin, X. and Lind, N.C. “Fast Probability Integration by Three-Parameter Normal Tail Approximation.” Structural Safety, Vo. 1, 1983, pp. 269-276.

Choi, K.K., Park, Y.H., and Youn, B.D., “Hybrid Analysis Method for Reliability-Based Design Optimization.” Journal of Mechanical Design, ASME, Vol. 125, No. 2, 2001, pp. 221-232.

Chou, T.W., “Microstructural Design of Fibrous Composites.” Cambridge University Press, Cambridge, 1992.

Cox, H.L., ‘The Elasticity and Strength of Paper and Other Fibrous Materials.” British Journal of Applied Physics, Vol. 3, No. 3, 1952. pp. 72-79.

Cui, Y., Cheung, M.S., Noruziaan, B., Lee, S., and Tao, J. “Development of ductile composite reinforcement bars for concrete structures.” Materials and Structures, Vol. 41, 2008, pp. 1509-1518.

Cui, Yi-Hua and Tao, Jie. “A new type of ductile composite reinforcing bar with high tensile elastic modulus for use in reinforced concrete structures.” Canadian Journal of Civil Engineering, Vol. 36, 2009. pp. 672-675

Der Kiureghian, A., Lin, H.Z., and Hwang, S.J. “Second Order Reliability Approximations.” Journal of Engineering Mechanics, ASCE, Vol. 113, No. 8, 1987, pp. 1208-1225.

Dingle, L.E. “Aligned Discontinuous Carbon Fiber Composites.” Proceeding 4th International Conference on Carbon Fibers, Their Composites and Applications, Plastic Institutes, London, 1974.

Eamon, D.C., and Charumas, B. “Reliability Estimation of Complex Numerical Problems Using Modified Conditional Expectation Method,” Computers and Structures, Vol. 89, No. 1-2, 2011, pp. 181-188.

Eamon, D.C. and Rais-Rohani, M. “Structural Reliability Analysis of Advanced Composite Sail.” SNAME Journal of Ship Research, Vol. 52, No. 3, 2008, pp 165-174.

Ellingwood, B.R., Galambos, T.V., MacGroger, J.G., and Cornell, C.A., “Development of Probability Based Load Criterion for American National Standards A58.” NBS Special Publication of Commerce, Washington DC, 1980.

Engelund, S., and Rackwitz, R. “A Bench Mark on Importance sampling Techniques in Structural Reliability.” Structural Safety, Vol. 12, No. 4, 1993, pp. 255-276.

Fiessler, B., Neumann, H. J. & Rackwitz, R “Quadratic Limit States in Structural Reliability.” Journal of Engineering. Mechanics, ASCE, Vol 1095, No. 4, 1979,. pp. 661–676.

Fu, S.Y., Hu, X., and Yue, C.Y., “The Flexural Modulus of Misaligned Short-Fiber-Reinforced Polymers.”, Composite Science and Technology, Vol. 49, No. 10, 1999. pp. 1533-1542.

Fu, S.Y., and Lauke, B., “An Analytical Characterization of the Anisotropy of the Elastic Modulus Misaligned Short-Fiber-Reinforced Polymers.” Composites Science and Technology, Vol. 58, No. 12, 1998, pp. 1961-1972.

Fu, S.Y., and Lauke, B., "The Elastic Modulus of Misaligned Short-Fiber-Reinforced Polymers." Composites Science and Technology, Vol. 58, No. 3-4, 1998, pp. 389-400.

Gabriele, G.A., and Ragsdell, K.M. "The Generalized Reduced Gradient Method: A Reliable Tool for Optimal Design." ASME Journal of Engineering for Industry, Vol. 99, 1977, pp. 384-400.

Galambos, T.V., and Ravindra, M.K. "Properties of Steel for Use in LRFD." Journal of the Structural Division, ASCE, Vol. 104 No. 9, 1978, pp. 1459-1468.

Gao, D., Benmokrane, B., and Masmoudi, R., "A Calculating Method of Flexural Properties of FRP Reinforced Concrete Beam: Part 1: Crack Width and Deflection." Technical Report, Department of Civil Engineering, University of Sherbrook, Sherbrook, Quebec, Canada, 1998.

Gill, P.E., Murray, W., and Saunders, M.A. "SNOPT: An SQP Algorithm for Large-Scale Constrained Optimization." SIAM Rev., Vol. 47, 2005, pp. 99-131.

Gomes, H.M., and Awruch, A.M., "Comparison of Response Surface and Nueral Network with Other Methods for Structural Reliability Analysis." Structural Safety, Vol. 26, No. 4, 2004, pp. 49-67.

Haldar, A., and Mahadevan, S. "Probability, Reliability, and Statistical Methods in Engineering Design." Wiley, 1999.

Han, S.P. "A Globally Convergent Method for Nonlinear Programming." Journal of Optimization Theory and Applications, Vol. 22, 1977, pp. 297-309.

Harbitz, A. "An Efficient Sampling Method for Probability of Failure Calculation." Structural Safety, Vol. 3, No. 2, 1986, pp. 109-115.

Harr, M.E., “Reliability Based Design in Civil Engineering.” Dover, 1997.

Hasofer, A.M., and Lind, N.C. “Exact and Invariant Second Moment Code Format.” Journal of Engineering Mechanics Division, ASCE, Vol. 100, No. EM1, 1974, pp. 111-121.

Hognestad, E., "A study on Combined Bending and Axial Load in Reinforced Concrete Members." University of Illinois at Urbana, Vol. 49, No. 22, 1951.

Hohenbichier, M., Gollwitzer, W., Kruse, W., and Rackwitz, R. “New Light on First-and Second-Order Reliability Methods.” Structural Safety, Vol. 4, 1987, pp. 267-284.

Hull, D. “An Introduction to Composite Materials.” Cambridge University Press, 1981.

Janney, M., Geiger, E., and Baitcher, N. “Fabrication of Chopped Fiber Preforms by the 3-DEP Process.” COMPOSITES & POLYCON, American Composites Manufacturers Association, 2007.

Jayaraman. K., and Kortschot, M.T. “Correction to The Fukuda-Kawata Young’s Modulus theory and Fukuda-Chou Strength Theory for Short Fiber-Reinforced Composite Materials.” Journal of Material Science, Vol. 31, 1996, pp. 2059-2064.

Kelly, A., and Tyson, W.R., “Tensile Properties of Fiber-Reinforced Metals.” Journal of Mechanical Physics Solids, Vol. 13, 1965, pp. 329-350.

Kelly, J.E. “The Cutting Plane Method for Solving Convex Problem.” Journal of SIAM, Vol. VIII, No. 4, pp. 703-712, 1960.

Kent, D.C., and Park, R., “Flexural Members with Confined Concrete.” Journal of the Structural Division, Vol. 97, No. 7, 1971, pp. 1969-1990.

Karamchandani, A. “Reliability Analysis of Truss Structures with Multistate Elements. II,” Journal of Structural Engineering, Vol. 118, No. 4, 1990, pp. 910-925.

Karamchandani, A., Bjerager, P., Cornell, A.C., “Adaptive Importance Sampling.” International Conference on Structural Safety and Reliability (ICOSSAR), 1989, p 855-862.

Karmarkar, N. “A New Polynomial Time Algorithm for Linear Programming.” Combinatorica, Vol. 4, No. 4, 1984, pp. 373–395.

Karush, W. “Minima of Functions of Several Variables with Inequalities as Side Constraints.” M.Sc. Dissertation. Department. of Mathematics, University of Chicago, Chicago, Illinois, 1939.

Kharmanda, G.; Olhoff, N.; and El-Hami, A. “Optimum Safety Factor Approach for Reliability-Based Design Optimization with Extension to Multiple Limit State Case” Structural and Multidisciplinary Optimization, Vol. 27, 2004, 421-434.

Krenchel, H., “Fiber Reinforcement.” Akademisk Forlag, Copenhagen, 1964.

Kuhn, H. W.; Tucker, A. W. “Nonlinear programming.” Proceedings of 2nd Berkeley Symposium. Berkeley: University of California Press. pp. 481–492, 1951

Lee, S.H., Kwak, B.M., “Reliability Based Design Optimization Using Response Surface Augmented Moment Method ", International Journal of Numerical Methods for Heat & Fluid Flow, Vol. 5, No., 4, 1995 pp.313 – 326.

Lee, T.W. and Kwak, B.M. “A Reliability-Based Optimal Design Using Advanced First Order Second Moment Method”, Mechanics of Structures and Machines, Vol. 15, No. 4, 1987, pp.523–542.

Lesay, J., and Marz, L. “Problems with reliability and safety of hot dip galvanized steel structures.” Welding & Material Testing, Bratislava, Slovakia, Vol. 14, No. 2, 2009, pp. 184-190.

Lutomirska, M. “Live Load Models for Long Span Bridges.” A Thesis Submitted to the University of Nebraska – Lincoln in Partial Fulfillment of the Degree of Doctor of Philosophy in Department of Civil Engineering, 2009.

MacGregor, J.G., “Safety and Limit State Design for Reinforced Concrete.” Canadian Journal of Civil Engineering, Vol. 3, No. 4, 1976, pp. 484-513.

MacGregor, J.G., and Wight, J.K. “Reinforced Concrete: Mechanics and Design” Prentice Hall; Sixth Edition, 2011.

Maghsoudia, A.A., and Bengarb, H.A., “Acceptable Lower Bound of The Ductility Index and Serviceability State of RC Continuous Beams Strengthened with CFRP Sheets.” Scientia Iranica, Vol. 18, 2011, pp. 36–44

Manera, M., “Elastic Properties of Randomly Oriented Short Fiber-Glass Composites.” Journal of Composites Materials, Vol. 11, 1977, pp. 235-247.

Mathews, F.L., and Rawlings, R.D “Composite Materials: Engineering and Science.” CRC Press, 1999.

Melchers, R.E., “Structural Reliability Analysis and Prediction.” Wiley, 1999.

Mertz, D.R., Kulicki, J.M., Prucz, Z., Clancy, C.M., and Nowak, A.S., “Updating The Calibration Report for AASHTO LRFD Code.” Final Report, Project No. NCHRP 20-7/186, 2007.

Naaman, A. E., and Jeong, S. M., “Structural Ductility of Concrete Beams Prestressed with FRP Tendons.”, “Non-Metallic (FRP) Reinforcement for Concrete

Structures." Proceedings of the Second International RILEM Symposium (FRPRCS), Ghent, Belgium, 1995, pp. 379-386.

NDS, "ASD/LRFD NDS for Wood Construction." National Design Specification, 2005.

Nosarev, A.V., "Elastic Constants for a Material Reinforced in Two Directions in The Planar Case." Polymer Mechanics, Vol. 3, No. 2, 1967, pp. 266-272.

Nowak, A.S., "Calibration of LRFD Bridge Design Code." NCHRP Report 368, Transportation Research Board, Washington, D.C., USA, 1999

Nowak, A.S., and Szerszen, M.M., "Calibration of Design Code for Building (ACI 318), Part 2: Reliability Analysis and Resistance Factors, ACI Structural Journal, Vol. 100, No. 3, 2003, pp. 383-391.

Nowak, A.S., and Collins, K.R., "Reliability of Structures." McGraw-Hill, 2000.

Pan, M., "Theoretical Determination of The Optimal Volume Fraction and Fiber-Matrix Property Compatibility of Short Fiber Composites." Polymer Composites, Vol. 14, No. 2, 1993, pp. 85-93.

PCI "PCI Bridge Design Manual.", 3rd edition, Precast/prestressed Concrete Institute, Chicago, IL, 2011.

Powell, M.J.D. "A fast algorithm for nonlinearly constrained optimization calculations." in Lecture Notes in Mathematics, Watson, G.A. et al., Eds., No. 630, Berlin, Springer Verlag, 1978, pp. 144-157.

Quayyum, S. "Bond Behavior of Fiber Reinforced Polymer (FRP) Rebars in Concrete." A Thesis Submitted to the University of British Columbia in Partial Fulfillment of the Requirements for the Degree of Master of Applied Science, 2010.

Rackwitz R., and Fiessler B. “Structural Reliability under Combined Random Load Sequences” Computers and Structures, Vol. 9, 1974. pp. 489-494

Rackwitz, R., Fiessler, B. “Note on Discrete Safety Checking When Using Non-Normal Stochastic Models for Basic Variables.” Load Project Working Session, MIT, Cambridge, MA, 1978.

Rao, S.S. “Engineering Optimization: Theory and Practice.” Wiley, 2009.

Rosen, J.B. “The gradient projection method of nonlinear programming.” Part I: linear constrains, SIAM journal, Vol. 8, 1960, pp. 181-217.

Rosen, J.B. “The gradient projection method of nonlinear programming.” Part II: nonlinear constrains, SIAM journal, Vol. 9, 1961, pp. 414-432.

Rosenthal, J. “A Model for Determining Fiber Reinforcement Efficienes and Fiber Orientation in Polymer Composites.’ Polymer Composites, Vol. 13, No. 6, 1992. pp 462-466-

Saikia, B., Thomas, J., and Nanjuda Rao, K.S., “Performance of Hybrid Rebars as Longitudinal Reinforcement in Normal Strength Concrete.” Materials and Structures, Vol., 38, 2005, pp. 857-864.

Shin, S., Kang, H., Ahn, J., and Kim, D., “Flexural Capacity of Singly Reinforced Beam with 150 MPa Ultra High-Strength Concrete.” Indian Journal of Engineering & Materials Science, Vo. 17, 2010. pp. 414-426.

Saliby, E. “Descriptive Sampling: An Improvement over Latin Hypercube Sampling.” Proceedings of the 1997 Winter Simulation Conference, 1997, pp. 230-233.

Shin, S., Kang, H., Ahn, J., and Kim, D. “Flexural Capacity of Singly Reinforced Beam with 150MPa Ultra High Strength.” Indian Journal of Engineering and Materials Science, Vol. 17, 2010, pp. 414-426.

Somboonsong, W., “Development of Ductile Hybrid Fiber Reinforced Polymer (D-H-FRP) Reinforcement for Concrete Structures.” A Thesis Submitted to the Drexel University in Partial Fulfillment of the Degree of Doctor of Philosophy in Department of Civil Engineering, 1997.

Tamuzs, V. and Tepfers, R., “Ductility of Non-Metallic Hybrid Fiber Composite Reinforcement for Concrete.”, “Non-Metallic (FRP) Reinforcement for Concrete Structures.” Proceedings of the Second International RILEM Symposium (FRPRCS), Ghent, Belgium, 1995, pp. 18-28.

Tarnopol’skil, Y.M., Portnov, G.G., and Zhigum, I.G., “Effect of The Fiber Curvature on The Modulus of Elasticity and Strength of Composites for Unidirectional Glass-Reinforced Plastic in Tension.” Polymer Mechanics, Vol. 3, No. 2, 1967, pp. 243-249.

Terry, T.K.Chung, “Behavior of Concrete Beams Reinforced with Hybrid FRP Composite Rebars.” A Thesis Submitted to the Hong Kong University of Since and Technology in Partial Fulfillment of the Requirements for the Degree of Master of Philosophy in Department of Civil Engineering, 2006.

Thomason, J.L., and Vulg, M.A., “Influence of Fiber Length and Concentration on The Properties of Glass Fiber-Reinforced Polypropylene: 1. Tensile and flexural modulus.” Composites Part A Applied Science and Manufacturing, Vol. 27, No. 6, 1996, pp. 477-484.

Thomason, J.L., Vlug, M.A., Schipper, G., and Kirkor, H.G.L.T., "Influence of Fiber Length and Concentration on the Properties of Glass-Fiber Polypropylene: Part 3. Strength and Strain at Failure." Composites Part A: Applied Science and Manufacturing, Vol. 27, No. 11, 1996, pp. 1075-1084.

Weng, G.J., and Sun, C.T., "Effects of Fiber Length on Elastic Moduli of Randomly-Oriented Chopped-Fiber Composites." Composite Materials: Testing and Design (Fifth Conference), ASTM STP 674, 1979, pp. 149-162.

Wierschem, N. and Andrawes, B. "Superelastic SMA-FRP composite reinforcement for concrete structures." Smart Materials and Structures, Vol. 19, 2010, pp. 1-13.

Wilson, R.B, "A Simplicial Method for Convex Programming." PhD thesis, Harvard University, 1963.

Won, J. P., Park, C.G., and Jang, C. "Tensile Facture and Bond Properties of Ductile Hybrid FRP Reinforcing Bars." Polymers & Polymer Composites, Vol. 15, No. 1, 2007, pp 9-16.

Wu, Y.F. "New Avenue of Achieving Ductility for Reinforced Concrete Members." ASCE Journal of Structural Engineering. Vol. 132, No. 9, September 2006. pp. 1502-1506.

Wu, Y.F. "Ductility Demand of Compression Yielding Fiber-Reinforced Polymer-Reinforced Concrete Beams." ACI Structural Journal, Vol. 105, No. 1, Jan-Feb 2008, pp 104-110.

Wu, Y.T. "Adaptive Importance Sampling Method for Structural System Reliability Analysis." Reliability Technology, American Society of Mechanical Engineers, Aerospace Division (Publication) AD, Vol. 28, 1992, p 217-231.

Yang, R.J., and Gu, L. “Experience with Approximate Reliability-Based Optimization Methods.” Vol. 26, No. 1-2, 2004, pp. 152-159.

Zhou, Y.W., Wu, Y.F., Leung, A.Y.T. “Ductility analysis of compression-yielding FRP-reinforced composite beams.” Cement & Concrete Composites, Vol. 31, 2009, pp. 682-691.

Zou, T., and S. Mahadevan, “A Direct Decoupling Approach for Efficient Reliability-Based Design Optimization.” Structural and Multidisciplinary Optimization, Vol. 31, No. 3, 2006, pp. 190-200.

Zoutendijk, G. “Methods of feasible directions.” Elsier, Amsterdam, 1960.

http://www.galvanizeit.org/images/uploads/drGalv/Galvanized_Rebar_versus_Epoxy_Coated_Rebar.pdf, 2011.

http://en.wikipedia.org/wiki/Hot-dip_galvanizing, 2011.

ABSTRACT

RELIABILITY MODEL FOR DUCTILE HYBRID FRP REBAR USING RANDOMLY DISPERSED CHOPPED FIBERS

by

BASHAR RAMZI BEHNAM

May 2012

Advisor: Dr. Christopher Eamon

Major: Civil Engineering

Degree: Doctor of Philosophy

Fiber reinforced polymer composites or simply FRP composites have become more attractive to civil engineers in the last two decades due to their unique mechanical properties. However, there are many obstacles such as low elasticity modulus, non-ductile behavior, high cost of the fibers, high manufacturing costs, and absence of rigorous characterization of the uncertainties of the mechanical properties that restrict the use of these composites. However, when FRP composites are used to develop reinforcing rebars in concrete structural members to replace the conventional steel, a huge benefit can be achieved since FRP materials don't corrode.

Two FRP rebar models are proposed that make use of multiple types of fibers to achieve ductility, and chopped fibers are used to reduce the manufacturing costs. In order to reach the most optimum fractional volume of each type of fiber, to minimize the cost of the proposed rebars, and to achieve a safe design by considering uncertainties in the materials and geometry of sections, appropriate material resistance factors have been developed, and a Reliability Based Design Optimization (RBDO), has been conducted for the proposed schemes.

AUTOBIOGRAPHICAL STATEMENT

BASHAR BEHNAM

BASHAR BEHNAM received his B.Sc. in Civil Engineering in 1992 and his first master degree in Civil Engineering in 1996 from University of Baghdad, Baghdad, Iraq. He received his second mater degree in Civil Engineering from Wayne State University in 2006. He has been studying towards his doctoral degree in Civil Engineering at Wayne State University Since 2007. His research interests are application of fiber reinforced polymer composites for civil infrastructure, reliability analysis, concrete technology, and modeling of structures.